2014-05-13

Production Data Analysis of Tight and Shale Reservoirs

Shahamat, Mohammad Sadeq

UNIVERSITY OF CALGARY

Production Data Analysis of Tight and Shale Reservoirs

by

Mohammad Sadeq Shahamat

A THESIS

SUBMITTED TO THE FACULTY OF GRADUATE STUDIES

IN PARTIAL FULFILMENT OF THE REQUIREMENTS FOR THE

DEGREE OF DOCTOR OF PHILOSOPHY

DEPARTMENT OF CHEMICAL AND PETROLEUM ENGINEERING

CALGARY, ALBERTA

MAY, 2014

Abstract

Production of oil and natural gas from challenging and unconventional (i.e. tight and shale) reservoirs has gained momentum and industry's attention because of the important role they will play in fulfilling future energy needs globally. Predicting reserves and forecasting future production of these types of reservoirs is crucial for evaluation of new investments and auditing of previous expenditures. One rapid way of examining dynamic response of a reservoir using solely production data is decline curve analysis. When applied to tight and shale reservoirs, traditional decline curve analysis can lead to unreasonable results. The main reasons are the extended transient flow (caused by very low permeabilities) and reservoir heterogeneities such as layering and compartmentalization.

The above observations led to the research presented in this thesis. The study, consisting of two parts, focused on modeling and forecasting of long-term oil and gas production from tight and shale reservoirs.

In the first part, a capacitance-resistance model (CRM) was developed which was the result of stepwise coupling of the material balance and fluid-flow equations. Using capacitance and resistance terms, the concept of continuous succession of pseudo-steady states was introduced to enable using the depletion equations through a stepwise procedure for performance analysis during transient and boundary dominated flow (BDF). The model was then extended to multilayered and compartmentalized reservoir cases. Verification of the approach was obtained by comparing results against those of a reservoir numerical simulator. It was shown that the proposed compartmentalized model is able to consider the effects of low permeability barriers as well as different reservoir properties across the compartments. In addition, it was shown that performance behaviour of multilayered and

compartmentalized reservoirs can be significantly different from that of a single compartment/layer reservoir; therefore the effect of additional compartments/layers should be accounted for.

In the second part of this work, an extensive simulation study was performed to elucidate the value of beta derivative for performing rate decline analysis. Based on the results, a new easy to use model for predicting future rate in conventional and unconventional oil and gas reservoirs was presented. Comparison of the model results with those of numerical simulation corroborated the reliability of the proposed method for forecasting production rates during transient and BDF.

This research demonstrated that physical complexities which are involved in production from the unconventional tight and shale reservoirs, including transient flow, layering, compartmentalization and natural fractures, can be simply captured by using the proposed approaches. They rely on simple reservoir engineering concepts. As a result, the proposed models offer new insights into production analysis of tight and shale reservoirs, using familiar and easy-to-understand reservoir engineering principles.

Acknowledgements

Many individuals have helped me throughout the course of my graduate studies at the University of Calgary. Their contributions to my research, their encouragement and motivation have proven invaluable. I would like to take this opportunity to thank them.

First and foremost, my heartfelt gratitude and respect goes to my supervisor and committee chairman, Dr. Roberto Aguilera and my co-supervisor, Mr. Louis Mattar for their continuous support of my PhD studies, for their motivation and enthusiasm. I learned numerous lessons not only technically from their immense knowledge and expertise, but also personally from their character, their way of approaching problems and their professional attitude and behaviour. I am deeply grateful to Dr. Roberto for his endless support and encouragements and for providing me a unique research environment through his amazing GFREE research group. I am also grateful to Louis who generously gave his time to offer me invaluable comments toward improving my work. Truly, I could not have imagined having better mentors for my PhD studies.

Besides my supervisor and co-supervisor, I would like to thank the rest of my thesis committee: Dr. Mehran Pooladi-Darvish, Dr. Tom Harding, Dr. Raj Mehta, Dr. Larry Lines and Dr. Robert Wattenbarger for their time and insightful comments.

I would like to thank my great friends in the GFREE group, Mr. Bruno Armando Lopez Jimenez, Mr. John Freddy Ramirez Vargas, Mrs. Liliana Zambrano and Mr. Mohammad Rahmanian for their friendship and fruitful discussions on technical issues. We accomplished some incredible jobs collaboratively on different topics which always remind me of those sweet days of working together.

In addition, I would like to thank all my friends and fellow graduate students, in particular: Mehdi Bahonar, Hamid Behmanesh, Hamidreza Hamdi, Mohammad Kariznovi, Hossein Nourozieh, Ehsan Ranjbar and Hamed Tabatabaie. Whether it was sharing analysis and discussing technical issues, a small talk during a tea/coffee break, or a weekend get-together, thank you. I consider your friendship a real treasure of my life.

I thankfully acknowledge the financial support from the Natural Sciences and Engineering Research Council of Canada (NSERC). I would like to thank Mr. Ross Laurie and Shaoyong Yu of ConocoPhillips Canada for providing me with field data for two example wells. Their help is gratefully acknowledged.

Finally, and most importantly, I would like to express gratitude to my wife (Maryam Nouri Zadeh), our parents (Namdar Shahamat and Nosrat Noureh Zadeh; and Abbas Nouri Zadeh and Sohaila Azargoun), all my brothers and sisters especially my oldest sister (Farkhondeh), for their love, support, timely encouragement, and endless patience, without which this work would never have been accomplished.

Dedicated to my Dear

Late Father, my Mother and my Wife.

I Have Your Love, Your Support, and

Your Blessings,

Therefore I Have Everything.

Table of Contents

List of Tables

List of Figures and Illustrations

List of Symbols, Abbreviations and Nomenclature

Symbol	Definition
A_c	Cross-sectional area, ft^2
b	Hyperbolic decline exponent, dimensionless
B	Liquid formation volume factor, bbl/Stb
B_g	Gas formation volume factor, ft^3/Scf
c	Total compressibility, 1/psia
c_f	Formation compressibility, 1/psia
c_g	Gas compressibility, 1/psia
c_t	Total compressibility (for gas cases), 1/psia
C	Electrical Capacitance, farad
C	Fluid flow Capacitance, Stb/psia or MScf/psia [see Eq. 3.4 or Eq. 3.10]
C_1	Fluid flow Capacitance of the higher permeability layer, Stb/psia or MScf/psia
C_2	Fluid flow Capacitance of the lower permeability layer, Stb/psia or MScf/psia
C_s	Flow Capacitance of the support compartment, Stb/psia or MScf/psia
C^*	Fluid flow Capacity, Stb/(ft.psia) or MScf/(ft.psia) [see Eq. 3.6]
C^*_1	Flow capacity of the higher permeability layer, Stb/(ft.psia) or MScf/(ft.psia)
C^*_2	Flow capacity of the lower permeability layer, Stb/(ft.psia) or MScf/(ft.psia)
D	Decline Rate, 1/day
F_c	Ratio of capacitance of the production to support compartment [see Eq. 4.8]
F_c^*	Ratio of capacity of the production to support compartment
F_R	Ratio of resistance of the production to support compartment [see Eq. 4.7]
F_R^*	Ratio of resistivity of the production to support compartment
G	Initial gas in place, Mscf
G_p	Cumulative gas production, MMScf
h	Net pay, ft
I	Electric current, amperes
k	Permeability, md
k_f	Fracture permeability in a dual porosity medium, md
k_m	matrix permeability in a dual porosity medium, md
k_s	Permeability of the damaged zone, md
L	Length, ft
m_b	Slope of the approximate BDF straight line on logarithmic plot of β vs. time
m_t	Slope of the approximate transient straight line on logarithmic plot of β vs. time
p	Pressure, psia
p_{avg}	Average pressure, psia
$p_{avg,s}$	Average pressure in the support compartment, psia
$(p_{avg})_D$	Dimensionless average reservoir pressure
p_D	Dimensionless pressure [see Table. A.1]
p_{DM}	Production tank dimensionless pressure [see Eq. 4.5 or 4.11]
p_{DMs}	Support tank dimensionless pressure [see Eq. 4.12]
$p_{DM,BDF}$	p_{DM} at the start of BDF
$p_{DM}{}^c$	Dimensionless pressure in compartmentalized model based on Δp^c [Eq. 4.20]
$p_{DM}{}^{cs}$	Dimensionless pressure in compartmentalized model based on Δp^{cs} [Eq. 4.21]
$\widehat{p_D}$	Dimensionless pressure defined as $\widehat{p_D} = 1 - p_D$
p_L	Langmuir pressure, psia

p_p	Normalized pseudo-pressure, psia
p_{pavg}	Normalized average pseudo-pressure, psia
p_{pwf}	Normalized wellbore pseudo-pressure, psia
$p_{pwf}{}^1$	Initial normalized wellbore pseudo-pressure, psia
p_{wf}	Wellbore flowing pressure, psia
$p_{wf}{}^1$	Initial wellbore flowing pressure, psia
p_{wD}	Dimensionless wellbore flowing pressure
$\overline{p_D}$	Dimensionless pressure in Laplace domain
$\overline{p_{wD}}$	Dimensionless wellbore flowing pressure in Laplace domain
q	Well production rate, StbD
q^1	Initial well production rate, StbD
q_{BDF}	Well-production rate at the start of BDF, MscfD
q_D	Dimensionless rate [see Table. A.1]
q_{Dd}	Dimensionless decline rate [see Eq. 6.7]
q_{DM}	Production tank dimensionless rate [see Eq. 4.13 or 4.16]
q_{DMs}	Support tank dimensionless rate [see Eq. 4.17]
$q_{DM,BDF}$	q_{DM} at the start of BDF
q_g	Gas well production rate, MscfD
q_i	Initial well-production rate, StbD
q_R	Ratio of production rate of higher to lower permeability layer [see Eq. 5.1]
q_s	Flow rate from the support to the production compartment, StbD [see Eq. 4.2]
q_{wD}	Dimensionless production rate at the wellbore
$\overline{q_D}$	Dimensionless rate in Laplace domain
R	Electrical resistance, ohms
R	Flow resistance, psia/StbD or psia/MScfD [see Eq. 3.5 or Eq. 3.11]
Ro%	Reflectance in Oil (percentage)
R_s	Flow resistance of the support compartment, psia/StbD or psia/MScfD
R^*	Flow resistivity, psia/(StbD.ft) or psia/(MScfD.ft) [see Eq. 3.7]
$R^*{}_1$	Flow resistivity of the higher k layer, psia/(StbD.ft) or psia/(MScfD.ft)
$R^*{}_2$	Flow resistivity of the lower k layer, psia/(StbD.ft) or psia/(MScfD.ft)
r_e	Reservoir size in r-direction, ft
r_{eD}	Dimensionless reservoir size in r-direction
r_{inv}	Radius of investigation, ft
r_w	Wellbore radius, ft
s	Skin factor, dimensionless [see Eq. 3.14 or 3.16]
s^*	Additional resistance due to skin $s^* = \Delta p_s/q$, psia/StbD [see Eq. 3.17]
t	Time, days
t_a	Normalized pseudo-time, days
t_i	Initial time at which $q = q_i$, days
t_{BDF}	Time to reach BDF, days
t_D	Dimensionless time [see Table. A.1]
t_{Dd}	Dimensionless decline time [see Eq. 6.6]
t_{DM}	Dimensionless time defined in compartmentalized model [see Eq. 4.6]
$t_{DM,BDF}$	t_{DM} at the start of BDF [see Eq. 4.23]
T	Reservoir temperature, °F
u	Lapalce space variable
V	Reservoir volume, bbl
V_L	Langmuir Volume, Scf
x_e	Reservoir length in x-direction, ft

x_f	Fracture half length, ft
y_D	Dimensionless distance in y-direction [see Table. A.1]
y_e	Reservoir length in y-direction, ft
y_{eD}	Dimensionless reservoir length in y-direction
y_{inv}	Distance of investigation, ft [see Eq. 3.1]
y_{invD}	Dimensionless distance of investigation
y_s	Size of the skin (damaged) zone near the hydraulic fracture, ft
Z	Gas compressibility factor, fraction
α_1	Constant used for defining y_{inv}; $\alpha_1 = 1.42$ for CTR and 2.55 for CTP
α_2	Constant used for determining liquid Resistance; $\alpha_2 = \frac{\pi}{6}$ for CTR and $\frac{2}{\pi}$ for CTP
β	Rate-based beta derivative, dimensionless [see Eq. 6.1]
β_{BDF}	Rate-based beta derivative at start of BDF, dimensionless
β_1	Constant used for defining p_D and q_D, $\beta_1 = 2\pi \times 141.2$ in field units
β_2	Constant used for determining dimensionless time; $\beta_2 = 0.00633$ in field units
ω	Storativity ratio, dimensionless [see Eq. 5.4]
λ	Interporosity flow coefficient, dimensionless [see Eq. 5.5]
λ_1	First eigenvalue of the matrix of coefficients, A
λ_2	First eigenvalue of the matrix of coefficients, A
μ	Viscosity, cp
μ_g	Gas viscosity, cp
γ_g	Gas gravity, fraction
θ	Langmuir Storage, Scf/ton
ϕ	Porosity, fraction
ΔE	Potential difference, volts
Δp	Pressure difference, psia
Δp^c	Pressure depletion of a dummy production compartment neglecting the support, psia [see Eq. 4.18]
Δp^{cs}	Pressure depletion of a dummy support compartment, psia [see Eq. 4.18]
Δp_{dep}	Pressure depletion, psia [see Eq. 3.2]
Δp_{pdep}	Pseudo-pressure depletion, psia
Δp_s	Additional pressure drop due to skin, psia [see Eq. 3.15]
Δt	Time interval, days

BDF	Boundary Dominated Flow
BHP	Bottom Hole Pressure
CRM	Capacitance-Resistance Model
CRR	Capacity to Resistivity Ratio, $(Stb/psia)^2/Day$ or $(MScf/psia)^2/Day$ [see Eq. 3.9]
CTP	Constant Terminal Pressure
CTR	Constant Terminal Rate
Der	Bourdet derivative
FMB	Flowing Material Balance
NFR	Naturally Fractured Reservoir
ODE	Ordinary Differential Equation
SPSS	Succession of Pseudo-Steady States
SRV	Stimulated Reservoir Volume
TCF	Trillion Cubic Feet
EUR	Expected Ultimate Recovery, MStb or MMScf
i	(subscription) initial

Chapter One: Introduction

Hydrocarbon resources can be assigned to various classes in a triangle where their relative positions reflect their abundance, reservoir quality and the technology required for their recovery (Masters 1979, Holditch 2006, Martin et al. 2010). Originally, Masters (1979) published the concept of the resource triangle. Later, Holditch (2006) stated that oil and gas resources are distributed lognormally in nature, similar to any other natural resources, such as gold, copper and uranium. This means that best quality (commonly termed conventional) resources are small in size and, once found, are easy to extract. Lower quality reservoirs, however, are abundant but more difficult to exploit. Unconventional petroleum reservoirs are lower quality reservoirs that require some extraordinary stimulation treatment or special recovery processes and technologies to produce economic volumes of oil and natural gas. Typical unconventional reservoirs are tight and shale oil and gas reservoirs, coalbed methane and gas hydrates, and heavy and extra-heavy oil reservoirs. They are critical for quenching the need for energy in the future.

The resource triangle concept is best explained by using the terms "endowment" and "activation index". The former was introduced by the USGS in 2000 and refers to the summation of hydrocarbon cumulative production, reserves and undiscovered resources (Aguilera 2013). The latter is a measure of the total investment required to establish access to new oil or gas expressed in dollars per unit volume per day (for example, $/barrel/day or $/Mcf/d) of stabilized production (Economides and Oligney 2000). Figure 1.1 depicts a resource pyramid for oil and gas resources, as postulated by Aguilera (2013), indicating the endowment and activation index. At the top of the resource triangle are the conventional

reservoirs with medium to high quality, i.e. higher permeabilities and/or higher API and lower viscosities. They are relatively small in size (hence their small endowment), easy to develop in terms of cost and required technology (smaller activation index), but more difficult to find. Deeper into the resource triangle, one encounters unconventional reservoirs that have large volumes of oil or gas endowment but are more difficult to develop. The downward increasing activation indices implicitly mean that increased oil and natural gas prices and/or improved technology are required for commercial development of unconventional reservoirs.

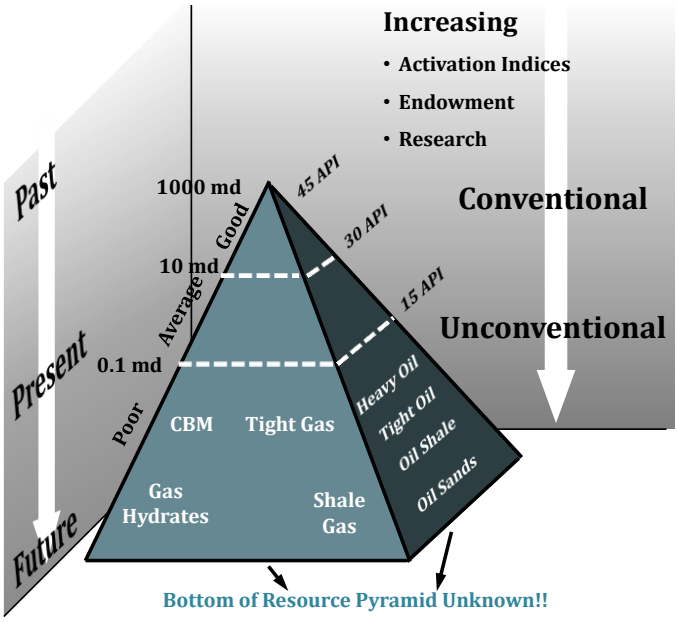

Figure 1.1: World oil and gas resource pyramid (adapted from Aguilera 2013).

As shown in the resource pyramid for oil and gas, going further to the bottom of the pyramid indicates larger resources. Unconventional oil resources accounts for more than 9.24 TBOE, 76% of the total oil endowment. Moreover, estimates demonstrate the contribution of unconventional gas reservoirs to be about 70,000 TCF, which is more than 75% of the total natural gas endowment (Aguilera 2013). The bottom of the resource

pyramid is unknown, and this opens significant possibilities for the future of unconventional petroleum resources throughout the world.

Among unconventional reservoirs, tight and shale oil and gas reservoirs have recently taken a great portion of the industry's attention because of their extent and the recently acquired technological ability to extract them. They are being pursued aggressively in both the US and Canada using horizontal wells and multi-stage hydraulic fracturing treatments. The advent of technology in these areas to extract oil and natural gas from once-impossible-to-get-at unconventional reservoirs has more than proved its value. Tight gas, for example, contributes approximately 56 percent (6.6 TCF) of the United States unconventional gas output. Shale gas production, on the other hand, amounted to 3.3 TCF in 2009, which was equivalent to 16 percent of the total US gas production (22.5 TCF), reported in April 2011 by the U.S. Energy Information Administration (EIA). The percentage increased to 23 percent of the total 24.1 TCF in 2010. Not only that, but the EIA projects a continual growth for shale gas share of the US natural gas production, anticipating almost 50 percent of the total produced gas volume by 2035. In Canada, the 2010 report by Canadian Society for Unconventional Gas (CSUG) estimated shale gas resources to be greater than 1100 TCF, mostly residing within the Western Canada Sedimentary Basin (WCSB).

All the above estimates point to the importance of unconventional resources in North America, and by extension the rest of the world, as viable alternatives for the rising energy demand. This in turn implies an ever-increasing need for reasonable production forecasting of unconventional oil and gas wells, and development of sound reserve estimation methodologies. In the following section, different methods available for forecasting

production and estimating reserves are described. This is followed by stating the research objectives and the scope of the present study.

1.1 Problem Statement

Evaluation of reservoir characteristics and prediction of future production performance have always been among the primary, as well as the most challenging, tasks for reservoir engineers. To choose a predictive method, the engineer has to take into account the availability of time and resources, reliability and uncertainty of the basic available data, and use sound engineering judgement for reasonable prediction and interpretation. Different methods are available for production prediction, and they range in complexity from those that provide an estimate of only ultimate recovery based on a simple empirical method to those that comprehensively simulate a reservoir to predict both reservoir and individual well performances.

Time and data requirements, which are directly proportional to the complexity of the method, and also cost constraints, are the main factors in selection of the evaluation technique. In some instances, a simple estimate of expected ultimate recovery (EUR) and rate decline forecasting may be required. However, there are other instances where detailed mathematical models and sometimes comprehensive reservoir simulation are more attractive because they can be used to appreciate the processes involved, in addition to enabling estimation of future production rate and recoveries as functions of time. The process of selection of the appropriate method for reservoir description and modelling is, therefore, a function of the analysis objectives and also availability of time, data and resources to perform the tasks. Figure 1.2 presents a pictorial comparison of the different

methods available for reservoir characterization and production forecasting. While offering the great advantage of being comprehensive and therefore enabling evaluation of complex reservoir behaviour, simulation requires availability of a lot of data. As a result, its data acquisition and also data preparation will be a time-consuming process. Comparably, the analytical methods that require less input data are faster to analyze and easier to understand while having the drawback of being less comprehensive. This is the result of assumptions required for solving the momentum (and sometimes energy) balance equations written over a differential element in the domain of interest.

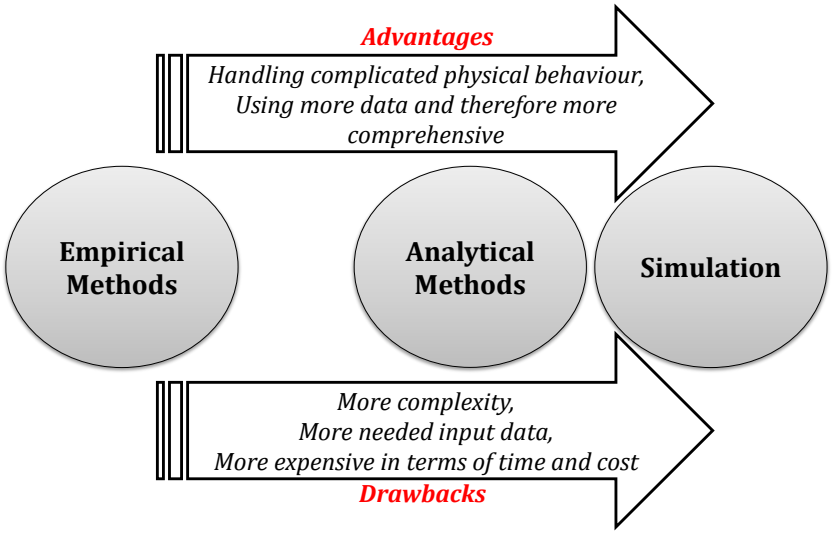

Figure 1.2: Comparison of the methods used for reservoir characterization and production forecasting.

In addition to the above methods and as shown in Figure 1.2, there are empirical methods that can be used for production prediction. They are simple and also require minimal data; therefore, they are convenient to use. They have received considerable attention in the industry. Among them, Arps (1945) is the single most commonly used method for describing the production rate behaviour. Since its introduction in 1945, this method has

become a commonly utilized tool for rapid evaluation of large quantities of production data. Its advantages over other techniques, including ease of use and minimal data requirement, and also its relative success in a wide range of formations with significantly different permeabilities has resulted in its almost universal applicability. The use of this method has become so entrenched as a common industry application that its inherent assumptions are often ignored or even forgotten.

Arps decline equations are purely empirical and subject to certain assumptions, most notably: the well produces at constant bottom-hole pressure (BHP), future production has to follow the past trend, and last but not least the analyzed production data belongs to the boundary dominated flow (BDF) period. In situations where any of the above assumptions are violated, using the Arps equations may lead to very pessimistic, optimistic and/or physically unreasonable reserve estimates. These situations can occur in tight and shale reservoirs.

In tight and shale reservoirs, geological complexities (the presence/absence of naturally occurring fractures and production contribution from different lithological layers), along with completion and fracture geometry complexities make their performance prediction a daunting task. In such reservoirs, commingling different layers is a common practice to establish an economical rate. Therefore, the amount of contribution by each layer to the total well's production, the starting time for sensible contribution of each layer, the types of flow regimes developed in each layer, and the collective combination of the layers can significantly change the Arps parameters, obtained based on a single layer assumption. In addition, the low to ultra-low permeability of these formations causes the transient flow period to last for years, if not tens of years, and therefore b-values in Arp's equation can be

greater than unity (Fetkovich et al. 1996, Lee and Sidle 2010). Many researchers (Cheng et al. 2008, Lee and Sidle 2010, Shahamat and Aguilera 2010) have pointed out that these higher-than-unity values of the exponent b can lead to very optimistic and physically unreasonable reserve estimates.

In addition to the above considerations, low deliverability of wells in low permeability reservoirs also forces the operators to use hydraulic fracturing treatments. This further complicates the flow behaviour of tight/shale reservoirs. In the case of shale reservoirs, hydraulic fractures essentially shatter the reservoir and therefore produce a huge contact surface area. Such reservoir shattering, which causes the creation of the so-called Stimulated Reservoir Volume (SRV), is in contrast to the conventional thinking about the hydraulic fracturing, bi-wing fractures (Mayerhofer et al. 2010). This tremendous surface area gives rise to the existence of an extensive linear flow period (Anderson et al. 2010), and fracture dominated flow (Duong 2011). These can be translated into the need for accommodation of transient flow in the traditional decline analysis in a manner consistent with reservoir engineering concepts.

1.2 Research Objectives

Reasonable evaluation of reservoir performance in a short period of time is a key concern in decision making. As depicted in Figure 1.2, more time and resources (data and expenses) are required as we move from simple empirical methods to comprehensive reservoir simulation. Because of their simplicity and minimal data requirements, empirical methods are appealing. Unfortunately, they suffer from some disadvantages, such as not

having a physical basis, and not being able to accommodate reservoir complexities (compared with the analytical and simulation methods).

In the same way that material (or energy) balance is written over the differential elemental volume in analytical methods, the material balance equation can be written over the entire reservoir domain to yield the capacitance-resistance method (CRM). This then implies that classical reservoir engineering concepts (i.e. material balance and fluid-flow equation) can be used to develop a simple, fast and inexpensive production forecasting method. In Figure 1.2, the utility and complexity of the CRM sits between empirical and analytical methods. The CRM, which is the focus of this research, is similar to the analytical method in that it has a physical basis. As a result, the parameters obtained using this method have physical meaning and therefore can be used to characterize a reservoir. In addition, some reservoir complexities can be accommodated in this methodology. The CRM is similar to empirical methods in the sense that it requires a minimum amount of data to perform the analysis (less than the data required by existent analytical methods and comparable with empirical methods). Because the CRM is the result of a material balance over the section of the reservoir affected by production, it represents the bulk characteristics of the reservoir.

The objective of this research is the development of an easy to use methodology for simple yet reasonable performance forecast of tight and shale oil and gas reservoirs. The following steps have been taken to achieve this objective:

(i) Capacitance Resistance model for simple reservoir geometries

   a. Develop BDF and transient flow models for production from tight and shale reservoirs.

b. Use the CRM to account for areal heterogeneities including composite and compartmentalized reservoirs.
c. Use the CRM to account for vertical heterogeneities (i.e. layering effects).
d. Study the effects of formation properties on the behaviour of the system.

(ii) Beta derivative[1] for making production forecasting of reservoirs with transient and BDF:

a. Study the effect of skin on beta derivative for radial and linear flow regimes.
b. Study the effect of reservoir properties on the beta derivative signature.
c. Develop of a methodology for production rate forecasting of tight and shale reservoirs, based on the beta derivative signature.

1.3 Scope of this Study

This study focuses on developing easy to use models that provide reasonable long-term forecasting production from tight and shale oil and gas reservoirs. The research is developed through eight chapters described next.

Chapter 1 (this chapter) provides an introduction of the thesis highlighting the vast hydrocarbon resources present in tight and shale reservoirs; and the objectives of the research.

[1] Elucidated in Chapter 6, beta derivative is defined as: $\beta = -\frac{dq/dt}{q/t}$.

Chapter 2 presents a brief review of properties of tight and shale reservoirs, and historic synopsis of approaches available in the literature for performing production data analysis. Existing empirical methods are discussed critically.

Chapters 3, 4 and 5 are devoted to the development of original capacitance-resistance methods introduced in this thesis for analysis of production data.

In Chapter 3, the analogy between electrical and petroleum engineering is discussed; capacitance and resistance terms are introduced and used through the concept of continuous succession of pseudo-steady states to describe the transient and boundary dominated flow behaviour of a homogeneous rectangular reservoir with a hydraulic fracture traversing it. This chapter uses a single tank for characterizing the homogeneous reservoir.

Chapter 4 discusses the use of two tanks (support and production tanks), and therefore two capacitances and resistances, for the analysis of compartmentalized and composite reservoirs. Simple analytical models are developed to describe the flow of fluids from one tank into the other and then to the wellbore. The models in Chapter 4 are developed for production scenarios of constant rate and constant wellbore pressure.

In Chapter 5, CRMs are used to explain the behaviour of multilayered and naturally fractured reservoirs producing at constant terminal rate. This chapter shows that the developed equations for compartmentalized/composite reservoirs can be used for performing production analysis of naturally fractured reservoirs.

Chapter 6 deals with rate decline analysis of simple reservoir geometries producing under constant terminal pressure. The main purpose of this chapter is to present a new and simple methodology similar to Arps method for rate forecasting and also reservoir

characterization. To achieve this goal, a series of simulation cases are created, and their production data are used to show the power of the beta derivative as a diagnostic parameter which can be used for rate decline analysis. Based on the results, two simple rate decline equations are derived for both transient and BDF, which enable generation of reliable type curves for analysis of production data. The proposed analysis approach is then validated by comparing its results against those of commercial numerical simulators. It has to be mentioned that all the development presented in Chapters 3, 4, 5 and 6 are original and solely developed as part of this work.

Chapter 7 presents field examples demonstrating the application of the models and resulting type curves for production analysis and rate forecasting.

Last, chapter 8 presents a brief summary of this work, the main conclusions drawn and recommendations for future work.

1.4 Technical publications

Portions of this research have been presented or will be presented in the near future at the following international conferences:

M.S. Shahamat, L. Mattar, R. Aguilera. 2014. Analysis of Decline Curves Based on Beta Derivative. Paper SPE 169570 prepared for presentation at the 2014 SPE Western North America and Rocky Mountain Joint Regional Meeting held in Denver, CO, USA, 16–18 April.

M.S. Shahamat, L. Mattar, R. Aguilera. 2014. A Physics-Based Method for Production Data Analysis of Tight and Shale Petroleum Reservoirs Using Succession of Pseudo-

Steady States. Paper SPE 167686 presented at the SPE/EAGE European Unconventional Conference and Exhibition held Vienna, Austria, 25–27 February.

M.S. Shahamat, R. Aguilera. 2010. A New Method for production Decline Analysis of Tight Gas Formations. Paper SPE 138149 presented at the CSUG/SPE Unconventional Resources and International Petroleum Conference held in Calgary, AB, Canada, 19–21 October.

Chapter Two: Literature Review

2.1 Scope of the Study

As mentioned in the previous chapter, unconventional reservoirs have greatly contributed to oil and gas production in North America. Reasonable performance analysis of these reservoirs requires understanding of the fundamental parameters and various processes which are involved in their production. This section provides a brief review of the major characteristics of tight and shale oil and gas reservoirs, and the common drilling and completion practices that have considerably affected their production behaviour. In addition, a historic review of the approaches used for their performance analysis is presented.

2.2 Unconventional Reservoir Characteristics

2.2.1 Tight gas reservoirs

The US Gas Policy Act of 1978 required in-situ gas permeability to be equal to or less than 0.1 md (100 microDarcies) for the reservoir to qualify as a tight gas formation (Aguilera and Harding 2008, Spencer 1989). While conventional core analyses of these types of rocks generally yield permeabilities on the order of tens of microDarcies, detailed special core analyses shows that the in-situ permeabilities for gas flow are much lower (Morrow et al. 1990). This is due to the combined effects of confining stress and water saturation which can cause approximately a two-order-of-magnitude reduction in gas permeability from the conventionally measured value, resulting in effective gas-flow permeabilities of 0.1–1.0 microDarcies in most of these reservoirs (Warpinski et al. 2009). As a result, tight

gas reservoirs can be considered as those having permeabilities less than 0.001 md (Blasingame 2008). Holditch (2006) provides a better definition of tight gas reservoirs as "reservoirs that cannot be produced at economic flow rates nor recover economic volumes of natural gas unless the well is stimulated by a large hydraulic fracture treatment, by a horizontal wellbore, or by use of multilateral wellbores."

There are two schools of thought that gained popularity about the geological setting of tight gas reservoirs. While the first characterizes tight gas formations as basin-centered (or continuous) gas accumulations which have large spatial dimensions and exist more or less independently of the water column (Law 2002, Schmoker 2002), the second considers them as gas reservoirs that occur in low permeability poor quality reservoir rocks in conventional structural and stratigraphic traps (Shanley et al. 2004). The controversy over acceptance of either one of these theories is significant because it substantially affects the estimates of gas in place volumes (extensively large values using the former to values in the range of conventional traps as a result of using the latter).

Production from tight gas reservoirs greatly depends on locating higher quality reservoir sections known as "sweet spots". Sweet spots are formed where various processes have enhanced the reservoir quality of gas saturated tight sandstones. They can occur in pervasive tight gas reservoirs and include either or all of the following criteria: (a) higher pressure, (b) greater reservoir thickness, (c) better reservoir quality (i.e. better permeability and porosity), (d) presence (or greater abundance) of natural fractures and (e) conventional traps within pervasive gas accumulations. An example of a sweet spot is the "Deep Basin" reservoir initially targeted in the Elmworth–Wapiti field in the western part of the WCSB foreland basin (Zaitlin and Moslow 2006). It is the aggradationally-stacked conglomeratic

shoreface deposits characterized by a higher reservoir quality with porosities in excess of 12% and permeabilities ranging from 1-1000+ md within thick successions of lower reservoir quality tight sandstones, siltstones, organic shales and coals (Figure 2.1). These original targets were considered to be classical "sweet spots" of higher permeability that are adjacent to the thermally mature gas bearing source rock with much lower permeability. Zaitlin and Moslow (2006) also present a schematic of the dual transmissivity nature of this reservoir, Figure 2.2, showing that the lower permeability rocks can be above, below, or lateral with respect to the reservoir connected to the wellbore.

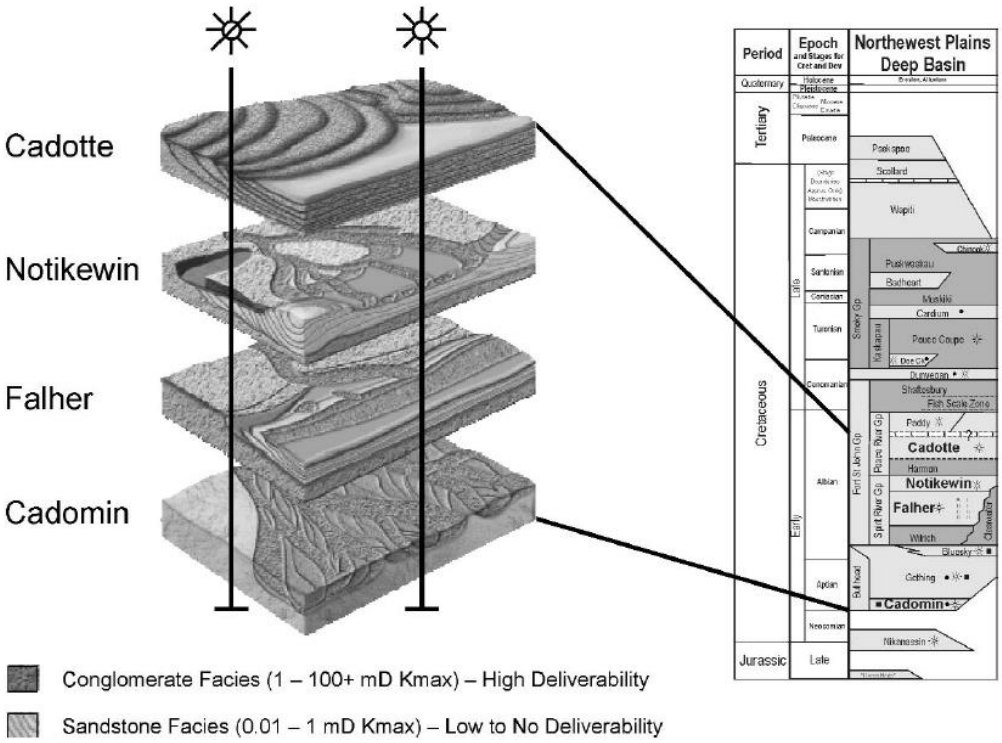

Figure 2.1: Example of the "Sweet Spot" in Western Canada Sedimentary Basin multi-zone deep basin (Zaitlin and Moslow 2006).

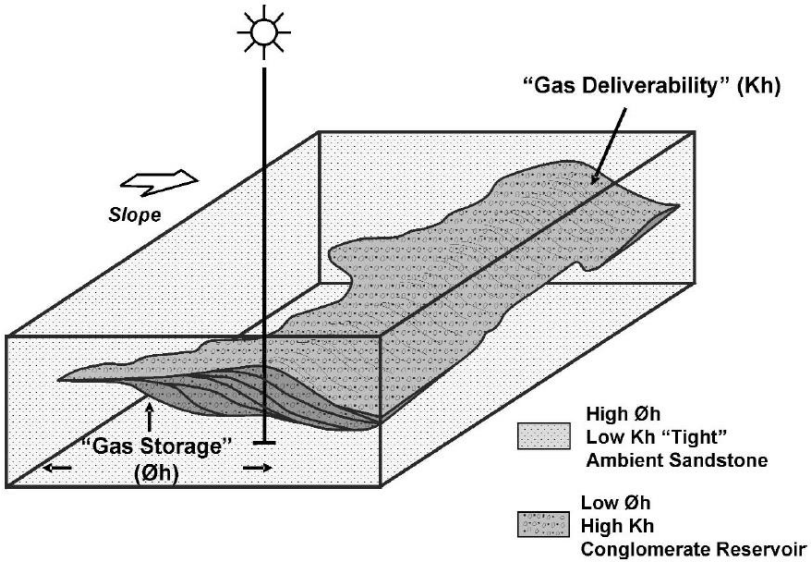

Figure 2.2: Schematic diagram depicting dual transmissivity nature of Deep Basin clastic reservoirs. Higher permeability conglomerate (sweet spot) encased in lower permeability tight sandstone reservoir (Zaitlin and Moslow 2006).

Similar to the conventional reservoirs, in tight formations natural gas is generated somewhere else (usually in shale) and migrates to the tight reservoir where it is trapped and stored in interparticle (matrix porosity), dissolution, slot, and micro-fracture porosity. Warpinski et al. (2009) discuss that natural fractures appear to be an important factor for economic gas production from tight reservoirs.

2.2.2 Shale gas reservoirs

Shale is by far the most abundant sedimentary rock comprising roughly two thirds of the sedimentary rocks in the Earth's crust (Spencer et al. 2010a) with a long history of gas production since the early 1900s from the Devonian shales of eastern North America (Warpinski et al. 2009). In spite of its abundance and production record, far less attention has been given to detailed study of shale than other rock types such as sandstone and limestone. In fact, extensive research and development of shale reservoirs is quite recent,

mainly due to the technological ability for massive multistage fracturing of horizontal wells. Because of the infancy of shale development, there is a large amount of uncertainty associated with the measurement of key properties, including porosity and permeability, from reservoir samples. This is a further complication to the problem of various definitions and usage of the term "shale" in different contexts.

According to ERCB Section 1.020(2) 27.1 of the Oil and Gas Conservation Regulations (OGCR), shale is defined as "a lithostratigraphic unit having less than 50% by weight organic matter, with less than 10% of the sedimentary clasts having a grain size greater than 62.5 micrometers and more than 10% of the sedimentary clasts having a grain size less than 4 micrometers. According to another definition, shales are fissile rocks composed of layers of fine grained sediments which are rich in clay and organic carbon (Martini et al. 1998). There are a number of other shale definitions available in the literature with difference of focusing more on some specific aspects of shales than others (Boggs 2001, Tucker 2001, Potter 2003). The common feature among all these definitions is that the grains and pores in shales are very small; smaller than tight and conventional formations (Ruppel and Loucks 2008, Wang and Reed 2009).

Unfortunately, there is not a clear protocol for determining shale properties like porosity, permeability and fluid saturation in the laboratory (Sondergeld et al. 2010, Spencer et al. 2010b). This is because there are different phenomena that play a role in production from shale reservoirs which sometimes can cause complications in their analysis. Aguilera (2010) discusses that shales exhibit all components of a petroleum accumulation and therefore they are unique; they are source rocks and reservoir rocks, in addition to being seals. He describes that gas is trapped and stored in shale in different ways (1) as adsorbed

gas into the kerogen material, (2) free gas trapped in nonorganic interparticle (matrix) porosity, (3) free gas trapped in microfracture porosity, (4) free gas stored in hydraulic fractures created during the stimulation of the shale reservoir, and (5) free gas trapped in a pore network developed within the organic matter or kerogen. As a result of their complexity, typically a hybrid of methods originally developed for coalbed methane or conventional reservoirs are applied for determining shale properties (Bustin et al. 2008). Table 2.1 below outlines the various sources for obtaining some of the shale reservoir properties. Explanation of some of these properties is given afterwards.

Table 2.1: Common sources for key reservoir and rock properties for shale gas reservoirs (modified from Sondergeld et al. (2010) and Clarkson et al. (2011b)).

Reservoir Property	Data Source
Porosity	Helium gas expansion, high-pressure mercury injection (MICP), nuclear magnetic resonance (NMR), log analysis (calibrated to core)
Permeability	Core Analysis: Steady-state and unsteady state (pressure- and pulse-decay), micro and nano CT scanning Well-test Analysis: (pre- and post-fracture) Injection / falloff (IFOT), diagnostic fracture injection test (DFIT), post-fracture flow and buildup Production Analysis: Rate-transient analysis, simulation history-matching
Water saturation	Core extraction (Dean Stark, Retort), capillary pressure, log analysis (using lab-based electrical property measurements)
Free and sorbed gas	Desorption canister testing and adsorption isotherms, calibrated log analysis
Total organic carbon	Leco TOC and RockEval (calculated), Log analysis
Thermal maturity	Vitrinite reflectance (Ro), RockEval (calculated)
Rock composition	X-Ray Diffraction, Fourier-Transform Infrared visual point count (for optically resolvable grains), electron microprobe

Shale's porosity and permeability are affected by many factors, including extent of microfractures, clay content and type, mineral and organic matter content, and type and thermal maturity of shale. Some of these factors are responsible for shale's unique behaviour. As an example, high stress-sensitivity of porosity and permeability in shales is

mainly attributed to the existence of microfractures. In general, matrix permeabilities of shales are extremely difficult to measure because they are so low, but various approaches to determine their value have yielded permeabilities on the order of 1–100 nanoDarcies. In order to determine water saturation, special lab procedures to determine capillary pressure are required to calibrate water saturation. Some shale gas reservoirs have moderate to high water saturations; others can have very low values.

An important parameter which is very useful for characterizing shale reservoirs is the level of their thermal maturity. Thermal maturity indicates the degree to which a formation has been exposed to high heat needed to break down organic matter into hydrocarbons. The amount of incident lights reflected by certain types of minerals, vitrinite macerals, gives a value (Ro%) that is used as an indication of thermal maturity, Figure 2.3. The reason for using vitrinite macerals as the candidate for determining thermal maturation is that it is the outcome of thermal alteration of lignin and cellulose in plant cell walls and is therefore abundant in coal and kerogen. While the sedimentary rocks that are rich in organic matter (such as shales) have considerable vitrinite content, carbonates, evaporites, and well-sorted sandstones have very low vitrinite content. Generally, the onset of oil generation is correlated with a reflectance of 0.5 to 0.6% and the termination of oil generation with reflectance of 0.85 to 1.1%. The wet gas and condensate prospective area has a Ro between 1.0% and 1.3%. Dry gas areas typically have a Ro greater than 1.3%. Figure 2.3 shows the value of the vitrinite reflectance as a function of hydrocarbon generation and their maturation stages.

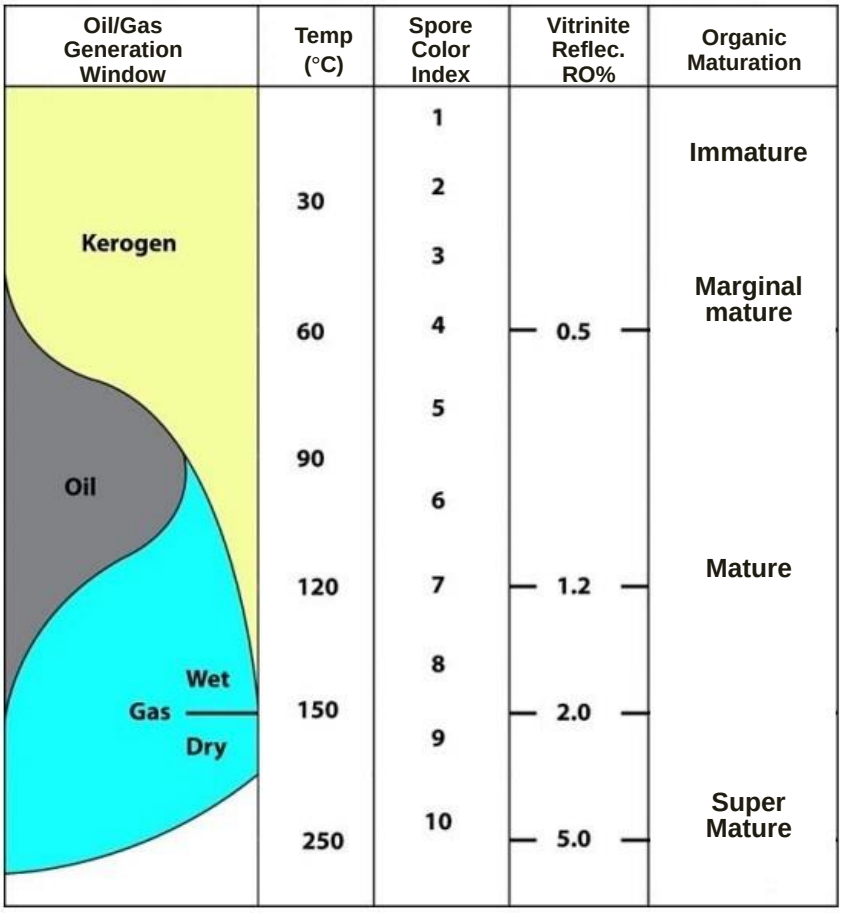

Figure 2.3: Hydrocarbon generation window and organic maturation with respect to the value of the vitrinite reflectance. Modified from Steyl and Van Tonder (2013).

Another important parameter for characterizing shales is the total organic carbon (TOC). This parameter is an indicator of potential hydrocarbon source rocks. There is usually a strong correlation between TOC and adsorbed gas in shale gas reservoirs. TOC correlations with gas content are sometimes used to predict specific gas content (G_c). Various methods for quantifying organic content from well logs have been published. Visual analysis for organic content is based on the porosity-resistivity overlay technique, widely used to locate possible hydrocarbon shows in conventional log analysis. By extending the method to radioactive zones instead of relatively clean zones, organic-rich shales (potential source

rocks, gas shales, oil shales) can be identified. Usually the sonic log is used as the porosity indicator but the neutron or density log would work, as well. Crossplots of porosity and resistivity (logarithmic) curves (Passey et al. 1990) can also be used to differentiate source rocks from non-source rocks. Low-resistivity shales are considered to be non-source rocks, while shales or silts with source-rock potential will show considerable crossover between the sonic and resistivity curves.

As mentioned previously, gas adsorption/desorption is an important characteristic of shale media and should be accounted for in a detailed shale analysis. According to Hill and Nelson (2000), between 20% and 85% of total storage in shales may be in the form of adsorbed gas. The subject of gas desorption has been studied extensively in coalbed methane reservoirs. Although the sorptive and transport properties of shale are not necessarily analogous to coal (Schettler and Parmely 1991), at least part of the knowledge is transferrable to shale reservoirs.

The adsorbed gas is a function of the content of the organic material and can be quantified by using either log analysis or calculations with sorption curves. There are many analytic and semi-analytic approaches that have been developed for modelling sorption curves in coalbed methane reservoirs, including the transient responses and multicomponent interactions (Clarkson and Bustin 2000). The one commonly used empirical model for single-component surface sorption is the Langmuir isotherm (King et al. 1986). Langmuir sorption isotherm is a relationship, at constant temperature, describing the volume of gas that can be sorbed to a surface as a function of pressure. It is expressed by the following equation:

$$\theta = \frac{pV_L}{p+p_L}$$ Eq. 2.1

The Langmuir sorption isotherms are typified by the total storage at infinite pressure (V_L) and the pressure at which half of this volume is stored (p_L). Figure 2.4 shows a typical Langmuir isotherm storage behaviour as a function of pressure. This model is based on the assumption of instantaneous equilibrium of the sorptive surface and the storage in the pore space. Gao et al. (1994) discuss that this is a good assumption in shale media, mainly due to the very low permeability and therefore slow flow through the kerogenic media in shales.

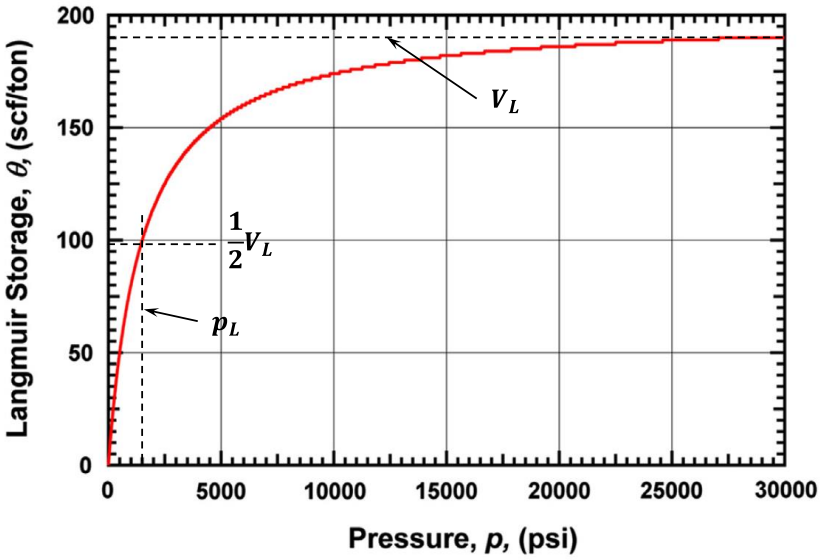

Figure 2.4: Typical Langmuir isotherm storage behaviour as a function of pressure.

The direct method of determining sorption isotherms involves drilling and cutting core that is immediately placed in canisters, followed by measurements of the volume of gas evolved from the shale over time (Crain 2011). The indirect method takes advantage of core or cuttings that have been stored and does not require fresh core, thus making this method more economical. Sorption isotherms are experimentally measured using a

powdered coal sample whose saturated methane content at a single temperature is measured at about six pressure points. The Langmuir equation is then used to predict the maximum gas storage capacity of a reservoir and the equilibrium pressure.

As mentioned before, shale is a rock with very fine-grained material, composed mostly of clay minerals and possibly other minerals, such as calcite or quartz. This is in spite of the fact that many rocks around the world are called shales, even though they contain small amounts of clays and kerogen (Crain 2011). This means that most of these so-called shales are really silts or silty shales or shaly silts with very low porosities and permeabilities. Sometimes, because of their radioactivity due to uranium (but little kerogen) they look a lot like shales on log analysis, i.e. their low resistivity, high radioactivity, large density-neutron separation, and high PE value (near 3) conspire to make the zone look like shale on logs. It would be extremely helpful, therefore, to examine the rock composition of a shale in order to reach a better completion, production and development planning. A ternary diagram of mineralogy of a shale is one way of presenting the results. Each corner of the triangle in such a diagram represents a group of minerals with more or less similar properties. Depending on the location of the points representing the rock composition, some conclusion can be drawn about the shale behaviour. Figure 2.5 shows the ternary diagram of Barnett mineralogy showing that the clay group content is smaller than the quartz group and therefore leading to the conclusion that the reservoir is brittle and thus favorable to a hydraulic fracturing job.

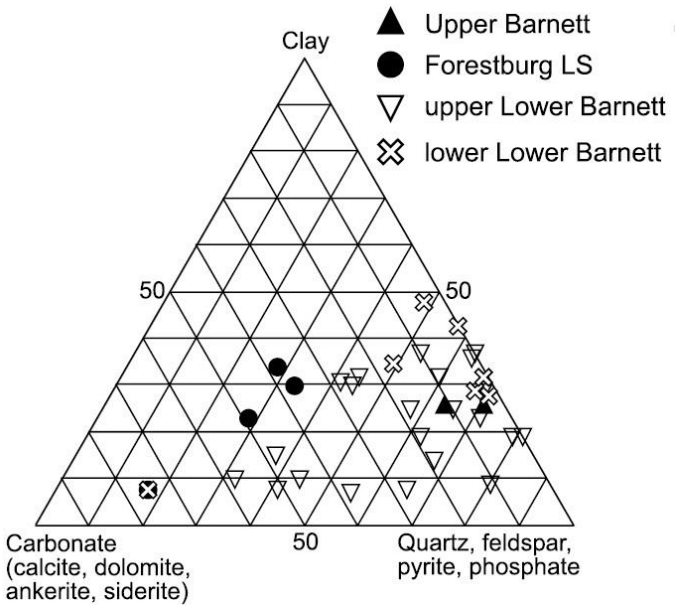

Figure 2.5: Ternary diagrams of Barnett mineralogy by member (Loucks and Ruppel 2007).

Shale gas reservoirs can be divided into two general categories: (a) the biogenic (like the Antrim shale) and (b) thermogenic (like the Barnett shale). In the case of the former, the organic matter has not been buried deep enough to generate hydrocarbons and instead the bacteria carried into the rock by water has generated biogenic gas that is sorbed to the organic matter. Therefore and as mentioned by Jenkins and Boyer II (2008) and Chan et al. (2011), biogenic shales can be considered as those shale formations that are at shallower depths (in the range of 500 – 4000 ft), thermally immature, and have high total organic content (TOC) often greater than 10 wt%. As a consequence of thermal immaturity, their smectitic clay contents have been only partially converted to illite which means they have higher smectite (or swelling clays) proportions. Biogenic shales are more susceptible to damage from reactions between aqueous fluids and swelling clays. Similar to other clay-rich rocks, they tend to be less consolidated and poorly cemented thus are not very brittle

and therefore they rely on existence of open natural fractures to provide conduits for water and gas production. After hydraulic fracturing of these types of shales, the induced and natural fractures have to be dewatered first before producing the sorbed gas. This means that the water production in these types of shales can be considerable.

Thermogenic shales, on the other hand, are generally found at depths greater than 3000 ft and have relatively smaller TOC compared with the biogenic shales (in the ranges of 2+%). This means that, most probably, the organic matter has been sufficiently cooked to generate gas which is held in the pore space and sorbed to the organic matter. The reason for their lower TOC is believed to be due to conversion of most of their organic content to hydrocarbon. Chan et al. (2011) mention that thermogenic shale gas plays contain significant amounts of Silica or Carbonate and "healed" natural fractures. Consequently they usually are brittle and therefore referred to as "fracturable" shales instead of "fractured" shales. As a result, initial gas rates for fractured horizontal wells in these types of shales are typically greater than those of the biogenic shales.

2.2.3 Tight/shale oil reservoirs

The terms "tight oil" and "shale oil" are used interchangeably in public discourse. "Tight oil formations" generally indicate all formations, including sandstone and carbonate as well as shales, that contain mostly oil and have low to ultralow permeabilities. This means that "shale oil reservoirs" are a subset of the more encompassing "tight oil reservoirs". As a result and due to its broader connotation, Energy Information Administration (2013) refers to tight oil production rather than shale oil production.

In addition, it should be mentioned that “shale oil” must not be confused with “oil shale”. Oil shale is a precursor of oil, sort of “a teenage oil” that constitutes the building blocks of conventional oil (Maugeri 2013). Therefore, the distinguishing characteristic of an oil shale is that it contains significant organic carbon, which has not yet transformed into oil. As such, it can be implied that oil shale rock exhibits low values of porosity and permeability and is closer to the surface. Oil shale is usually termed a source rock with a kerogen which is predominantly Type I, as opposed to coal and coal bed methane reservoirs which mostly contain type III kerogen. Some adsorbed and some free gas may also exist.

Similar to the shale gas reservoirs, shale oil reservoirs are rich with clay and are fissile, meaning they can split in layers, especially where there is massive clay content. These layers may stretch horizontally for hundreds and thousands of miles (Maugeri 2013). Shale oil formations are deeper than oil shales, with depths sometimes reaching 15,000 feet or even more.

2.3 Common Drilling and Completion Practices

Evident from their definition, successful development of unconventional reservoirs is a direct function of the advent of technology in setting the stage for their commercial production. In this section, we briefly discuss the main technologies that are mainly responsible for commercial development of tight and shale oil and gas reservoirs.

As mentioned in the previous sections, irrespective of the fluid type (oil or gas) and geology setting (tight sandstone, shale or combination) the permeabilities of tight/shale oil/gas reservoirs are low to ultra-low, in the orders of micro- to nano-darcies. Because of the extremely low permeability of these systems, the key for their economic production is

creating an enormous conductive surface area in contact with the wellbore, either through rejuvenation of the existing natural fractures or the development of a fracture "network" during stimulation.

The well-established method in the industry for increasing the contact area of a wellbore with the reservoir is the fracturing treatment. Examining different methods for performing such a task in tight and shale reservoirs has revealed that the optimum choice of fracturing fluid is slickwater. This is not to say that slickwater is a panacea, as it may not function well in situations that require higher conductivity hydraulic fractures (ex. for ductile shales) or even can cause serious issues when applied to water-sensitive shales (King 2010).

Slickwater is a water-based fluid with very few additives (therefore a very low viscosity) which is combined with proppant, such as sand, to provide a low-cost fluid type of choice for hydraulic fracturing. Benefiting from its low viscosity, the slickwater leaks off into the microfractures and flow laminations in tight and shale reservoirs and therefore enhances the contacted surface area with apparently minimum formation damage. Important operational considerations that affect the success of slickwater fracturing include pump-rates, fluid volumes and sand tonnages (King 2010). Upon designing an optimum job and as evidenced by microseismic monitoring, slickwater fracturing does create a complex network of fractures which leads to high contacted surface area (Fisher et al. 2005, Warpinski et al. 2009, Mayerhofer et al. 2010). Fisher et al. (2005) and Warpinski et al. (2009) illustrated the possible fracture geometries as a result of hydraulic fracturing of tight and shale reservoirs, Figure 2.6, and discussed that the simple bi-wing planar fracture is an

oversimplified description of the fracturing job and physical fracture verifications indicate a very complex fracture network around the wellbore.

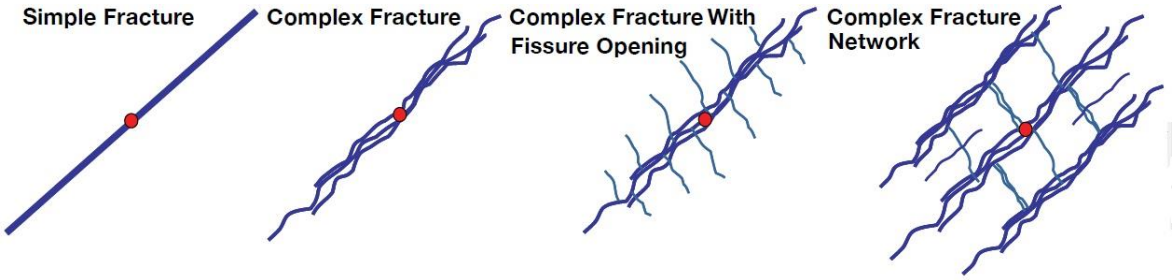

Figure 2.6: Comparison of possible fracture geometries created in tight and shales reservoirs (Warpinski et al. 2009).

In the quest of maximizing the contact area by a single wellbore, long horizontal wells oriented in a direction to promote transverse fracturing have emerged as a key technology. Multi-stage hydraulic fracturing of horizontal wells has been applied to both open-hole and cased-hole wells with various kinds of stage isolation. In the open-hole scenario, packers are typically used to isolate stages and shiftable valves are used to convey the hydraulic fracture treatment to the formation–balls of decreasing diameter per stage are used to open frac ports for each successive stage (Clarkson et al. 2011a). In the cased-hole scenario, effective isolation of stages requires a good cement job. Cased and cemented completion is more common because it allows for better control of number and location of fracture initiation (at perforation clusters). It is generally believed that more perforation clusters and stages in cased and cemented completions increase the probability of dense fracturing (King 2010). As a result of such massive stimulation, the fracture complexity creates an enhanced permeability region called stimulated reservoir volume (SRV). Mayerhofer et al. (2010) discussed the importance of horizontal lateral orientation relative to fracture

network azimuth and well placement and also fracture spacing on SRV coverage. Moreover, they illustrated that although maximized using the slickwater treatment, the SRV of individual wells are relatively small, therefore, multiple wells with closer well spacing (sometimes with overlapping SRVs) should be drilled and massively fractured to essentially shatter the entire volume between wells and thus improve recovery (Figure 2.7). Advocated by some operating companies, variations of this approach include fracturing of multiple parallel laterals simultaneously (simul-frac) or in short alternating sequences (zipper-frac). These applications benefit from stresses created through the fracturing of one stage for diverting the direction of fracture propagation from an offsetting stage and therefore contacting new rock.

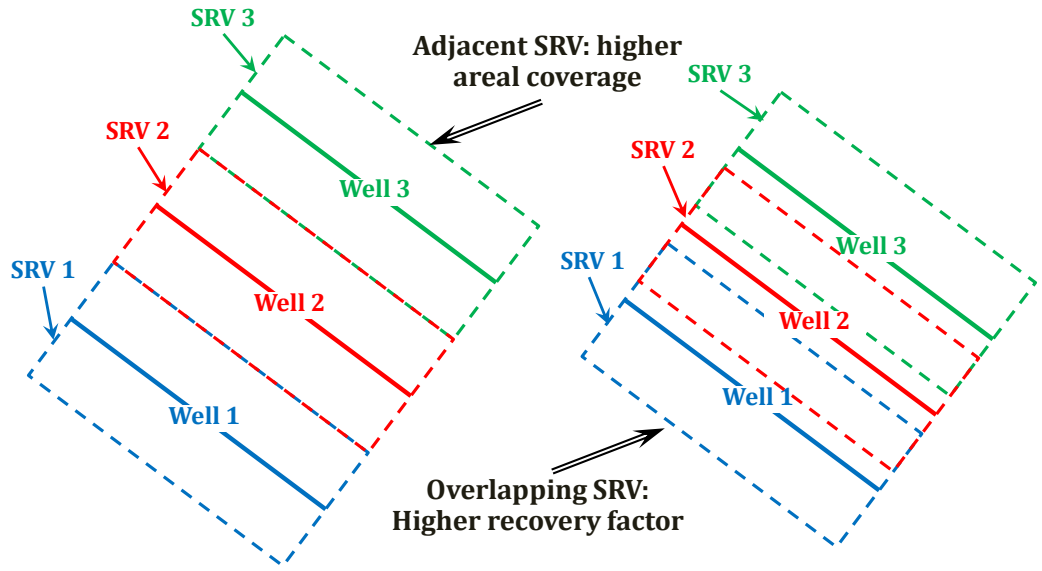

Figure 2.7: Importance of horizontal well placement strategy on SRV coverage, modified from Mayerhofer et al. (2010).

2.4 Common Production Data Analyses

A cursory look at the portion of the total endowment attributed to tight and shale oil and gas reservoirs indicate their crucial role for quenching the thirst for energy in the future. Explained in the previous section, their recent production evolution is definitely indebted to the advances in drilling and fracturing technology. To our chagrin, however, a common characteristic of production from these reservoirs is their inevitable rate decline. Shale oil and gas wells exhibit a peak in production rates during the first weeks of operation referred to as initial production. Afterwards, their production record generally displays a rate decline behaviour, i.e. about 40–60 percent and then further 30–40 percent lower rates by the end of the first and second years of production, respectively (Maugeri 2013). The immediate implication of the observed rate decline behaviour is an increasing need for predicting future performance of unconventional reservoirs through either using the methods available in the literature (which are proved to be relatively successful in conventional reservoirs) or developing new approaches to account for unconventional reservoirs complexities. As a result, a critical review of the available production data analysis approaches is in order.

2.4.1 Traditional decline curve analysis

Among the methods for production prediction that have gained popularity are the traditional decline curves. After the seminal work of Arps (1945), traditional decline curve or decline curve analysis was introduced as a graphical procedure that includes a curve fit of past production performance using certain standard curves and then extrapolating the trend to predict potential future performance. Arps decline equations were obtained based

on the decline curve loss-ratio proposed originally by Johnson and Bollens (1927). Defined as the fraction of production rate to loss in production with respect to time, Arps noticed that the loss-ratio formulation was a valuable tool for statistical analysis and extrapolation of various types of curves, i.e. exponential and hyperbolic declines. He discussed that whereas in the case of the former the loss-ratio (D) is a constant value, in the latter case its first derivative is constant. Based on this observation, he introduced the equations for exponential (Eq. 2.2) and hyperbolic declines (Eq. 2.3).

$$q = q_i exp(-D \times t) \qquad \text{Eq. 2.2}$$

$$q = \frac{q_i}{(1+bD_i t)^{\frac{1}{b}}} \qquad \text{Eq. 2.3}$$

Later and through extensive work, Fetkovich recognized that Arps decline curve equations are only applicable during BDF period (Fetkovich 1980, Fetkovich et al. 1987, Fetkovich et al. 1996). In addition, he proved the empirical exponential equation is, in actual fact, the theoretical solution for flow of a liquid with constant fluid properties during BDF period. Fetkovich (1980) combined the Arps decline equations with theoretical transient flow equations to provide the well-known Fetkovich typecurves for rate decline analysis. Moreover, he attempted to provide a physical basis for the hyperbolic decline equation for oil and gas reservoirs with different production drive mechanisms. As such, Fetkovich et al. (1996) showed that solution gas drive reservoirs typically exhibit b=0.3 and also gas wells show b=0.4–0.5.

Implicit in his analysis, Arps decline equations are purely empirical and subject to certain assumptions, most notably: the well produces at constant bottom-hole pressure (BHP), future production has to follow the past trend, and last but not least the analyzed

production data belongs to the boundary dominated flow (BDF) period. In situations where any of the above assumptions is violated, using the Arps equations may lead to very pessimistic, optimistic and/or physically unreasonable reserve estimates. These situations commonly occur in tight and shale reservoirs because (1) permeabilities are low and therefore their transient flow is extended (which delays the onset of boundary dominated flow), and (2) production is from multilayers and therefore contrasting layers cause complications. Moreover, Ye and Ayala (2013) showed analytically that even the BDF assumption is subjective. Gas wells exhibit a hyperbolic rate decline with a constant b-value only under the true wide-open condition, i.e. $p_{wf} = 0$. For gas wells producing at less than full potential, however, they showed that the decline behaviour does not display a hyperbolic decline with a constant b-value but rather a hybrid decline comprising of variable b-value hyperbolic decline during early boundary-dominated flow followed by an exponential decline at later times. The decreasing b-value decline was previously reported in numerical simulations of gas wells by Okuszko et al. (2008).

In attempts to make reasonable rate decline forecasting in tight and shale reservoirs, different approaches have been proposed by researchers. Each of the proposed methodologies has their own specific merits and drawbacks. In the following sections, an elaborate discussion of the methods introduced to predict future performance and estimate reserves in tight and shale reservoirs is presented.

2.4.1.1 Transient Flow Studies

This is the main concern in analysis of production data from low permeability reservoirs using decline curves. Violation of the Boundary Dominated Flow (BDF) assumption in

tight and shale reservoirs, implicit in the Arps method, has made researchers think about modification of the approach and/or revision of the formulation. Examples for modification of the approach are the works by Cheng et al. (2008) and Kupchenko et al. (2008), where they stick with the Arps formulation but modify the parameters at different times during production history of the well to encompass both transient and BDF periods. Because of the empirical nature of the Arps formulas, some other researchers have suggested using other empirical relations that have the ability to account for transient, or both transient and BDF periods. The works that are categorized under "revision of the formulation" include the Power Law Exponential Decline suggested by Ilk et al. (2008), Stretched Exponential Decline proposed by Valko (2009), Fracture Dominated Linear Flow Model proposed by Duong (2011) and Logistic Growth Model proposed by Clark et al. (2011). A brief review of each of these methods follows.

To start the discussion, Arps stated the b-value (or exponent in the hyperbolic equation) to be between zero and one, which is strictly true for data during BDF. Later, when transient data were analysed using Arps hyperbolic decline, b-values greater than unity were obtained (Fetkovich et al. 1990). Using this decline exponent for estimating reserves would result in either infinite values (which is meaningless from a theoretical point of view) or very large values (which is unrealistic from a practical point of view) (Cheng et al. 2008, Lee and Sidle 2010).

In order to circumvent the above problems in low permeability reservoirs with long transient flow periods and to be able to reasonably forecast their production rate, Cheng et al. (2008) proposed an alternative approach which includes determining a priori BDF b-value, and then determining q_i and D_i by extrapolating trends in calculated values from

best fits of the production data. In another approach, Kupchenko et al. (2008) used the Arps hyperbolic decline relation along with the idea of transient decline exponent introduced by Spivey et al. (2001). Calculation of transient b-values by taking the derivative of the inverse of decline ratio, which essentially implies the second derivative of the production rates, can be difficult considering the noise in the rate data.

Kupchenko et al.'s methodology was a two-step procedure; the first step was to fit a decline exponent (a best fit regression) to actual production history (e.g. a b-value equal to 2), and the second step was to determine the time after which a rate decline exponent of less than 0.5 occurs ($t_b = 0.5$). This time was calculated using the radius (or distance) of investigation concept. Production forecast using each of these approaches resulted in better and more conservative reserves estimates, compared to hyperbolic decline with b-values of higher than unity.

A different class of attempts has also been made to analyze rate data considering transient flow. With tight gas being the focal point in recent years, Power Law Exponential Decline (PLE) as shown in Eq. 2.4 was proposed by Ilk et al. (2008) to serve reservoir engineers in unconventional settings as do Arps hyperbolic equation in conventional reservoirs:

$$q = \hat{q}_i exp\left(-\hat{D}_i t^n - D_\infty t\right) \qquad \text{Eq. 2.4}$$

where $\hat{q}_i$ is the initial (time zero) rate, $\hat{D}_i$ is the initial decline rate (this is different from D_i in Arps equations) and D_∞ is the decline rate at infinite time. There are a number of studies focusing very specifically on application of the PLE for decline analysis (Kabir et al. 2011, Lee and Sidle 2010, Mattar and Moghadam 2009, McNeil et al. 2009). The common result of almost all of these studies is that there are different combinations of parameters that give

the same rate match, but can lead to completely different forecasts. This indicates the non-uniqueness of the result from the PLE decline, which is attributed to the larger number of parameters used in its formulation, as compared to Arps hyperbolic decline.

Stretched Exponential Production Decline (SEPD) model (Valko 2009) is another empirical method proposed for rate decline analysis of reservoirs with predominant transient flow. It is shown in the equation below:

$$q = q_i exp\left[-\left(\frac{t}{\tau}\right)^n\right] \qquad \text{Eq. 2.5}$$

where τ is a characteristic number of periods; and n is a dimensionless model parameter. The method has gained more attention than PLE and is believed to be more appealing for evaluation of unconventional reservoirs (Can and Kabir 2012, Kabir et al. 2011, Lee and Sidle 2010). SEPD involves a two-step process: first, data fitting is needed to generate the recovery potential or EUR and second, various ranges of production data may be fitted to describe the rate decline. Can and Kabir (2012) presented a probabilistic performance-forecasting method using the SEPD model and reached the conclusion that SEPD is superior to Arps hyperbolic relation with regard to estimating future performance in unconventional reservoirs. More recently, Yu et al. (2013) developed a modified form of the SEPD where they employed a specialized logarithmic plot of $\ln\left(\frac{q_0}{q}\right)$ versus time, with q_0 as the initial maximum production rate, to obtain a straight line for finding the related SEPD parameters. Compared with the SEPD, his approach is claimed to yield more reliable EUR for dry, wet and retrograde gas as well as tight oil wells.

In another effort, Anh Duong (2011) introduced a totally different empirically derived decline model that is based on long term linear flow in tight and shale reservoirs. His

method relies on a log-log plot of q/G_p vs. time, which for dominant linear flow gives a straight line whose slope and intercept are the parameters used to forecast the rate behaviour. Radial flow and boundary dominated flow cause upward and downward concavity to this straight line, respectively. This method focuses on analyzing linear flow data and has the ability to provide a statistical method to forecast the production of resource plays.

Another empirical method developed by Clark et al. (2011) is the Logistic Growth Model. Logistic growth is a family of mathematical models used to forecast growth in numerous applications, examples of which are modeling population growth, regeneration of organs and penetration of new products into the market. They attempted to use the logistic growth model along with a "carrying capacity" concept to predict production rate of unconventional reservoirs. In their formulation, the carrying capacity (which is in fact the total amount of oil or gas recoverable from primary depletion and can be obtained from volumetric calculations) is used to constrain the total predicted cumulative production values. They believe that this is an advantage of the method, and forces the model not to extrapolate to non-physical values.

There are references that discuss the application and comparison and also modification of the above methods for analysis of production information (Freeborn and Russell 2012, Lee and Sidle 2010, Mishra 2012, Yu 2013, Yu et al. 2013). In general, these methods give better results compared to the Arps equations under certain conditions, but they may lead to unreasonable forecasts if used without giving due consideration to the associated assumptions.

2.4.1.2 Multi-layers Studies

Fetkovich et al. (1990) provided the first paper dealing with the subject of depletion and long-term performance forecasting of non-communicating layered reservoirs. They used the backpressure curve concept along with the material balance equation to reach some conclusions about the applicability of Arps method in forecasting long-term performance of multi-layered reservoirs. They confirmed that commingled shut-in pressures basically track the pressure curve of the more permeable layer. They also noticed higher-than-expected Arps b-values for multi-layer reservoirs. In addition, they pointed out that the magnitude of the b-value may provide an indication of permeability and volume contrast between layers. Most important of all, they discussed that in case of existence of layered crossflow; layers could be combined into a single equivalent layer with average reservoir properties of the crossflowing layers. If there is no crossflow then layers can be combined into either a single layer, if each layer has the same diffusivity property, or two layers, otherwise.

El-Banbi and Wattenbarger (1996) developed a model to match constant p_{wf} production data from multi-layer no-crossflow systems during BDF. They coupled individual-layer material balance and BDF rate equations to obtain a rate forecasts and to estimate properties of each layer. They mentioned that a suitable range of permeability for reasonable application of this method was between 10 and 0.1 md. Reservoirs with permeabilities higher than 10 md and lower than 0.1 md are subject to errors because of non-Darcy flow effects and transient flow effects, respectively.

Suabdi (2001) presented new analysis and modeling techniques for no-crossflow multi-layered gas reservoir performance, producing at constant wellbore pressure. He coupled an

approximate form of the stabilized flow equation with the gas material balance equation to develop his semi-analytical solutions. In his work, he primarily demonstrated that the semi-analytical solution developed by Ansah et al. (2000), which was developed for a single layer system, can be used to analyze a multi-layered system as part of a performance-based reservoir characterization. He didn't discuss the behaviour of the multilayered no-crossflow system during the transient flow period.

Cheng et al. (2008) used Arps method for analysis of production rates from a multi-layer tight gas well with extended transient period. They determined a priori b-value for the multi-layered reservoir (which was greater than that of a single layer) and then determined q_i and D_i from a backward analysis scheme. Their results were superior to Arps decline curve with parameters obtained from matching the late time production data. Note that the b-value they used was an arbitrary value of between 0.5 and 1.0, as suggested by Fetkovich et al. (1990). In short, matching the rate-time data from multi-layer reservoirs results in high b-values that are strictly empirical and only based on fitting the hyperbolic decline equation to the production data.

It can be concluded from the discussion above that empirical methods can provide reasonable estimates of production rate, yet they may not add to the understanding of the reservoir and flow behaviour because of their empirical nature. They can work very well in some cases but can also lead to real fiascos, if wrong decisions are made based on their use. As noted by Lee and Sidle (2010), incomplete understanding of the basic physics of fluid flow and stimulation effectiveness in complex tight and shale reservoirs limits the ability to develop models in which there is high confidence. Despite this lack of complete

understanding, however, it is crucial to forecast future performance and to estimate and report reserves for the purpose of future development.

2.4.2 Modern production data analysis

All the methods discussed in the previous section are empirical relations, which are subjective by their own nature. They only require the production rate information to perform the analysis and as a result of this minimal data requirement have gained widespread attention in the industry. Pressure data, however, are important information which upon availability should be used in production data analysis. Reservoir signals embedded in the pressure information have the potential to significantly affect the analysis and, as a result can change the conclusions made based solely on analysis of rate data. Very specifically, incorporation of the pressure information is of great importance for high deliverability reservoirs (including unconventional plays) which are characterized by rate-controlled flow for extended periods of time.

Recently some methods have been proposed that use the pressure and rate data with the empirical methods to perform production analysis. As an example, Anderson et al. (2012) proposed a straightforward methodology for forecasting the production of high pressure unconventional wells under controlled drawdown. Their method was based on a linear relationship between pressure normalized rate and cumulative production when plotted on a semi-log scale. They used such a decline curve analysis of pressure normalized rates to forecast production and estimate ultimate recovery. More recently, Ilk and Blasingame (2013) proposed utilization of the convolution/superposition theory along with the recently developed empirical rate-time equations in pressure normalized form.

These above two references are essentially empirical methods that attempt to account for both pressure and rate data in their analysis. Hereafter, the modern production data analysis methods are briefly discussed. They are the methods that have a solid mathematical and physical basis for analyzing pressure and rate information.

2.4.2.1 Analytical Models

There are specific reservoir configurations with simplified production constraints that are of practical significance. Under certain assumptions, one can model their behaviour by writing the diffusivity equation for such systems, specifying initial and boundary conditions and using dimensionless variables to obtain their exact fluid flow solutions. These solutions are mostly obtained using Laplace transform, Fourier transform or Green's function which if required can be inverted into real time domain either directly or by using numerical inversion algorithms. Analytical models use these exact closed-form solutions for history matching of available pressure and rate data and then forecasting production. They are appealing because they are fast and enable engineers to study the effect of different parameters on the behaviour of the system of interest.

There are numerous models (for different well and reservoir configurations) available in the literature that have been solved analytically and the choice of one model over another can drastically change the outcome of a forecast. The answer to the question of which model to choose requires consideration of a number of factors including seismic data, geology, log data, and information provided from other wells drilled into the same formation. This section is essentially a brief synopsis of some of the analytical models (i.e. models with analytical solutions) commonly used for production data analysis.

Gringarten and Ramey (1973) used Green's function to present analytical solutions to a vertical well within a rectangular reservoir of no-flow outer boundaries with homogeneous properties. Later and again by means of the Green's function, Gringarten and Ramey (1974) presented an analytical expression for pressure distribution created by a hydraulically-fractured well in a homogeneous reservoir. The solution was developed for a uniform flux into the fracture, with a modification for the case of infinite conductivity fracture.

Clonts and Ramey (1986) presented an analytical solution for pressure response of a horizontal well in a finite anisotropic rectangular reservoir. Their solution was again based on Green's function. Thompson et al. (1991) addressed the issue of computational expense associated with solutions based on Green's function during very early times and offered a practical approach of switching between alternative solutions at different times, i.e. using cylindrical source solution during very early times and Green's function solutions during late times. Their approach is applicable to horizontal wells, fractured wells and any flow problem that involves Green's function solutions.

Wattenbarger et al. (1998) used the reservoir configuration shown in Figure 2.8 and provided analytical constant rate and constant wellbore pressure solutions from infinite conductivity fractured wells in such reservoirs. They also provided simple and practically useful early-time and late-time approximations for these solutions.

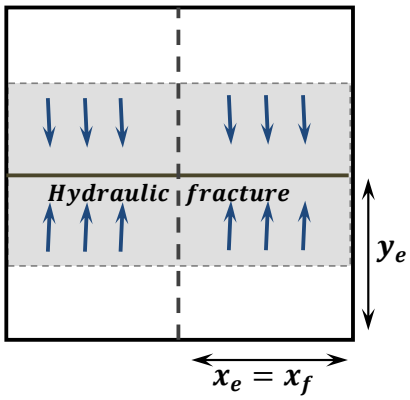

Figure 2.8: Reservoir geometry used by Wattenbarger et al. (1998); a hydraulically fractured well in a rectangular reservoir.

El-Banbi (1998) presented linear dual porosity models for the same reservoir configuration. His model was later extended by Bello and Wattenbarger (2010) to account for skin. They assumed that there is no drainage from the outer reservoir and did not account for desorption in their work. They identified five flow regions with their model and stated that field production data in most shale gas wells exhibit linear flow from the matrix into the fractures with an observed skin effect. They provided a new analytical equation and asymptotic solutions to model the effect of skin on linear flow behaviour.

Brown et al. (2011) suggested using a configuration shown in Figure 2.9 to model pressure-transient and production behavior of multi-fractured horizontal wells in low permeability shale reservoirs. As the figure demonstrates, their model considers a naturally fractured medium in the Stimulated Reservoir Volume (SRV) surrounded by an outer reservoir region of lower permeability. In this model, the outer-reservoir feeds the inner-reservoir via linear flow; the inner-reservoir feeds the fractures via linear flow, and the fluid within the fractures travels linearly towards the wellbore. The flow within the transverse vertical fracture towards the horizontal well has a radial flow pattern whose

effect in the trilinear model is taken into account by a convergence skin. The trilinear-flow solution is obtained in Laplace domain which is numerically inverted to time domain. Their model was validated by using the semi-analytical solution developed by Medeiros et al. (2008).

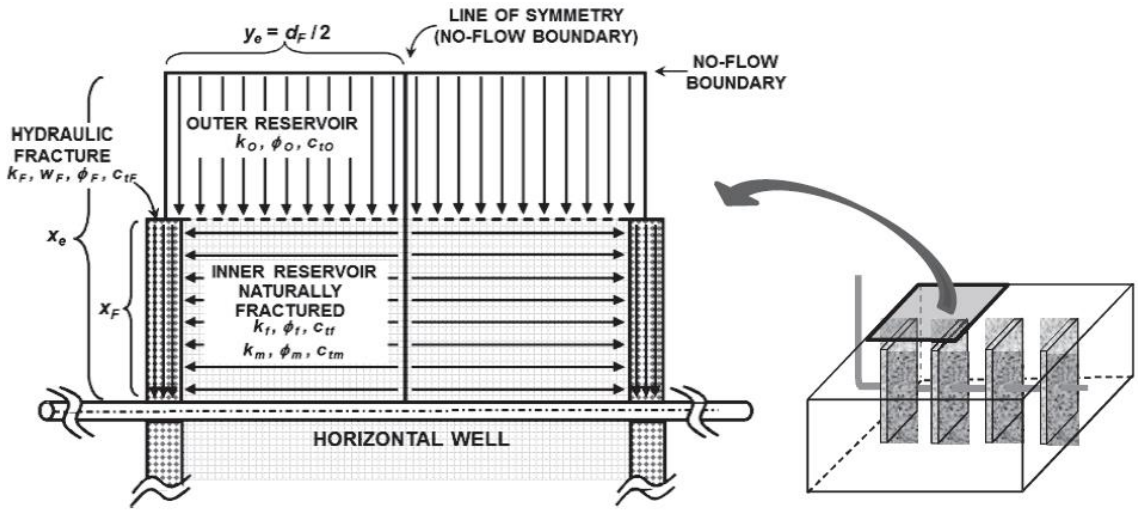

Figure 2.9: Schematic of the trilinear-flow model representing three contiguous flow regions for a multiple-fractured horizontal well (Brown et al. 2011).

Brohi et al. (2011) presented a linear composite model that uses dual porosity flow solution for the inner reservoir and a single porosity solution for the outer reservoir combined with continuity of pressure and flux at their interface. In essence, their solution in Laplace domain is for the same model as that of Brown et al. (2011) with the difference in coupling of the three regions. They used a numerical simulator to examine the validity of some of the assumptions made in the development of their work.

The model and solutions suggested by Brown et al. (2011) and Brohi et al. (2011) describe the pressure distribution for a system in which the SRV region of enhanced permeability occupies all the space between hydraulic fractures. They considered that the model consists

of three regions: fracture, high-permeability region, and low-permeability region. A more general form of their work was presented by Stalgorova and Mattar (2013). This model is called the horizontal multifrac enhanced fracture region model and is a rectangular reservoir that consists of a non-contributing horizontal well and transverse fractures (Figure 2.10). It is based on the hypothesis that the propagation of a hydraulic fracture may create a branching pattern (Daneshy 2003), which as a consequence results in a stimulated region around each hydraulic fracture. This, therefore, can be modeled by introducing a region of higher permeability around each fracture, all surrounded by a lower permeability region, see Figure 2.10.

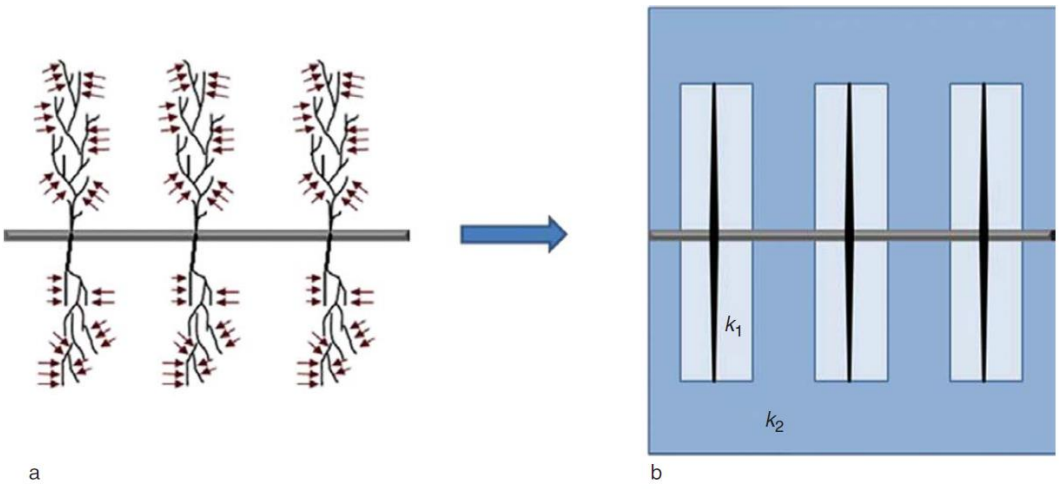

Figure 2.10: Schematic of (a) a horizontal well with multiple branch fractures and (b) its representation by a model ($k_1 > k_2$) (Stalgorova and Mattar 2013).

This model considers five different regions with linear flow. Figure 2.11 shows a cross-section of a quarter of a reservoir and uses arrows to depict each of these regions. As can be seen, there is linear from the non-stimulated region (region 2, 3 and 4) to the inner-reservoir region (region 1), from the inner-reservoir region to the hydraulic fracture and finally from hydraulic fracture towards wellbore.

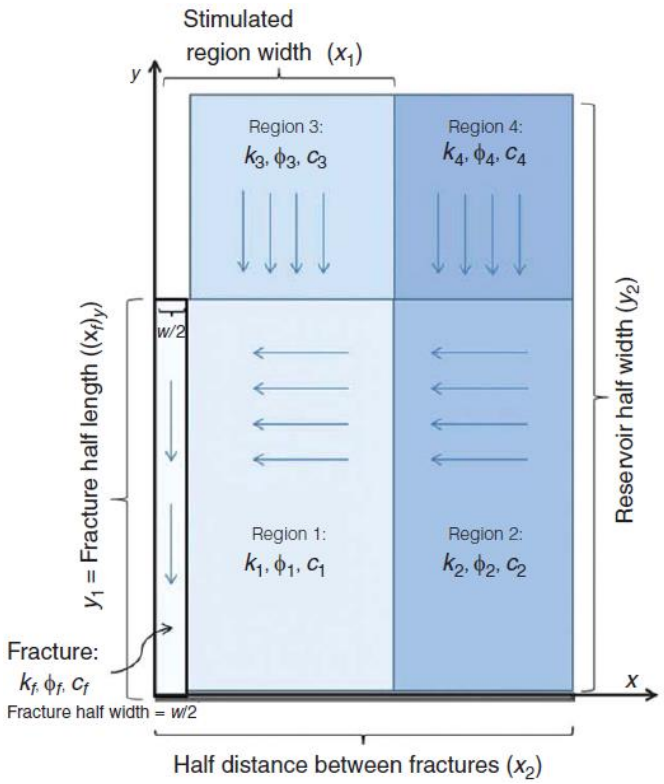

Figure 2.11: Schematic and dimensions of the five region model for one quarter of a fracture (Stalgorova and Mattar 2013).

They developed the solutions in Laplace domain, inverted into real time domain using Stehfest Algorithm (Stehfest 1970), and compared them against numerical simulation. They discussed that analytical and numerical models are in good agreement only when the geometry of the system falls within certain limitations.

Solutions to the analytical models mentioned above are derived with the assumption of constant viscosity (μ) and compressibility (c) to ensure a linear governing partial differential equation within the systems of interest. This assumption is reasonable for liquid flow problems. Gas, however, exhibits a compressibility that is not constant, but changes with pressure. Additionally, its viscosity and compressibility factor (Z-factor) also change with pressure. As a result, flow of a gas through a porous medium gives a nonlinear partial

differential equation for which there is no analytical solution available in the literature. A number of researchers attempted to remove the nonlinearity from the governing equation by defining pseudo-pressure and pseudo-time. Original definition of pseudo-pressure was given by Al-Hussainy and Ramey (1966). This definition was later subtly modified by Meunier et al. (1987), Eq. 2.6, to retain the unit of pressure and thus relieve one of having to deal with the abstract units of pseudo-pressure ($psia^2/cp$).

$$p_p = \frac{\mu_{gi} Z_i}{p_i} \int_{p_b}^{p} \frac{p}{\mu_g(p) Z(p)} dp \qquad \text{Eq. 2.6}$$

Evident in the above definition, the integrand is a function of pressure and the variable of integration is also pressure. Therefore one can rigorously calculate pseudo-pressure. Gas pseudo-time, however, is not amenable to a completely rigorous solution. Reminiscent of the definition of pseudo-pressure, pseudo-time (introduced by Agarwal (1979)) is a transformation that accounts for the changes in gas compressibility and viscosity. Similar to pseudo-pressure, a useful variation of pseudo-time is obtained by its normalization (Fraim and Wattenbarger 1987, Meunier et al. 1987):

$$t_a = \mu_{gi} c_{ti} \int_0^t \frac{1}{\mu_g(p) c_t(p)} dt \qquad \text{Eq. 2.7}$$

Pseudo-time is an approximate transformation because the integrand is a function of pressure while the variable of integration is time. While Agarwal (1979) defined pseudo-time in terms of viscosity and compressibility evaluated at the wellbore pressure, Fraim and Wattenbarger (1987) and also Palacio and Blasingame (1993) suggested calculating pseudo-time at the average reservoir pressure for long term production analysis. Later, Anderson and Mattar (2007) showed that the use of average reservoir pressure for pseudo-

time calculation was not valid during transient flow period and therefore proposed calculating pseudo-time at the average pressure within the region of influence. They utilized the well-established concept of radius of investigation to find the region of influence and therefore the volume to be used for the average pressure calculation. Recently, Tabatabaie et al. (2013) proposed using the liquid type curve to find the volume of investigation. For this purpose, they used an iterative procedure. Their method applies to a constant rate production. They mentioned that the extension of the method to variable flow rate scenarios using the principle of superposition is still problematic and requires further investigation.

Transforming pressure to pseudo-pressure and time to pseudo-time partially linearizes the governing differential equation and therefore allows for using the liquid solutions for gas flow problems.

2.4.2.2 Type curves

Solutions to analytical models expressed in dimensionless form can be used to obtain type curves which, through a type curve matching process, provide a direct reservoir characterization method. In the context of production data analysis, there are numerous type curves that have received widespread attention in the industry. Fetkovich (1980) is the pioneer in using type curves for production data analysis. He used liquid analytical solutions to constant flowing pressure production of a well at the center of a closed circular reservoir and combined them with the empirical Arps decline curve equations to present a set of type curves used for parameter estimation and production forecasting. The Fetkovich

type curve does not consider variations in bottomhole flowing pressure (p_{wf}) and also changes in PVT properties with reservoir pressure for gas wells.

Carter (1985) presented a modified version of the Fetkovich decline type curves for gas flow to take into account changes in pressure dependent gas properties during reservoir depletion. Blasingame and Lee (1986) introduced a superposition time function (material balance time) for analysis of variable well rate data for oil reservoirs. Later, Palacio and Blasingame (1993) introduced material balance pseudo-time to convert gas well variable pressure production data into constant rate liquid equivalents. They showed that when the typecurves are plotted using material balance time function, the analytical exponential stem of the Fetkovich type curve becomes a unit-slope straight line on log-log coordinates. Based on this observation and the smoothing nature of integral functions, Blasingame and his coworkers introduced new plotting functions (pressure-integral, rate-integral and rate-integral derivative) for construction of new sets of type curves. Analyzing variable rate and variable pressure production data, Palacio and Blasingame (1993) worked on analysis of gas wells, Doublet et al. (1994) focused on analysis of oil wells, Marhaendrajana and Blasingame (2001) developed the analysis methods for multiwell reservoir systems and Pratikno et al. (2003) dealt with hydraulically fractured wells. All these related type curves were based on solutions of models that assume a circular outer boundary.

Araya and Ozkan (2002) provided important perspectives on the use of production decline type curve analysis for vertical, fractured, and horizontal wells. Amini et al. (2007) presented the development of an elliptical boundary model and a series of decline type curves for a system consisting of a hydraulic fracture at the center of an elliptical reservoir. Wattenbarger et al. (1998), on the other hand, focused on extended linear flow in very tight

and shale reservoirs and, as a result chose the model to be a rectangular reservoir that is hydraulically fractured and with the fracture extended to the boundaries of the reservoir (according to Figure 2.8). Based on the solution, they presented new typecurves to analyze the production data of wells with linear flow.

2.4.2.3 Flowing Material Balance (FMB)

The material balance equation is the building block of all reservoir engineering calculations. Traditionally, static material balance requires the well to be shut-in at several points during its producing life to obtain the average reservoir pressure. Upon obtaining average reservoir pressures (p_{avg}), a material balance formulation is employed to calculate original hydrocarbons in place. For gas wells, for example, this means obtaining a straight line in the plot of $\left(\frac{p}{Z}\right)_{avg}$ versus cumulative gas production. Obtaining average pressure by shutting the well in is sometimes impractical, and the duration of the shut-in is often not long enough to obtain an accurate measurement. The flowing material balance is an alternative to the static material balance that uses the concept of boundary-dominated flow or pseudo-steady state flow, as well as flowing pressures and rates to calculate original hydrocarbons in place. Introduced by Mattar and McNeil (1998), it is generally accepted as the most accurate procedure for estimating original hydrocarbons in place because it uses actual reservoir performance data.

FMB uses the fact that during stabilized constant rate production from a well, the pressure at all locations within the reservoir declines at the same rate. This means that the pressure drop measured at the wellbore is the same as the pressure drop that would be observed

anywhere in the reservoir, including the location which represents average reservoir pressure. As a result, one can write the flow equation in a format that would lead to a straight line which can be extrapolated to evaluate the original hydrocarbons in place. In the case of a liquid reservoir, for example, a plot of normalized rate (i.e. $\frac{q}{(p_i - p_{wf})}$) vs normalized cumulative production ($\frac{N_p}{c_t(p_i - p_{wf})}$) results in a straight line whose x-intercept is used to calculate the original hydrocarbons in place, see Figure 2.12.

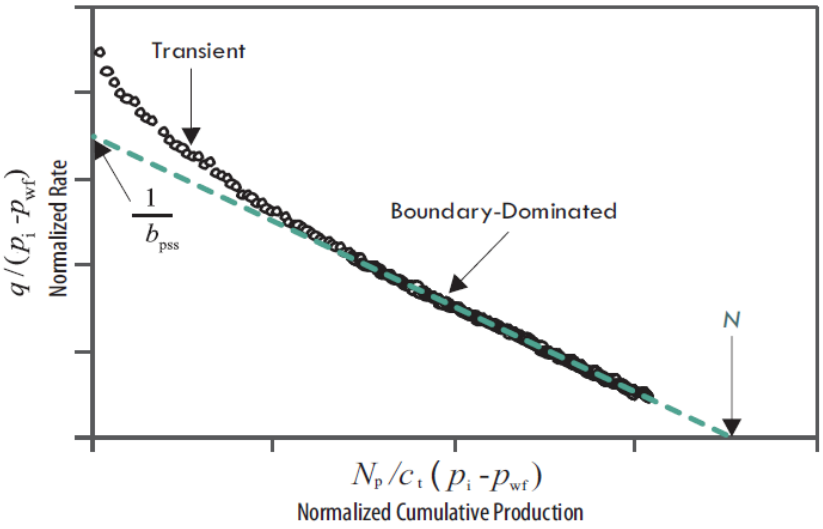

Figure 2.12: Oil flowing material balance (Fekete RTA poster).

For gas flow, however, one would require calculating pseudo-pressure and pseudo-time to be used to construct a plot of normalized pseudo-pressure $\left(\frac{p_{pi} - p_{pwf}}{q}\right)$ vs. material balance pseudo-time $\left(\frac{G_{pa}}{q}\right)$, Figure 2.13. Note that G_{pa} is the cumulative production calculated based on pseudo-time (i.e. $G_{pa} = \int_0^{t_a} q dt_a$). As mentioned before, pseudo-time accounts for the dependence of gas viscosity-compressibility product on reservoir pressure, which itself is a function of the size of the reservoir, which itself is the objective of the FMB procedure. This therefore indicates that the FMB in gas wells involves an iterative process.

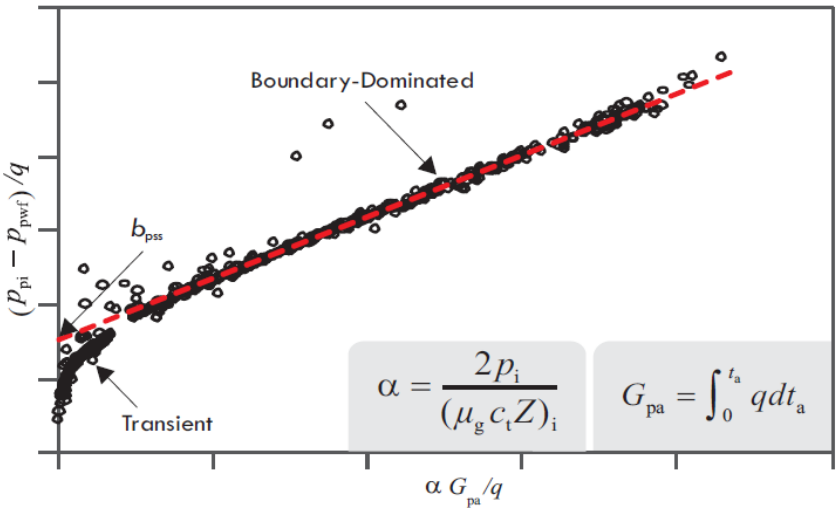

Figure 2.13: Plot of normalized pseudo-pressure vs. material balance pseudo-time used for flowing material balance of gas reservoirs (Fekete RTA poster).

The intercept of the straight line in the above plot (b_{pss}) is used to plot the p/Z versus G_p which upon extrapolating the late time straight line gives the original gas in place, see Figure 2.14.

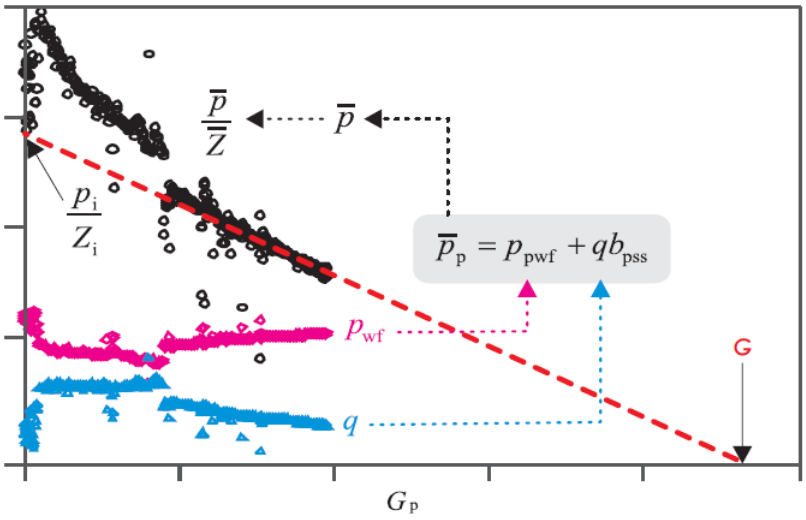

Figure 2.14: Gas flowing material balance (Fekete RTA poster).

The graphical simplicity of the flowing material balance analysis has made it quite popular. Although FMB was originally developed for a volumetric gas reservoir, it was extended to account for other complexities including the effects of the formation compressibility, residual fluids expansion, other sources of energy such as aquifer support and other sources of gas storage such as connected reservoirs, or adsorption in coal/shale. These have been done by modification of the gas compressibility factor from Z to Z** (Moghadam et al. 2011).

2.4.2.4 Specialized plots

Specialized plots are among the simplest methods available for analyzing production data. They are plots that seek a straight line for examining the reservoir behaviour during a specific flow regime. In the context of production data analysis of unconventional reservoirs (fractured tight and shale) linear flow is the dominant flow regime for long periods of time and therefore using its specialized plot is of particular importance. The square-root-of-time plot is its specialized plot and is probably the most important plot for analyzing linear flow (Anderson et al. 2010). As reported in the literature, linear flow appears as a straight line on the square-root-of-time plot whose slope can be used to calculate the product of the fracture half-length and square root of permeability. Therefore, using a very simple diagnostic plot, some of the reservoir properties can be calculated. Examples of application of this method for unconventional oil and/or gas reservoirs are the comprehensive works of Wattenbarger on linear flow (Bello and Wattenbarger 2010, Ibrahim and Wattenbarger 2006, Wattenbarger et al. 1998) and Nobakht's work (Nobakht and Clarkson 2012a, b, Nobakht et al. 2012, Nobakht and Mattar 2012). These studies

focus on different aspects of analysis of production data using the square root of time plot. Changes in calculated reservoir parameters associated with the effect of skin in constant rate and constant p_{wf} production, and also changes in reservoir properties with production and the application of pseudo-time are among the topics of special interest in these studies.

2.4.3 Capacitance-resistance method for production data analysis

Fluid flow in petroleum engineering is akin to flow of electricity in electrical engineering. The correspondences between petroleum and electrical engineering have long been used in the petroleum industry for reservoir modeling and simulation. Initial attempts in utilizing electrical analogues include those of Bruce (1943) where he presented the theory of using electrical capacitance and resistance, and built the actual electrical network, to model the flow of fluids in the reservoir. Wahl et al. (1962) constructed an extremely large-sized resistance-capacitance network and the associated control equipment for simulating four of the most prolific reservoirs in Saudi Arabia. They employed a trial and error procedure in which the resistance values, and occasionally capacitance values, were adjusted until the voltage history of each controller agreed with the pressure history of the oil wells it represented. The resulting model was then used for forecasting the reservoir and individual well performance.

Recently, capacitance-resistance models (CRM) have received renewed interest for predicting performance of water and gas flood projects and determining interwell connectivities in mature reservoirs (Albertoni and Lake 2003, Sayarpour et al. 2009, Weber et al. 2009, Yousef et al. 2006). In a nutshell, they based their analysis on the assumption of constant productivity index (i.e. boundary dominated flow condition), treated the

injection rates as input signals and production rates as output signals and then used the signal processing and nonlinear multivariate regression techniques to determine the inter-well connectivity and response delay as their unknown system parameters.

In addition to the above analysis approaches and based on the geologic observation presented in Figure 2.2, Shahamat and Aguilera (2010) used CRM models to develop a new method for evaluation of production decline analysis of a single well in tight gas formations. The method solved the continuity and flow equations for low and ultra-low permeability formations, which correspond for example, to tight and/or shale gas reservoirs. The new solution permitted integrating the rates at which the well is producing and the rates at which the low or ultra-low permeability source was feeding the reservoir connected to the wellbore. Equilibrium was reached when the contribution from the ultra-low permeability reservoir is equal to the rate contributed by the production reservoir to the wellbore.

Figure 2.15 shows a conventional material balance plot for the tight Falher formation in the WCSB. The plot shows a deviation of the conventional straight line resulting in values of original gas-in-place that increase by two or three times (maybe even more) with respect to the conventional extrapolation with the initial points. This is interpreted to be due to the dual or possibly triple transmissivity nature of the Falher formation (Zaitlin and Moslow 2006). The methodology developed by Shahamat and Aguilera (2010) using tanks (CRM), with a concept that had been utilized by Pulle (1982), permitted generating the same material balance signature as shown in Figure 2.16.

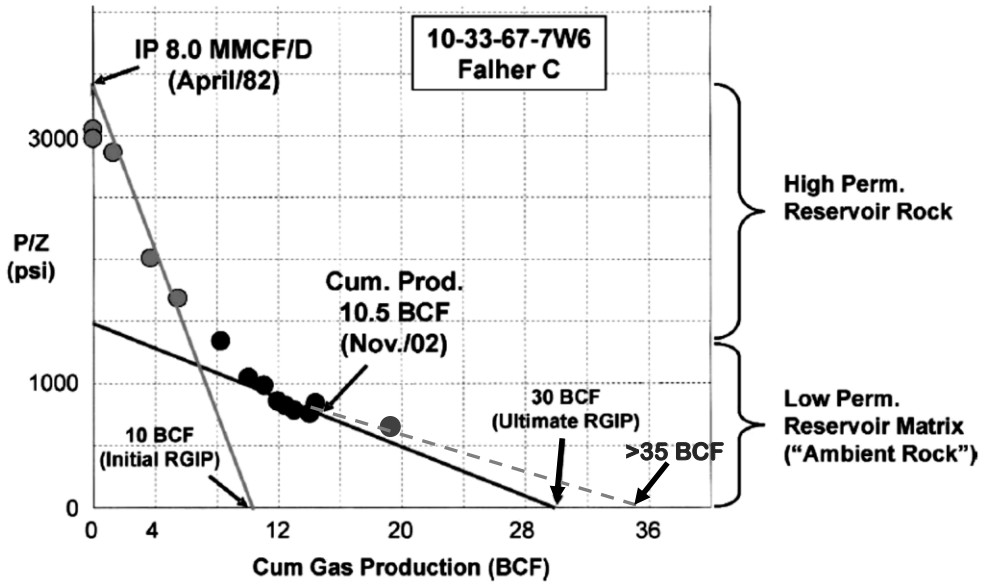

Figure 2.15: Characteristic P/Z curve depicting the dual- or tri-transmissivity nature of a Deep Basin reservoir as observed in the 10-33-67-7w6 well (Adapted from Moslow, 2005).

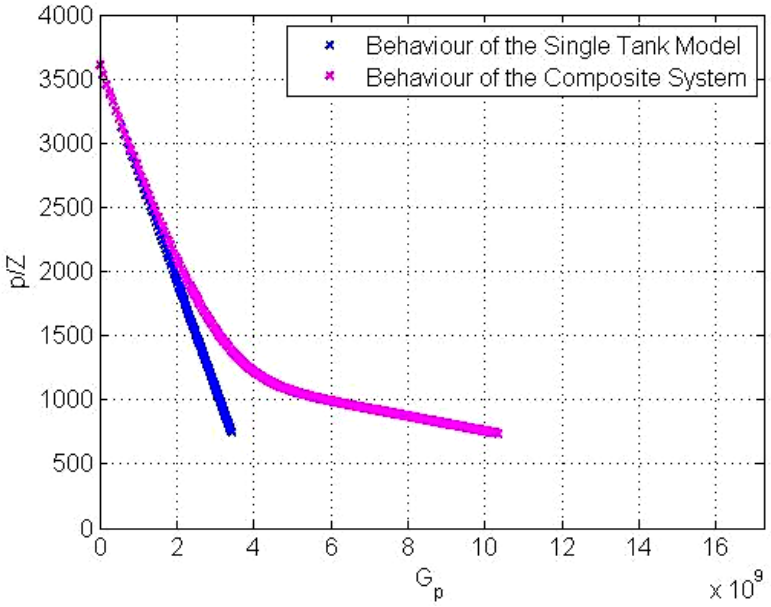

Figure 2.16: Typical plot of p/Z vs. cumulative gas production. Notice similarity in the signature of this curve with the one for the WCSB well shown in Figure 2.15 (Source: Shahamat and Aguilera, 2010).

The model (Shahamat and Aguilera 2010) was applied to field data presented by Kupchenko et al. (2008). The results are shown on Figure 2.17, which presents a Cartesian plot of gas rate vs. cumulative gas production. The proposed model predicts an original gas-in-place, which is in close agreement with the best realistic result obtained by the work of Kupchenko et al. (2008). The graph also shows the gas contribution from the tight source.

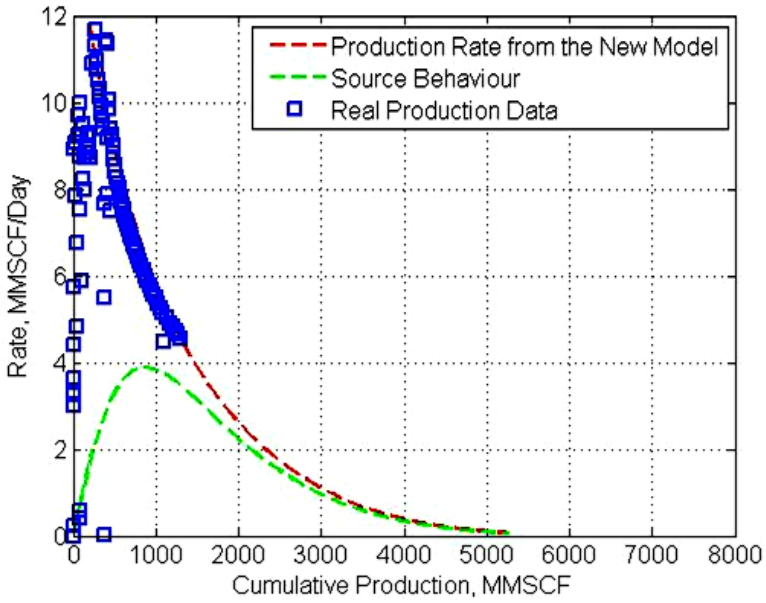

Figure 2.17: Plot of rate vs. cumulative gas production, showing Shahamat and Aguilera (2010) model prediction and source contribution for the field example in paper SPE 114991 (Kupchenko et al. 2008). Blue squares are real gas rate data, brown dashed line is theoretical performance (including an excellent history match), and green dashed line is the calculated contribution from the tight or ultra-tight formation to the producing reservoir.

The analogy between flow of fluid and electricity and therefore the capacitance-resistance models (CRM) has been used for developing original methodologies in this thesis to forecast pressure and rate in reservoirs with dominant transient linear flow regime. This is the subject of the next chapters in this research.

Chapter Three: Capacitance-Resistance Model

3.1 Scope of the Study

Reservoir fluid flow is a fundamentally complex process which involves complicated interaction of rock mechanics, fluid dynamics and thermodynamics within complex, anisotropic and discontinuous geological structures. As a result, prediction of performance of a reservoir is challenging. The usual practice in the industry is to use a simulator where the reservoir is divided into small gridblocks (cells). The governing flow equations along with the empirical laws are then written for each of these cells and solved numerically to obtain saturation and composition of different phases within each cell. In addition, pressure is calculated at a fixed point such as the grid-cell center or as an average cell pressure. Upon obtaining a satisfactory match of the available production data, the constructed model with associated properties can then be used with a reasonable degree of confidence for production forecasting. In spite of the problems associated with simulating more complex physical phenomena in unconventional (such as naturally fractured or shale) reservoirs, simulation is by far the most comprehensive method for modeling reservoir behaviour. As such, it is used as a tool to validate the results of other methods.

Comparable with the approach used in numerical simulation, a reservoir may be represented as a single tank (cell) that has the size of the entire reservoir and a pressure equal to the average reservoir pressure. Modeling the reservoir performance using this single tank is based on the introduction of capacitance and resistance terms (taken from analogy with electrical engineering). It forms the so-called Capacitance-Resistance Model

(CRM) and certainly has advantages, as well as limitations, for analysis and prediction of production performance.

In this chapter, the analogy between the flow of fluid and electricity is described, and a brief introduction into CRM is given with emphasis on forecasting of pressure and rate in reservoirs with dominant transient linear flow regime. First single phase liquid reservoir is considered, and then the approach for a single phase gas reservoir is illustrated.

3.2 Equivalence between Electrical and Petroleum Engineering

Flow of fluids in a porous medium is in many respects analogous to flow of current in a conductor. The electric current (I) through a conductor (such as a wire) is the result of a potential difference (ΔE) across its length. In the electrical world, flow of current is expressed according to Ohm's Law, $I = \Delta E/R$ where R is the electrical resistance and is a function of cross-sectional area of the conductor, its length and the intrinsic properties of the conductor (called resistivity, whose inverse is named conductivity). Similarly, in the petroleum world there is Darcy's Law that relates the pressure difference to the rate of production. It can be expressed in terms of the difference between average reservoir pressure and wellbore pressure to yield the so-called deliverability equation, $q = \Delta p/R$ where $\Delta p = p_{avg} - p_{wf}$. Note that in order to describe flow of fluids through porous media and for the sake of generality the term *fluid-flow equation*, rather than Darcy's Law or deliverability equation, is used in this research. Expressing fluid-flow equation in terms of average pressure is important because average pressure and its changes in production (time) play a critical role in calculation of rock and fluid characteristics and therefore reservoir performance forecasting, economic evaluation and management. By analogy, the

resistance (R) is a function of the properties of the reservoir, cross-sectional area (A_c) and length (L) over which the flow takes place. The term resistivity does not have a direct analog in the petroleum field but the term conductivity does. Conductivity is equivalent to mobility (k/μ). This means that in the same way that the conductivity implies the ease of flow of electricity, the mobility signifies the ease of flow of fluids in the reservoir.

In addition, in the electrical analysis there is a capacitance term which is the ability of electrical elements to store energy (electrical charge). Capacitance is the ratio of the stored energy to the voltage across the terminals (ΔE). A pure capacitance (C) that experiences a constant current (I) will exhibit a constant rate of voltage change over time, i.e. $I = C\frac{dE}{dt}$. Likewise in petroleum engineering, capacitance (or Storage Capacity) is the ability of a reservoir to supply energy (pressure). It is the ratio of the cumulative produced fluid to the pressure depletion (difference) resulting from this production. Using the compressibility equation ($c = -\frac{1}{V}\frac{dV}{dp}$), the capacitance (C) can be expressed as the product of the total system compressibility and the reservoir volume from which the production is taking place ($C = \frac{c \times V}{B}$). The definition for capacitance is similar in form to the wellbore storage constant defined by van Everdingen and Hurst (1949). The difference lies in the fact that instead of the wellbore volume and compressibility, here the volume and compressibility of the reservoir are used. Table 3.1 provides a summary of the analogies between the electrical and petroleum engineering. It is noted that in the case of the latter, both the capacitance and resistance are functions of length through V (reservoir volume) and L, respectively. It is also noted in Table 3.1 that f_1 and f_2 demonstrate different functions operating on the arguments inside the parentheses.

Table 3.1: Summary of analogy between flow of fluid in a porous medium and flow of electricity in an electrical conductor.

	Electrical Engineering	Petroleum Engineering
Driving force:	Voltage difference, ΔE	Pressure difference, Δp
Flow eq.:	Ohm's Law, $I = \frac{\Delta E}{R}$	Fluid $-$ flow equation, $q = \frac{\Delta p}{R}$
Storage eq.:	Faraday equation	Compressibility equation
Resistance, R:	$R = f_1(\text{material property}, A_c, L)$	$R = f_2(\text{fluid and rock property}, A_c, L)$
Capacitance, C:	$C = \frac{Idt}{dE}$	$C = -\frac{qdt}{dp}$

The correspondence between electrical and petroleum systems mentioned above can be used to explain production behaviour of any reservoir, during both transient flow and BDF periods. Explaining a liquid reservoir behaviour during BDF is straightforward, because the reservoir has been fully investigated, fluid properties can be assumed constant, and therefore the capacitance and resistance terms are constant. Under this condition, production at the wellbore means depletion of a tank. As mentioned before, a number of studies have been carried out to illustrate the utility of the CRM for waterflood performance forecasting of reservoirs with high permeabilities (Albertoni and Lake 2003, Sayarpour et al. 2009, Weber et al. 2009, Yousef et al. 2006). Explaining the reservoir behaviour during transient flow period is more complex. This is because the investigated size of the reservoir changes with time, which results in corresponding changes in both capacitance and resistance. As will demonstrated later, provided that the flow regime is known (or can be assumed), the concept of continuous succession of pseudo-steady states can be used for applying the tank-type depletion to the transient flow period, as well.

3.3 Basic Model

The basic reservoir model used in this work is similar to that of Wattenbarger (El-Banbi and Wattenbarger 1996, Wattenbarger et al. 1998) and Nobakht (Nobakht and Clarkson 2012a, b, Nobakht et al. 2012) and shown in Figure 3.1(a). This figure shows a rectangular reservoir with a hydraulic fracture in the center. The fracture completely traverses the reservoir, hence its production exhibits transient linear flow until the investigated distance (y_{inv}) is equal to the reservoir length in the y-direction (y_e); thereafter the flow regime is boundary dominated. This geometry is chosen because production data analysis of low permeability tight and shale reservoirs exhibit linear flow for long periods of time. Figure 3.1(b) also demonstrates the tank representation of the model of Figure 3.1(a). Resistance in this figure represents all the barriers to fluid flow from the production tank to the wellbore. The pressure in the production tank is uniform throughout because there is no resistance that would create a pressure gradient. It is assumed that wellbore skin to be equal to zero. Skin effect will be discussed in a separate section at the end of the chapter.

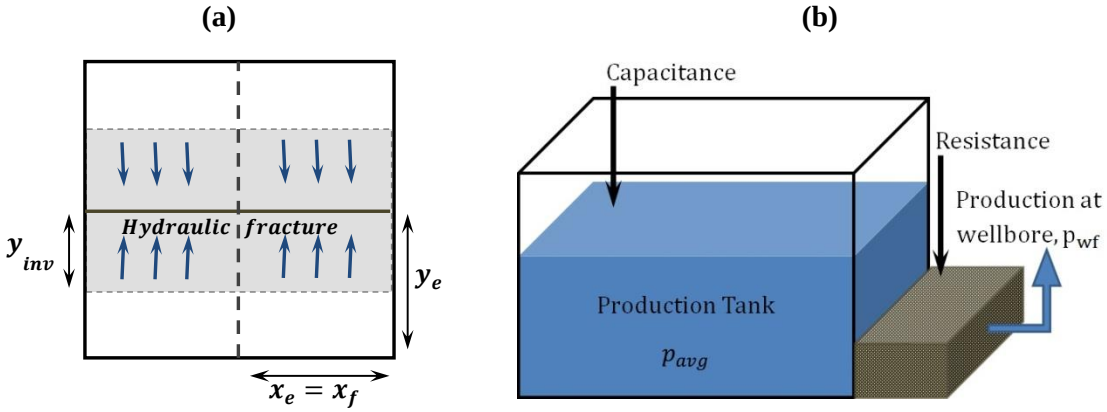

Figure 3.1: Schematic of a hydraulically fractured well in the center of a rectangular reservoir (a) and its tank representation (b).

The region that is investigated represents the propagation of the pressure disturbance into the reservoir, and is obtained using the distance of investigation equation (y_{inv}), Eq. 3.1. This equation states that depending on the nature of the rock, the fluids and the duration of flow, there is a region that has been considerably affected by (and therefore has notably contributed to) the production at the wellbore.

$$y_{inv} = \alpha_1 \sqrt{\frac{\beta_2 kt}{\phi \mu c}} \qquad \text{Eq. 3.1}$$

In this equation, k is the permeability in md, μ is the viscosity in cp, ϕ is the porosity, c is the compressibility in 1/psia and time is in days. $\beta_2 = 0.00633$ and α_1 is a constant which depends on the criterion used for defining the distance of investigation. α_1 depends on the type of production at the wellbore. Wattenbarger et al. (1998) proposed $\alpha_1 = 1.42$ and 2 for constant rate and constant pressure production, respectively. Later, Nobakht and Clarkson (2012a) suggested a modification of the distance of investigation equation over that of Wattenbarger et al. (1998) for constant pressure production, giving $\alpha_1 = 2.55$. In this study and based on simulation studies, we use $\alpha_1 = 1.76$ and 2.23 for constant rate and constant pressure production, respectively. It should be mentioned that the definition of y_{inv} in the above equation is applicable only for $t < t_{BDF}$, where t_{BDF} is the time to reach BDF. This upper limit of time for y_{inv} ensures that the calculated reservoir distance in the y-direction is limited to the size of the reservoir, y_e.

3.4 Depletion during Transient and BDF-Liquid Reservoirs

The change in the average reservoir pressure with time as a result of production is called depletion. In order to determine the amount of depletion for any production time interval,

the material balance (i.e. the compressibility) equation can be written in the following form:

$$\Delta p_{dep} = \frac{q\Delta t}{C} \qquad \text{Eq. 3.2}$$

In this equation, C is the reservoir capacitance in Stb/psia and Δp_{dep} is the pressure depletion as a result of production for a time interval Δt.

In addition to the above equation and as mentioned before, the fluid-flow equation is a relation between average reservoir pressure, the wellbore pressure and the rate of production. This equation is shown below:

$$q = \frac{1}{R}\left(p_{avg} - p_{wf}\right) \qquad \text{Eq. 3.3}$$

Resistance, R, in the above equation is equivalent to the inverse of the productivity index (psia/StbD).

Capacitance (C) and resistance (R) in the above equations depend on the flow geometry and can be obtained analytically for simple reservoir geometries. For flow of a liquid within the reservoir geometry shown in Figure 3.1, C and R can be easily obtained as below:

$$C = \frac{4x_f ch\phi}{5.615B} \times y_{inv} \qquad \text{Eq. 3.4}$$

$$R = \frac{\beta_1 B\mu}{2\pi k h x_f} \times (\alpha_2 \times y_{inv}) \qquad \text{Eq. 3.5}$$

where $\beta_1 = 2\pi \times 141.2$ and α_2 is a constant determined from the deliverability equation (Wattenbarger et al. 1998) and is equal to $\frac{\pi}{6}$ and $\frac{2}{\pi}$ for constant rate and constant pressure production, respectively. Because of their dependence on the distance of investigation,

y_{inv}, the obtained C and R parameters vary with time. It is more convenient to define parameters that are only representative of the reservoir characteristics and independent of the production scenario. One can therefore introduce the terms capacity (C^*) and resistivity (R^*) through the following equations:

$$C^* = C/y_{inv} \quad \text{Eq. 3.6}$$

$$R^* = R/(\alpha_2 \times y_{inv}) \quad \text{Eq. 3.7}$$

Introducing capacity and resistivity through the above equations gives two unique advantages for production forecasting specific to the case of zero skin. First, multiplication of the capacity and resistivity gives hydraulic diffusivity, which is a reservoir property that determines the speed at which the pressure disturbance travels through the reservoir, Eq. 3.8. This property is used for obtaining the distance of investigation, Eq. 3.1. Second, division of the capacity by the resistivity gives a parameter (CRR, Eq. 3.9) that is characteristic of linear flow and can be used for performance prediction. It is noted that the analysis of constant rate linear flow by Clark (1968) and Gringarten et al. (1974) also shows the same combination of parameters for determining the pressure change with time.

$$\frac{1}{C^* \times R^*} = \frac{\pi}{2}\left(\frac{\beta_2 k}{\phi \mu c}\right) \quad \text{Eq. 3.8}$$

$$CRR = \frac{C^*}{R^*} = \frac{8\pi}{5.615\beta_1}\frac{kc\phi}{\mu}\left(\frac{x_f h}{B}\right)^2 \quad \text{Eq. 3.9}$$

The capacitance-resistance terminology can be used to explain the depletion behaviour during BDF of both constant terminal rate and constant terminal pressure production. Knowing that C and R are constant during BDF, Eq. 3.2 shows that constant terminal rate

production for equal time intervals results in equal pressure depletion. In addition, Eq. 3.3 suggests that any pressure drop at the wellbore caused by constant rate production results in dropping of average reservoir pressure by the same amount. This means that in constant rate production wellbore pressure tracks the average reservoir pressure during BDF. However, for constant terminal pressure production, constancy of wellbore pressure means that the production rate used for determining the depletion is a declining rate.

The situation is different when one applies the above reasoning for describing the behaviour during transient flow. In order to explain this flow behavior, the transient solution of the reservoir configuration shown in Figure 3.1, derived in Appendix A, is used. The distance of investigation equation (Eq. 3.1) is employed to calculate p_{avg} as the average pressure within the investigated volume. Using the integral method to determine the location at which the pressure is equal to the average pressure, Figure 3.2 is obtained. Figure 3.2 (a) shows the constant rate pressure profile at three consecutive times during transient flow with their corresponding average pressure values.

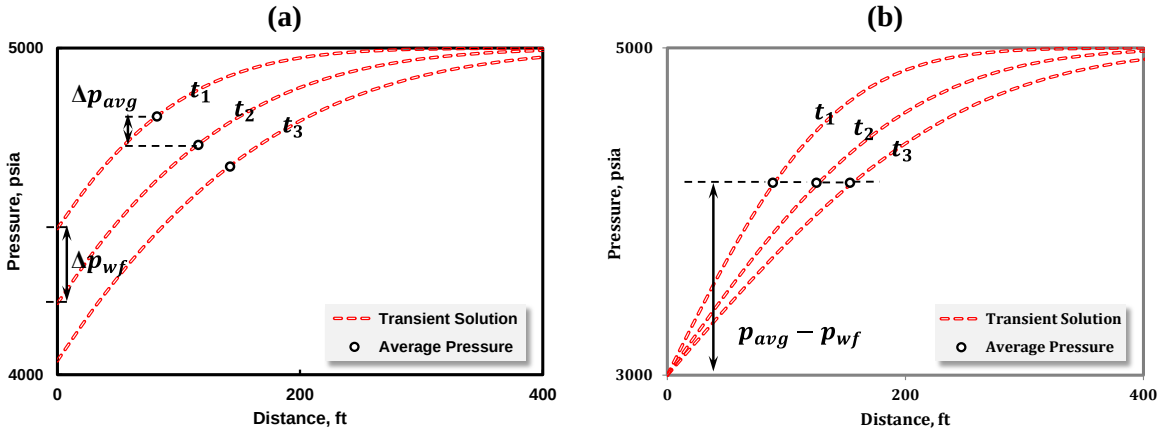

Figure 3.2: Pressure profile during transient linear flow; (a) constant rate, (b) constant pressure production.

Comparison of the calculated wellbore pressure and average pressures for each time demonstrates that p_{avg} and p_{wf} drop by different amounts. In fact, the change in average pressure during any time period is smaller than half (≅0.46) the pressure change at the wellbore; see Appendix A. This is due to the effect of the changing size of the reservoir (i.e. y_{inv}) during the transient flow period and is different from BDF where p_{avg} and p_{wf} track each other.

Constant pressure production of the same reservoir shows another story. Here the constant pressure complete solution derived in Appendix A is used to obtain the pressure profile and similar to the constant rate production, calculate the volumetric average pressure. Figure 3.2 (b) depicts the pressure profile and the associated average pressure for three consecutive times. This plot demonstrates that during transient linear flow, the average pressure stays at a constant value which is neither the initial pressure nor the wellbore pressure. As a result, during this flow period the pressure difference $(p_{avg} - p_{wf})$ in the fluid-flow equation is constant but the increasing Resistance with time as a result of increasing y_{inv} causes the rate to decline.

The discussion above demonstrates that in order to use the depletion equation during transient flow, one need to consider the distance of investigation in the related calculations. As a result, the concept of continuous succession of pseudo-steady states is introduced to represent the transient flow period, for constant rate and constant pressure production using simple depletion and resistance equations.

3.5 Continuous Succession of Pseudo-Steady States (SPSS)

Continuous succession of (steady) states was introduced by Muskat (1937) as a method that enables the use of the simple steady-state solutions for dealing with time varying systems where the time transient play a minor role in the physical behaviour of the system. He discussed that the methodology is useful for systems where transmission of the pressure disturbances in the porous medium may be considered as effectively instantaneous. It is required, therefore, for the reservoir to have small dimensions and high permeability, and the fluids to be either incompressible or slightly compressible. Whittle and Gringarten (2008) introduced a method to determine minimum tested volume from a well-testing response by imposing a unit-slope line on the derivative plot at each point in time. Their method was based on the assumption of successive pseudo-steady states meaning that, during the transient flow period, the system was thought to behave like a growing tank. Their method was later used by Tabatabaie et al. (2013) for calculation of the volume of the influenced region and therefore obtaining an appropriate pseudo-time function during transient flow.

Building on this concept and based on the electrical analogy, the concept of succession of pseudo-steady states is proposed. With this concept, the transient flow behaviour of a reservoir producing under constant rate or constant p_{wf} can be reasonably represented by a continuous succession of the pseudo-steady state equations provided that:

- The main flow regime (e.g. linear or radial) can be reasonably approximated,
- The changes in capacitance and resistance are obtained by using the distance of investigation equation,

- Production from one time step to the other causes depletion of the associated capacitance according to the material balance equation,
- The resistance and therefore the pressure and/or rate at the new time step are obtained using the fluid-flow equation and the reservoir pressure resulting from depletion of the capacitance at the previous time step.

The procedure consists of the stepwise coupling of the material balance equation for the investigated volume with the fluid-flow equation. It should be mentioned that irrespective of the production scenario, the depletion calculations between two consecutive time steps (t_j and t_{j+1}) are performed assuming a constant rate of production, hence the name pseudo-steady states.

The above discussion about applying depletion and fluid-flow equations in the CRM is valid for liquid reservoirs having constant fluid properties (viscosity and compressibility). The approach can be used for the case of gas provided that the changes in gas compressibility and viscosity are accounted for. As is shown in Appendix F, the gas compressibility equation can be written according to Eq. 3.10. This equation is the well-known gas material balance equation.

$$\Delta\left(\frac{p}{Z}\right)_{dep} = \frac{q_g \Delta t}{C} \qquad \text{Eq. 3.10}$$

In addition, for gas reservoirs the fluid-flow equation can be written in terms of pseudo-pressure to yield:

$$q_g = \frac{(p_{p,avg} - p_{p,wf})}{R} \qquad \text{Eq. 3.11}$$

Where p_p is the normalized pseudo-pressure (psia). Similar to the liquid flow cases discussed in the previous sections, for gas reservoirs Eq. 3.6 and Eq. 3.7 are used to relate capacitance with capacity and resistance with resistivity. Again here the capacity and resistivity terms are independent of the production scenario, and their multiplication should give the hydraulic diffusivity.

It should be noted that Eq. 3.10 gives the depletion in terms of p/Z while Eq. 3.11 requires pseudo-pressure for its calculation. In order to convert pressure to pseudo-pressure and to p/Z, one can obtain a table of gas properties and perform linear interpolation between its entries to calculate p_p and p/Z for any value of pressure.

3.6 Implementation of the CRM

As mentioned in the previous sections, CRM consists of stepwise calculation of depletion at each time and coupling it with the fluid-flow equation. What CRM does is a simplified version of what is performed in a numerical simulator. Having produced from a reservoir and obtained some rate and pressure data, the CRM uses an initial data point (rate and wellbore pressure at the first time step) and minimal parameters representing reservoir characteristics (CRR and t_{BDF}) to history match the available rates and pressures and then predict the future behaviour. In CRM for linear flow, only knowledge of the ratio of capacity to resistivity (and not both capacity and resistivity) is required for analysis, because use of the initial declining rate/pressure data constrains the CRM results and consequently decreases the number of parameters required to history match the rest of the data. This means that under the condition of using reasonable initial rate/pressure data, different combinations of C^* and R^* that result in the same CRR parameter will give

similar results. In order to simplify calculation of the distance of investigation (y_{inv}) it is assumed here that $R^* = 1$. It can be stated, therefore, that the CRM effectively lumps all the reservoir characteristics into the ratio of capacity to resistivity (CRR).

In this section, the procedures required for using CRM to analyze constant rate and constant pressure production data of liquid and gas reservoirs is described.

3.6.1 Liquid reservoirs

For constant rate production of a liquid reservoir, the procedure to follow is shown in Figure 3.3. The first step includes specifying the input parameters shown in the Figure 3.3. The second step is calculating the hydraulic diffusivity from the inverse of multiplication of capacity and resistivity, i.e. $\frac{1}{C^* \times R^*}$. Having obtained the hydraulic diffusivity, Eq. 3.1 is used at each time to determine the investigated distance, with the upper limit obtained using t_{BDF}. Then the resulting distance of investigation is used along with the capacity to obtain capacitance and thereby the pressure depletion, Eq. 3.2. Thereafter, the pressure depletion and the first wellbore pressure are used in a stepwise procedure to calculate the subsequent wellbore pressures.

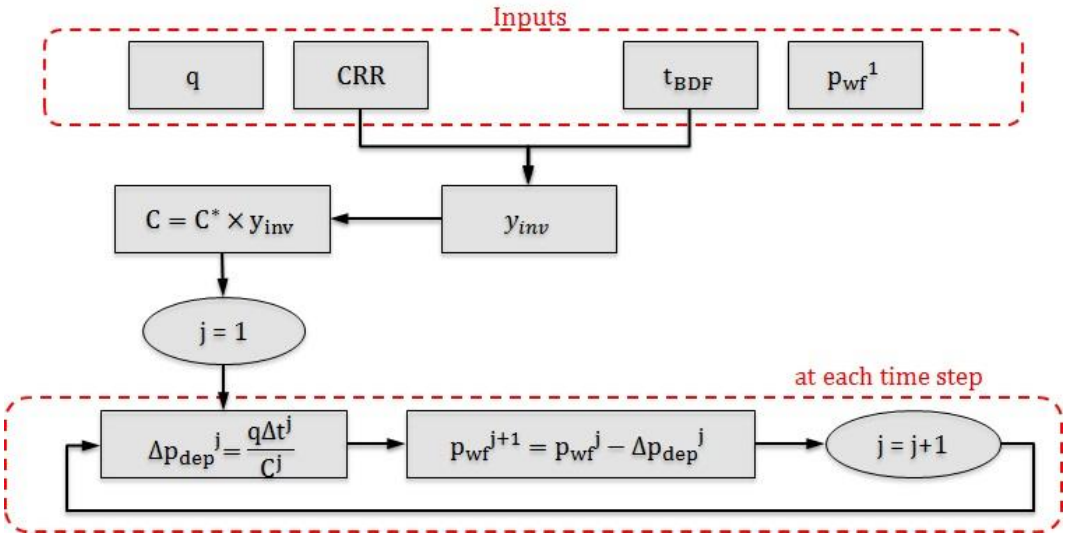

Figure 3.3: The procedure for applying CRM for constant rate production of liquid reservoirs.

For constant pressure production of a liquid reservoir, the procedure to follow is shown in Figure 3.4. It is almost similar to the case of constant rate production, with the difference that the obtained distance of investigation and capacity and resistivity are used for obtaining the pressure depletion and new average pressure (through the material balance equation, Eq. 3.2) and also the new production rates (through the fluid-flow equation, Eq. 3.3). Thereafter, by knowing the first production rate and utilizing a stepwise procedure, the subsequent rates can be calculated.

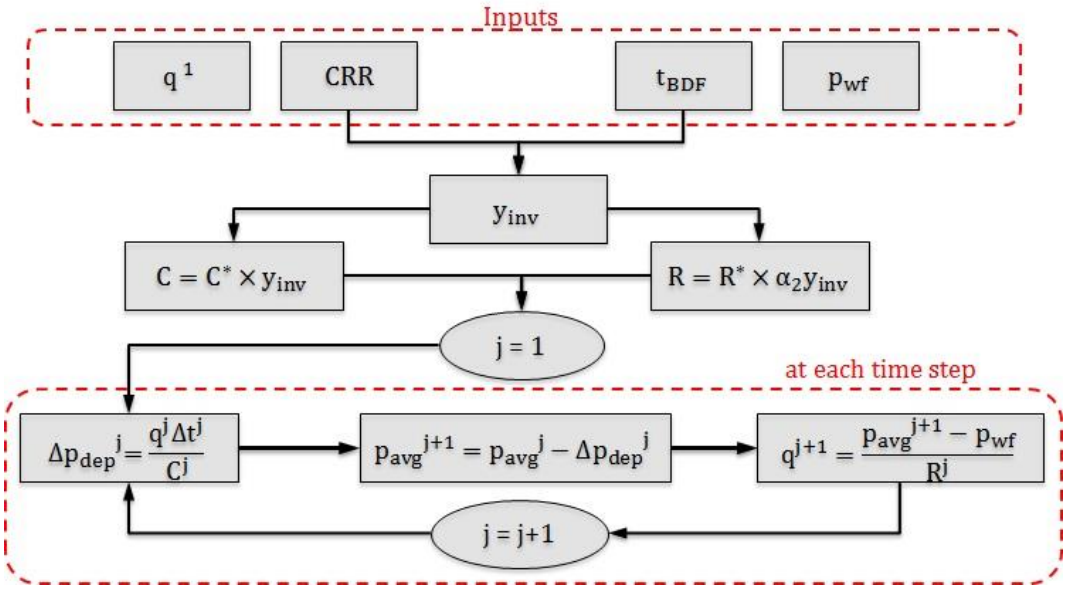

Figure 3.4: The procedure for applying CRM for constant pressure production of a liquid reservoir.

3.6.2 Gas reservoirs

As mentioned in the previous section, CRM for gas is based on pseudo-pressure formulation of the fluid-flow equation, Eq. 3.11, whereas the gas depletion calculation is according to Eq. 3.10, which is based on pressure (p/Z). In order to couple these equations, pressure has to be converted to pseudo-pressure and vice versa for the related calculations by using a simple table lookup.

Similar to the liquid reservoir cases, using the CRM for constant rate production of a gas reservoir involves using capacity, resistivity and the time to BDF. Capacity and resistivity define the hydraulic diffusivity which is used for calculating y_{inv} at each time. Combining capacity and resistivity with the obtained distance of investigation through Eq. 3.6 and Eq. 3.7 gives capacitance and resistance that would allow the calculation of pressure depletion by applying Eq. 3.10. Through the table lookup, one can obtain the new average and

wellbore pseudo-pressures and wellbore pressure as a result of the depletion that occurred at the previous time step. These pseudo-pressures are then used in the fluid-flow equation to calculate new p/Z corresponding to the average pseudo-pressure. Having calculated the gas depletion value for this time step, one can calculate the new p/Z which can be converted back to pseudo-pressure through another table lookup. The new pseudo-pressures are then used for the next round of calculations. This procedure is depicted in Figure 3.5. T in this Figure indicates Table lookup.

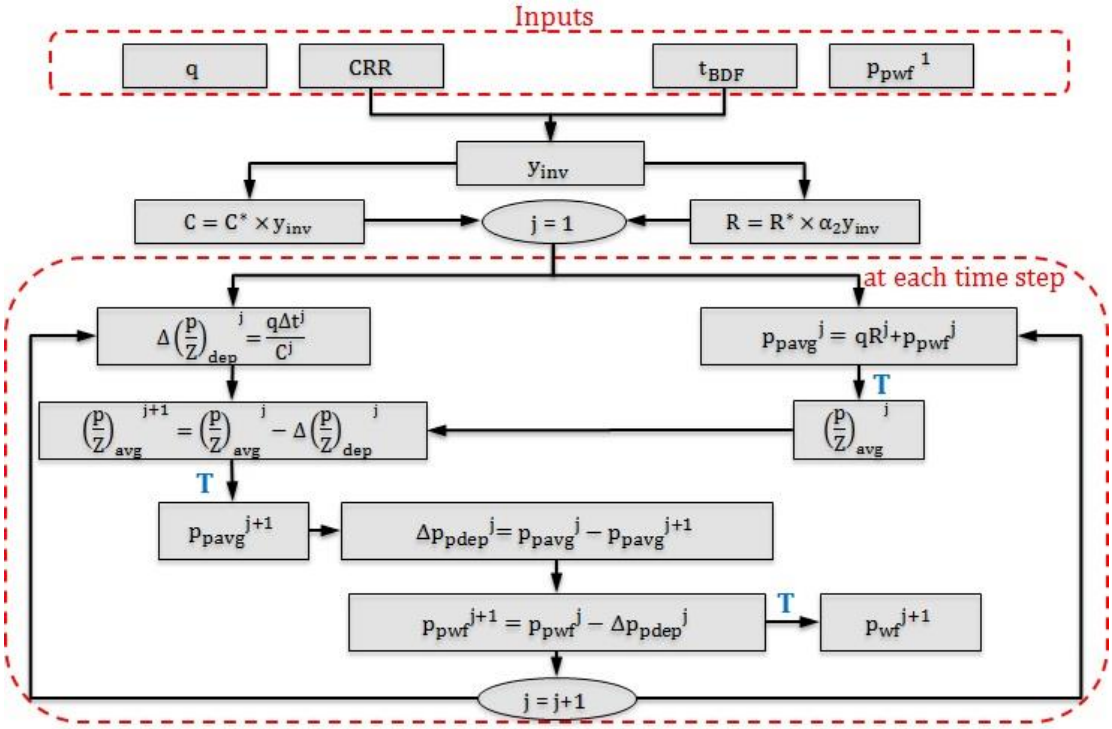

Figure 3.5: The procedure for using CRM for constant rate production of a gas reservoir.

For constant pressure gas production, a procedure almost similar to that of the constant rate gas production is applied, see Figure 3.6. Again the CRM involves using capacity, resistivity and the time to BDF. Capacity and resistivity define the hydraulic diffusivity which is used for determining y_{inv}. Combining capacity and resistivity with obtained

distance of investigation through Eq. 3.6 and Eq. 3.7 gives capacitance and resistance that would allow calculation of depletion and fluid-flow equations by applying Eq. 3.10 and Eq. 3.11. Through the table lookup (T in Figure 3.6), one can calculate the p/Z corresponding to the average pseudo-pressure from the fluid-flow equation. Using this and the depletion value for this time step, the new p/Z is calculated which can be converted back to pseudo-pressure through another table lookup. The new pseudo-pressure is then used in the fluid-flow equation to calculate a new production rate and therefore a next round of calculations.

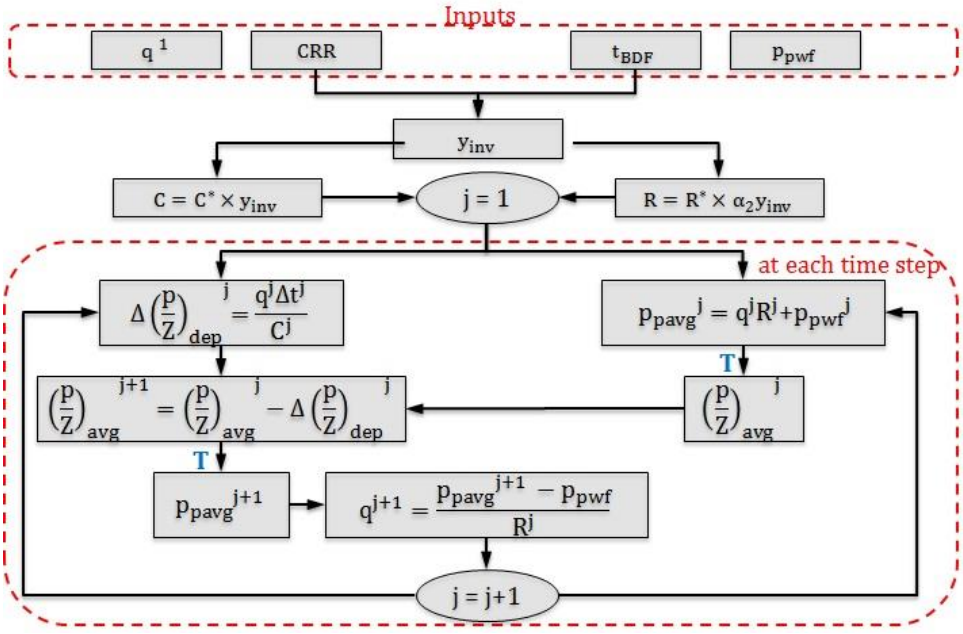

Figure 3.6: The procedure for using CRM for constant pressure production of a gas reservoir.

3.7 Validation of CRM

In this section, first synthetic rate/pressure data for liquid and gas reservoirs are generated, using rigorous approaches (either analytical or numerical methods). Then the methodologies outlined in the previous section are used to demonstrate the behaviour of CRM for matching the production data. Achieving reasonable results compared with those of the rigorous approaches confirms the validity of the CRM.

3.7.1 Liquid reservoirs

In order to validate the CRM procedures for the constant rate and constant pressure liquid cases, analytical complete solutions are employed. The complete solutions involve writing the dimensionless diffusivity equation and different boundary and initial conditions for a finite reservoir and then obtaining the solutions analytically and expressing them in real time domain. The complete solutions are valid for all time and therefore encompass both transient flow and BDF.

Constant rate production of a liquid reservoir with geometry shown in Figure 3.1 gives a declining wellbore pressure whose behavior during both transient and BDF can be described using the analytical complete solution shown in Eq. 3.12. Constant pressure production of the same reservoir, on the other hand, gives a declining rate behavior that can be described using the analytical complete solution in Eq. 3.13. These complete solutions are shown in Appendix B.

$$p_D = \frac{\pi}{2}\left(\frac{t_D}{y_{eD}}\right) + \pi y_{eD} \sum_{n=1}^{\infty} \left\{ \frac{1}{(n\pi)^2} \left(1 - e^{-\left(\frac{n\pi}{y_{eD}}\right)^2 t_D} \right) \right\} \qquad \text{Eq. 3.12}$$

$$q_D = \frac{4}{\pi y_{eD}} \sum_{n=1}^{\infty} \left\{ e^{-\left(\frac{(2n-1)\pi}{2y_{eD}}\right)^2 t_D} \right\} \quad \text{Eq. 3.13}$$

In the above equations, t_D and y_{eD} are dimensionless time and distance, respectively, p_D the dimensionless pressure for constant rate production and q_D is the dimensionless rate for constant wellbore pressure production. They are defined in Appendix A.

These complete solutions give the correct behavior of a liquid reservoir with linear flow. They involve the summation of a large number of terms (at least 100) to produce acceptable results during transient flow. During BDF, though, the solutions can be simplified to yield the well-known pseudo-steady state equation and exponential decline equation for constant rate and constant pressure production, respectively.

Utilizing Eq. 3.12 and the parameters in Table 3.2(a), a set of wellbore pressure data were generated for the constant rate production case. In addition, the parameters in Table 3.2(a) were used in Eq. 3.13 to yield a set of declining rate data for a specified constant wellbore pressure of 500 psia. The production rate and pressure data for each of the production scenarios were then used to examine the CRM methodology.

Using Eq. 3.1 and Eq. 3.4 – Eq. 3.9 and reservoir characteristics outlined in Table 3.2(a), parameters to be used in CRM for constant rate and constant pressure production are obtained. They are listed in Table 3.2(b). It is noted in this table that instead of determining two parameters C^* and R^*, only their ratio parameter (i.e. CRR) are shown. The reason for this is that our analysis indicates that determining only their ratio parameter (i.e. CRR) suffices for obtaining reasonable results. Figure 3.7 demonstrates comparison of the CRM results (solid red lines) with those of the complete solution (black circles) for constant rate production.

Table 3.2(a): Reservoir geometry and properties used for generating the complete solutions.

Parameters	Values
p_i, psia	5000
k, md	0.01
h, ft	100
y_e, ft	500
x_e, ft	500
x_f, ft	500
μ, cp	0.6
ϕ, fraction	0.1
B, bbl/Stb	1.0
c, 1/psia	7.5×10^{-6}
s (skin factor)	0
q, StbD (for constant rate production)	10
p_{wf}, psia (for constant wellbore pressure production)	500

Table 3.2(b): Parameters used in CRM for constant rate and constant pressure production of the liquid reservoir with specified properties in Table 3.2(a).

Constant Rate Parameters	Values
$p_{wf}{}^1$, psia	4840.7
q, StbD	10
CRR, $(Stb/psia)^2/Day$	0.158
t_{BDF}, days	574
Constant Pressure Parameters	**Values**
p_{wf}, psia	500
q^1, StbD	180
CRR, $(Stb/psia)^2/Day$	0.158
t_{BDF}, days	360

Figure 3.7 shows that using the parameters in Table 3.2(b) and employing the procedure outlined in Figure 3.3, an excellent match of the complete solution is obtained. Figure 3.7 (a) shows the Cartesian plot of wellbore pressure versus time and Figure 3.7 (b) demonstrates the logarithmic plot of the pressure difference $(p_i - p_{wf})$ versus time. The

straight lines of slopes half and unity shown in Figure 3.7(b) clearly depict the dominant flow regimes to be linear flow and BDF.

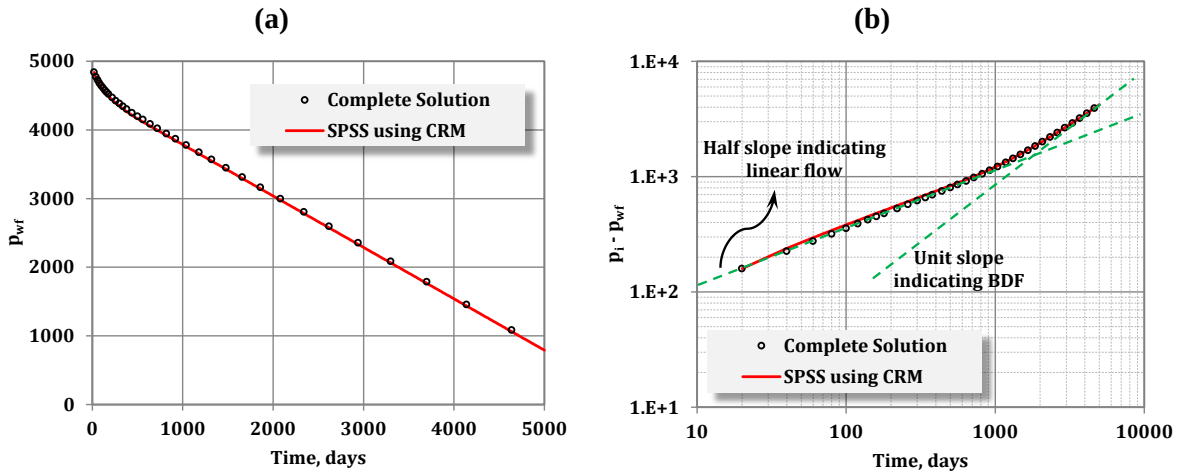

Figure 3.7: Comparison of the CRM and the complete solution for constant rate production; (a) Cartesian plot of p_{wf} versus time, (b) Loglog plot of (p_i - p_{wf}) versus time.

Figure 3.8 and Figure 3.9 demonstrate comparison of the CRM results (solid red lines) with those of the complete solution (black circles) for constant wellbore pressure production. Calculated parameters for this case are shown in Table 3.2(b). As can be seen in this table, the calculated t_{BDF} for constant pressure is smaller than the constant rate production. This is due to the smaller α_1 used in Eq. 3.1 for the constant pressure and reflects the difference in the speed of propagation of the sensible pressure disturbance between these two production scenarios.

Figure 3.8 shows Cartesian and Loglog comparison of the resulting rates. As can be seen, the match is not satisfactory. This is because in the CRM, calculation of the reservoir depletion during any time period is based on the constant rate assumption. As a result, a higher initial production rate during early time gives higher pressure depletion, and therefore leads to a sudden drop in the subsequent calculated rate.

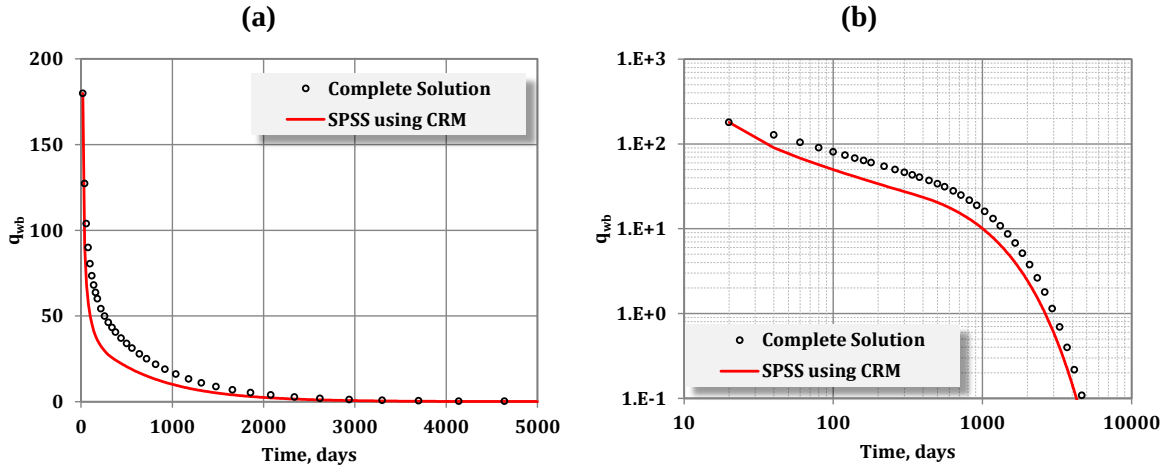

Figure 3.8: Comparison of the CRM and the complete solution for constant p_{wf} production; (a) Cartesian and (b) loglog plot of q versus time.

A better match of the declining rates can be obtained by using either smaller time steps and/or iteration on the rate used for the depletion calculations. Figure 3.9 shows the match when three iterations on the calculated rate were used. The obtained excellent match demonstrates the validity of the approach for this case. It is worth mentioning that use of smaller time steps produces results that are similar to those obtained using iteration.

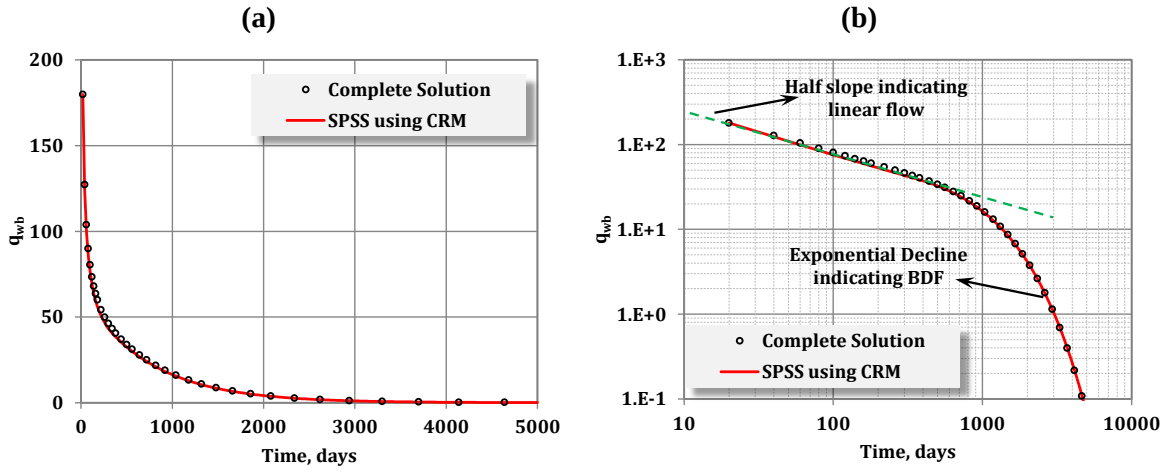

Figure 3.9: Comparison of the CRM (with 3 iterations on rates) and the complete solution for constant p_{wf} production; (a) Cartesian and (b) loglog plot of q versus time.

The obtained matches between the CRM and the complete solutions for the constant rate and constant pressure production of the above liquid reservoir confirm the validity of the proposed CRM procedures. This reveals that by knowing two parameters about the reservoir (CRR and t_{BDF}) and the initial pressure and rate of production, one can follow the CRM stepwise procedures outlined in the previous section to calculate the subsequent rates.

3.7.2 Gas reservoirs

A synthetic set of gas production data can be obtained by using either the complete solutions of the previous section (with pseudo-pressure in place of pressure and pseudo-time in place of time) or numerical simulation. In this section, a commercial numerical simulator with properties shown in Table 3.3(a) is used to obtain the gas production data for constant rate and constant wellbore pressure production.

Table 3.3(a): Reservoir geometry and fluid properties used for numerical simulation of a gas reservoir.

Parameters	Values
p_i, psia	5000
T, °F	200
k, md	0.01
h, ft	100
y_e, ft	500
x_e, ft	500
x_f, ft	500
μ, cp	0.025
ϕ, fraction	0.1
γ_g, fraction	0.65
s (skin factor)	0
q, MscfD (for constant rate production)	350
p_{wf}, psia (for constant wellbore pressure production)	500

Numerical simulation of a gas reservoir with the above properties and the reservoir geometry shown in Figure 3.1(a) results in a set of declining wellbore pressure (for constant rate production) or rate (for constant wellbore pressure production). Utilizing Eq. 3.1 and Eq. 3.4 – Eq. 3.9 and reservoir characteristics in Table 3.3(a), parameters to be used in the CRM are obtained according to Table 3.3(b). Again it is noted in Table 3.3(b) that instead of determining two parameters C* and R*, only their ratio parameter (i.e. CRR) is actually required for obtaining reasonable results.

Table 3.3(b): Parameters used in CRM for constant rate and constant pressure production of the gas reservoir with specified properties in Table 3.2(a).

Constant Rate Parameters	Values
$p_{wf}{}^{1}$, psia	4806
q, MscfD	350
CRR, $(\text{MScf/psia})^2/\text{Day}$	79.5
t_{BDF}, days	422
Constant Pressure Parameters	**Values**
p_{wf}, psia	500
q^{1}, MscfD	3922
CRR, $(\text{MScf/psia})^2/\text{Day}$	79.5
t_{BDF}, days	375

Figure 3.10 demonstrate comparison of the CRM results (solid red lines) with those of the numerical simulation (black circles) for constant rate production. Figure 3.10(a) gives a Cartesian plot of wellbore pressure with time. In addition, Figure 3.10(b) demonstrates the logarithmic plot of the pressure difference ($p_i - p_{wf}$) versus time. As evident in this Figure, CRM is able to reasonably history match constant rate production of the simulated gas reservoir.

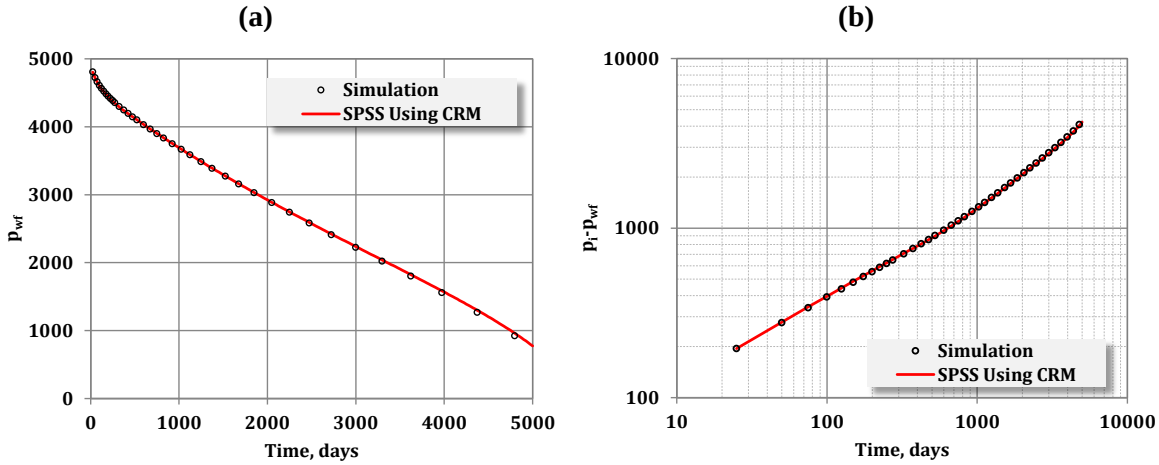

Figure 3.10: Comparison of the CRM and the numerical simulation for constant rate production of a gas reservoir; (a) Cartesian plot of p_{wf} versus time, (b) Loglog plot of (p_i - p_{wf}) versus time.

Figure 3.11 (a) and (b) show the CRM match of the simulation results for constant pressure production. Similar to the case of a liquid constant pressure production, here again constant rate assumption for calculation of depletion can cause results that might not follow the simulation signature. Using iteration and/or smaller time steps in the CRM can significantly improve the history matching of the simulation results.

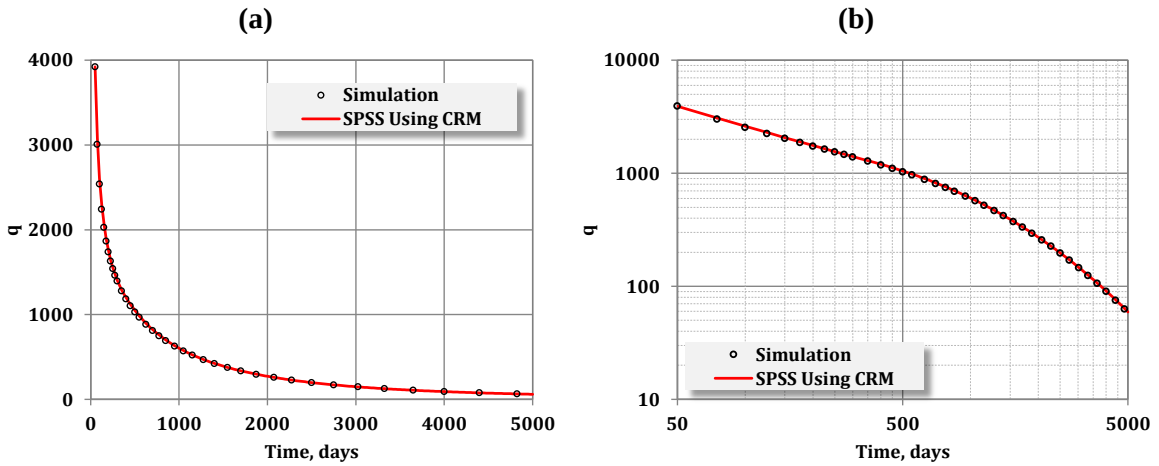

Figure 3.11: Comparison of the results of the CRM (with small time steps) and the numerical simulation for constant pressure production of a gas reservoir; (a) Cartesian and (b) Loglog plots of rate versus time.

The results obtained above for liquid and gas cases using the approaches mentioned up to here demonstrate the SPSS approach through the CRM can yield appropriate behaviour of a reservoir during not only BDF but also transient (linear) flow. In other words, BDF and transient (linear) flow can be written using the capacitance and resistance terms.

3.8 Effect of Skin

As mentioned previously, the analysis methods mentioned in the previous sections are applicable to cases where there is no skin. In this section, first a briefly description of skin is given and then the way to consider its effects in CRM is explained.

There are different factors in, and in the vicinity of, the wellbore that can alter the pressure measured at the well. In tight and shale wells the additional pressure drop can be due to multiphase flow, liquid loading, incomplete recovery of the injected fracturing fluid, damage on the fracture-face, near-fracture saturation changes or emulsions, pressure-dependent fluid and/or rock properties, finite fracture conductivity, adsorption/diffusion of gas near the wellbore region (where the pressure is lower). Combinations of these and other effects often complicate analysis of production data. There are different ways to account for these effects in well testing and production data analysis. In his original work in (1953), van Everdingen noted that the effect of damage or stimulation rarely exceeds 20 ft around the bore hole and as such he defined skin as a dimensionless additional pressure drop at the wellbore. This way, he was able to consider damage/stimulation effects mathematically in well testing (constant rate) solutions. Later, Hawkins (1956) defined a region near the wellbore, affected by damage/stimulation. Focused on radial flow geometry

and using Darcy's Law, Hawkins obtained a relation between skin factor (s) and the size and permeability of the damaged region near wellbore:

$$s = \left(\frac{k}{k_s} - 1\right) \ln\left(\frac{r_s}{r_w}\right) \qquad \text{Eq. 3.14}$$

The additional pressure drop due to damage is calculated according to the following equation:

$$\Delta p_s = \frac{141.2 q B \mu}{kh} s \qquad \text{Eq. 3.15}$$

Figure 3.12 shows effect of skin on pressure distribution within a reservoir. Evident in this figure, the damaged region (the dashed area between r_s and r_w) exhibits a different pressure profile (solid blue curve) than it would if there was no damage (dashed red curve):

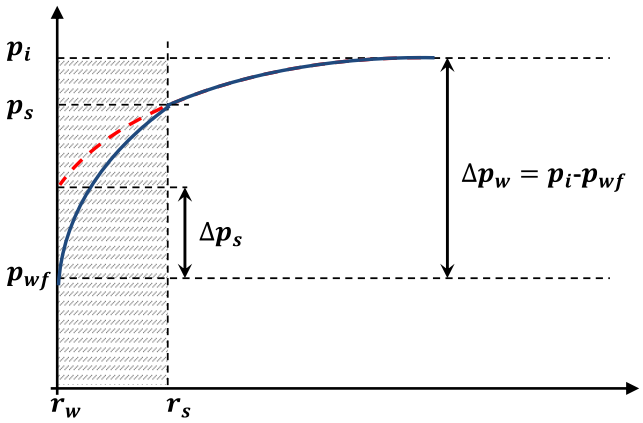

Figure 3.12: Effect of skin (damage) on pressure profile around the wellbore.

For fractured reservoirs, the same concept is applied. Linear flow theory is employed to obtain a skin formulation. Writing Darcy's Law (linear flow) for the damaged and undamaged regions and then using continuity of pressure and rate at the skin boundary results in the following definition of skin:

$$s = \left(\frac{\pi}{2}\right)\left(\frac{k}{k_s} - 1\right)\left(\frac{y_s}{x_f}\right) \qquad \text{Eq. 3.16}$$

Similar to the radial flow, the pressure drop due to skin is obtained according to Eq. 3.15. It is noted that Eq. 3.16 is the definition for fracture face skin for a hydraulically fractured reservoir, as introduced by Cinco-Ley and Samaniego-V. (1981).

In Appendix B, the constant rate and constant pressure complete solutions with skin effect for a liquid reservoir are derived. For constant rate production, inclusion of skin effect is through addition of s to the dimensionless pressure solution at the wellbore. This means that all the pressure values from the start to the end of production exhibit the same additional pressure drop due to skin (Δp_s). As a result, since the CRM approach involves using the first pressure value which has the skin effect embedded in it, skin effect for constant rate production is implicitly included in the CRM analysis. Therefore the constant rate approaches mentioned in the previous sections are also applicable to situations where there is skin. Figure 3.13 is an illustration of the skin effect in constant rate production.

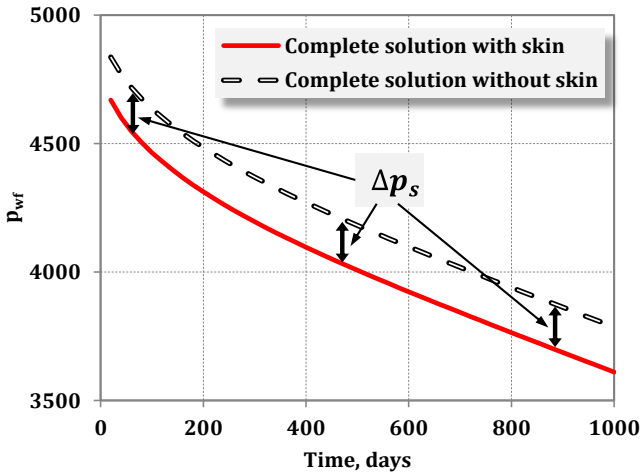

Figure 3.13: Comparison of the constant rate behaviour with and without skin during BDF and transient linear flow.

For constant pressure production, however, the situation is different. As demonstrated by Bello and Wattenbarger (2010), the additional pressure drop due to skin causes a diminishing effect on the production rate. Unlike the constant rate case, skin is not simply additive in constant pressure production (Nobakht and Mattar 2012). This is because the additional pressure drop (Δp_s) depends on the wellbore rate, which declines with time and in turn has a decreasing effect. Bello and Wattenbarger (2010) used the linear flow specialized plot ($1/q_D$ vs. $\sqrt{t_D}$) to illustrate this behaviour, see Figure 3.14.

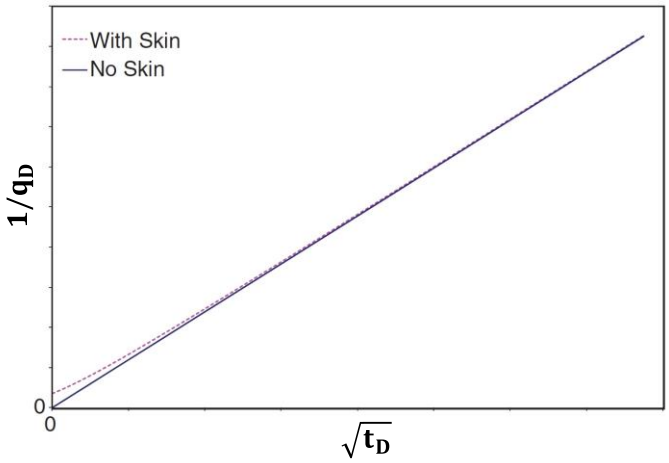

Figure 3.14: Effect of skin on the specialized linear flow plot for constant pressure production.

In this situation, the CRM approaches in the previous sections are not applicable because the skin effect should be included in the resistance (R). Skin causes additional resistance to flow, therefore its effects can be considered in the CRM by using an additional term (s^*), through the following equation.

$$R = R^* \times (\alpha_2 \times y_{inv}) + s^* \qquad \text{Eq. 3.17}$$

In this equation $s^* = \frac{\Delta p_s}{q}$.

Simple addition of s^* in the resistance term allows for inclusion of the skin effect in the analysis. This means that by calculating the resistance according to Eq. 3.17, constant pressure approaches developed in the previous sections can be used for cases where skin is significant and its effects should be considered in the analysis.

Figure 3.15 shows the application of CRM for a reservoir with skin effect exhibiting linear flow. The complete solution was obtained for a rectangular reservoir of y_e, x_e, and x_f equal to 500 ft, with permeability of 0.005 md and s = 2. Using the CRM approach in Figure 3.4 with Eq. 3.17, the initial rate of 29.6 StbD, $\text{CRR} = 0.15\ (\text{Stb/psia})^2/\text{Day}$ and $s^* = 5.8\ \text{psia/StbD}$, excellent results are obtained. Figure 3.15 shows that the CRM can be used for analysis of cases with skin effect.

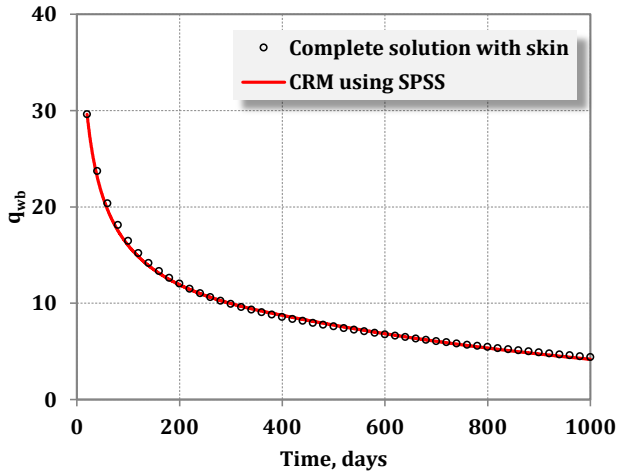

Figure 3.15: Comparison of the CRM and the complete solution with skin effect for constant p_{wf} production.

Notwithstanding the behaviour of idealized reservoirs producing at constant p_{wf} discussed up to this point, Nobakht and Mattar (2012) argue that the practical observation from numerous shale-gas wells essentially producing at constant flowing pressure indicate that they yield a "straight-line-with-intercept" rather than the "curve-with-intercept" shown in

Figure 3.14. This behaviour is contrary to the theoretical work by Bello and Wattenbarger (2010) and is used to present a simple method of removing the (apparent) skin from the data. The modified production data then can be analyzed using linear flow specialized plots for analysis. Along the same line, it can be stated that when analyzing the constant p_{wf} production data with apparent skin, one can remove the skin effects from all data by the method that Nobakht and Mattar (2012) proposed. Having done that, the modified rate data are analyzable using the CRM approach without the need for using an additional parameter i.e. skin effect (s^*), in the analysis.

3.9 Chapter Summary and Conclusions

This chapter presented a new methodology for predicting future rate or pressure of oil and gas reservoirs having linear flow geometry. The methodology consisted of simple coupling of equations for material balance, distance of investigation and boundary dominated flow, using the concept of continuous succession of pseudo-steady states (SPSS). Tested against analytical solutions for liquids and numerical simulations for gas reservoirs during both transient and boundary dominated flow, the approach showed excellent agreement which confirmed the ability of the method for reliably forecasting production. Key conclusions from this work are as below:

- The approach requires very little input data yet is based on rigorous engineering concepts which work during the transient as well as the boundary dominated flow periods.

- Skin causes additional pressure drop (or additional flow resistance) at the wellbore. In order to account for the skin in the CRM, resistance term has to be modified.
- The depletion equations can be used not only for analysis of late time production data, where BDF prevails, but also for early time data where transient flow is dominant. This indicates that complex systems with complicated mathematical (e.g. Laplace space) solutions can be represented adequately using simple concepts.

Chapter Four: Performance Analysis of Compartmentalized and Composite Reservoirs Using CRM

4.1 Scope of the study

In Chapter three the capacitance–resistance methodology for performing production forecasting was presented (Shahamat et al. 2014). During the course of that study, it was found that providing the flow regime is known or can be predicted, the succession of pseudo-steady states can be used to obtain reasonable pressure and rate information comparable with analytical or simulation methods during transient and boundary dominated flow regimes.

This chapter focuses on using the capacitance and resistance terms to develop a mathematical model for obtaining information related to the contrast in rock and fluid properties from the analysis of compartmentalized or composite systems. As such, first a brief description of compartmentalized reservoirs is given, followed by a review of the methods for their characterization. Then, the CRM is used to model flow of a liquid within a compartmentalized reservoir. The developed solutions are expressed using the capacitance and resistance terminology. Two tanks (and therefore two capacitance and resistance terms) are considered in the model – production and support. The length component in the capacitance and resistance terms for the support tank is treated as either a constant value or a variable according to the distance of investigation. The former implies that the support tank is a pure capacitance with no resistance, therefore no pressure gradient within it. This means instantaneous depletion (i.e. BDF) of the support tank. The latter, however, accounts for support tank transient flow. The derived mathematical solutions for these cases enable the generation of production type curves. Similarities

between constant rate and constant pressure scenarios are discussed and two simulation examples are implemented to validate the obtained solutions and type curves.

4.2 Background

Compartmentalized reservoirs are the result of segregation of a petroleum accumulation into a number of individual fluid/pressure compartments. They occur when flow is restricted across some form of boundaries in the reservoir. These boundaries are caused by a variety of geological features and processes and can be either completely sealed, across which no flow can occur, or partially sealed in which case the boundaries exhibit low to very low permeability (permeability barriers). The latter allows fluids and pressures of the compartments to equilibrate over geologic time-scales, and retards cross-flow between compartments during production. As a result, there will be pressure discontinuities across the reservoir, which according to Stewart and Whaballa (1989) can occur over near horizontal events such as shales or micaceous streaks and/or near vertical events such as partially communicating faults or turbidite lobe interfaces.

Evidence of compartmentalization has been observed in both oil and gas reservoirs (Junkin et al. 1992). A number of compartmentalized reservoirs have been discovered in different parts of the world including those in the North Sea (Fox et al. 1988), Texas Gulf Coast (Junkin et al. 1992), Australia (Malavazos and McDonough 1991) and Middle-East (Stewart 2011). Malavazos and McDonough (1991) presents a well-test case study of the Katnook reservoir located in South Australia, where the unit slope on the derivative plot of the extended draw-down of one of the wells indicates a charging-recharge mechanism. This extended draw-down test is shown in Figure 4.1, evidently indicating the effect of a

supporting compartment. The compartmentalized behaviour can also occur in particular meandering fluvial reservoirs. In these environments, the depletion and the lateral cross-flow between the laterally avulsing point bar deposits separated by the semi-permeable channel fills can effectively create a compartmentalized system (Hamdi 2012). Corbett et al. (2012) present an interesting well-test response in a meandering channelized system, where numerical well-test simulations and a multi-point statistics approach support the analytical well-test interpretation and the existence of effective sand bar compartments. Malavazos and McDonough (1991) demonstrated another channelized reservoir example where there is communication between the stacked channel compartments.

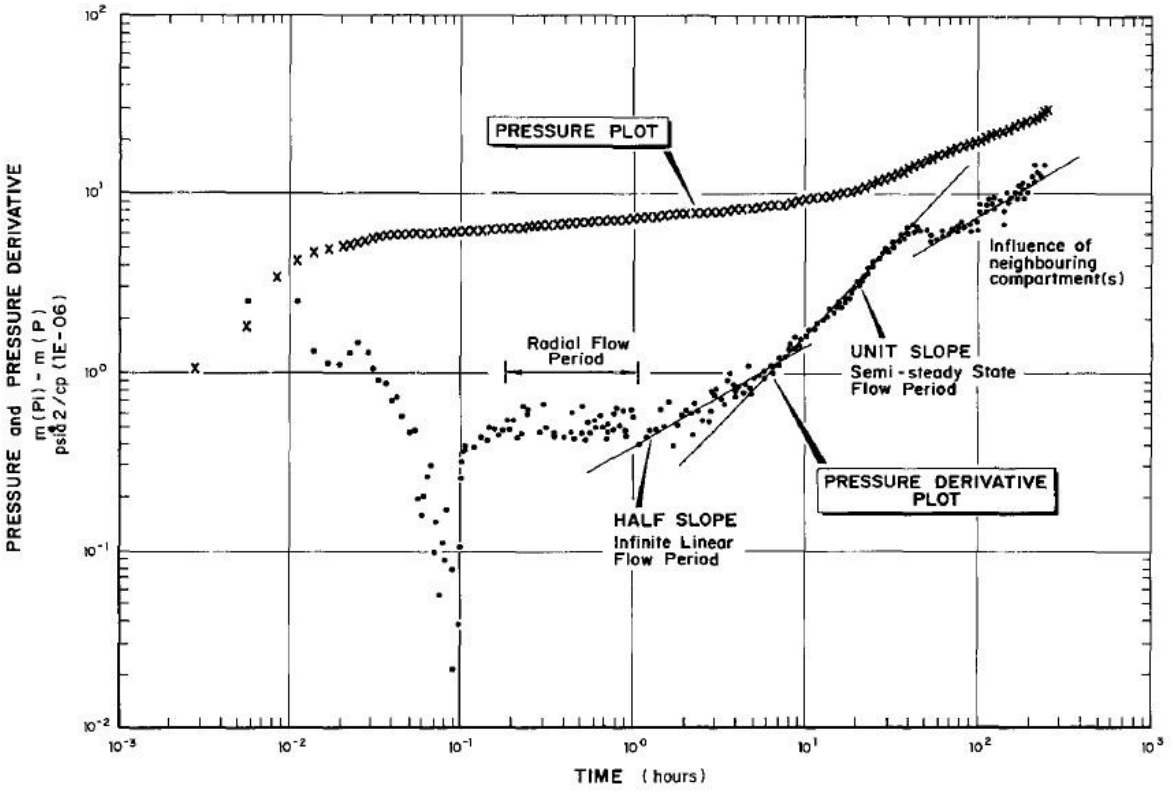

Figure 4.1: Extended draw-down response of an Australian compartmentalized reservoir, well Katnook 3 (Malavazos and McDonough 1991).

An important aspect of reservoir compartmentalization is a stacked channel realization where two sand bodies communicate hydraulically with each other through an overlapping area (interface). Chilingarian et al. (1992) gave an account of geologic and engineering aspects of compartmentalization in carbonate reservoirs and pointed out that reservoir compartmentalization may result not only from vertical and lateral lithofacies changes, but also from spatial variations stemming from processes of post-depositional diagenesis that create secondary porosity in the rocks.

Reservoir compartmentalization can also be considered in unconventional reservoirs, where multi-frac completion of horizontal wells create an SRV (Stimulated Reservoir Volume) region of enhanced permeability around the horizontal well that is surrounded by an unstimulated region of much lower permeability (Stalgorova and Mattar 2012). It is therefore reasonable to model the production behaviour of such a reservoir using a model where the production and support tanks are attributed to the SRV and unstimulated reservoir sections, respectively.

4.3 Compartment Detection and Analysis

Reservoir compartmentalization is detected primarily from observations of pressure discontinuities both areally and vertically (Stewart and Whaballa 1989). Such pressure variations over a producing field can be monitored using wireline formation testers (WFTs) and are due to differential depletion of the system caused by permeability barriers or reservoir heterogeneities of one kind or another (Stewart 2011). Bradley and Powley (1994) indicate other ways for the detection of reservoir compartmentalization, including the changes in mineralogy and drilling rates and also using electrical resistivity, sonic

velocity and density of shales. Reservoir simulation is another method which can be used to detect compartmentalization. Because of its complexity and associated degrees of freedom, though, this method is not justified in most cases before identifying and quantifying the major flow units and barrier resistances using other methods (Rahman 1998, Stewart and Whaballa 1989, Aguilera 2013).

There are also well-testing and production data analysis methods which can contribute to an improvement of the understanding of geology. Analytical models and related solutions can lead to a simplified description of the geological heterogeneities around the well and can provide good insights into the significance of various parameters affecting the transport phenomena (Massonnat et al. 1993). Stewart and Whaballa (1989) argue that an extended drawdown test should be performed to detect the limits of the producing compartment. They developed type curves to identify the extent of faulted boundaries between compartments. By matching the late time data, they estimated the resistance to flow of fluid at the boundary (which they call transmissibility). Their approach is based on the use of single phase material balance equations, the concepts of boundary pressure time delay and desuperposition to predict pressures over different flow regimes. Along the same lines, Rahman (1998) develops analytical 1D, 2D and 3D solutions for constant rate transient flow in compartmentalized systems.

Stewart (2011) presented a mathematical method for well-test analysis of a two-cell compartmentalized system. He presented the material balance equations in dimensionless terms and discussed the existence of two derivative unit slopes in Logarithmic scales indicating depletion of the well and support compartments. He considered the effect of compartment volumes, neglecting the variations in other reservoir parameters, e.g.

permeability, between the compartments. This work does not involve the mathematical complexities of Rahman (1998) and is appealing from a practical point of view.

In the following sections, the capacitance and resistance terms introduced in the previous chapter are used to model the behaviour of a compartmentalized reservoir. Two tanks (and therefore two capacitance and resistance terms) are considered in the model – production and support. The support tank feeds the production tank; therefore, its contribution starts after investigating the production tank. The length component in the capacitance and resistance of the support tank is first assumed to be constant, equal to the size of the support tank in the y-direction. This assumption implies instantaneous depletion (i.e. BDF) of the support tank. Based on this assumption and by using the fluid-flow and material balance equations for both tanks, simple analytical solutions are derived for constant rate and constant pressure production of a compartmentalized system. Using the distance of investigation equation in the capacitance and resistance terms, it is shown that the solutions can be easily modified to account for transient flow within the support tank. The derived mathematical solutions enable the generation of production type curves which can be used to characterize a compartmentalized system and obtain meaningful information related to the contrast in rock and fluid properties between the compartments.

4.4 Mathematical Development

The mathematical framework of this study is based on the capacitance-resistance approach. Adapted from Shahamat and Aguilera (2010), the configuration of the different sections of a compartmentalized reservoir is depicted using a tank model (Figure 4.2). The production tank is directly connected to the wellbore through the sand pack which implies a flow

resistance (R) to the wellbore. In addition, there is a support tank which is connected to the production tank through another barrier with a flow resistance, R_s. Depending on the values of flow capacitance (C and C_s) and resistance (R and R_s) there are various degrees of pressure communication between these compartments. The base geometry of each resistance is according to Figure 3.1(a) which implies transient linear flow.

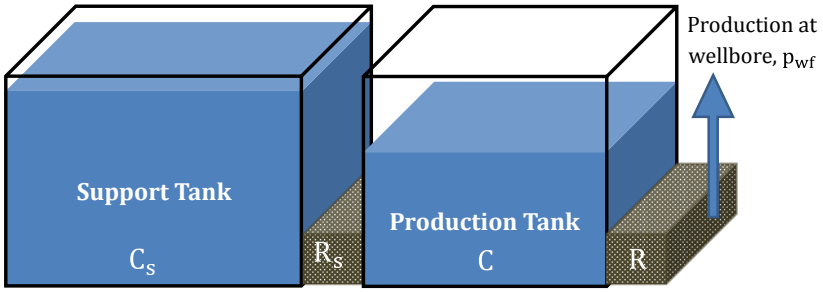

Figure 4.2: Tank representation of a compartmentalized reservoir.

It is assumed that the contribution of the support tank starts after investigating the production tank. This means that by the time the support tank starts feeding the production tank, the characteristics of the production tank (i.e. its C, R and t_{BDF}) are known (methodologies in the previous chapter can be used to determine them). These properties are used for modeling the compartmentalized reservoir behaviour.

As mentioned in chapter two, there is a length component in the capacitance and resistance terms that changes during transient flow according to the distance of investigation ($y_{inv,s}$, for the support tank). For simplicity, the support length component is assumed constant and equal to the size of the support tank in the y-direction ($y_{e,s}$). This way, the support tank in Figure 4.2 represents a pure capacitance, it exhibits no pressure gradient and therefore its pressure can be reported by one single pressure value, i.e. $p_{avg,s}$.

Using the fluid-flow equation for relating the production rate to the average pressure of the production tank (Eq. 3.3), one gets:

$$q = \frac{1}{R}\left(p_{avg} - p_{wf}\right) \quad \text{Eq. 4.1}$$

Moreover, for relating the average pressure of the support tank with the average pressure of the production tank fluid-flow equation is used through the following formula:

$$q_s = \frac{1}{R_s}\left(p_{avg,s} - p_{avg}\right) \quad \text{Eq. 4.2}$$

Linear flow regime within the support resistance leads to the following definition, $R_s = \left(\frac{\beta_1 B\mu}{2\pi kh}\right)_s \times \left(\frac{y_{e,s}}{x_f}\right)$. In the above two equations, q and q_s are expressed in StbD.

In addition to Eq. 4.1 and Eq. 4.2 for describing the behaviour of a compartmentalized system, the material balance equations for both tanks are employed. The material balance equation (i.e. compressibility equation) for the production tank is according to Eq. 4.3:

$$C\frac{dp_{avg}}{dt} = q_s - q \quad \text{Eq. 4.3}$$

Similarly, the compressibility equation for the support tank is according to Eq. 4.4.

$$C_s\frac{dp_{avg,s}}{dt} = -q_s \quad \text{Eq. 4.4}$$

In the above two equations, capacitances (C and C_s) are expressed in Stb/psia. It is noted that capacitance is the multiplication of pore volume and total compressibility.

Eq. 4.1 through Eq. 4.4 are the building blocks of the proposed methodology. Solutions to different production constraints (i.e. constant terminal rate or constant terminal pressure) are obtained by defining different dimensionless parameters, as shown in the following sections.

4.4.1 Constant terminal rate production (Reservoir Limit Testing):

For the constant terminal rate production (CTR) the dimensionless pressure and time, p_{DM} and t_{DM}, are defined as follows:

$$p_{DM} = \frac{(p_i - p)}{q \times R} \qquad \text{Eq. 4.5}$$

and,

$$t_{DM} = \frac{t}{C \times R} \qquad \text{Eq. 4.6}$$

It is noted that the dimensionless pressure defined in Eq. 4.5 is different from the definition used in the classical well-testing literature. In well-testing literature the dimensionless pressure is defined based on wellbore pressure, whereas Eq. 4.5 is written in terms of average reservoir pressure (to be used in Eq. 4.1 through Eq. 4.4).

In addition, two additional dimensionless parameters are introduced to characterize reservoirs with two communicating compartments. The first parameter, F_R, is the ratio of resistances, and reflects the combined effect of contrast in permeability, viscosity, formation thickness and skin factor, between the production and support tanks:

$$F_R = \frac{R}{R_s} \qquad \text{Eq. 4.7}$$

The second parameter, F_c, is the ratio of flow capacitances, and reflects the combined effect of changes in reservoir pore volume and compressibility of the production tank with respect to the support tank:

$$F_c = \frac{C}{C_s} \qquad \text{Eq. 4.8}$$

While normally one would expect to define the ratios of resistance and capacitance with respect to the production tank (i.e. $\frac{R_s}{R}$ and $\frac{C_s}{C}$), defining F_R and F_c according to Eq. 4.7 and Eq. 4.8 simplify the formulations and obtained solutions in a concise form. As such, smaller values of F_R (or F_c) indicate larger values of resistance (or capacitance) of the support tank compared with the production tank.

Using the dimensionless variables defined in Eq. 4.5 through Eq. 4.8, and upon some mathematical manipulations, Eq. 4.3 and Eq. 4.4 take the following dimensionless forms, respectively:

$$\frac{dp_{DM}}{dt_{DM}} = F_R(p_{DMs} - p_{DM}) - 1 \qquad \text{Eq. 4.9}$$

$$\frac{dp_{DMs}}{dt_{DM}} = -F_R F_c(p_{DMs} - p_{DM}) \qquad \text{Eq. 4.10}$$

In these equations, p_{DM} and p_{DMs} are the dimensionless pressures of the production and support compartments. Eq. 4.9 and Eq. 4.10 construct a system of linear differential equations, which can be solved to obtain the pressure of the support and production tanks. This system can be solved using matrix algebra routines. The detailed procedure for the solution is given in Appendix C. The resulting dimensionless pressure of the production tank (p_{DM}) is given by the following closed form:

$$p_{DM} = p_{DM,BDF} + \left(1 + \frac{F_R}{\lambda_2}\right)(t_{DM} - t_{DM,BDF}) + \frac{F_R}{\lambda_2}\left(\frac{1}{\lambda_2} + p_{DM,BDF}\right)\left(1 - e^{\lambda_2(t_{DM} - t_{DM,BDF})}\right) \qquad \text{Eq. 4.11}$$

and the solution for the support tank (p_{DMs}) is:

$$p_{DMs} = \left(1 + \frac{F_R}{\lambda_2}\right)\left\{(t_{DM} - t_{DM,BDF}) + \left(\frac{1}{\lambda_2} + p_{DM,BDF}\right)\left(1 - e^{\lambda_2(t_{DM} - t_{DM,BDF})}\right)\right\} \qquad \text{Eq. 4.12}$$

where, $\lambda_2 = -F_R(1 + F_c)$ is the smallest eigenvalue of the matrix of coefficients for the system of Eq. 4.9 and Eq. 4.10. In these equations $t_{DM,BDF}$ and $p_{DM,BDF}$ are the dimensionless time and pressure at the beginning of the BDF for the production tank and can be determined using the CRM in the previous Chapter. Detailed explanation of these equations is given in section 4.5.

4.4.2 Constant terminal pressure production (Rate Transient Analysis):

For the case of constant terminal pressure (CTP) production, the dimensionless rate variable, q_{DM}, is defined as follows:

$$q_{DM} = \frac{q \times R}{(p_i - p_{wf})} \qquad \text{Eq. 4.13}$$

The dimensionless rate as defined in this equation is based on the average reservoir pressure and therefore is the equivalent linear flow form of the Fetkovich rate decline parameter (Fetkovich 1980). Employing the dimensionless rate (Eq. 4.13) and time (Eq. 4.6) in Eq. 4.1 through Eq. 4.4, the constant pressure behaviour of the compartmentalized system is obtained based on the solution of a system of ordinary differential equations:

$$\frac{dq_{DM}}{dt_{DM}} = -q_{DM} + q_{DMs} \qquad \text{Eq. 4.14}$$

$$\frac{dq_{DMs}}{dt_{DM}} = F_R q_{DM} - (F_R + F_c F_R) q_{DMs} \qquad \text{Eq. 4.15}$$

In these equations, $q_{DM}$and q_{DMs} are dimensionless rates for the production and support compartments. Similar to the constant terminal rate solution, these equations can be solved using matrix algebra routines to obtain the declining rate behaviour of compartmentalized

reservoirs. The detailed procedure for the solution is outlined in Appendix D. The resulting dimensionless rate of the production tank (q_{DM}) is given in the following closed form:

$$q_{DM} = q_{DM,BDF}\left\{\left(\frac{\lambda_2+1}{\lambda_2-\lambda_1}\right)\times e^{\lambda_1(t_{DM}-t_{DM,BDF})} - \left(\frac{\lambda_1+1}{\lambda_2-\lambda_1}\right)\times e^{\lambda_2(t_{DM}-t_{DM,BDF})}\right\} \qquad \text{Eq. 4.16}$$

Similarly, the solution for the support tank (q_{DMs}) is obtained according to Eq. 4.17:

$$q_{DMs} = q_{DM,BDF}\left(\frac{(\lambda_1+1)(\lambda_2+1)}{(\lambda_2-\lambda_1)}\right)\left\{e^{\lambda_1(t_{DM}-t_{DM,BDF})} - e^{\lambda_2(t_{DM}-t_{DM,BDF})}\right\} \qquad \text{Eq. 4.17}$$

It is noted that in these two equations, $\lambda = \frac{-(1+F_R(1+F_c))\pm\sqrt{(1-F_R(1+F_c))^2+4F_R}}{2}$, adopting the convention that λ_1 and λ_2 correspond to positive (+) and negative (-) signs, respectively. In these equations $t_{DM,BDF}$ and $q_{DM,BDF}$ are the dimensionless time and rate at the beginning of the BDF for the production tank and can be determined using the CRM in the previous Chapter. Detailed explanation of these equations is given in the next section.

4.5 Examination of the Results

In order to discuss the behaviour of the obtained equations in a systematic manner, first the equations obtained for the constant rate production are elaborated and after that the constant pressure production behaviour is discussed.

4.5.1 Constant terminal rate production

The behaviour of a compartmentalized reservoir can be better understood using the principle of superposition. The pressure change in the production tank is expressed as the depletion of a single tank without any support (Δp^{c}) subtracted by the pressure maintenance caused by the support tank (Δp^{cs}). This means that the pressure change of a single tank can be expressed as below:

$$\Delta p = \Delta p^{c} - \Delta p^{cs} \qquad \text{Eq. 4.18}$$

Rearranging and writing the above equation in dimensionless form, one gets:

$$p_{DM}{}^{cs} = p_{DM}{}^{c} - p_{DM} \qquad \text{Eq. 4.19}$$

As evident from the definition of $p_{DM}{}^{c}$, an equation for its behaviour can be obtained by using Eq. 4.11, when R_s approaches infinity and therefore $F_R = 0$. This leads to the following relation:

$$p_{DM}{}^{c} = p_{DM,BDF} + \left(t_{DM} - t_{DM,BDF}\right) \qquad \text{Eq. 4.20}$$

Using Eq. 4.20 and Eq. 4.11 inside Eq. 4.19 gives:

$$p_{DM}{}^{cs} = -\frac{F_R}{\lambda_2}\left(t_{DM} - t_{DM,BDF}\right) - \frac{F_R}{\lambda_2}\left(\frac{1}{\lambda_2} + p_{DM,BDF}\right)\left(1 - e^{\lambda_2\left(t_{DM} - t_{DM,BDF}\right)}\right) \qquad \text{Eq. 4.21}$$

Note that this equation is different from Eq. 4.12 and is useful for illustrating the contribution of the support tank. Figure 4.3 and Figure 4.4 demonstrate the behaviour of a compartmentalized reservoir and the support contribution compared with a single tank reservoir model. Figure 4.3 shows dimensionless pressure versus dimensionless time in logarithmic scales while the right hand side of the figure gives the Cartesian plot of pressure versus time. It is evident from these figures that during transient flow, the behaviour of both single and double tank models are identical. However, the effects of the support tank are felt after reaching the boundaries of the production tank. During this period, the log-log plot gives a straight line of unit slope for the single tank model which corresponds to a straight line on the Cartesian plot shown on Figure 4.4. Deviation from this behaviour (unit slope on the log-log plot or late time straight line on the Cartesian plot) is due to the pressure contribution of the support tank. The double-sided black arrows on

the Cartesian plot clearly demonstrate that the amount of deviation is equal to the support contribution. It is noted that at late times, i.e. total system pseudo-steady state, the two compartments are depleted at the same rate with a constant pressure difference between them. Subtracting Eq. 4.12 from Eq. 4.11 and evaluating the result at late time gives the pressure difference according to the following relation:

$$p_{DM} - p_{DMs} = -\frac{1}{\lambda_2} \qquad \text{Eq. 4.22}$$

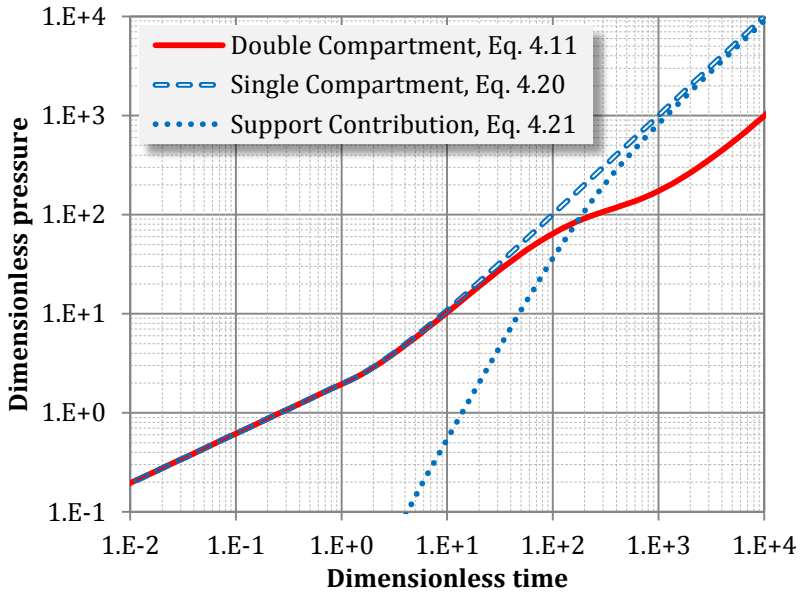

Figure 4.3: Log-log plot of p_{DM} vs. t_{DM}, comparing behaviour of single tank and 2-compartment (F_R = 0.01 and F_c = 0.1) models. Also shown is the contribution of the support tank.

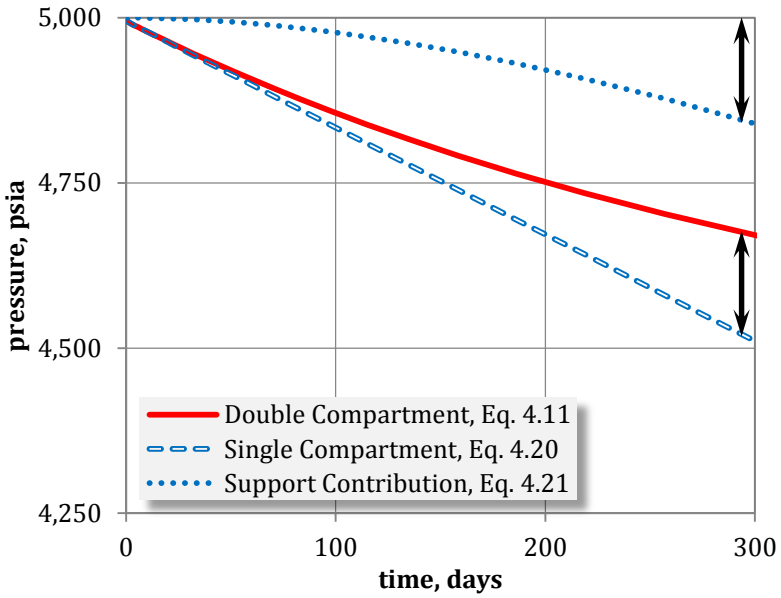

Figure 4.4: Cartesian plot of pressure vs. time, comparing behaviour of single tank and 2-compartment (F_R = 0.01 and F_c = 0.1) models. Also shown is the contribution of the support tank.

One can also determine the points where there are major changes in the plot of pressure versus time. These points include the start of boundary dominated flow (BDF) for the production tank, the time where deviation from the first unit slope on the log-log plot of p_{DM} versus t_{DM} takes place, and the time attributed to the start of the total system behaviour. The equation for the distance of investigation (Eq. 3.1) is used to identify the time at which these changes occur in the behaviour of a compartmentalized reservoir (see Appendix E). Writing this equation in terms of dimensionless variables defined in this work, one can obtain the time at which BDF of the production tank starts:

$$t_{DM,BDF} = \frac{\pi}{2}\frac{1}{\alpha_1{}^2\alpha_2} \qquad \text{Eq. 4.23}$$

The time where deviation from the single tank behaviour happens is determined from the following equation:

$$t_{DM} = t_{DM,BDF}\left(\frac{F_R+1}{F_R}\right) \quad \text{Eq. 4.24}$$

and the time at which the total system BDF occurs can be determined using the distance of investigation equation for the total system:

$$t_{DM} = t_{DM,BDF}\left(\frac{F_R F_c+1}{F_R F_c}\right) \quad \text{Eq. 4.25}$$

These characteristic points are derived based on the distance of investigation equation and are detailed in Appendix E.

In addition to the above characteristic points, one can calculate the well-testing or semilog derivative (Der) of Eq. 4.11 according to the following equation:

$$\text{Der} = \left(1+\frac{F_R}{\lambda_2}\right)t_{DM} - F_R\left(\frac{1}{\lambda_2}+p_{DM,BDF}\right)t_{DM}e^{\lambda_2(t_{DM}-t_{DM,BDF})} \quad \text{Eq. 4.26}$$

Figure 4.5 shows a plot of dimensionless pressure and the well-testing derivative versus dimensionless time with inclusion of the points at which the transient flow in the production tank ends (point A), the support tanks becomes active (B) and the BDF for the composite system begins (C). This figure demonstrates the powerful ability of the well-testing derivative for detecting different flow regimes. Compared with the dimensionless pressure plot, the well-testing derivative shows the start of joint BDF at a much earlier time. In addition, it is noted that while the dimensionless pressure curve manifests a half slope during the transition period between points B and C, the welltesting derivative does not exhibit a half slope and therefore indicates that the flow regime during this period is not linear flow. This powerful diagnostic feature of derivative plot is used to advantage in well-test analysis for the detection of different flow regimes. In the context of production data analysis, however, the sensitive nature of the derivative amplifies the inherent noise in

the production data so much that it makes the derivative plot essentially useless. Accordingly, it is reasonable to use the developed pressure solutions (rather than their derivatives) to make acceptable production analysis and therefore use the points with significant changes in the production behaviour to simply characterize a compartmentalized system (via Eq. 4.24–Eq. 4.26).

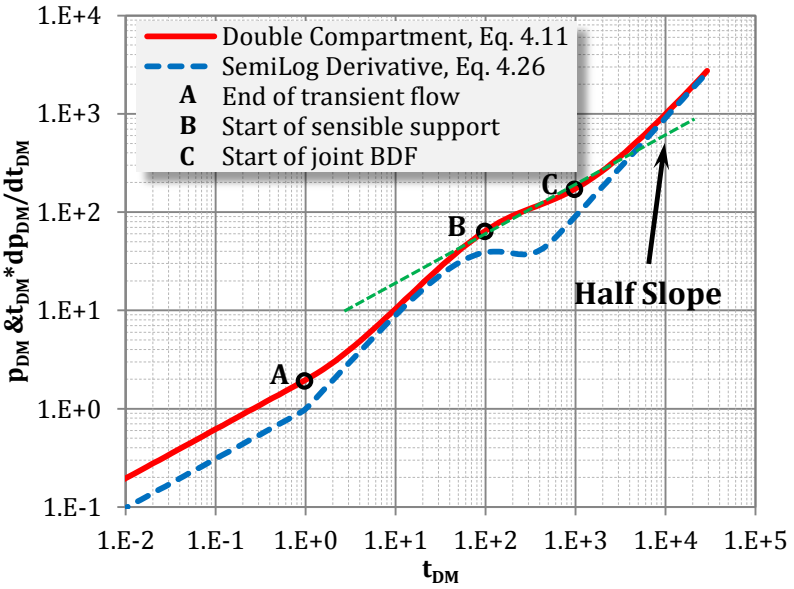

Figure 4.5: Log-log plot of p_{DM} and well-testing derivative (Der) versus t_{DM}, along with the position of the characteristic points for the behaviour of the compartmented reservoir.

Evident from Eq. 4.11, the behaviour of the double compartment model is a function of the value of F_c and F_R. These parameters determine the time at which the straight line attributed to the behaviour of the total system takes place. Figure 4.6 and Figure 4.7 show the effect of F_c and F_R on the behaviour of the double tank model, respectively. As mentioned previously, smaller values of F_R (or F_c) indicate larger resistance (or capacitance) of the support tank compared with the production tank and therefore later appearance of the total system unit slope.

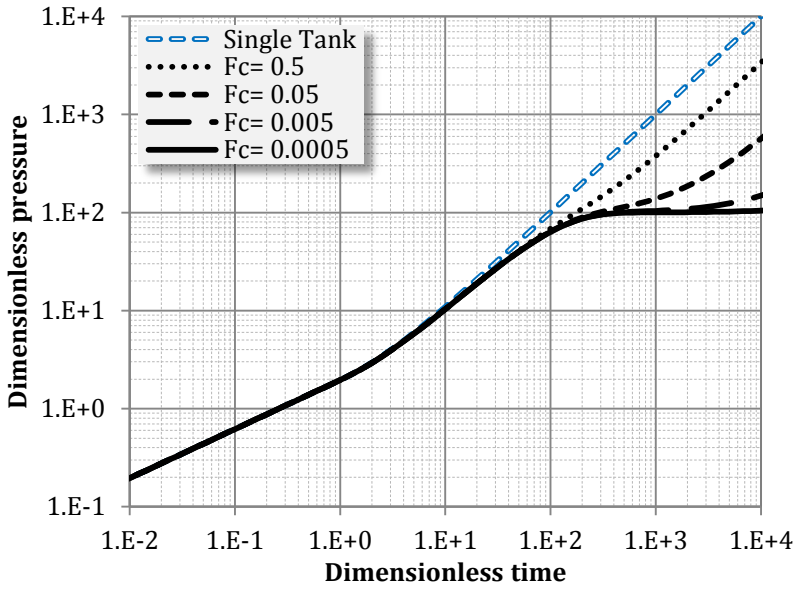

Figure 4.6: Effect of F_c on the CTR response of a compartmentalized system with F_R = 0.01. Smaller value of F_c indicates a support tank with larger capacitance and therefore lower p_{DM}.

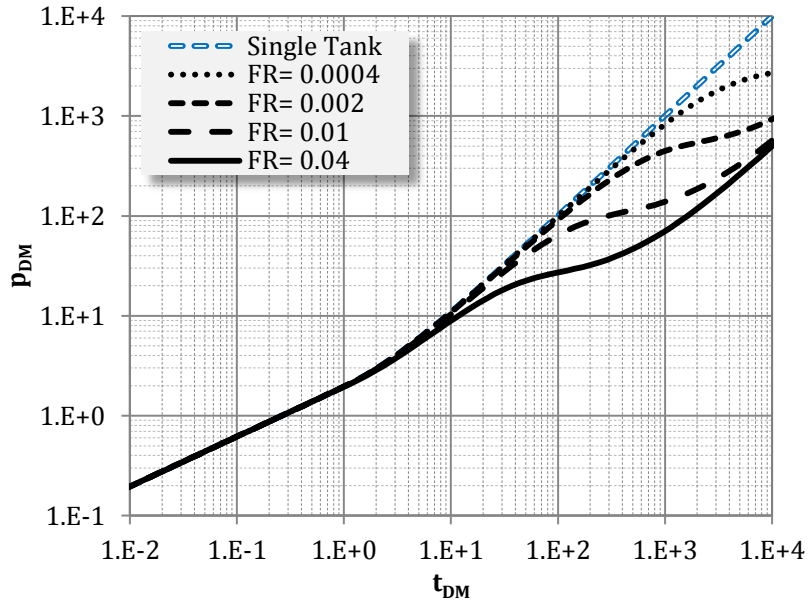

Figure 4.7: Effect of F_R on the CTR response of a compartmentalized system with F_c = 0.05. Smaller value of F_R indicates a support tank with larger resistance and therefore higher p_{DM}.

Using Eq. 4.11, type curves for different values of F_c and/or F_R can be easily generated which, through a simple type curve matching approach, can be used for estimating the contrast of capacitance (F_c) and resistance (F_R) between production and support compartments. These parameters can be used to compare the hydraulic diffusivity of the two reservoir sections.

4.5.2 Constant terminal pressure production

Constant pressure production from a two-compartment reservoir yields a double exponential decline in rate; each is attributed to depletion of one compartment. A log-log plot of dimensionless rate versus dimensionless time (Eq. 4.16) for typical values of $F_R = 0.01$ and $F_c = 0.05$ is given in Figure 4.8. This figure demonstrates the difference between the behaviour of a single tank and that of a two-tank reservoir. Depletion of a single tank results in the well-known exponential decline (Fetkovich 1980) which can be obtained by substitution of $\lambda_1 = 0$ and $\lambda_2 = -1$ in Eq. 4.16:

$$q_{DM} = q_{DM,BDF} \times e^{-(t_{DM} - t_{DM,BDF})} \qquad \text{Eq. 4.27}$$

Based on these parameters and using the equation for the distance of investigation, the points where major changes take place in the plot of rate versus time can be determined. The first point is the start of the boundary dominated flow (BDF) for the production tank, which as in the case of constant rate can be determined with the use of Eq. 4.23. The second point is the time where deviation from the single tank behaviour happens. This can be determined according to the equation:

$$t_{DM} = t_{DM,BDF} + \frac{1}{\lambda_1 + 1} \times ln\left(\frac{\lambda_2 - \lambda_1}{\lambda_2 + 1}\right) \qquad \text{Eq. 4.28}$$

The time for the total system BDF can be determined using the distance of investigation equation for the total system, similar to the case of constant rate production, Eq. 4.25. Figure 4.8 shows the location of the characteristic points (end of transient flow in the production tank (A), start of sensible support tank contribution (B) and start of BDF for the composite system (C)) on the log-log plot of q_{DM} vs. t_{DM} for $F_R = 0.01$ and $F_c = 0.1$. It depicts that the rate decline associated with such a compartmentalized system exhibits a period following depletion of the production tank where the flow rate is constant. q_{DM} for this period can be obtained from the second exponential term in Eq. 4.16.

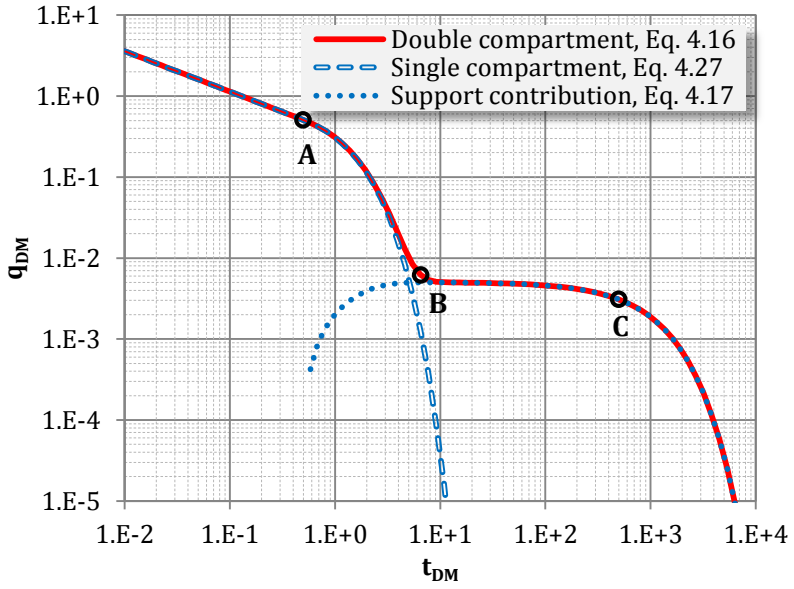

Figure 4.8: Log-log plot of q_{DM} vs. t_{DM} showing the behaviour of a double tank model, $F_R = 0.01$ and $F_c = 0.1$, the position of its characteristic points and its comparison with the single tank model.

Similar to the CTR, deviation from the single tank behaviour is because of the pressure contribution of the support tank and is a function of the values of F_c and F_R. These parameters determine the behaviour of the system. Figure 4.9 and Figure 4.10 show the effect of F_c and F_R on the double tank model rate decline.

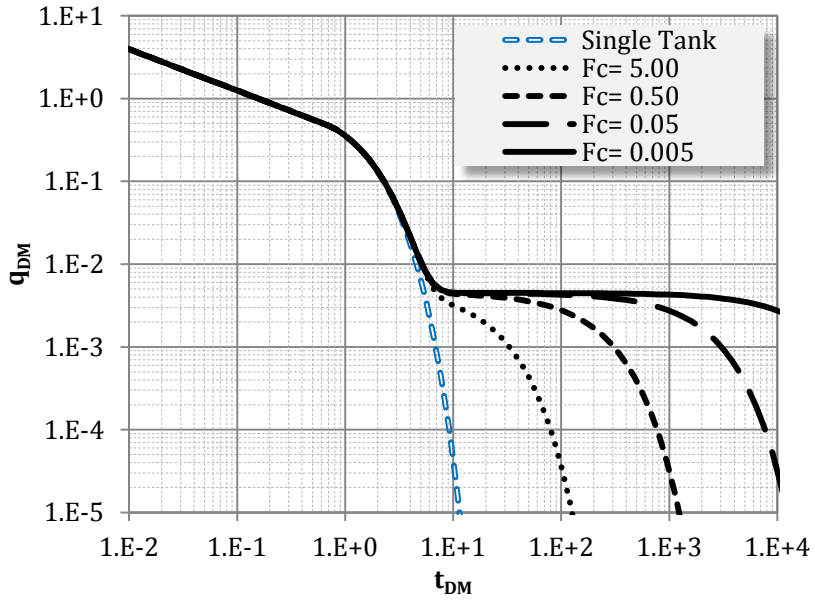

Figure 4.9: Effect of F_c on the CTP response of a compartmentalized system with F_R = 0.01. Smaller value of F_c indicates a support tank with larger capacitance and therefore higher q_{DM}.

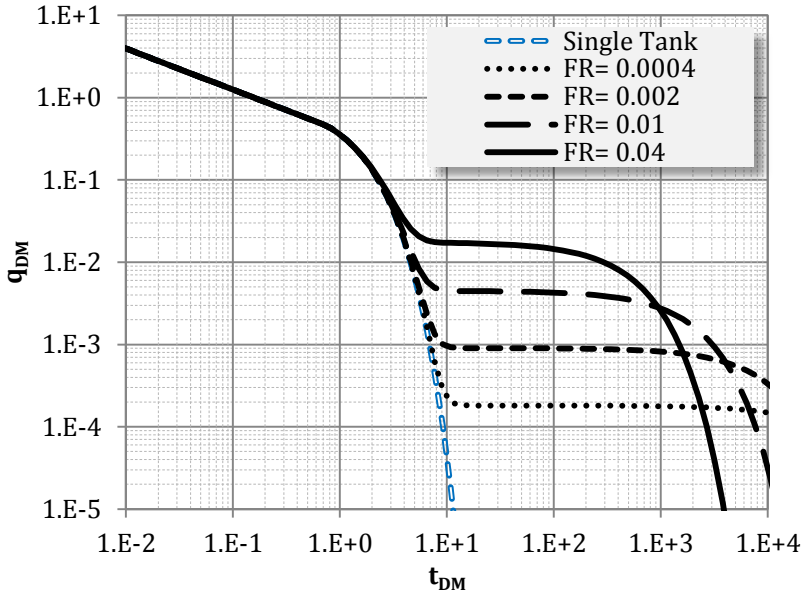

Figure 4.10: Effect of F_R on the CTP response of a compartmentalized system with F_c = 0.05. Smaller value of F_R indicates a support tank with larger resistance and therefore lower q_{DM}.

Using Eq. 4.16, type curves for different values of F_c and/or F_R can be easily generated which can be used through a simple type curve matching approach to estimate the contrast of capacitance (F_c) and resistance (F_R) between production and support compartments. These parameters reflect the effective variation of reservoir and fluid properties across the compartments.

4.6 Transient Flow within the Support Tank

The equations developed so far are based on the premise of instantaneous (or relatively instantaneous) depletion of the support tank. This means that in the above equations the transient flow in the support tank is ignored. As a result, immediately after the start of support tank contribution, its flow regime is assumed to be BDF. This is a reasonable assumption for cases where the size of the support and production tanks and also their permeabilities are very close to each other. However in cases where the size of the support tank is bigger than that of the production compartment, the support permeability should be higher in order to satisfy its relative instant depletion. In practice, this may not be the case and the production tank may be surrounded by a number of lower (instead of higher) permeability sections. Moreover, having a lower-permeability support tank would require extended transient flow to be considered.

In order to extend the application of the proposed model for capturing transient flow within the support tank, the distance of investigation concept is employed. The length components in the capacitance and resistance parameters of the support tank are allowed to change with time according to the distance of investigation equation (Eq. 3.1) until reaching its BDF. This implies that parameters F_c and F_R decrease with time and become constant only at late

times, therefore they cannot be used for type curve generation. For the purpose of producing the appropriate type curves, F_c^* and F_R^* are defined, where $F_c^* = F_c \times \frac{y_{inv,s}}{y_e}$ and $F_R^* = F_R \times \frac{y_{inv,s}}{y_e}$. These parameters indicate the ratios of the capacity and resistivity of the production to support tank, rather than their capacitance and resistance, and exclude the effect of variable distance introduced in the support compartment by $y_{inv,s}$ (Shahamat et al. 2014). Using these parameters and just for demonstration purposes, the obtained CTR and CTP type curves for typical values of F_R^* and F_c^* are shown in Figure 4.11 and Figure 4.12, respectively.

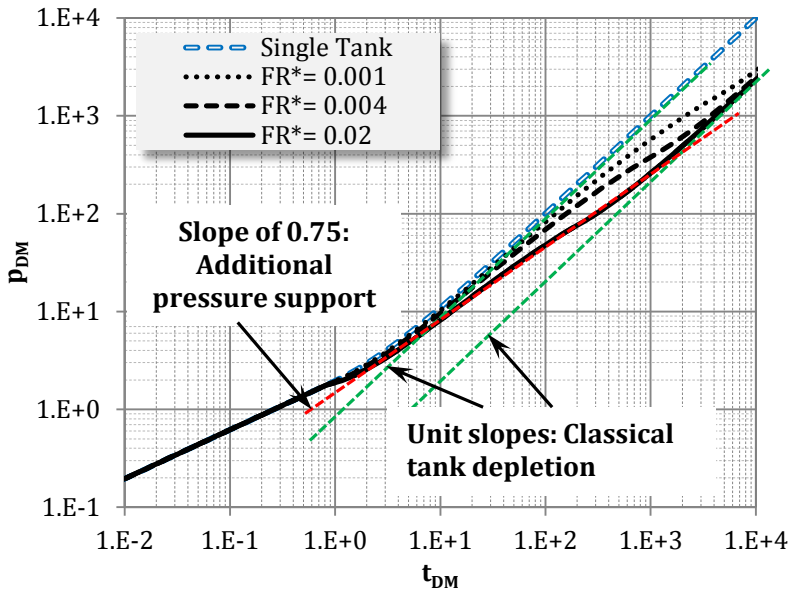

Figure 4.11: Effect of F_R^* on the CTR response of a compartmentalized system with F_c^* = 0.3.

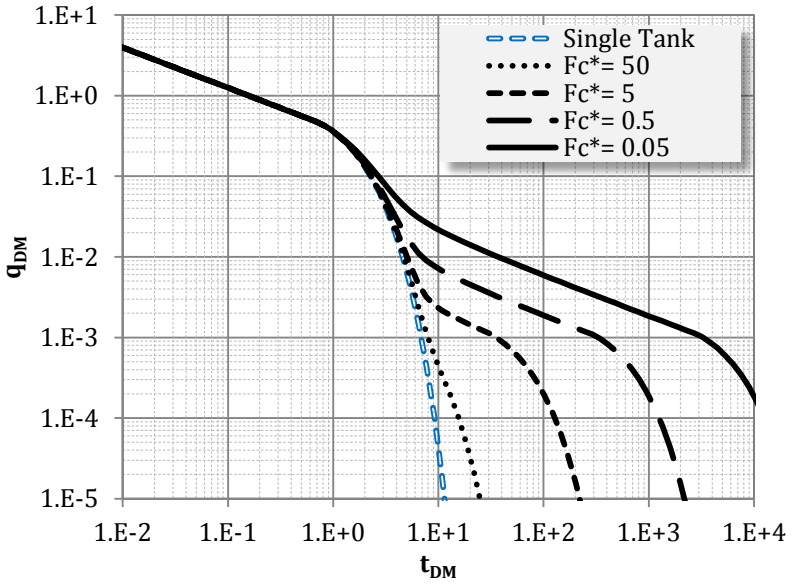

Figure 4.12: Effect of F_c^* on the CTP response of a compartmentalized system with $F_R^* = 0.005$.

Figure 4.11 is the CTR response of a compartmentalized system considering the effect of transient flow within the support tank. It shows that contribution of the support tank can considerably alter the production signature in such a way that the classic half or unit slopes may not exist for long times. In this figure, there is one case with a slope of 0.75 during the transition period for almost 3 log cycles. Figure 4.12 depicts the effect of F_c^* on the CTP response of a reservoir. It illustrates two straight line of slope -0.5 on the log-log plot of q_{DM} versus t_{DM} indicating linear flow regime. Each of these linear periods is followed by significant drops in dimensionless rate that correspond to exponential declines signifying depletion in the associated compartment.

The proposed tank model and developed type curves can be used to characterize a compartmentalized or composite reservoir. Examples of their application are given in the next section through two simulation examples.

4.7 Validation

4.7.1 Simulation Example, Case 1

Using a commercial numerical simulator, Case 1 is a single phase liquid composite reservoir with contrasting reservoir properties shown in Table 4.1 and reservoir schematic depicted in Figure 4.13. The production well is in the center of the higher permeability reservoir section, is hydraulically fractured and is put on production for about 12 years.

Table 4.1: Reservoir and fluid properties used for constructing simulation results.

Parameter	Region 1	Region 2
k (md)	0.5	0.01
ϕ (fraction)	0.04	0.06
c_f (psia^{-1})	3×10^{-6}	9×10^{-6}

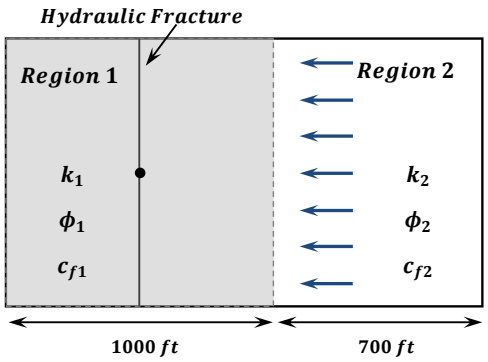

Figure 4.13: Reservoir geometry used for simulation of a composite reservoir.

Constant rate and constant pressure production of the well are shown in Figure 4.14 and Figure 4.15, respectively. Using the developed type curves in Figure 4.11 and Figure 4.12 and through a type curve matching process, the parameters are determined to be $F_c^* = 0.28$ and $F_R^* = 0.02$. Calculation of these parameters based on the simulation input data give identical values. This consistency validates the approach and developed equations for production data analysis of a composite reservoir.

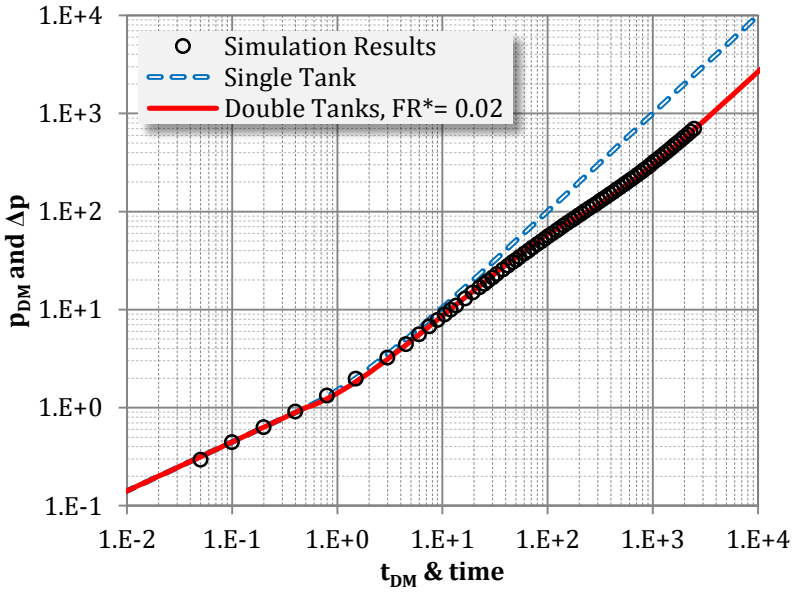

Figure 4.14: Type curve match results for CTR production of Case 1.

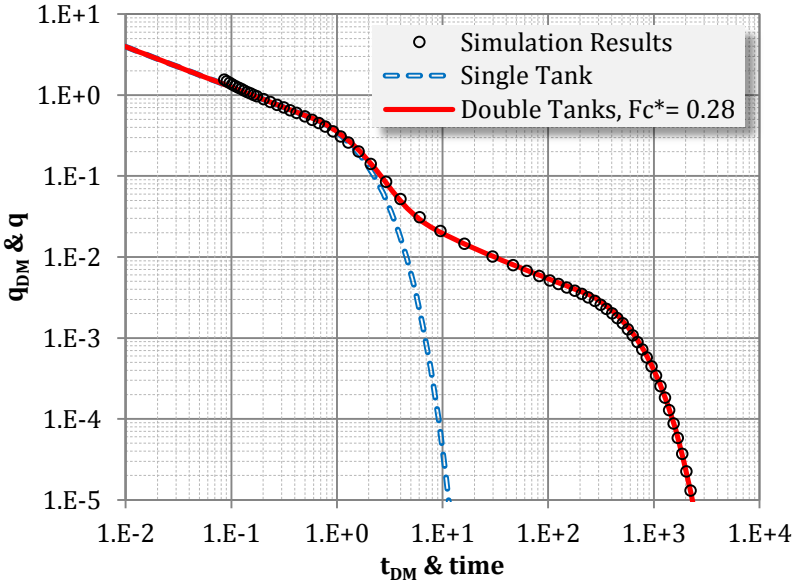

Figure 4.15: Type curve match results for CTP production of Case 1.

4.7.2 Simulation Example, Case 2

In this case, a compartmentalized reservoir with similar properties and reservoir configuration as the previous example is used. Compartmentalization is imitated using a thin lower permeability region between the two reservoir sections. Such a lower permeability region (which in this case is 5% of the lower permeability region) represents a fault or low permeability shale barrier and is used to simulate a compartmentalized reservoir. The production well in the center of the higher permeability region is hydraulically fractured and is put on production for 12 years under either constant rate or constant pressure production.

Existence of the low permeability barrier delays the production from the lower permeability region in such a way that its transient flow (half slope) is absent from the well's production signature. As a result, one can assume instantaneous support and simply use Eq. 4.11 and Eq. 4.16 for its production analysis. For the CTR production data and using type curves similar to what presented in Figure 4.6, one can obtain a perfect match as illustrated in Figure 4.16 showing $F_R = 1.2 \times 10^{-3}$ and $F_c = 0.2$. It is noted here that F_R represents the ratio of the flow resistance between the production and support compartments. For the simulation case defined in this example, it fuses the effect of a flow barrier (low permeability region) in addition to the contrast of permeability between the two reservoir sections. This is an advantage of this method as it combines the effect of different factors affecting production at the wellbore in a single term to be used in the type curve analysis. On the other hand, F_c represents the ratio of capacitance of production and support compartments. This term represents the combined effects of the drainage volume and compressibility associated with each compartment.

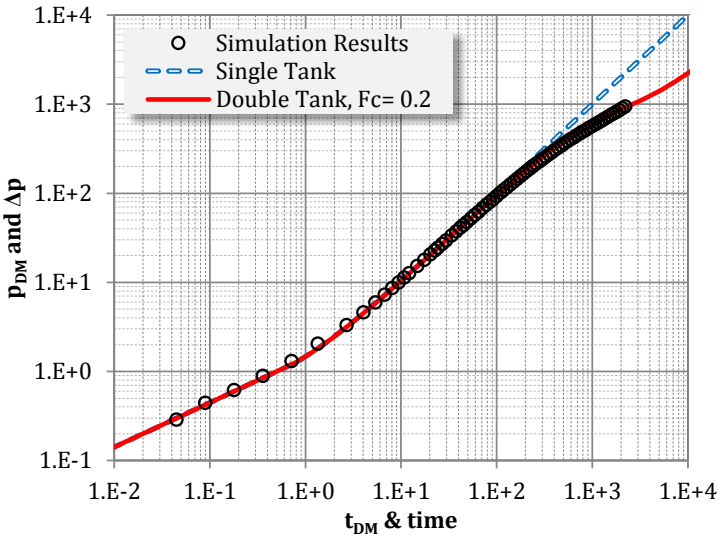

Figure 4.16: Type curve match results for CTR production of Case 2.

Analyzing the CTP production data and using type curves similar to those in Figure 4.9, the match (Figure 4.17) yields $F_R = 2.3 \times 10^{-3}$ and $F_c = 0.2$. Comparison of the matching parameters for CTP and CTR indicates different values of F_R for the same compartmentalized system. The difference is attributed to the effect of transient flow within the support compartment for each of these production scenarios. In other words, the propagation of pressure disturbance in the reservoir as a result of constant terminal rate and constant terminal pressure is different for systems that exhibit linear flow. This leads to different values of F_R obtained from analysis of constant rate and constant pressure solutions.

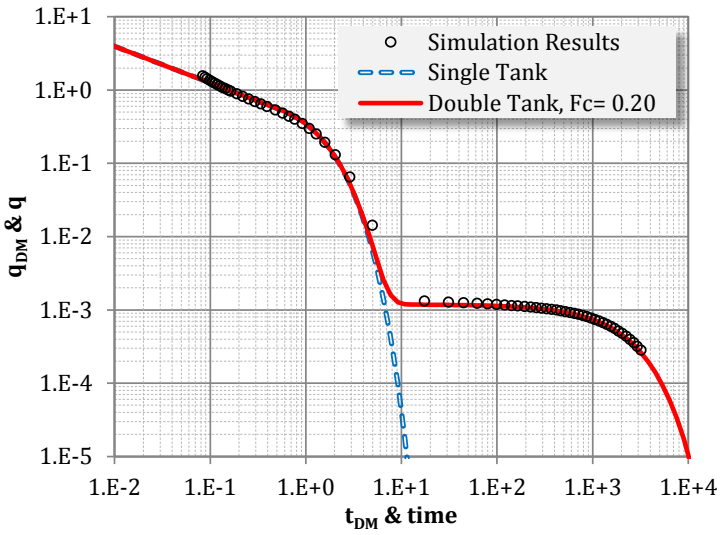

Figure 4.17: Type curve match results for CTP production of Case 2.

4.7.3 Discussion

Comparison of the results for the composite and compartmentalized reservoir models in the above examples show that CTR and CTP of a composite model yield similar values for F_c^* and F_R^*. However, for the compartmentalized model with BDF within the support tank, type curve matching of the CTR and CTP gives different values of F_R for the same reservoir. This reveals that F_R is not only dependent on the reservoir and fluid characteristics of the two compartments, but also on the production mechanisms. Intuitively, it has a resemblance to the skin factor that is used extensively in well-testing analysis. The skin factor explains the additional pressure drop at the wellbore and has different effects for CTR compared with CTP. While the skin factor is defined as the ratio of the permeabilities and the sizes of damaged and undamaged zones, F_R is the ratio of the permeability, viscosity and size of the production and support compartments.

Our extensive numerical experiments with different contrast in properties and with low permeability barrier showed that not only the permeability and size of the support tank, but also its compressibility and porosity greatly influence the performance behaviour of a compartmentalized reservoir. For smaller values of hydraulic diffusivity of the support compartment, lower permeability barrier results in a production signature which can be adequately modeled using the simplified solution (with constant F_c and F_R). In general, for a system with relatively equally-sized production and support regions and with a barrier that has smaller than 1% permeability of the lower permeability region, the BDF assumption of the support compartment is valid and its performance can be reasonably modeled using the developed solution with constant F_c and F_R.

This study illustrates that the parameters F_c and F_R (or F_c^* and F_R^*) can be used as parameters to characterize a compartmentalized/composite reservoir. Type curves can be generated for different values of F_c and F_R (or F_c^* and F_R^*). Here it should be stressed that when analyzing production data, these parameters are not known a priori. Therefore type curve matching process may not be very practical. Although a type curve matching process was used for obtaining these parameters, a history matching process can be employed instead to determine F_c and F_R (or F_c^* and F_R^*).

It is worth mentioning that even though F_c and F_R are based on physical properties (e.g. permeability, porosity, compressibility etc.) of the system, the history matched F_c and F_R may not reflect these exact properties but are more likely a combination of the various complexities in the system (transient flow, existence of barrier, constant rate vs. constant pressure production, etc.). Nevertheless, because they are based on system properties, they are meaningful, and their value obtained from the history matching should be much more

useful than a purely empirically derived match (as in the Arps curves). In essence, it can be stated that these parameters are matching parameters that qualitatively have physical meaning as they are related to physical properties of the system, but quantitatively can have different values under different production scenarios (as in the case of F_R).

4.8 Chapter Summary and Conclusions

In this chapter, the long term performance of compartmentalized and composite reservoirs under constant rate and constant pressure production were studied. Using the capacitance and resistance concepts, a mathematical model was developed and detailed analytical solutions were presented. Different scenarios for BDF and transient flow within the support compartment were considered. The model allowed for considering the effects of low permeability barriers as well as different reservoir properties across the compartments. Key conclusions are as follows:

- The analytical solutions are obtained in real time domain and therefore can be easily implemented in a spreadsheet application.
- Depletion of each compartment is revealed by two unit slopes on a log-log plot of pressure versus time for CTR. For CTP, however, the depletions display two exponential declines. These depletion signatures are separated by transition periods which depend on the support cell contribution (i.e. BDF or transient).
- Expressed in dimensionless form, the solutions provide type curves which can be used through a matching process for estimating the contrast of capacitance and resistance (i.e. F_c and F_R or F_c^* and F_R^*). These parameters reflect the combined effect of

variation of reservoir and fluid properties across the compartments and control the flow performance of compartmentalized systems.

- The basic equations are developed based on the BDF as the prevailing conditions. However, the distance of investigation concept is then used to model the transient effect of the supporting compartment. This is considered as a generalization of two-region linear composite model with inclusion of a leaky interface (permeability barrier).
- The difference in distance of investigation for the CTR and CTP leads to different values of F_R (for instantaneous depletion of the support) which are obtained from the type curve matching process of pressure and rates for the same system.

Chapter Five: Performance Analysis of Multi-Layered and Naturally Fractured Reservoirs

5.1 Scope of the Study

Most reservoirs consist of several layers whose characteristics are different from each other. Wells in such reservoirs may produce from more than one layer. Pressure/rate behavior in these kinds of vertically heterogeneous systems are not necessarily similar to that of a single layered system. Sometimes, the pressure/rate behaviour only reveals the average properties of the entire system because of the pressure communication (crossflow) between the layers. There are many other instances where layers behave independently of each other and, as a result, a complex wellbore pressure/rate response is obtained. Fetkovich et al. (1990) indicated that existence of crossflow may be of considerable importance in long-term production forecasting. They also mentioned that it is possible to reduce multilayer systems into equivalent two-layer systems for obtaining reasonable production forecasting. Moreover, they pointed out that a no-crossflow layered reservoir can exhibit the same type of response as that of a naturally fractured reservoir; a double depletion type of rate decline where the early depletion of the higher permeability layer resembles fracture-volume depletion and the late depletion of the lower permeability layer appears analogous to matrix depletion.

As mentioned in the literature review, Chapter two, a common practice for establishing economic rates in tight and shale reservoirs is commingling of different layers. The amount of contribution by each layer to the total well's production, the starting time for sensible contribution of each layer, the types of flow regimes developed in each individual layer

and their collective combination can significantly complicate the performance behaviour of such reservoirs. As a result, reasonable prediction of their production performance is directly linked with accounting for the effect of multilayered completion of these reservoirs.

This chapter extends the application of the CRM for performance analysis of multi-layered and naturally fractured reservoirs. Similar to the case of compartmentalized/composite reservoirs discussed in Chapter four, the effects of another layer(s) or another medium (matrix) can be accounted for by using additional tanks in the capacitance-resistance model. As such, two basic situations that are of significance in analysis of multilayered reservoirs (i.e. production with crossflow and without crossflow) produced at constant terminal rate are considered. Similarity between dual porosity models available in the literature and the CRM approach for analysis of naturally fractured reservoirs is also discussed. Similar to the previous chapters, linear flow is assumed to be the dominant flow regime during transient period.

5.2 Multilayered Reservoir Analysis Using CRM

The logical way for representing a multilayered reservoir in CRM is to use multiple tanks with distinct reservoir properties signifying the different layers. Such an approach is especially suitable for situations where a permeability barrier between layers could effectively eliminate the possibility of existence of crossflow between layers. Under these conditions, each layer behaves independent of the other layers and therefore differential depletion of the various layers occurs. Figure 5.1(a) shows tank representation of a two layered reservoir without crossflow between layers.

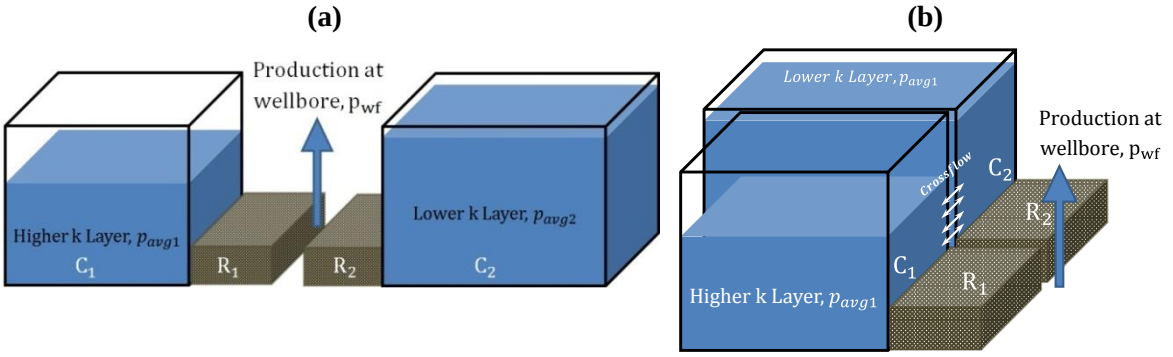

Figure 5.1: Schematic of a multi-layered reservoir (a) without and (b) with crossflow.

In performing the analysis using the CRM for this situation, one needs the rate of production of individual layers to be able to determine the depletion of each layer. Our analysis shows that the fraction of the total production attributed to each layer depends on the ratio of its capacitance to the capacitance of the total system. As a result, production rate of each layer can change with time during transient flow and can become a constant value during the BDF of the lower permeability layer. Therefore, allocation of the rate at each time step is performed according to q_R, which is the ratio of the capacitance of each layer to the total capacitance:

$$q_R = \frac{C_1}{(C_1+C_2)} \qquad \text{Eq. 5.1}$$

Figure 5.1(b) demonstrates the tank representation of a reservoir having two layers that possess crossflow in between layers. When there is crossflow and the difference between the resistivity of the layers is moderate, the different layers can interact with each other in terms of pressure. As a result of this pressure communication one can use a single tank with the equivalent properties (i.e. capacity and resistivity) of the layers to forecast the total system production performance.

Equivalent resistivity of the layers can be obtained using the electrical analogy of resistivities in parallel, as follows:

$$\frac{1}{R^*} = \left(\frac{1}{R^*_1} + \frac{1}{R^*_2}\right) \quad \text{Eq. 5.2}$$

In addition the equivalent capacity can be obtained according to the following equation:

$$C^* = (C^*_1 + C^*_2) \quad \text{Eq. 5.3}$$

It would be advantageous to examine the performance behaviour of a two layered system producing under the constant terminal rate using the capacitance-resistance approach. This can be achieved by considering the following numerical simulation examples of a two layered liquid reservoir (with and without crossflow) and then using the CRM for analyzing their production behaviour.

5.2.1 Example case 1-with crossflow

In this example, a two layered reservoir that exhibits crossflow between layers is numerically simulated. The well and reservoir geometry of each layer is shown in Figure 3.1(a), indicating linear flow. Table 5.1 shows the basic reservoir properties used for obtaining the simulation results. This reservoir is put on production for 4000 days with the production rate of 100 StbD.

According to Section 3.6.1, the CRM is based on using two parameters for characterizing each layer (CRR and t_{BDF}) in addition to the constant rate of production and initial wellbore pressure. The procedure to be followed here is similar to that of chapter three (Figure 3.3) with the difference that CRR and t_{BDF} are based on equivalent capacity and resistivity of layers. Therefore, capacity and resistivity of each layer are calculated

analytically (using equations in Chapter 3, Eq. 3.4 – Eq. 3.7). Because there is no permeability barrier between the layers, crossflow exists between them. Therefore, Eq. 5.2 and Eq. 5.3 are employed and the equivalent capacity and resistivity are obtained to yield the parameters to be used in CRM, Section 3.6.1. These parameters are $\mathrm{CRR} = 96\ (\mathrm{Stb/psia})^2/\mathrm{Day}$ and $\mathrm{t_{BDF}} = 141$ days.

Table 5.1: The basic reservoir properties used for numerical simulation of a two-layered reservoir.

Parameters	Layer 1	Layer 2
Initial reservoir pressure, psia	5000	5000
Permeability, md	0.2	0.02
Thickness, ft	100	250
y_e, ft	1000	1000
x_e, ft	1000	1000
x_f, ft	1000	1000
μ, cp	0.295	0.295
ϕ, fraction	0.1	0.1
B_i, bbl/Stb	1.021	1.021
c_t, 1/psia	5.97×10^{-6}	6.97×10^{-6}

Figure 5.2(a) and (b) are logarithmic and Cartesian plots of Δp vs. time and show the comparison of the results of the CRM using the equivalent capacity and resistivity with those of the simulation. In addition, CRM results using the properties of the higher permeability layer are shown. Evident in Figure 5.2(a), during early time the transient linear flow within both layers result in a bilinear flow. Slope of 0.28 as opposed to 0.25 (which is characteristic of dual-linear flow) is the result of crossflow between the layers. Moreover, during late time, the BDF of both layers results in a slope of unity in this plot. Figure 5.2(b) clearly confirms the BDF of the total system during late time by showing a straight line. Note that the results of the CRM with properties of the higher (or lower)

permeability layer is not useful. These figures clearly demonstrate the excellent match of the numerical results obtained using the CRM with equivalent properties of the two layers.

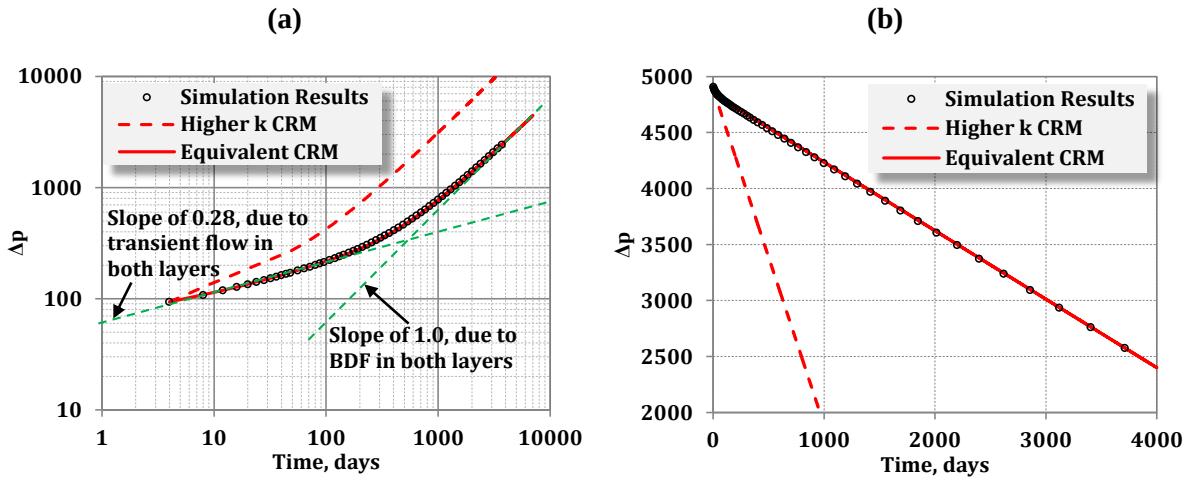

Figure 5.2: Comparison of the CRM with the equivalent properties of the layers, CRM with the properties of the higher permeability layer, and simulation results.

The above example depicts the ability of a single tank model for performance analysis of multilayered reservoirs with crossflow. Therefore for a multilayered reservoir exhibiting cross flow, the CRM can be used to infer the equivalent reservoir properties of the multiple layers.

In addition to the above example where one tank with equivalent properties of the layers in the capacitance-resistance model is used, there are cases where the analysis of multiple layers having crossflow using a single tank cannot give reasonable results. Sensitivity analysis on the different parameters reveal that if the ratio of the resistivity of the two layers is greater than 40, then one cannot use the single layer CRM for its production prediction. This means that for values of resistivity ratio greater than 40 the existing crossflow between layers is considered insignificant and therefore depletion of each layer takes place independently of the other layer. Figure 5.3 is an example of this situation,

where the same reservoir properties as those in Table 5.1 were used; except that the permeability of the second layer is set equal to 0.002 which results in a larger resistivity ratio.

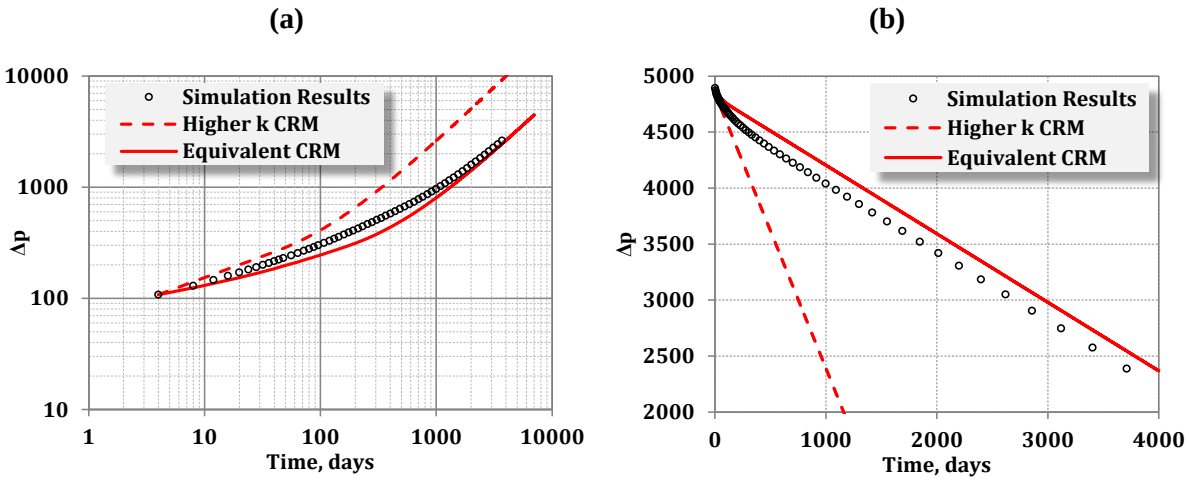

Figure 5.3: Comparison of the CRM with the equivalent properties of the layers, CRM with the properties of the higher permeability layer, and simulation.

It should be mentioned that in Figure 5.3, the equivalent tank properties were calculated based on the new permeability to obtain $\mathrm{CRR} = 78.6\,(\mathrm{Stb/psia})^2/\mathrm{Day}$ and $t_{BDF} = 172$ days.

Evident in the above figure, using the single tank CRM with the equivalent properties of the two layers doesn't yield the expected match of the simulation results. Already stated, the reason for this is the differential depletion of the two layered system. It is noted that as the difference in permeability of the two layers gets larger, differential depletion becomes more prevailing.

5.2.2 Example case 2-without crossflow

In this section, a reservoir with two layers without crossflow is simulated. Again, the reservoir configuration for each layer is identical to that of Figure 3.1(a). Pertinent reservoir properties used for construction of this case are listed in Table 5.2. An impermeable layer in between the two producing layers was used in order to ensure no pressure communication between them. The reservoir is produced for 4000 days with a production rate of 50 StbD.

Table 5.2: The basic reservoir properties used for numerical simulation of a two-layered reservoir without crossflow.

Parameters	Layer 1	Layer 2
Initial reservoir pressure, psia	5000	5000
Permeability, md	0.2	0.002
Thickness, ft	100	250
y_e, ft	1000	1000
x_e, ft	1000	1000
x_f, ft	1000	1000
μ, cp	0.295	0.295
ϕ, fraction	0.1	0.1
B_i, bbl/Stb	1.021	1.021
c_t, 1/psia	5.97×10^{-6}	6.97×10^{-6}

According to the results in Chapter 3, CRM is based on using two parameters for characterizing each layer (CRR and t_{BDF}) in addition to the constant rate of production and initial wellbore pressure. The procedure to be followed here is similar to that of chapter three (Figure 3.3) with the difference that production rate to be used for depletion calculation of each layer is a function of the capacitance of both layers, according to q_R. This means that $q_1 = q_R \times q$ and $q_2 = (1 - q_R) \times q$, where q is the wellbore rate. Here the subscripts 1 and 2 refer to the higher and lower permeability layers, respectively. For

this set of simulation production data, the parameters in Table 5.3 were used to get a match of flowing pressures. These values are consistent with their analytical calculations.

Table 5.3: Double tank properties used for analysis of two layered reservoir.

Parameter	Value
CRR_1, $(Stb/psia)^2/Day$	19.6
t_{BDF1}, Day	45
CRR_2, $(Stb/psia)^2/Day$	0.9
t_{BDF2}, Day	5244

A comparison of the obtained results is given in Figure 5.4. Figure 5.4(a) shows the contribution of each layer. Evident in this figure, the contribution of each layer to total production varies with time. This variation continues until BDF of the lower permeability layer is reached. Although not clearly shown in the figure, during the period where both layers are in transient period (i.e. first 45 days) contribution of each layer will be a constant value. Note that calculation of the q_R confirms this statement. Calculation of time for reaching BDF of the lower permeability layer (layer 2) shows that it occurs at $t_{BDF2} = 5244$ days. As a result, the contribution of each layer shows a continuously changing trend. Figure 5.4(b) is a logarithmic plot of Δp vs. time and compares the results of the double-tank CRM and single tank equivalent CRM with those of the simulation. Predictably, excellent match is obtained using the double tank CRM. During early times a slope of 0.25 is obtained which indicates dual-linear flow (as a result of linear flow in each layer). This is followed by a slope of 0.67 which suggests BDF of the higher permeability layer and transient flow of the lower permeability layer. As can be seen, single tank equivalent CRM does not give appropriate results for describing the behaviour of this system. This example

demonstrates the ability of the double-tank CRM to reasonably track the multilayered simulation results.

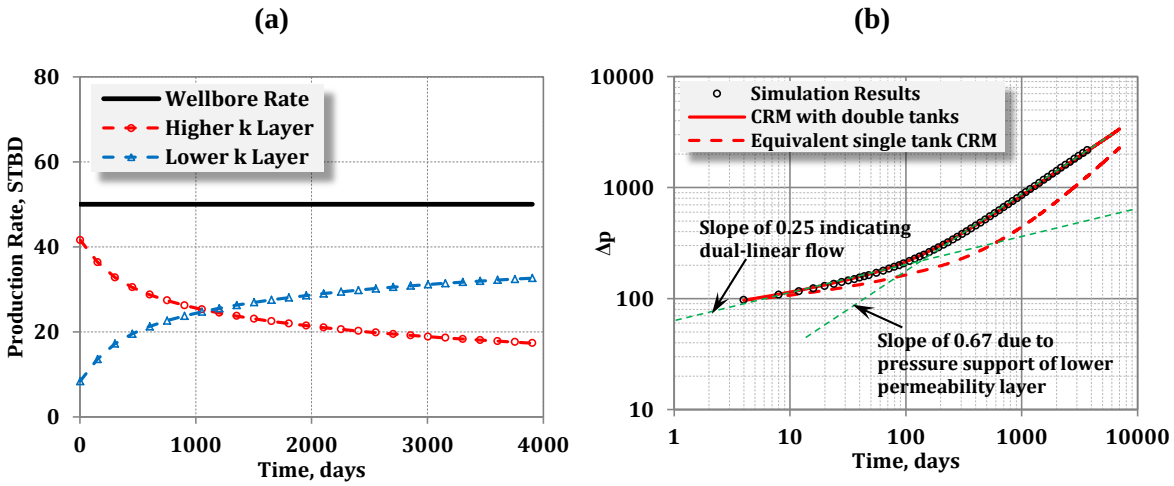

Figure 5.4: (a) Comparison of the production rate from layers 1 and 2 and the wellbore; (b) results of the CRM with double tanks compared with those of the numerical simulation.

Using the double tank CRM, one can perform a sensitivity analysis on the rate of production from the wellbore to illustrate the effect of production rate on depletion of each layer. The data of the above example were used and the rates of production were chosen to be 50, 100, 150, 200 and 250 StbD. The Cartesian plot of cumulative production of the lower permeability versus cumulative production of the higher permeability for these production rates are shown in Figure 5.5. This figure depicts the rate dependency of the constant rate production from a two layered system. Increase in wellbore production rate causes the contribution of the lower permeability layer (layer 2) to the total cumulative production to become smaller. This means that for multilayered wells with higher production rates, the bulk of the well's production comes from the higher permeability layer. As a result of this observation it can be stated that lower production rates can result in more even depletion of the layers.

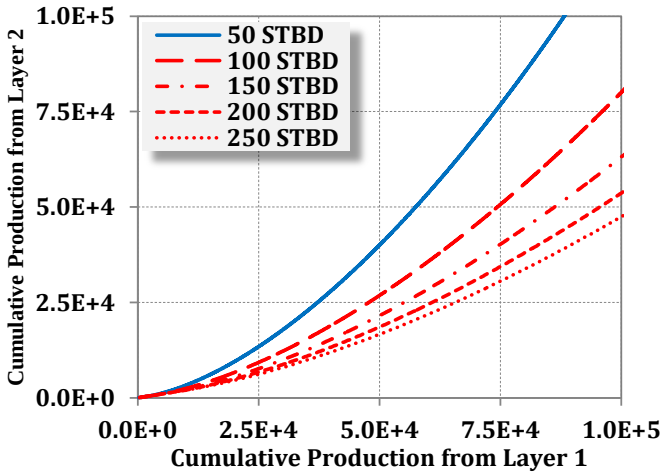

Figure 5.5: Effect of wellbore production rate on depletion of layers in a two layered reservoir.

5.3 Naturally Fractured Reservoirs (NFR)

Naturally fractured reservoirs are similar to conventional reservoirs in terms of deposition of the sediments with intergranular porosity (matrix), but different from them because of the disruption of their continuity as a result of stresses created by Mother Nature. They occur in many reservoirs due to local tectonic events happening during their geological time or even due to dessication and/or thermal gradients. Events like folding, faulting, tensile failure, thermal effects and subsidence create primary fracturing, which can be later altered by dissolution and/or precipitation. These discontinuities (called natural fractures) are pathways of higher permeability that may or may not have strong storage capacity (relative to the matrix). Classically, naturally fractured media are described by a dual porosity model. In the dual-porosity approach, the matrix media feed the fracture media which are drained by the wellbore (Warren and Root 1963). This means that the fracture medium essentially supplies the main flow paths for the reservoir rock, while the matrix

acts as the major source of the fluid storage. A dual-porosity model is characterized by the following two parameters, storativity ratio (ω) and interporosity flow coefficient (λ). The former is defined according to Eq. 5.4 and is the ratio of the storage capacity of the fracture to that of the total system:

$$\omega = \frac{(\phi c)_f}{(\phi c)_f + (\phi c)_m} \qquad \text{Eq. 5.4}$$

The interporosity flow coefficient represents how fast the fluids can flow from the matrix to the fracture medium, and is defined according to Eq. 5.5:

$$\lambda = x_f{}^2 \alpha \frac{k_m}{k_f} \qquad \text{Eq. 5.5}$$

In the above equation, α is the shape factor and can be obtained according to Eq.1.6:

$$\alpha = \frac{4n(n+2)}{L_m{}^2} \qquad \text{Eq. 5.6}$$

Where L_m is a characteristic length and n is the number of sets of fractures (1, 2 or 3 for slabs, match sticks and cubes, respectively). Note that the choice of α is not important in production data analysis (Hassanzadeh et al. 2009, Moghadam et al. 2010) because this parameter is lumped with others into λ to be obtained from the data analysis.

Numerous studies have been performed on analyzing the behaviour of dual porosity media. As an example, Da Prat (1981) focused on constant pressure production of such media, used the Warren and Root model of a circular reservoir with a vertical well in the center and obtained solutions in Laplace domain which were inverted back into real time domain using a numerical inversion algorithm. He proposed short term and long term

approximations of the obtained solution, according to the following equations, respectively:

$$q_D = \frac{1}{\left(\ln(r_{eD})-\frac{3}{4}\right)} \exp\left(-\frac{2}{{r_{eD}}^2\left(\ln(r_{eD})-\frac{3}{4}\right)}\frac{t_D}{\omega}\right) \quad \text{Eq. 5.7}$$

$$q_D = \frac{\lambda\left({r_{eD}}^2-1\right)}{2} \exp\left(-\frac{\lambda}{(1-\omega)} t_D\right) \quad \text{Eq. 5.8}$$

Where q_D and t_D are dimensionless parameters. These solutions are shown in the following Figure:

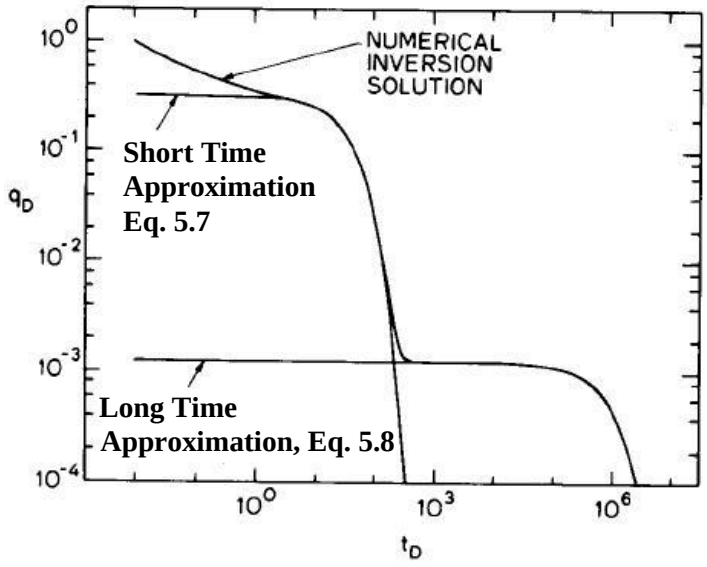

Figure 5.6: Plot of dimensionless rate vs. dimensionless time using numerical inversion of the Laplace solution, along with its short time and long time approximations (Adapted from Da Prat et al (1981)).

The above brief description of the NFRs and the analysis by Da Prat shown in the Figure above, clearly demonstrate the similarity of the dual porosity modeling approach with the CRM described for compartmentalized/composite reservoirs, discussed in the previous chapter. The beauty of the capacitance-resistance model is the simple coupling of early and

late time solutions without the need for expressing them in Laplace domain. If used for analysis of dual porosity media, CRM effectively combines all the fractures into one production tank and all the matrix media into one support tank. Therefore, interaction of these two distinct media depends not only on ω and λ, but also on the size of the reservoir. Since the focus of our investigation is linear flow, the following substitutions are required to express the CRM in terms of the dual porosity parameters:

$$F_c = \frac{\omega}{(1-\omega)} \qquad \text{Eq. 5.9}$$

$$F_R = \frac{3}{\lambda {y_{eD}}^2} \qquad \text{Eq. 5.10}$$

Employing the F_c and F_R parameters defined according to these equations, solutions in Chapter 4 can be used to analyze the performance behaviour of a dual porosity reservoir with pseudo-steady state interporosity flow using the CRM. Moreover, using the solution with transient support (matrix) tank, one can simply obtain the dual porosity solutions with transient interporosity flow.

5.4 Chapter Summary and Conclusions

In this chapter, the application of the capacitance-resistance model for production data analysis of multilayered and dual porosity reservoirs were shown. Although the discussion was only for liquid reservoirs, by virtue of the results in preceding chapters it can be stated that the results are also applicable to gas reservoirs. Key conclusions of this chapter are:

- A two layered reservoir with crossflow produces a rate/time and pressure/time production performance behaviour similar to that of a single layer reservoir.

- A two layered reservoir without crossflow produces a rate/time and pressure/time production performance behaviour that a single layer reservoir cannot reproduce.
- In situations where the ratio of the resistivities is smaller than 40, one can use a single tank model to analyze the behaviour of a two layered system without crossflow.
- Behaviour of dual porosity reservoirs can be easily reproduced using the double tank composite CRM (discussed in Chapter four). The support tank then takes the role of combined matrix media and production tank resembles combined fracture network.

Chapter Six: Analysis of Decline Curves Based on Beta Derivative

6.1 Scope of the Study

The literature survey mentioned in Section 2.4.1 shows that the Arps decline curve equations are obtained for constant pressure production scenarios and based on behaviour of loss-ratio (i.e. fraction of production rate to loss in production with respect to time). He obtained simple exponential and hyperbolic decline equations for cases where the loss-ratio or its derivative with respect to time is constant, respectively. Their application for rate forecasting is limited to production data during boundary dominated flow (BDF), meaning that during transient flow they give unreasonable results.

This chapter presents the development of a simplified method which follows the Arps analysis steps, but uses the beta derivative (instead of loss-ratio) for obtaining a new set of equations for rate decline analysis during transient and BDF. It is shown that under ideal condition of perfect rate decline, i.e. constant terminal pressure and minimal noise in rates, the log-log plot of beta-derivative gives a reasonable straight line during transient flow period (radial or linear flow regimes). In addition, during the BDF another straight line is obtained with a slope different from that of the transient flow. Using the equations of straight lines for each of these flow regimes leads to decline equations which have a power-law nature and can be used for rate prediction. Parameters associated with the proposed equations include slopes of transient and BDF straight lines on the log-log plot of the beta derivative versus time, the time that BDF starts and value of beta derivative at the start of BDF. Combining the transient and BDF equations and expressing them in dimensionless form, type curves are easily generated which can be used for determining

the required parameters. Matched against the results of numerical simulation during transient and BDF, better rate forecasting is achieved using the proposed method compared with the other (empirical) methods available in the literature.

6.2 Beta Derivative Background

Introduction of the semilog derivative (Bourdet et al. 1983, Bourdet et al. 1989) as a useful diagnostic tool spurred a lot of efforts to develop other simple diagnostic methods for performing well test analysis and interpretation. Among them, the work of Onur and Reynolds (1988), Duong (1989) and Onur et al. (1989) are noteworthy, as they formed the basis for beta derivative. Dividing pressure drop by the associated Bourdet derivative, these researchers proposed a plotting function that was believed to alleviate the non-uniqueness issue inherent in well testing problems. This plotting function was later revived by Sowers (2005) and Hosseinpour-Zonoozi et al. (2006) and its inverse was named beta derivative. Hosseinpour-Zonoozi et al. (2006) looked for specific application of the beta derivative for performing pressure transient analysis and concluded that the beta derivative function can provide new insights into analysis and interpretation of pressure transient data. Beta derivative was later redefined by Ilk et al. (2007) as a rate-based function to analyze production data. As demonstrated by Hosseinpour-Zonoozi et al. (2006) for pressure transient analysis and Ilk et al. (2007) for rate transient analysis, the beta derivative and its auxiliary functions can be used to provide characteristic signatures for unfractured and fractured wells. They state that the beta derivative can be used mainly as a diagnostic function, not a function used to provide an exact estimate of reservoir parameters.

Idorenyin et al. (2011) analyzed various implementations of the beta derivative based on constant rate and constant pressure production and found that the classic signature of these plotting functions is altered by the presence of skin. They also showed that the beta derivative has significant diagnostic value for identifying power-law types of flow regimes (wellbore storage, linear flow, bilinear flow, boundary-dominated flow, etc.) because it possesses a recognizable unique character for each of these flow regimes. For instance, the beta derivative (for constant rate) is 0.5 for linear flow, 0.25 for bilinear flow and 1.0 for boundary dominated flow. They also mentioned that being a dimensionless parameter, it can be used to differentiate the performance of wells producing from the same field or from different resource plays.

6.3 Beta Derivative Behaviour

In this section, the behaviour of the beta derivative calculated from rate decline of different reservoirs (water, oil or gas) during both transient and BDF is studied (throughout the rest of the chapter beta derivative is used to indicate beta derivative based on rate). This beta derivative (Ilk et al. 2007) is defined according to Eq. 6.1:

$$\beta = -\frac{dq/dt}{q/t} \qquad \text{Eq. 6.1}$$

Its behaviour for linear and radial flow geometries is of interest to us. Analysis of linear flow of liquid reservoirs (with constant viscosity and compressibility) is easy since there are simple analytical solutions available in the literature which are expressed in real time domain and can be used for calculation of the rate decline and therefore the beta derivative. For radial flow, however, the solutions in Laplace domain cannot be inverted analytically

into real time domain and this results in complicated equations for beta derivative which will not be presented here, because that would distract from the focus of this work. As a result and for consistency, a commercial numerical simulator is used to obtain the linear and radial rate decline data from which one can calculate the associated beta derivatives. The base reservoir geometries chosen for this study to maintain pure linear and radial flow are shown in Figure 6.1 (a) and (b), respectively.

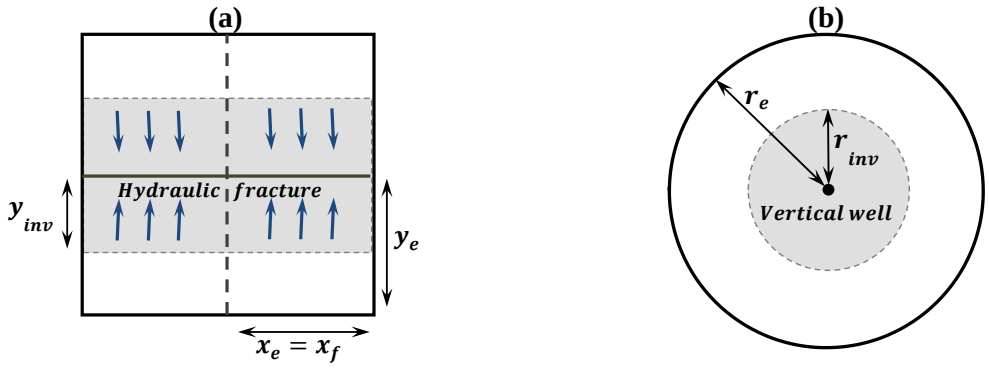

Figure 6.1: Schematic of (a) a hydraulically fractured well in a rectangular reservoir (b) a vertical well in the center of a circular reservoir.

Figure 6.1 (a) shows a rectangular reservoir with a hydraulic fracture that completely traverses it. Obviously, transient flow of such a reservoir exhibits linear flow. In addition, Figure 6.1 (b) demonstrates a reservoir geometry whose transient flow displays pure radial flow. For the reservoir with linear flow geometry, it is assumed that reservoir size in the x and y directions are equal, in order to have the closest reservoir configuration to the case of reservoir with radial flow geometry. In Figure 6.1 (a) and (b), y_{inv} and r_{inv} demonstrate the investigated distance for the linear and radial flow regimes, respectively. Evidently, during transient flow period these distances increase with time until reaching a maximum which is equal to the external size of the reservoir.

Table 6.1 shows the pertinent information regarding the setup of the simulations. Simulation studies include using water, live single-phase oil and dry gas as the reservoir fluids. Producing from these reservoirs under constant flowing pressure and using the production record of each simulation case, the beta derivatives are numerically calculated and the similarities observed in the signature of their beta derivatives are used for proposing appropriate rate decline equations.

Table 6.1: Reservoir simulation model parameters.

Parameters	Values
Initial pressure, psia	5000
Flowing bottomhole pressure, psia	500
Porosity, %	10
Reservoir size in x direction (For linear flow), ft	500
Reservoir size in y direction (For linear flow), ft	500
Fracture half length (For linear flow), ft	500
Reservoir size in r direction (For radial flow), ft	500
Formation compressibility, $1/psia$	3×10^{-6}
Net pay thickness, ft	100

In the next section, the behaviour of different (water, oil and gas) reservoirs with dominant linear flow, reservoir geometry shown in Figure 6.1 (a), is discussed. This is then followed by discussion of the behaviour of reservoirs with dominant radial flow, reservoir geometry shown in Figure 6.1 (b).

6.3.1 Linear flow

6.3.1.1 Liquid Reservoir with Constant Properties (Water reservoir)

For this case, a permeability of 0.01 md was used. Linear flow theory for a liquid reservoir (with constant fluid viscosity and compressibility) indicates that a log-log plot of rate versus time during early-time (transient flow) regime is described by a straight line trend with a -1/2 slope. The beta derivative for this flow regime also gives a constant value of 0.5. During the late-time (boundary-dominated) flow regime, the decline trend has an exponential nature and its beta-derivative is a straight line with a unit slope. Analytical solutions for this case are given by Idorenyin et al. (2011). Calculating the beta derivative for this simulation case confirms the analytical solutions, i.e. a constant value during transient flow and rising with slope of unity during BDF, see Figure 6.2. It is noted that the time for start of BDF (t_{BDF}) can be obtained using the intersection point of the transient and BDF straight lines.

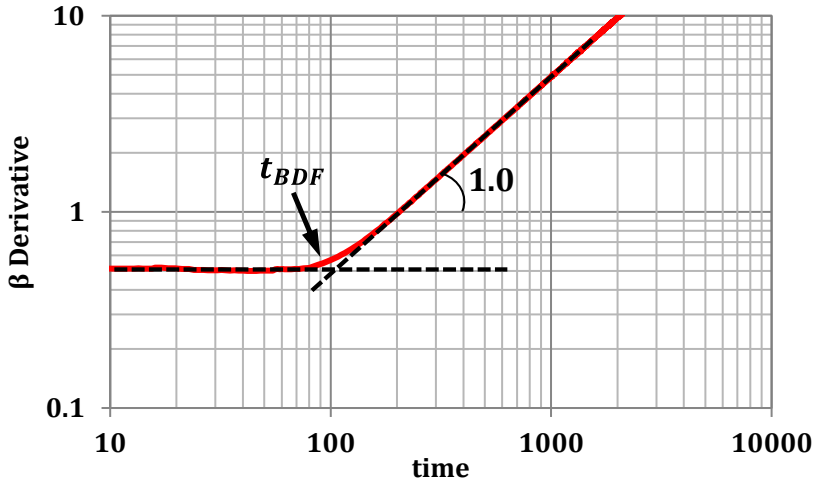

Figure 6.2: Logarithmic plot of the beta derivative for a water reservoir with linear flow.

In an attempt to investigate some of the parameters that affect the behaviour of the beta derivative, the values of the reservoir size and the skin were changed. The reservoir size (y_e) was increased from 500 ft in the previous case to 1000 and 2000 ft. This resulted in a horizontal shift of the beta derivative in the x-direction, as shown in Figure 6.3(a). Figure 6.3(b) also shows the effect of changing skin from 0 to 0.2 and 0.4. Not only did the change in skin value alter the slope of the transient straight line, but it also shifted the late time straight line in the x-direction. It has to be mentioned here that the skin values used for linear flow cases (0.2 and 0.4) represent the fracture face skin and are large values because of the definition of skin for linear flow (See Section 3.8 for more details on skin formulation in linear and radial flow).

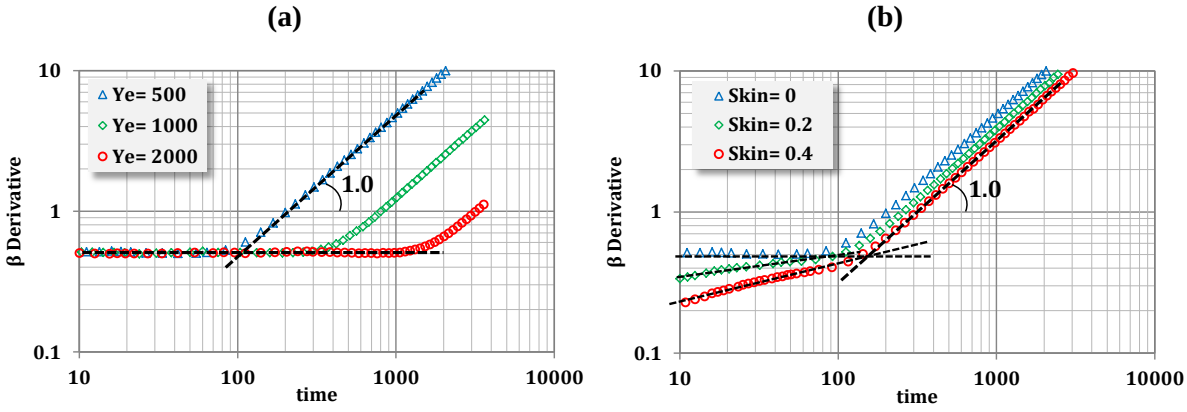

Figure 6.3: Effect of (a) reservoir size and (b) skin value on the calculated beta derivative of a water reservoir with linear flow.

6.3.1.2 Liquid Reservoir with Varying Properties (Oil reservoir)

Here a permeability of 0.1 md with an oil of 45 API flowing through the reservoir and constant viscosity of 0.8 cp were used. Similar to the previous case; the simulation was run for different values of reservoir size and skin and the results shown in Figure 6.4(a) and (b), respectively, were obtained.

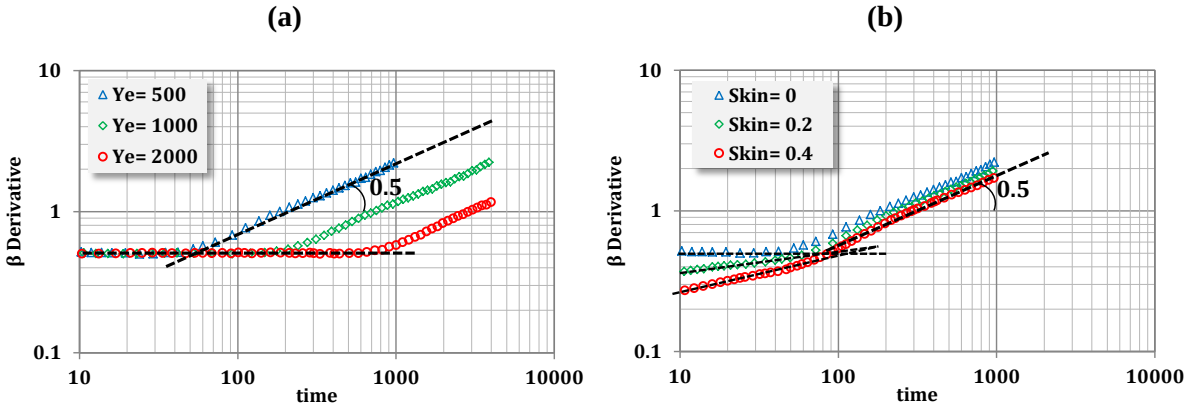

Figure 6.4: Effect of (a) reservoir size and (b) skin factor on the calculated beta derivative of an oil reservoir with linear flow.

The beta derivative during transient linear flow was equal to a constant value of 0.5.This was not surprising. However, during the late-time flow regime, the beta derivative assumed an approximately straight line trend, but with a slope of 0.5 instead of 1.0 (this unexpected result is discussed later). As before, increasing the reservoir size resulted in a delay in observing the start of the BDF straight line. In addition, increasing the skin value caused the transient slope to become more positive. It also caused shifting to the right of the BDF straight line. All the simulation test cases for oil reservoir with linear flow geometry exhibited the BDF approximate straight line with slope of a half.

The half slopes obtained for BDF is in contrast to slope of unity obtained for flow of water through the same system. This difference is attributed to the changing oil compressibility with pressure compared with a constant compressibility used for water simulation cases. In order to observe the effect of compressibility on the calculated beta derivative for the oil cases, constant oil compressibility of $c_o = 5 \times 10^{-6}$ was used for one of the above simulation cases. The resulting change in its calculated beta derivative is shown in Figure 6.5. While the BDF straight line shows a slope of unity for the case of constant oil

compressibility, a changing oil compressibility (according to Vazquez and Beggs correlation) resulted in a beta derivative signature with a slope of 0.5 during BDF.

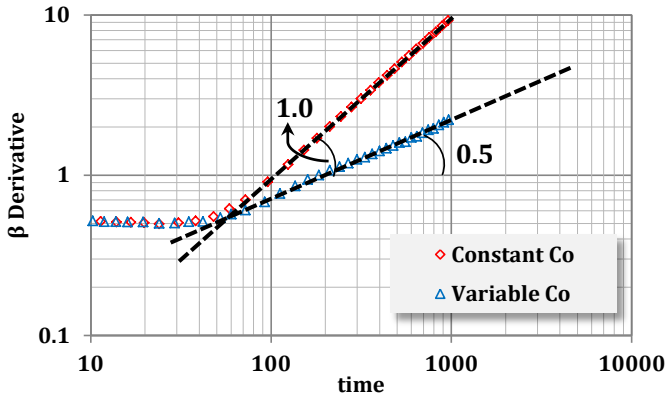

Figure 6.5: Effect of oil compressibility on beta derivative for an oil reservoir with linear flow.

6.3.1.3 Gas Reservoir

In this case, a permeability of 0.01 md and a gas with specific gravity of 0.7 as the reservoir fluid were used. As before, a number of simulation cases were run with different values of reservoir size and skin and numerically calculated their beta derivatives, as shown in Figure 6.6(a) and (b), respectively. Again the beta derivative during transient flow was equal to a constant value of 0.5 for cases where skin was equal to zero. Interestingly, during BDF a straight line whose slope is equal to 0.5 was obtained, similar to the oil case. Sensitivity on the size of the reservoir indicated that the smaller the reservoir is, the earlier is the BDF beta derivative straight line, Figure 6.6(a). In addition, performing a sensitivity study on the skin value depicted that the more damaged the well is (i.e. having more positive skin) the more positive is the transient beta derivative slope. In addition, skin causes shifting to the right of the BDF beta derivative straight line. These are clearly seen in Figure 6.6(b).

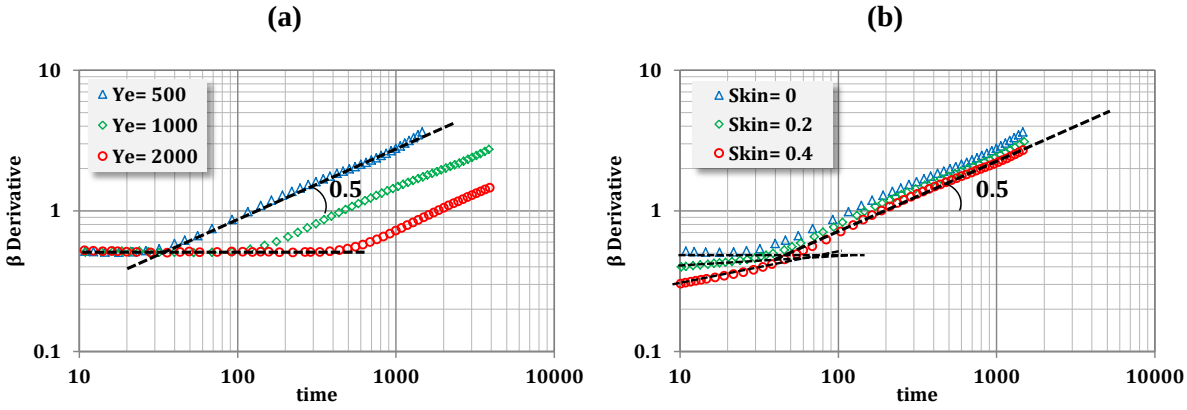

Figure 6.6: Effect of (a) reservoir size and (b) skin factor on the calculated beta derivative of a gas reservoir with linear flow.

Results obtained for the oil and gas cases indicate that regardless of the type of fluid flowing through the reservoir, during BDF the slope of the beta derivative is equal to 0.5. This is an interesting observation which can be used for making oil or gas production forecast. In order to further confirm this result, the properties of the flowing fluids were changed (oil API from 45 to 25 and 65; gas specific gravity from 0.7 to 0.56 and 0.9). Upon applying these changes to the oil and gas simulation cases and calculating their appropriate beta derivatives, Figure 6.7(a) and (b) were obtained. As can be seen in Figure 6.7(a) higher API, which is indicative of lighter oil, led to earlier propagation of the pressure wave (as a result of production) into the reservoir. This implied earlier observation of the BDF beta derivative straight line. Figure 6.7(b) shows the effect of changing the gas gravity on the beta derivative of the dry gas simulation cases. Evident in this plot, the gas gravity has a minor effect on the obtained beta derivative signature. Plots in Figure 6.7(a) and (b) demonstrate that independent of the type of oil or gas flowing in the reservoir, the trend of beta derivative during BDF for reservoirs with dominant linear flow geometry exhibits a straight line of slope 0.5.

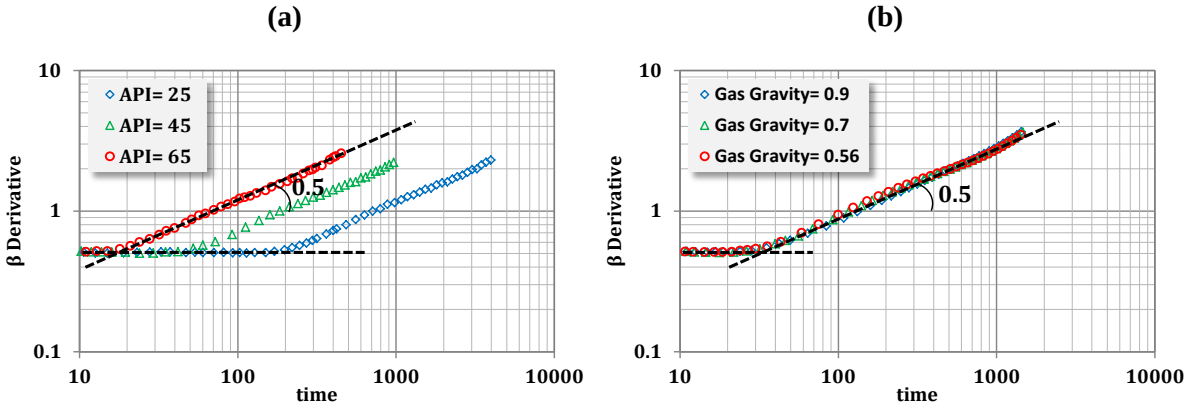

Figure 6.7: Effect of (a) oil API and (b) gas specific gravity on the calculated beta derivative single phase reservoirs with linear flow.

6.3.2 Radial flow

6.3.2.1 Liquid Reservoir with Constant Properties (Water reservoir)

This section is similar to Section 6.3.1 with the difference being a reservoir geometry that exhibits pure radial flow, Figure 6.1 (b). Constant pressure production gives a rate decline whose BDF can be explained using simple analytical solutions – an exponential decline as discussed by Idorenyin et al. (2011). During the transient flow period, however, the analytical solutions involve complex equations in Laplace domain. Notwithstanding the analytical complexity of the related equations, one can simply use the simulation rate decline to numerically calculate the associated beta derivative. Plotted in logarithmic coordinates, the calculated beta derivative shows an approximate straight line of slope -0.09 during transient flow and another straight line with a slope of unity during BDF, Figure 6.8. The intersection of these approximate straight lines can be used for determining the time for start of BDF (t_{BDF}).

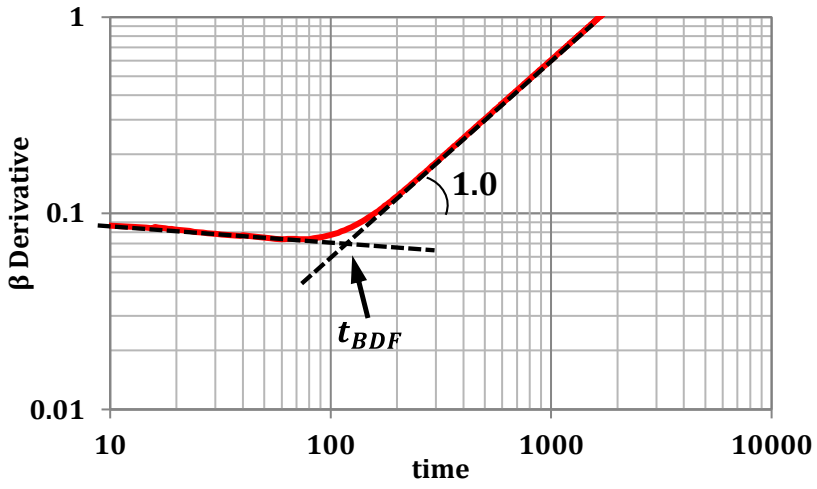

Figure 6.8: Logarithmic plot of the beta derivative for a water reservoir with radial flow.

In an attempt to investigate some of the reservoir parameters affecting the behaviour of beta derivative, the values of the reservoir size and skin were changed. The reservoir size in the r-direction was increased from 500 ft to 1000 ft and 2000 ft. This shifted the beta derivative, as shown in Figure 6.9(a). Figure 6.9(b) also shows the effect of changing skin from 0 to - 4.0 and + 4.0. Introduction of positive skin resulted in significant downward shifting of the calculated beta derivative. Not only that, but the slope of the transient straight line also increased (became less negative). Introduction of a negative skin, on the other hand, resulted in upward shifting of the entire beta derivative in addition to making the slope more negative for the transient straight line. The BDF line maintained its unit slope for all reservoir sizes and skin values.

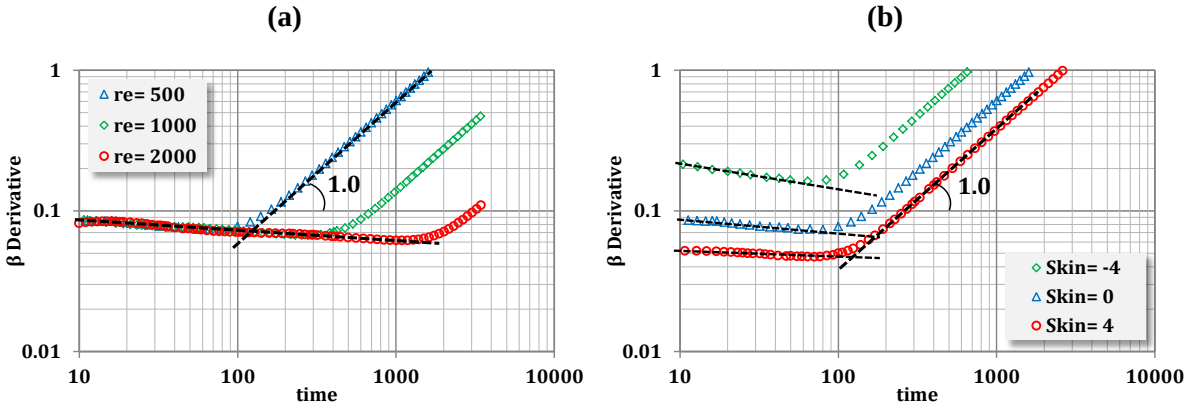

Figure 6.9: Effect of (a) reservoir size and (b) skin value on the calculated beta derivative of a water reservoir with radial flow.

6.3.2.2 Liquid Reservoir with Varying Properties (Oil reservoir)

In this case, a permeability of 0.01 md with an oil of 45 API and compressibility that varies with pressure (according to Vasquez and Beggs correlation) was used. Similar to the previous case, different values of reservoir size and skin were tested. Then, the beta derivatives were calculated numerically and the results were plotted on logarithmic coordinates, Figure 6.10(a) and (b).

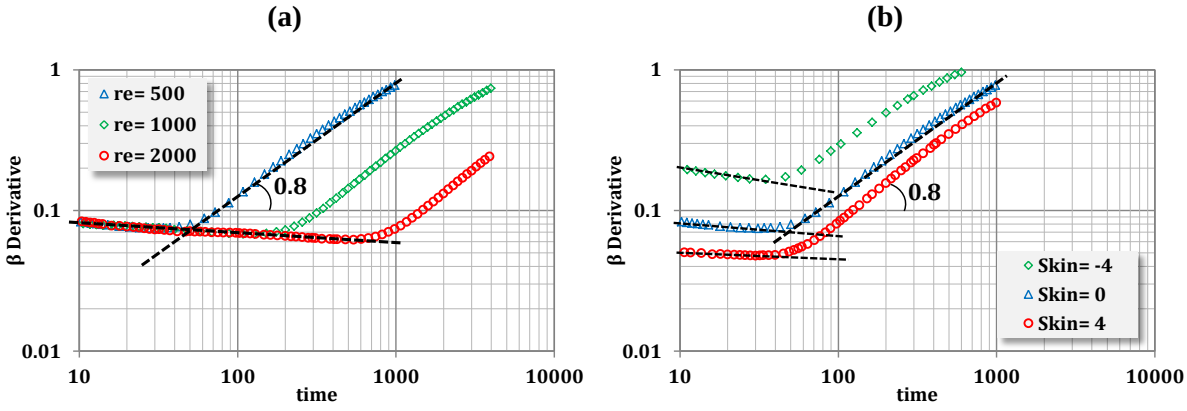

Figure 6.10: Effect of (a) reservoir size and (b) skin value on the calculated beta derivative of an oil reservoir with radial flow.

Figure 6.10(a) depicts that increasing the reservoir size caused delay in obtaining the BDF straight line. In addition, adding positive skin to simulation cases resulted in downward shifting of the associated beta derivatives, as well as a slight change in the slope of the approximate transient straight line (Figure 6.10(b)). Evident in these figures, the BDF approximate straight line showed a slope equal to 0.8 regardless of skin value.

6.3.2.3 Gas Reservoir

In this case, a permeability of 0.01 md and a gas with specific gravity of 0.7 as the reservoir fluid was used. The same procedure as discussed in previous sections was followed. First the simulation was performed for different values of reservoir size and skin, then the beta derivatives were calculated numerically and finally the results were plotted on logarithmic coordinates, Figure 6.11(a) and (b). The obtained beta derivative signatures were quite similar to those of oil reservoir, showing slope of 0.8 during BDF. Increasing the reservoir size caused a delay in obtaining the BDF straight line. In addition, adding positive skin to simulation cases caused the associated beta derivative to shift downward. It also slightly changed the slope of the approximate transient straight line.

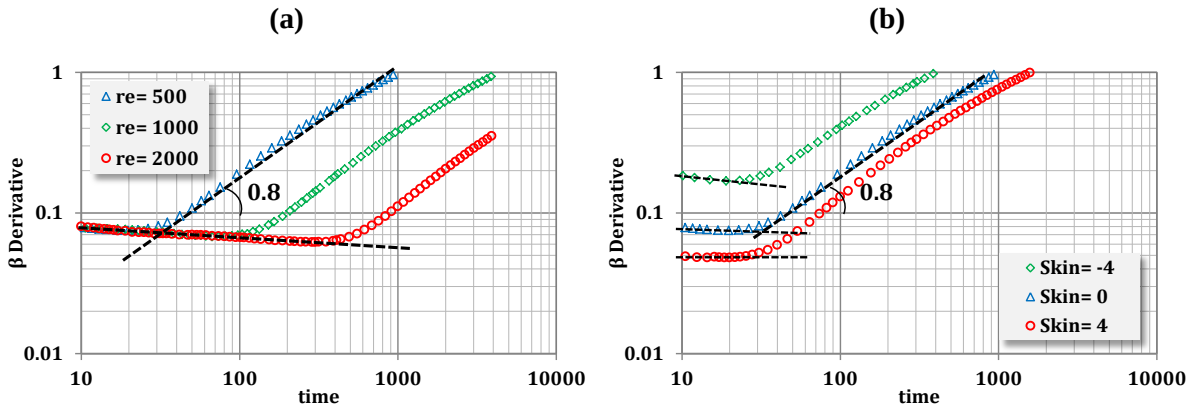

Figure 6.11: Effect of (a) reservoir size and (b) skin on the calculated beta derivative of a gas reservoir with radial flow.

The results for the oil and gas cases indicate that regardless of the type of fluid (oil or gas), the calculated beta derivative during radial BDF gives a reasonable straight line with slope of 0.8. This is in contrast to the slope of 0.5 obtained for linear BDF flow. In order to further confirm this result, the properties of the flowing fluids were changed (changed the oil API from 25 to 45 and 65 for oil cases and gas specific gravity from 0.7 to 0.56 and 0.9 for gas cases). Upon applying these changes and calculating their appropriate beta derivatives, Figure 6.12(a) and (b) were obtained. As can be seen in Figure 6.12(a), higher API led to earlier onset of the BDF beta derivative straight line (because of the higher mobility). Figure 6.12(b) shows the effect of changing gas gravity on the beta derivative of dry gas simulation cases. Evident in this plot, the gas gravity had a minor effect on the obtained beta derivative signature. These results demonstrate that independent of the type of oil or gas flowing in the reservoir, the trend of beta derivative during BDF for a reservoir having radial flow exhibits a straight line of slope 0.8.

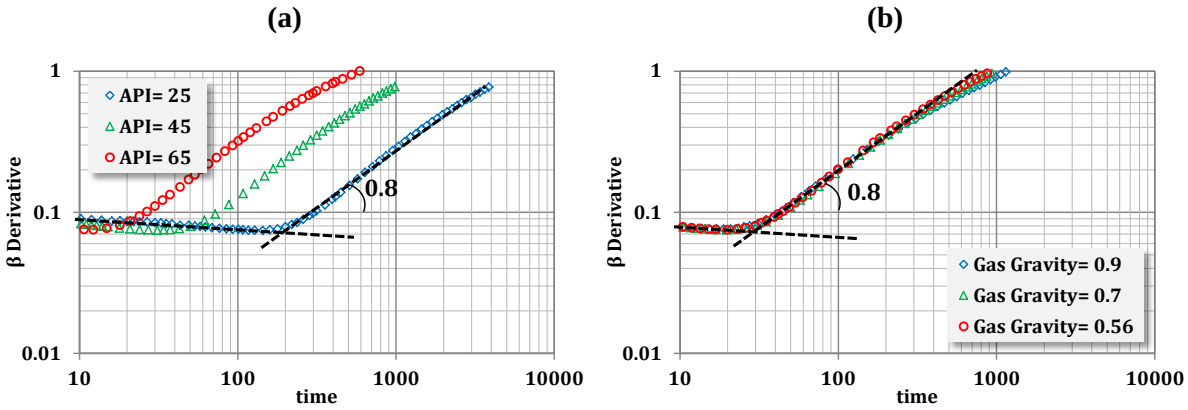

Figure 6.12: Effect of (a) oil API and (b) gas specific gravity on the calculated beta derivative single phase reservoirs with radial flow.

The results obtained so far, demonstrate that beta derivative displays two approximate straight line segments, one associated with transient flow and the other with BDF. The

transient and BDF straight lines have different slopes and their intersection give the time for the start of BDF. It is found that in cases where constant fluid properties during production and reservoir depletion can be assumed (i.e. water as the reservoir fluid) the BDF straight line gives a slope of unity, regardless of the flow regime (i.e. radial or linear). However, when the fluid properties are allowed to change with pressure (i.e. single-phase live-oil or gas), it has been shown that the flow geometry determines the slope during BDF. While the BDF slope is 0.5 for linear flow, it is approximately equal to 0.8 for radial flow. This finding applies irrespective of whether the reservoir fluid is oil or gas.

6.4 New Rate Decline Equations Based on Beta Derivative

Transient and BDF straight lines on a log-log plot of beta derivative versus time reflect the nature of rate decline and therefore can be used for production forecasting. As a result, and similar to Arps in using the loss ratio (or decline rate) for obtaining rate decline equations, the β derivative can be use to model the declining rate behaviour of reservoirs producing at constant pressure. The equation of a straight line on logarithmic coordinates can be employed to obtain the following relation for the beta derivative during transient flow (i.e. $t \leq t_{BDF}$):

$$\beta = \beta_{BDF}\left(\frac{t}{t_{BDF}}\right)^{m_t} \qquad \text{Eq. 6.2}$$

In this equation, m_t is the slope of the transient straight line, t_{BDF} is the time that BDF starts and β_{BDF} is the beta derivative at t_{BDF}. β_{BDF} depends mainly on the type of flow regime and skin value. It is an important parameter which, based on simulation results can

range between 0.5 as for the case of linear flow without skin to 0.01 for the case of radial flow with large values of positive skin.

In a similar fashion, the equation of a straight line of the beta derivative on logarithmic coordinates during BDF (i.e. $t > t_{BDF}$) gives the following relation:

$$\beta = \beta_{BDF}\left(\frac{t}{t_{BDF}}\right)^{m_b} \quad \text{Eq. 6.3}$$

In this equation m_b is the slope of the BDF straight line on the log-log plot of the beta derivative. Using the definition of beta derivative, Eq. 6.1, Eq. 6.2 can be integrated to obtain the relevant equation for rate during transient flow period, Eq. 6.4:

$$q = q_i exp\left(-\frac{\beta_{BDF}}{m_t} \times \left\{\left(\frac{t}{t_{BDF}}\right)^{m_t} - \left(\frac{t_i}{t_{BDF}}\right)^{m_t}\right\}\right) \quad \text{Eq. 6.4}$$

In this equation, q_i is the observed rate at the initial time t_i. One can also perform integration of Eq. 6.3 from the time in which the reservoir boundaries are sensed (t_{BDF}) to obtain the following rate equation during BDF:

$$q = q_{BDF}\exp\left(-\frac{\beta_{BDF}}{m_b} \times \left\{\left(\frac{t}{t_{BDF}}\right)^{m_b} - 1\right\}\right) \quad \text{Eq. 6.5}$$

In this equation, q_{BDF} is the rate at t_{BDF} which can be obtained using Eq. 6.4. Expressing Eq. 6.4 and Eq. 6.5 in terms of dimensionless parameters enables the construction of type curves. Using the Fetkovich (1980) style of terminology, the dimensionless decline time and rate are defined according to the following equations:

$$t_{Dd} = \frac{t}{t_{BDF}} \quad \text{Eq. 6.6}$$

$$q_{Dd} = \frac{q}{q_{BDF}} \qquad \text{Eq. 6.7}$$

Dimensionless rate defined above is identical to that of Fetkovich, while the dimensionless time defined here is different from that of Fetkovich by a constant multiplier. Substituting these definitions in Eq. 6.2 to Eq. 6.5, one can construct different type curves for analysis of rate data during both transient and BDF flow regimes. Such type curves are convenient for determining the rate decline parameters through a type curve matching process. An example of the resulting type curve for $m_t = 0$ and $m_b = 1.0$ and different values of β_{BDF} are shown in Figure 6.13(a) and (b). The former shows the type curve for the beta derivative and the latter shows the corresponding dimensionless rate decline with time. These type curves can be used as diagnostic plots only for obtaining an idea about the value of β_{BDF} and not for m_t and m_b.

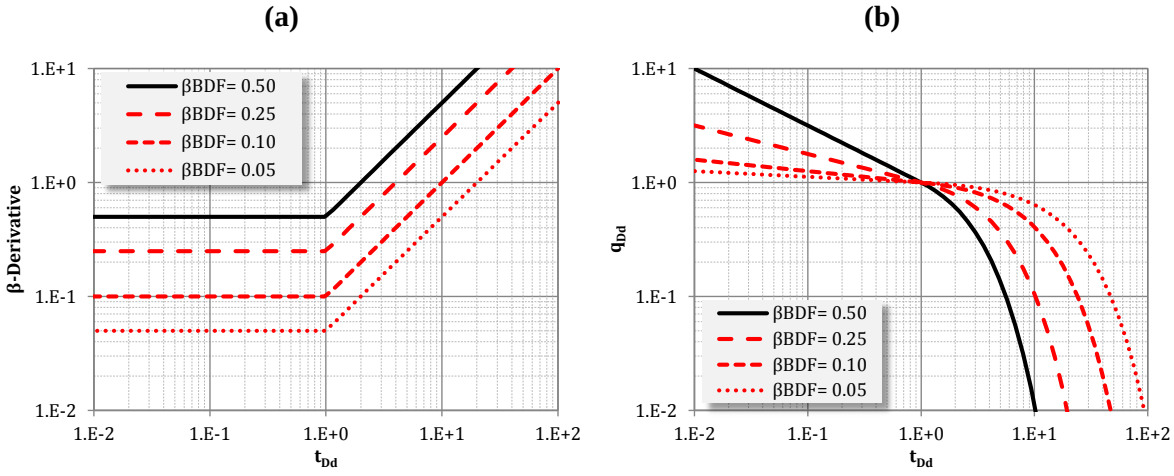

Figure 6.13: Logarithmic plot of (a) beta derivative and (b) dimensionless rate decline versus dimensionless time, for $m_t = 0$ and $m_b = 1.0$.

In addition, for any value of β_{BDF}, one can construct another set of type curves to be used for obtaining estimates of m_t and m_b. Figure 6.14(a) and (b) show the type curves for

$\beta_{BDF} = 0.5$. Juxtaposition of the type curve for beta derivative (Figure 6.14(a)) and dimensionless rate decline (Figure 6.14(b)) shows that during transient flow (i.e. $t_{Dd} < 1$) positive values of m_t, which in most cases correspond to a positive skin value, create downward curvature in the rate decline. This is in contrast to an upward curvature as a result of a negative m_t, attributed to the effect of negative skin.

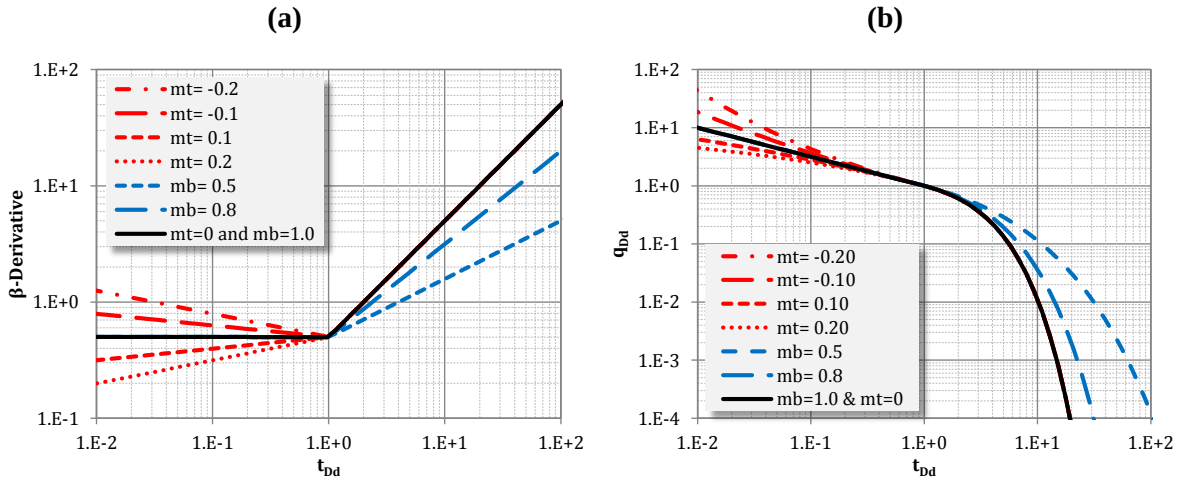

Figure 6.14: Log-log plot of (a) beta derivative and (b) dimensionless rate versus dimensionless time for various values of m_t and m_b, for linear flow ($\beta_{BDF} = 0.5$).

During BDF, these plots show the curves for m_b equal to 0.5 and 0.8, as these correspond to BDF linear and BDF radial depletion. In addition to these stems, the black solid curve is for $m_b = 1.0$ which represents the decline behaviour of a fluid with constant fluid properties (i.e. exponential decline).

Plots in Figure 6.13 and Figure 6.14 depict how the rate decline type curves are related to beta derivative type curves. Although theoretically both of these type curves (i.e. beta derivative and rate decline) can be used for parameter estimation, the difficulty in obtaining reasonable beta derivative from noisy rate data makes the beta derivative type curve impractical. As a result, the rate decline type curves are the recommended type

curves for parameter estimation. In the next sections, the recommended procedure for parameter estimation and rate forecasting is outlined and an example of its application is given afterwards.

6.5 Forecasting Procedure

Using the above observation and resulting type curves, a simple and systematic procedure for forecasting production is presented:

1. Determine the first reliable measured rate and the corresponding time (q_i and t_i). For practical application and due to data uncertainty and quality issues one can make use of an approach similar to that of Duong (2011), i.e. using the best 1-month or 3-month average rate instead of the first measured rate.
2. Use type curve shown in Figure 6.13(b) to obtain an idea about the type of dominant flow regime and therefore a rough estimate of the value of β_{BDF}. One can also use other methods available in the literature to determine the dominant flow regime. As an example, one can use linear specialized plot where $1/q$ is plotted versus $\sqrt{t}$ on Cartesian coordinates which upon achieving a reasonable straight line indicates that the dominant flow regime is linear. As demonstrated in the previous sections, for pure linear flow without skin $\beta_{BDF} = 0.5$.
3. Use the β_{BDF} obtained in the previous step to generate another set of type curve similar to that of Figure 6.14(b) for determining the slope of the transient straight line, i.e. m_t. Upward or downward concavity of the logarithmic plot of the early time rate data indicate positive or negative transient slope (m_t), respectively.

4. After matching the early time data and therefore obtaining a rough estimate of β_{BDF} and m_t, determine m_b through matching the rate data plot with the late time portion of the type curve obtained in the previous step (similar to Figure 6.14(b)). It is noted that $m_b = 1.0$ indicates no change in reservoir fluid properties (i.e. exponential decline), $m_b = 0.5$ and 0.8 indicate a reservoir fluid whose properties change with depletion and the dominant flow regime is linear and radial flow, respectively.
5. Calculate t_{BDF} and also q_{BDF} from the corresponding coordinates of rate data plot at $t_{Dd} = 1$ and $q_{Dd} = 1$.
6. Use the parameters (m_t, m_b, β_{BDF} and t_{BDF}) corresponding to the obtained matched type curve in Eq. 6.4 and Eq. 6.5 to calculate (and forecast) the rates during transient and BDF.

Note. Tight and shale reservoirs exhibit pure linear flow for long times. Knowing this, for these reservoirs one can use $\beta_{BDF} = 0.5$ and $m_b = 0.5$ and a value for m_t which correspond to their skin value.

6.6 Simulation Example

In order to validate the proposed approach and equations, the linear flow gas simulation case (Section 6.3.1.3 with no skin) is used for analysis. For this case, one year of the synthetic production data was used for analysis. The data were analyzed as discussed in steps 1 through 5 in the forecasting procedure described in the preceding section. The satisfactory match for this case corresponded to $\beta_{BDF} = 0.5$, $m_t = -0.05$ and $m_b = 0.5$, as shown in Figure 6.15. Figure 6.16, on the other hand, shows the satisfactory match by

using the method proposed by Nobakht et al. (2012). Nobakht et al. presented a simplified approach by combining the linear flow equations during the transient period with Arps equations during BDF. They simulated a similar case and proposed using Fetkovich b-value equal to 0.5 for BDF. Plots in Figure 6.15 and Figure 6.16 demonstrate perfect matches of the available rate data using both methods.

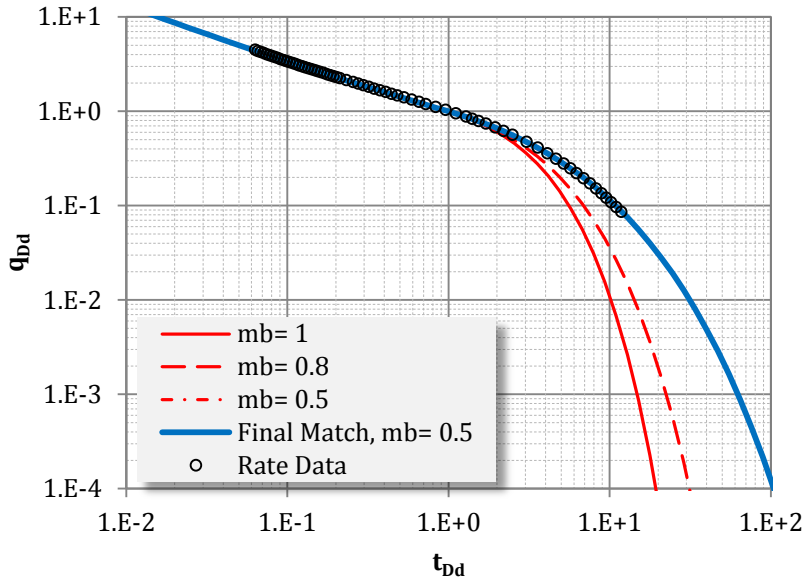

Figure 6.15: Type curve matching for the simulation example using the proposed approach (β_{BDF} = 0.5).

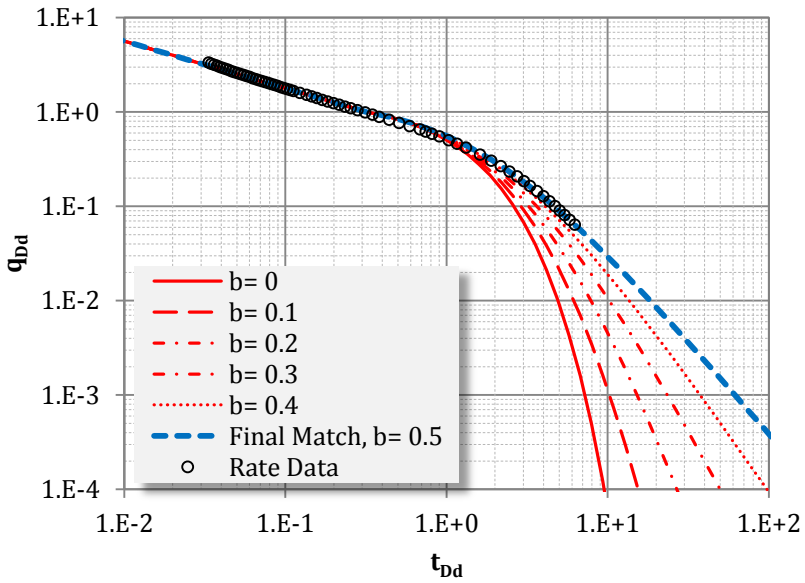

Figure 6.16: Type curve matching for the simulation example using Nobakht et al. (2012) approach.

The resulting parameters were then used to calculate the rates for 10 more years of production. Comparison of the calculated rates against the original numerically generated synthetic rates are given in Figure 6.17. This figure shows the calculated rates using the proposed approach compared against the calculated rates using Nobakht et al. approach. Simple comparison of these rates with the simulation results depicts the ability of the proposed methodology to generate more reasonable long-term production forecasts.

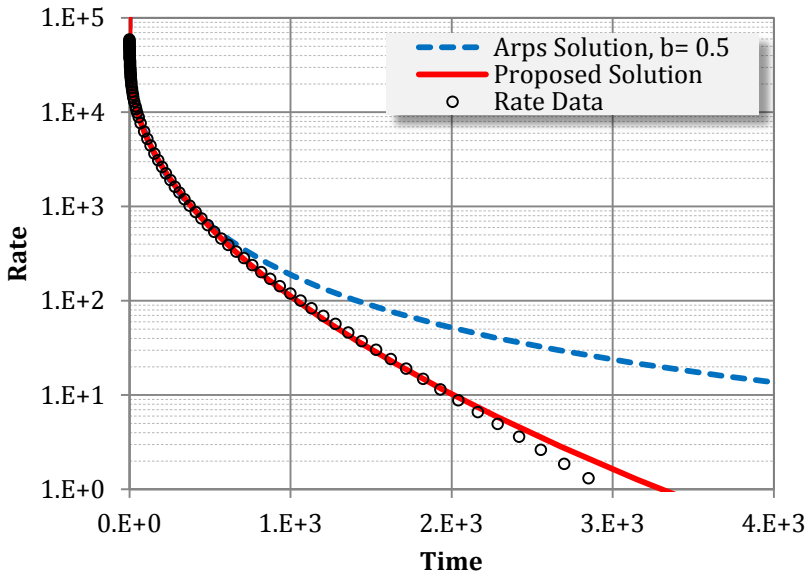

Figure 6.17: Comparison between the simulated production rate (symbols), the rates obtained using the proposed method (solid line) and Nobakht et al. (2012) method (Arps b=0.5) (dashed line).

The reason for the overestimation of rates as a result of using Nobakht approach (with Arps b=0.5 during BDF) can be simply explained in Figure 6.18 and Figure 6.19. While Figure 6.18 demonstrates excellent match of the entire production period using the proposed methodology, Figure 6.19 shows that while b=0.5 is reasonable early in BDF, this value does not stay constant. Instead, in reality, the b-value varies due to changes in properties of gas with depletion.

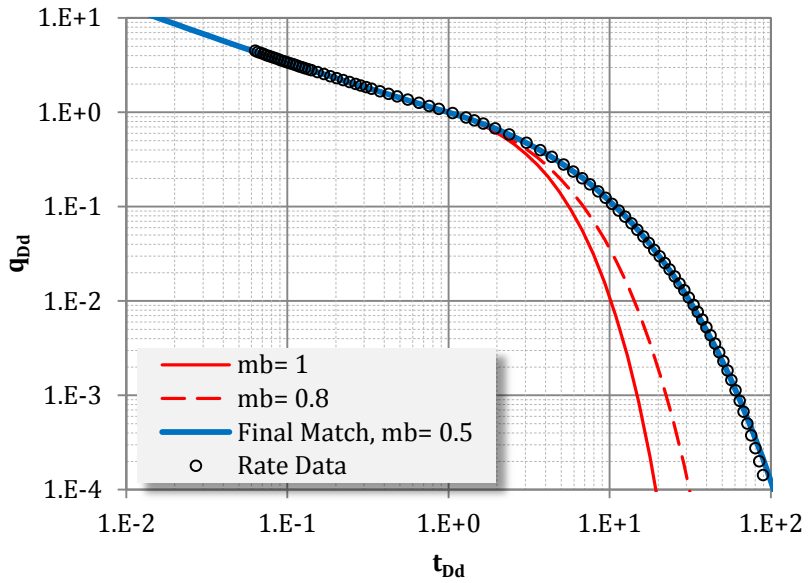

Figure 6.18: Type curve matching of the simulation rates using the proposed type curves which is based on beta derivative.

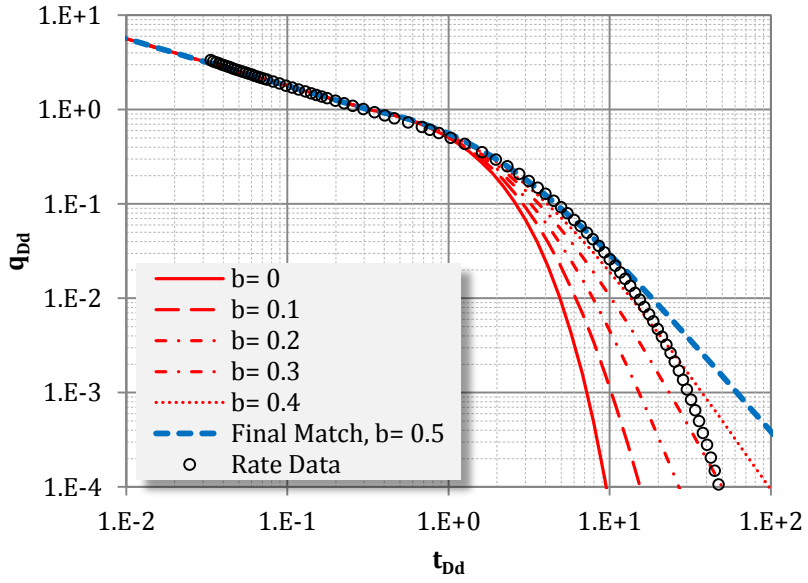

Figure 6.19: Type curve matching of the simulation rates using the approach presented by Nobakht et al. (2012) which is based on Arps method.

6.7 Discussion

Forecasting production and estimating reserves have been among the most challenging tasks for petroleum engineers. It becomes a more daunting task in the case of tight and shale reservoirs with extended transient flow. Lack of knowledge of the basic reservoir properties, like the permeability and the areal/vertical extent, often forces analysts to resort to empirical methods which are easy to use. Recently, Power Law and Stretched Exponential decline models have received considerable attention for rate prediction and reserve estimation in unconventional plays. The problem with these methods, though, is that their involved parameters lack physical meaning, from a reservoir engineering standpoint, and therefore they suffer from arbitrariness.

The method presented in this work is based on meaningful interpretation of a simple diagnostic parameter (beta derivative). Simulation results show that the logarithmic plot of beta derivative versus time results in one reasonable straight line during transient flow and another one during BDF. This is used as a framework to propose rate decline equations which exhibit a form similar to the SEDM proposed by Valko (2009). The advantage of the method proposed in this chapter is that the equations involve tangible parameters that can be obtained (or reasonably estimated) using other available methods, or type curve matching. These parameters are β_{BDF} which mainly reflects the type of flow regime, m_t which determines the upward or downward curvature during transient flow and m_b which determines the degree of curvature during BDF.

Our numerical simulation results show that the value of BDF slope (m_b) depends mainly upon the type of flow regime and fluid type. In the case of constant fluid properties this value is equal to unity, indicating exponential decline. For cases where fluid properties can

change with production, pure linear flow results in m_b values near 0.5. Pure radial flow regime yields m_b near 0.8. Although the BDF slope value is also influenced by the type of oil and gas flowing toward the wellbore, numerical studies show that this effect is overshadowed by the type of flow regime. Obviously, for flow geometries that do not exhibit a pure radial or linear flow, it is expected that during BDF beta derivative show a slope between 0.5 and 0.8. Figure 6.20(a) shows a gas simulation case with a reservoir geometry that is neither radial nor linear. Numerical calculation of beta derivative obtained for this case is given in Figure 6.20(b) showing a BDF slope equal to 0.65.

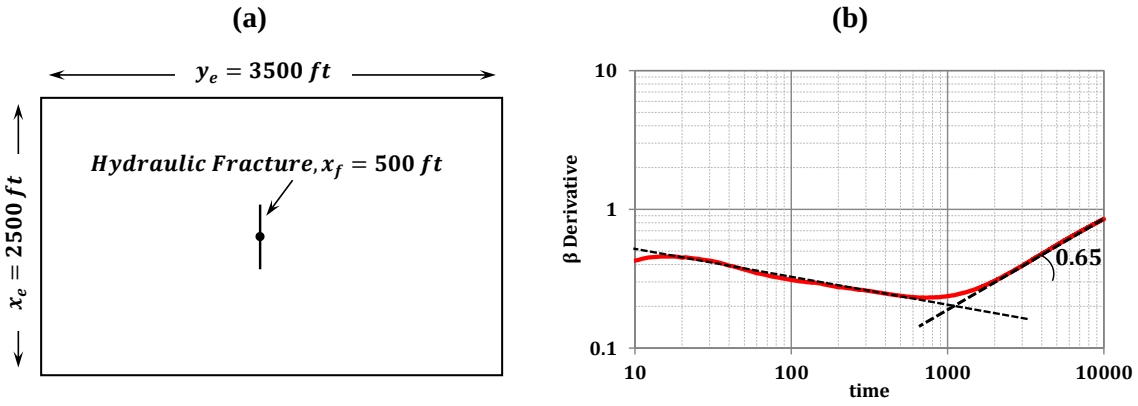

Figure 6.20: Schematic of a hydraulically fractured well in the center of a rectangular reservoir (a) and its calculated beta derivative (b).

Comparison of the radial and linear flow beta derivatives for the different oil/ gas cases and the case in the above figure shows a unique feature of two of the main parameters (i.e. β_{BDF} and m_b). Several numerical experiments show that for the calculated beta derivatives in all simulation cases, there exists a relationship between β_{BDF} and m_b. Although further scrutiny is required, it is observed that lower β_{BDF} results in higher m_b. Obtaining an appropriate simple relationship between these parameters in terms of reservoir variables

(e.g. permeability, porosity and …) reduces the uncertainty concomitant with choosing m_b for reasonable rate forecast, using limited rate data.

In short, the proposed methodology is appealing because it is not limited to a specific flow regime. As can be shown rigorously using analytical solutions, the method is appropriate for the case of linear flow of constant compressibility liquid (transient and BDF). It works also reasonably well for other types of reservoir fluid during transient (radial and linear) and BDF, with and without skin. The main assumptions associated with the method include: (1) production is at a constant wellbore pressure, and (2) the future production trend follows that of the past. Under these limiting conditions, which are similar to those of Arps, the method can be used with a reasonable degree of accuracy for production forecasting.

6.8 Chapter Summary and Conclusions

An easy to use new approach for predicting future rate in conventional and unconventional oil and gas reservoirs is presented. The method relies principally on the observation that a plot of rate-based beta derivative versus time on log-log coordinates gives a straight line during transient flow and a second straight line during BDF. Numerical simulation of reservoirs with dominant linear and radial flow, with and without skin, confirmed this observation. Using the equations of straight lines and upon simple integration, a new methodology was developed that can be used for forecasting decline in production rate. Key conclusions from this work are as below:

- The proposed equations are simple, easy to use and enable the generation of reliable transient and BDF type curves.

- The beta derivative at the start of BDF (β_{BDF}) is directly related to the type of flow regime and skin value.
- Extensive numerical simulation revealed that only for cases where the fluid properties do not change with time, i.e. water as the reservoir fluid, the slope of beta derivative during BDF (m_b) is equal to unity. This behaviour gives well-known exponential decline. For oil and gas cases where the fluid properties change with time, m_b mainly depends on the dominant flow geometry. While $m_b = 0.5$ for pure linear type of depletion, $m_b = 0.8$ for pure radial depletion.
- The numerical simulation corroboration presented in this Chapter indicates that the proposed method provides reliable production rate forecasting while staying away from the analytical complexities of using pseudo-time and its iterative procedure. The observation holds true in the cases of water, oil and gas production rates.

Chapter Seven: Field Applications

7.1 Scope of the study

Welltesting and production data analysis problems are generally inverse problems, meaning that the system (model) characteristics are to be determined by examining the input (pressure or rate) and output (rate or pressure) data. Ubiquitous in all inverse problems is the non-uniqueness issue, i.e. there are many models that can be used to generate the same set of input-output data. As a result, one has to be cautious not to rely on a single model or method to analyze the welltesting and/or production data.

Notwithstanding the need for using both traditional and modern decline curves for analysis of production data, in this chapter only the type curves and procedures developed in the previous chapters are used. As such, six field examples are presented. The first two are analysis of synthetic variable rate/pressure data. Their results confirm the ability of the proposed models to reasonably forecast production rate of field cases. Then four tight and shale field cases previously reported in the literature are examined. Their rate-time data are analyzed, future rates are forecasted and consistent results are obtained.

7.2 Field examples

7.2.1 Case 1 – Dry gas multi-fractured well in WCSB (Yu et al. 2013)

This example well is a dry open-hole horizontal well that is hydraulically fractured in multiple stages, with pertinent details given by Yu et al. (2013). The historical pressure and rate data for this well are shown in Figure 7.1(a). Using the BHP data, a synthetic set of rate data corresponding to a Fekete's horizontal multi-stage fracture model was created. A

comparison plot of the synthetic rate data with the field data is shown in Figure 7.1(b). The model used to create this synthetic rate data set has an OGIP of 1805 MMScf.

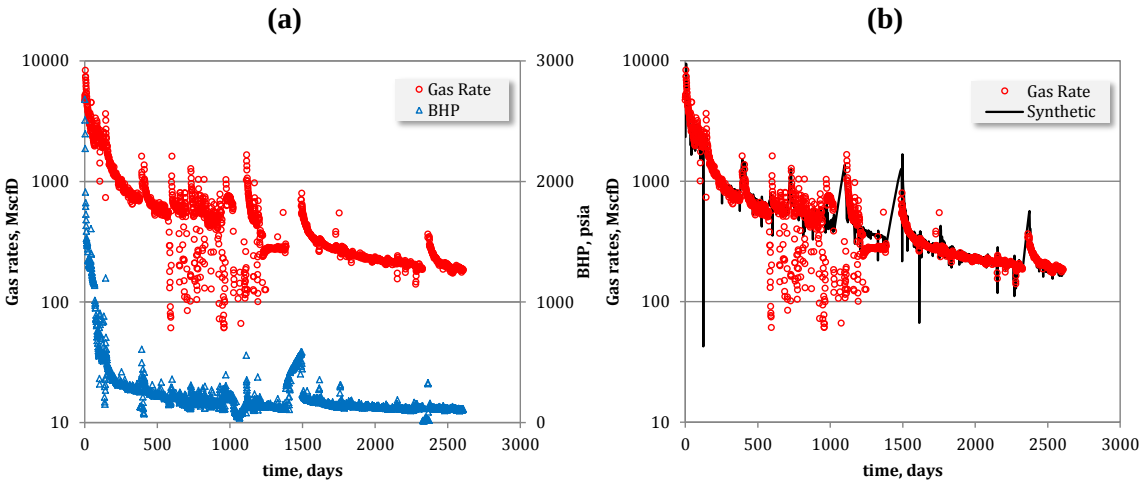

Figure 7.1: (a) Cartesian plot of historical BHP and rate, Case 1 (Yu et al. 2013); (b) comparison of the generated synthetic rates with field rates (this study).

The variable pressure and (synthetic) rate data were then analyzed using the CRM. Looking at the pressure plot, it was assumed that the BHP is constant and equal to 150 psia. Gas gravity of 0.621 was used to generate the table of pressure-pseudo-pressure-p/Z. The required parameters for obtaining a reasonable match of the declining rate data were determined to be: $q^1 = 15000$ MScfD, $CRR = 6800$ $(MScf/psia)^2/Day$, $t_{BDF} =$ 475 days. The result of examining these parameters in CRM are shown in Figure 7.2(a). As it can be seen, the CRM reasonably forecasts the rate decline. In addition, the rate-time decline equation based on beta derivative was used to forecast production rate of this example case. The following parameters ($m_t = 0.01, m_b = 0.5, \beta_{BDF} = 0.5$ and $t_{BDF} =$ 475 days) were used to obtain a reasonable match of the declining rate. Value of β_{BDF} indicates pure linear flow for this example. Figure 7.2(b) gives a comparison of the forecasted rates using the beta derivative approach.

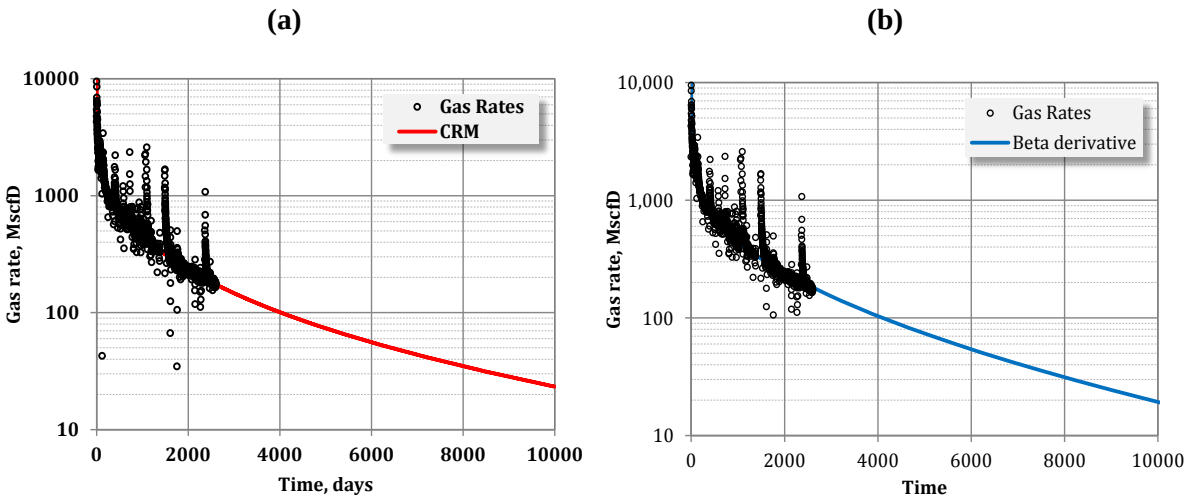

Figure 7.2: Analysis of synthetic rate data using the (a) CRM and (b) the Beta Derivative – Case 1.

Using an abandonment rate of 15 MScfD, the expected ultimate recovery (EUR) based on the beta derivative was determined to be 1766 MMScf. This is in close agreement with the original gas in place used for construction of the synthetic rates. Evaluation of the data using Arps method with b=0.5 and b=1.0 yielded EUR equal to 1924 and 2408 MMScf, respectively. These results demonstrate the overestimation of EUR using Arps method.

7.2.2 Case 2 – Dry gas multi-fractured well in WCSB (Yu 2013)

This example is a horizontal well that is hydraulically fractured in multiple stages, with pertinent details given by Yu (2013). The historical pressure and rate data for this well are shown in Figure 7.3(a). This well is in a reservoir having a lower permeability compared with the previous case. Similar to the previous example and using the BHP data, a synthetic set of rate data corresponding to a Fekete's horizontal multi-stage fracture model was created. Comparison of the synthetic rate data with the field data is shown in Figure 7.3(b). The model used to create the synthetic rate has an OGIP of 2091 MMScf.

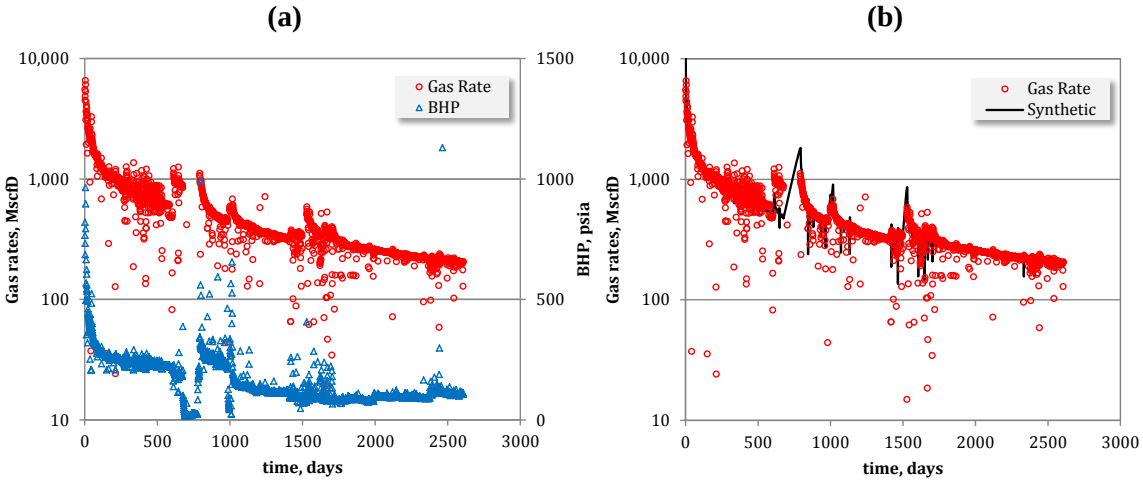

Figure 7.3: (a) Cartesian plot of historical BHP and rate, Case 2 (Yu 2013); (b) comparison of the generated synthetic rates with field rates (this study).

The variable pressure and (synthetic) rate data were then analyzed using the CRM. Looking at the pressure plot, it was assumed that the wellbore flowing pressure is constant and equal to 110 psia. Gas gravity of 0.65 was used to generate the table of pressure-pseudo-pressure-p/Z. The parameters determined for matching the declining rate data were: $q^1 = 11000$ MScfD, $\text{CRR} = 55\ (\text{MScf/psia})^2/\text{Day}$, $t_{BDF} = 700$ days. The result of examining these parameters in CRM are shown in Figure 7.4(a). Evidently, the CRM reasonably forecasts the rate decline. The smaller value of CRR compared with the previous example illustrates either a higher resistivity (lower permeability) or lower capacity (smaller porosity and/or total compressibility) of the reservoir in this case. The synthetic rate data was also analyzed using the rate-time decline equation based on beta derivative. These parameters ($m_t = 0.01, m_b = 0.5, \beta_{BDF} = 0.5$ and $t_{BDF} = 700$ days) were used to obtain a reasonable match of the declining rate. Again, the value of β_{BDF} in this case indicates pure linear flow. Figure 7.4 (b) gives a comparison of the forecasted rates using the beta derivative approach.

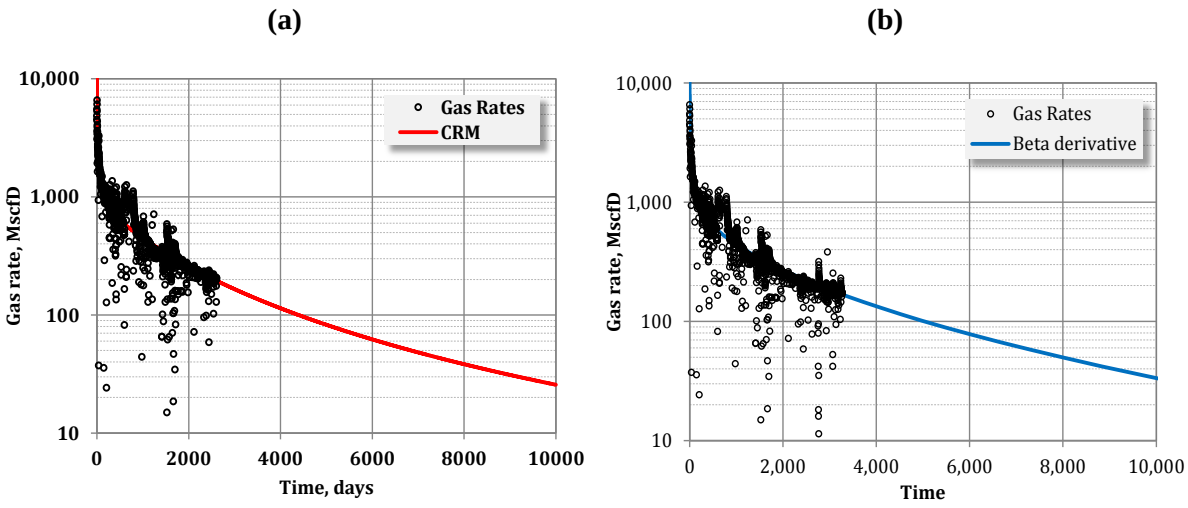

Figure 7.4: Analysis of synthetic rate data using the (a) CRM and (b) the Beta Derivative – Case 2.

Using an abandonment rate of 15 MScfD, the EUR based on the beta derivative was determined to be 2086 MMScf. This is in close agreement with the original gas in place used for construction of the rate data. Evaluation of the same data using Arps method with b=0.5 and b=1.0 resulted in EUR equal to 1915 and 2691 MMScf, respectively. These results are indicative of the overestimation of EUR using Arps method.

7.2.3 Case 3 – East Texas Tight Gas Sand Well (Ilk 2010, Pratikno et al. 2003)

This case is a hydraulic fractured tight gas well in east of Texas reported by Ilk (2010). Average porosity and calculated permeability for this case are determined to be 9% and 0.015 md, respectively. Ilk (2010) applied analytical, semi-analytical and different empirical models to obtain predictions of the declining rates. He mentioned that based on knowledge of the well completion, as well as prior analysis of the data done by Pratikno et al. (2003), the reservoir model should be that of a vertically fractured well with low fracture conductivity.

The CRM (discussed in chapter 3) was used to analyze the rate-time data of this well. Assuming a gas gravity of 0.7, the table of pressure, pseudo-pressure and p/Z were generated and used in the procedure described in Figure 3.6. The logarithmic plot of rate vs. time showed that the early time data give an almost 0.5 slope, indicating no possible skin effect. Using $\mathrm{CRR} = 200$ and $\mathrm{t_{BDF}} = 300$ days and $\mathrm{s^*} = 0$ psia/StbD, the results shown in Figure 7.5 were obtained.

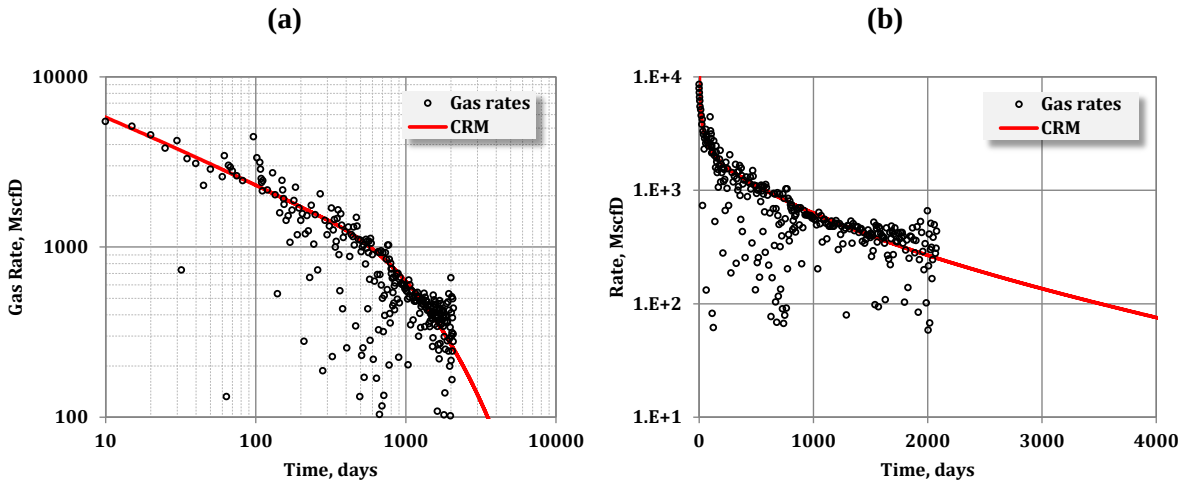

Figure 7.5: Analysis of declining rate data using the CRM – Case 3.

In addition, the rate-time data from this well were analyzed using the rate decline equations based on beta-derivatives. Based on the procedure proposed in Chapter 6, the parameters used for matching the rate data (shown in Figure 7.6(a)) were determined to be: $\beta_{BDF} = 0.5$, $m_t = 0.01$ and $m_b = 0.5$. Consistent with the results of the CRM, the value of m_t was greater than zero and indicated skin effect at early times. In addition, $\beta_{BDF} = 0.5$ confirmed existence of linear flow during transient period. As shown in Figure 7.6(a) and (b), the resulting calculated rate decline reasonably compares with the well rate history during early and late times. Included in these graphs are the rate declines obtained by using

$m_b = 0.8$ and also $m_b = 1.0$. Hence $m_b = 1.0$ represents the conventional exponential decline. As can be seen, using $m_b = 0.5$ gives the most reasonable rate decline for this case.

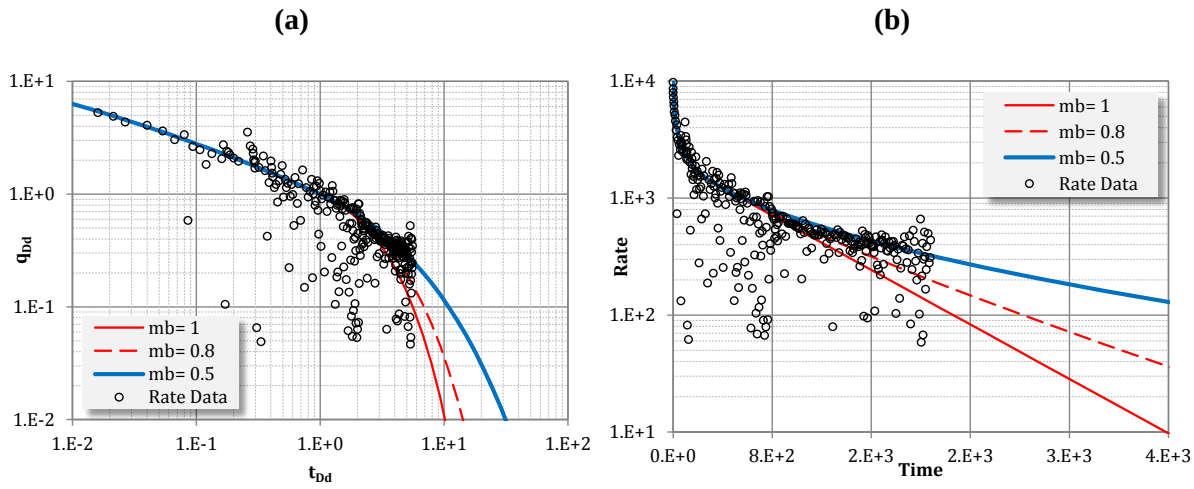

Figure 7.6: Analysis of declining rate data using the β-derivative – Case 3.

7.2.4 Case 4 – Mexico Tight Gas Well (Amini et al. 2007)

This example is a tight gas reservoir with a permeability of less than 0.001 md. The hydraulically fractured vertical well of interest in this reservoir has over 40 years of high quality production data and as a result is literally considered a "near textbook" example which can be used for production data analysis. Amini et al. (2007) developed elliptical models to analyze the declining production rate of this case.

Using the CRM analysis procedure (Figure 3.6) to analyze the rate-time data for this well, the parameters were determined to be CRR = 730 and $t_{BDF} = 4100$ days. It should be mentioned that a gas gravity of 0.65 was used for generating the results. Moreover, the skin was considered to be negligible ($s^* = 0$). As can be seen in both plots of this figure, the CRM perfectly matched the rate decline. Here it was assumed that $p_i = 5000$ psia.

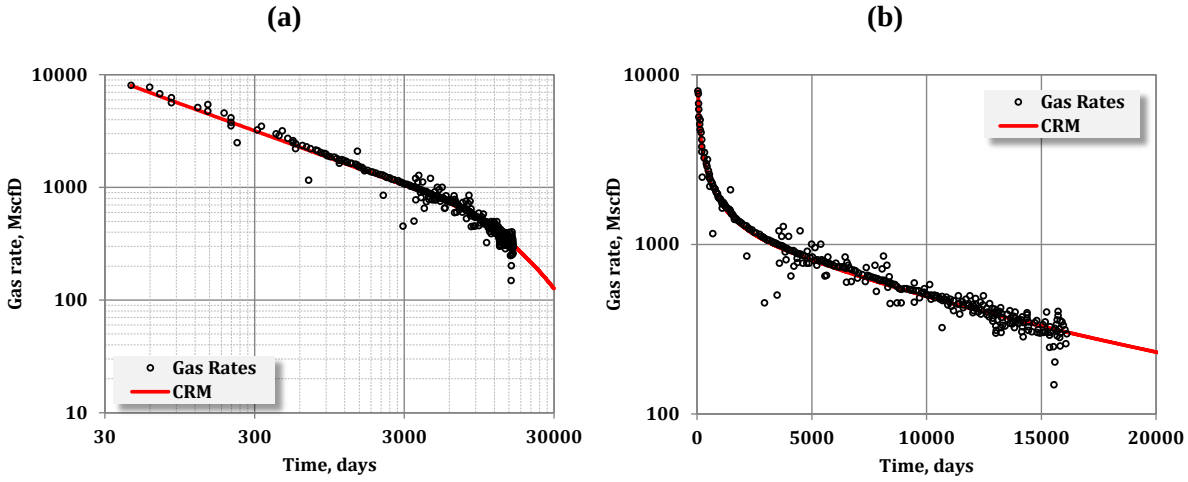

Figure 7.7: Analysis of declining rate data using the CRM – Case 4.

Similar to Case 3, the rate-time data from this well were analyzed using the procedure presented in chapter 6. The following parameters for matching the data and therefore making a forecast were obtained: $\beta_{BDF} = 0.5$, $m_t = 0.001$ and $m_b = 0.5$. The obtained logarithmic type curve match is shown in Figure 7.8(a). The semilog comparison of the calculated rate with the historical rate data is shown in Figure 7.8(b).

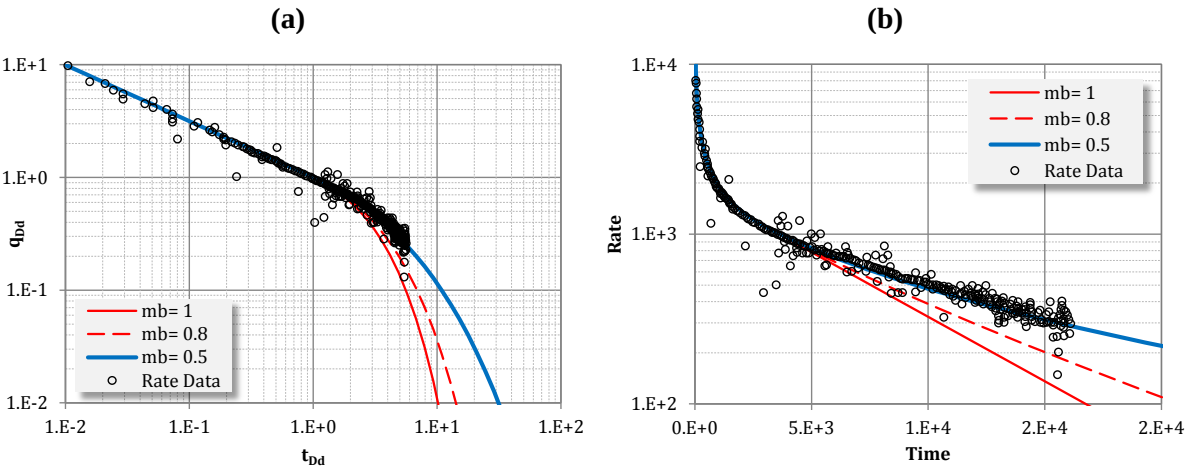

Figure 7.8: Analysis of declining rate data using the β-derivative – Case 4.

The perfect type curve match for this case confirms reasonable long term production forecasting using this decline model. Again, $\beta_{BDF} = 0.5$ confirms linear flow during

transient period, and $m_t = 0.001$ shows existence of small skin effect. These results are similar to the CRM results obtained previously.

7.2.5 Case 5 – Shale Gas Well (Ilk 2010)

This case is a horizontal well with multiple fractures in a shale gas reservoir, reported by Ilk (2010). This example has only 340 days of available production data. Ilk (2010) mentioned that this well exhibits considerable skin effect.

The CRM approach (Figure 3.6) with a table of gas properties generated for an assumed gas gravity of 0.65 were employed. Parameters used for obtaining the match were CRR = 1800 and $t_{BDF} = 130$ days, and $s^* = 0.03$ psia/StbD. As can be seen in the logarithmic plot of rate vs. time, the early time slope was considerably smaller than 0.5, therefore indicating significant skin effect.

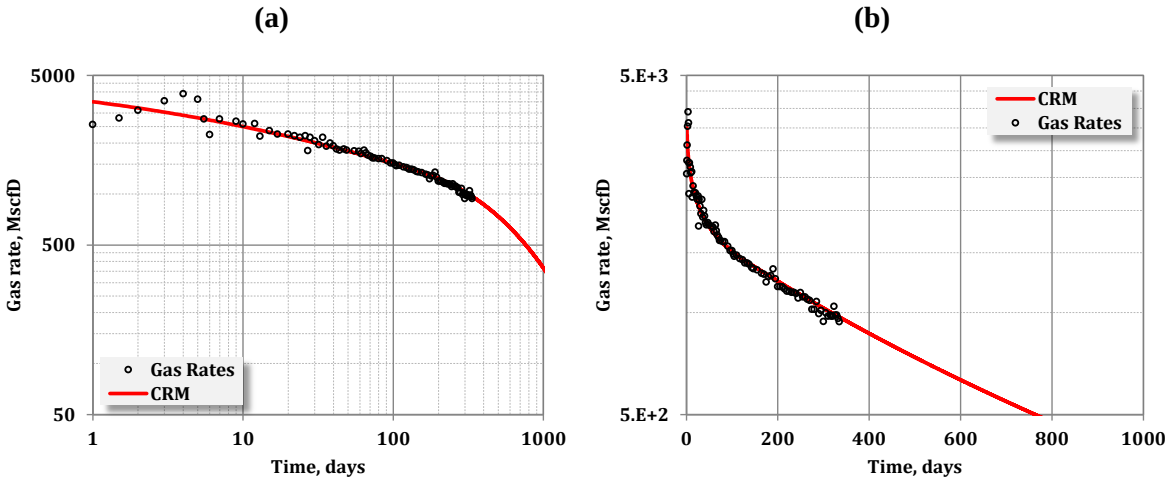

Figure 7.9: Analysis of declining rate data using the CRM – Case 5.

Using the beta derivative type curves, the following parameters for matching the data and therefore producing a forecast were obtained: $\beta_{BDF} = 0.5$, $m_t = 0.35$ and $m_b = 0.5$. The resulting logarithmic type curve match is shown in Figure 7.10(a). The semilog

comparison of the calculated rate with the historical rate data is shown in Figure 7.10(b). Again, $\beta_{BDF} = 0.5$ indicates linear flow and $m_t = 0.35$ shows existence of considerable skin in the data. These results were also obtained by the CRM method. The difference with the CRM, though, is that these type curves indicate that the data is still in transient flow period. While the CRM shows the end of transient flow to happen at approximately 130 days, the match in Figure 7.10(a) shows the start of BDF to be the end of the measured data (hence the end of the data on type curve at $t_{Dd} = 1$). This means that the reservoir has not yet reached the boundaries and the calculated rates might provide a conservative forecast of the future rates.

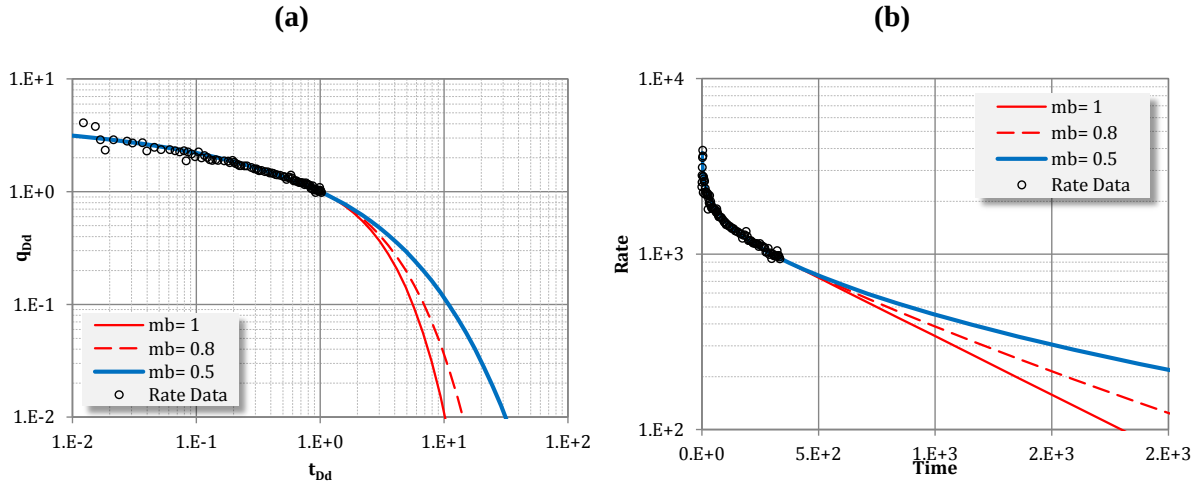

Figure 7.10: Analysis of declining rate data using the β-derivative – Case 5.

7.2.6 Case 6 – Wet Gas Well, WCSB (Yu et al. 2013)

This case is a horizontal well producing wet gas from a naturally fractured reservoir in WCSB with a condensate yield of approximately 5 bbls/MMscf. The rate-time data for this well is from a public database and has been reported by Yu et al. (2013).

The CRM with a table of pressure–pseudo-pressure–p/Z constructed for gas gravity of 0.72 was employed. The following parameters were used for obtaining a match of the rate-time decline data: CRR = 120 and t_{BDF} = 450 days, and $s^* = 0$. As can be seen, the early time data show a slight deviation from half slope. This is probably due to skin effect. In addition, the late portion of the data was not matched by the model. This is due to the effect of liquid loading, as mentioned by Yu et al. (2013).

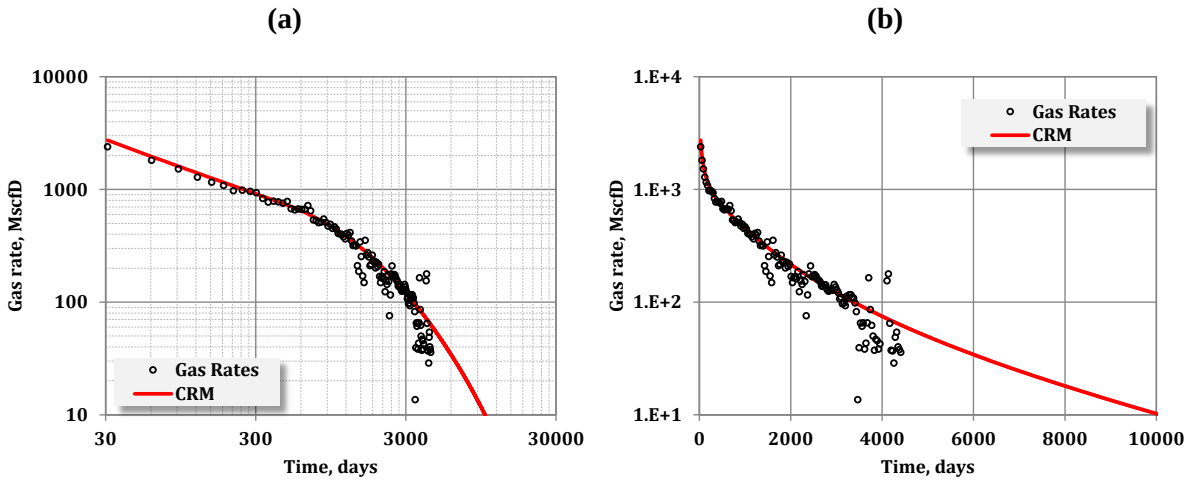

Figure 7.11: Analysis of declining rate data using the CRM – Case 6.

This set of rate-time data was then analyzed by using the beta-derivative method. Following the described procedure, the type curve match and the semilog comparisons, shown in Figure 7.12(a) and (b), were obtained. The match obtained by using $\beta_{BDF} = 0.5$, $m_t = 0.1$ and $m_b = 0.5$ is very reasonable. As can be seen, the last portion of the data was also not matched on this type curve. As mentioned by Yu et al. (2013), the rate during that period dropped more, due to the problem of liquid loading.

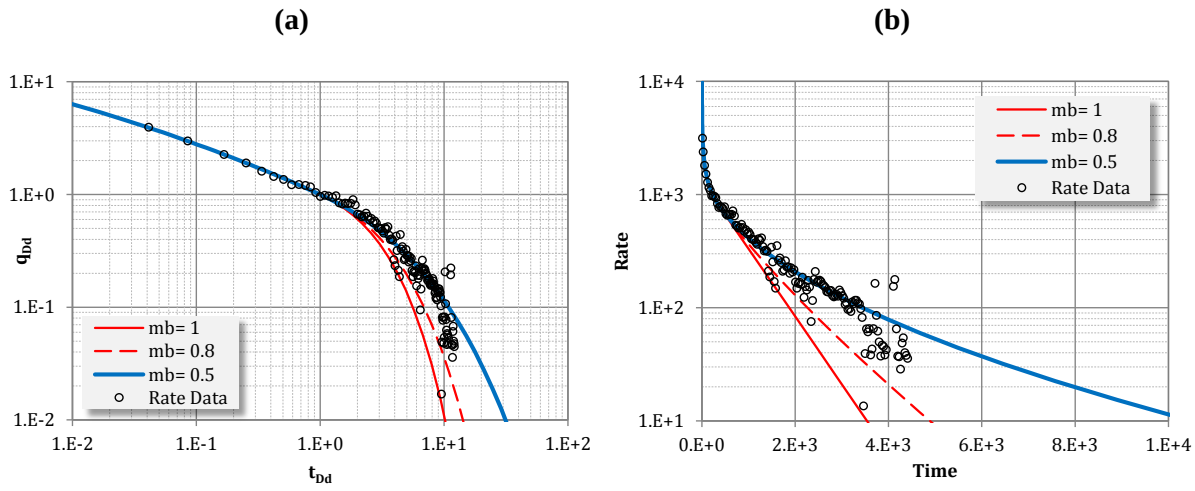

Figure 7.12: Analysis of declining rate data using the β-derivative – Case 6.

7.3 Chapter summary and conclusions

Analysis of the simulation results, shown in the previous chapters, depicted the validity of the developed models and type curves for reliable forecasting of transient and BDF rate and pressure declines. This chapter described their utility for predicting future production in low to ultra-low permeability reservoirs. Only cases where wellbore pressure was relatively constant were considered. As a result, the following conclusions were made:

- Early time data may not reflect longer decline trends. As a result, for obtaining a match using CRM, an initial rate (or pressure) different from the first data point may be used.
- Although not mentioned in this chapter, using skin in the CRM may cause non-uniqueness, i.e. different combinations of s^* and CRR may give the same rate decline.
- The procedure outlined in Chapter 6 provides an easy and useful way of determining the decline parameters during transient and BDF.

Chapter Eight: Summary, Conclusions and Recommendations

8.1 Summary and Conclusions

The goal of this research was to develop a simple methodology for reasonable performance forecasting of unconventional (tight and shale) reservoirs with extended transient flow. The capacitance-resistance model (CRM) was developed which was the result of stepwise coupling of the material balance and fluid-flow equations. Using the distance of investigation equation, it was shown that the methodology can be used for transient and BDF of oil, gas and water reservoirs. The model was extended to multilayered and compartmentalized reservoir cases. In addition, a simple rate decline forecasting model was developed that relies on simulation observation of the rate-based beta derivative. As a result, its parameters are not totally arbitrary, as is the case of the stretched exponential decline model. The developed models were compared against the corresponding numerical models, i.e. box-shaped reservoirs with fractures traversing the reservoir and circular reservoirs with vertical well in the center implying linear and radial flow, respectively, during their transient period. Under these limiting geometric conditions, excellent results were obtained.

Although the conclusions of each chapter were drawn separately and stated in the corresponding sections of this dissertation, the following major conclusions are made as a result of this study:

- Using the distance of investigation and the depletion equations, minimal data is required for analyzing a reservoir performance and forecasting its production during transient and BDF.

- The physical processes which are involved in production from the unconventional tight and shale reservoirs are complex functions of different phenomena and their performance can be considerably and distinctively influenced by reservoir heterogeneities, including layering, compartmentalization and natural fractures. Their combined effects can be simply captured by adapting the capacitance and resistance parameters in the CRM.
- A two layered or compartmentalized reservoir produces a production performance behaviour (rate/time and/or pressure/time) that a single layer, single compartment reservoir cannot reproduce. As a result, using a tank model with consideration of the layering/compartmentalization effects may be warranted.
- Analysis of rate decline (constant terminal pressure) can be performed based on the behaviour of beta derivative. As a result, simple and easy to use type curves can be generated that are reliable during transient and BDF.
- The parameters involved in the type curves based on beta derivative are functions of the type of fluid, the dominant flow regimes and skin values.

8.2 Recommendations

Based upon the results of this study, the following topics are recommended for further study:

- Capacitance-resistance model developed in this work is based on linear flow regime. This is due the assumption that the hydraulic fracture completely traverses the reservoir. In situations where this assumption is not reasonable, other flow regimes

may develop, leading to an investigated volume that cannot be reasonably calculated based on the distance of investigation equation. New simple methods for calculating volume of investigation may generalize the application of the developed CRM for other flow regimes.

- This research did not consider the effect of desorption in the production data analysis. Considering the adsorption/desorption effects using a tank model is of considerable value especially for shale reservoirs where it can be significant.
- This research focused on single-phase flow of fluids within porous media. Multi-phase flow through porous media certainly complicates analysis of production data. As a result, comprehensive investigation of multi-phase flow using the proposed approaches is recommended.
- Our numerical experiments indicated that there is a relationship between the main parameters (β_{BDF} and m_b) in the developed decline rate based on beta derivative. As mentioned in the Section 6.7, further scrutiny and research for obtaining a correlation between these parameters in terms of reservoir variables can reduce the uncertainty associated with choosing reasonable BDF parameters during transient and early BDF.

References

Agarwal, R.G. 1979. "Real Gas Pseudo-Time" A New Function for Pressure Buildup Analysis of MHF Gas Wells. Paper SPE 8279 presented at the SPE Annual Technical Conference and Exhibition, Las Vegas, Nevada, USA, 23–26 September.

Aguilera, R. 2010. Flow Units: From Conventional to Tight Gas to Shale Gas Reservoirs. Paper SPE 132845 presented at the Trinidad and Tobago Energy Resources Conference, Port of Spain, Trinidad, 27–30 June.

Aguilera, R. 2013. Flow Units: From Conventional to Tight Gas to Shale Gas to Tight Oil to Shale Oil Reservoirs. Paper SPE 165360 presented at the SPE Western Regional & AAPG Pacific Section Meeting, Joint Technical Conference, Monterey, CA, USA, 19–25 Apr.

Aguilera, R., Harding, T.G. 2008. State-of-the-Art Tight Gas Sands Characterization and Production Technology. *Journal of Canadian Petroleum Technology* **47** (12). PETSOC-08-12-37.

Al-Hussainy, R., Ramey, H.J. 1966. Application of Real Gas Flow Theory to Well Testing and Deliverability Forecasting. *Journal of Petroleum Technology* **18** (5): 637–642. SPE-1243-B-PA.

Albertoni, A., Lake, L.W. 2003. Inferring Interwell Connectivity Only From Well-Rate Fluctuations in Waterfloods. *SPE Reservoir Evaluation & Engineering* **6** (1): 6–16. SPE-83381-PA.

Amini, S., Ilk, D., Blasingame, T.A. 2007. Evaluation of the Elliptical Flow Period for Hydraulically-Fractured Wells in Tight Gas Sands--Theoretical Aspects and Practical Considerations. Paper SPE 106308 presented at the SPE Hydraulic Fracturing Technology Conference, College Station, Texas, USA, 29–31 January.

Anderson, D.M., Mattar, L. 2007. An Improved Pseudo-Time for Gas Reservoirs With Significant Transient Flow. *Journal of Canadian Petroleum Technology* **46** (7). PETSOC-07-07-05.

Anderson, D.M., Nobakht, M., Moghadam, S., Mattar, L. 2010. Analysis of Production Data From Fractured Shale Gas Wells. Paper SPE 131787 presented at the SPE Unconventional Gas Conference, Pittsburgh, Pennsylvania, USA, 23–25 February.

Anderson, S., Anderson, D.M., Epp, K.L., Edwards, K., Stalgorova, E. 2012. Pressure Normalized Decline Curve Analysis for Rate-Controlled Wells. Paper SPE 162923 presented at the SPE Hydrocarbon Economics and Evaluation Symposium, Calgary, Alberta, Canada, 24–25 September.

Ansah, J., Knowles, R.S., Blasingame, T.A. 2000. A Semi-Analytic (p/z) Rate-Time Relation for the Analysis and Prediction of Gas Well Performance. *SPE Reservoir Evaluation & Engineering* **3** (6): 525–533. SPE-66280-PA.

Araya, A., Ozkan, E. 2002. An Account of Decline-Type-Curve Analysis of Vertical, Fractured, and Horizontal Well Production Data. Paper SPE 77690 presented at the SPE Annual Technical Conference and Exhibition, San Antonio, Texas, USA, 29 September–2 October.

Arevalo-Villagran, J.A. 2001. Analysis of long-term behavior in tight gas reservoirs: Case histories. PhD Thesis, Texas A&M University, College Station, TX.

Arps, J.J. 1945. Analysis of Decline Curves. *Transactions of the AIME* **160**: 228–247.

Bello, R.O. 2009. Rate transient analysis in shale gas reservoirs with transient linear behavior. PhD Thesis, Texas A&M University, College Station, TX.

Bello, R.O., Wattenbarger, R.A. 2010. Modelling and Analysis of Shale Gas Production With a Skin Effect. *Journal of Canadian Petroleum Technology* **49** (12): 37–48. SPE-143229-PA.

Blasingame, T.A. 2008. The Characteristic Flow Behavior of Low-Permeability Reservoir Systems. Paper SPE 114168 presented at the SPE Unconventional Reservoirs Conference, Keystone, Colorado, USA, 10–12 February.

Blasingame, T.A., Lee, W.J. 1986. Variable-Rate Reservoir Limits Testing. Paper SPE 15028 presented at the Permian Basin Oil and Gas Recovery Conference, Midland, Texas, USA, 13–15 March.

Boggs, S. 2001. *Principles of Sedimentology and Stratigraphy*, 3rd edition, Prentice Hall.

Bourdet, D., Ayoub, J.A., Pirard, Y.M. 1989. Use of Pressure Derivative in Well Test Interpretation. *SPE Formation Evaluation* **4** (2): 293-302. 00012777.

Bourdet, D., Whittle, T.M., Douglas, A.A., Pirard, Y.M. 1983. A New Set of Type Curves Simplifies Well Test Analysis. *World Oil*.

Bradley, J.S., Powley, D.E. 1994. Pressure Compartments in Sedimentary Basins: A Review. In *Basin Compartments and Seals*, ed. Peter J. Ortoleva. The American Association of Petroleum Geologists.

Brohi, I., Pooladi-Darvish, M., Aguilera, R. 2011. Modeling Fractured Horizontal Wells As Dual Porosity Composite Reservoirs – Application to Tight Gas, Shale Gas and Tight Oil Cases. Paper SPE 144057 presented at the SPE Western North American Region Meeting, Anchorage, Alaska, USA, 7–11 May.

Brown, M., Ozkan, E., Raghavan, R., Kazemi, H. 2011. Practical Solutions for Pressure-Transient Responses of Fractured Horizontal Wells in Unconventional Shale Reservoirs. *SPE Reservoir Evaluation & Engineering* **14** (6): 663–676. SPE-125043-PA.

Bruce, W.A. 1943. An Electrical Device for Analyzing Oil-reservoir Behavior. *Transactions of the AIME* **151** (1): 112–124.

Bustin, R.M., Bustin, A.M.M., Cui, A., Ross, D., Pathi, V.M. 2008. Impact of Shale Properties on Pore Structure and Storage Characteristics. Paper SPE 119892 presented at the SPE Shale Gas Production Conference, Fort Worth, Texas, USA, 16–18 November.

Can, B., Kabir, C.S. 2012. Probabilistic Production Forecasting for Unconventional Reservoirs With Stretched Exponential Production Decline Model. *SPE Reservoir Evaluation & Engineering* **15** (1): 41–50. SPE-143666-PA.

Carter, R.D. 1985. Type Curves for Finite Radial and Linear Gas-Flow Systems: Constant-Terminal-Pressure Case. *Society of Petroleum Engineers Journal* **25** (5): 719–728. SPE-12917-PA.

Chan, P., Etherington, J., Aguilera, R., Clarkson, C.R., Barker, G.J., Jenkins, C. 2011. Unconventional Resources Estimation. In *Guidelines for Application of the Petroleum Resources Management System*, Chap. 8.

Cheng, Y., Lee, W.J., McVay, D.A. 2008. Improving Reserves Estimates From Decline-Curve Analysis of Tight and Multilayer Gas Wells. *SPE Reservoir Evaluation & Engineering* **11** (5): 912–920. SPE-108176-PA.

Chilingarian, G.V., Mazzullo, S.J., Rieke, H.H. 1992. Introduction. In *Carbonate Reservoir Characterization: A Geologic-Engineering Analysis, Part I*. Elsevier Science Publishers B.V.

Cinco-Ley, H., Samaniego-V., F. 1981. Transient Pressure Analysis: Finite Conductivity Fracture Case Versus Damaged Fracture Case. Paper SPE 10179 presented at the SPE Annual Technical Conference and Exhibition, San Antonio, Texas, USA, 4–7 October.

Clark, A.J., Lake, L.W., Patzek, T.W. 2011. Production Forecasting with Logistic Growth Models. Paper SPE 144790 presented at the SPE Annual Technical Conference and Exhibition, Denver, Colorado, USA, 30 October–2 November.

Clark, K.K. 1968. Transient Pressure Testing of Fractured Water Injection Wells. *Journal of Petroleum Technology* **20** (6): 639–643. SPE-1821-PA.

Clarkson, C.R., Aguilera, R., Pedersen, P.K., Spencer, R.J. 2011a. SHALE GAS: Part 6 - Influence of Technology on Shale Gas Development. *Canadian Society of Petroleum Geologists* (2): 23–29.

Clarkson, C.R., Aguilera, R., Pedersen, P.K., Spencer, R.J. 2011b. SHALE GAS: Part 8 - Shale Gas Development Optimization. *Canadian Society of Petroleum Geologists* (4): 25–31.

Clarkson, C.R., Bustin, R.M. 2000. Binary gas adsorption/desorption isotherms: effect of moisture and coal composition upon carbon dioxide selectivity over methane. *International Journal of Coal Geology* **42** (4): 241–271.

Clonts, M.D., Ramey, H.J. 1986. Pressure Transient Analysis for Wells With Horizontal Drainholes. Paper SPE 15116 presented at the SPE California Regional Meeting, Oakland, California, 2–4 April.

Corbett, P.W.M., Hamdi, H., Gurav, H. 2012. Layered fluvial reservoirs with internal fluid cross flow: a well-connected family of well test pressure transient responses. *Petroleum Geoscience* **18**: 219–229.

Crain, E.R. 2011. UNICORNS IN THE GARDEN OF GOOD AND EVIL: Part 4 - Shale Gas. *Canadian Society of Petroleum Geologists* (2): 19–22.

Daneshy, A.A. 2003. Off-Balance Growth: A New Concept in Hydraulic Fracturing. *Journal of Petroleum Technology* **55** (4): 78–85. SPE-80992-MS.

DaPrat, G., Cinco-Ley, H., Ramey, H.J. 1981. Decline Curve Analysis Using Type Curves for Two-Porosity Systems. *Society of Petroleum Engineers Journal* **21** (3): 354–362. SPE-9292-PA.

Doublet, L.E., Pande, P.K., McCollum, T.J., Blasingame, T.A. 1994. Decline Curve Analysis Using Type Curves--Analysis of Oil Well Production Data Using Material Balance Time: Application to Field Cases. Paper SPE 28688 presented at the International Petroleum Conference and Exhibition of Mexico, Veracruz, Mexico, 10–13 October.

Duong, A.N. 1989. A New Set of Type Curves for Well-Test Interpretation With the Pressure/Pressure-Derivative Ratio. *SPE Formation Evaluation* **4** (2): 264-272. 00016812.

Duong, A.N. 2011. Rate-Decline Analysis for Fracture-Dominated Shale Reservoirs. *SPE Reservoir Evaluation & Engineering* **14** (3): 377–387. SPE-137748-PA.

Economides, M.J., Oligney, R.E. 2000. *The color of oil: the history, the money and the politics of the world's biggest business*, Round Oak Pub. Co.

El-Banbi, A.H. 1998. Analysis of tight gas well performance. PhD Thesis, Texas A&M University, College Station, TX.

El-Banbi, A.H., Wattenbarger, R.A. 1996. Analysis of Commingled Tight Gas Reservoirs. Paper SPE 36736 presented at the SPE Annual Technical Conference and Exhibition, Denver, Colorado, USA, 6–9 October.

Energy Information Administration (EIA). 2013. Technically Recoverable Shale Oil and Shale Gas Resources: An Assessment of 137 Shale Formations in 41 Countries Outside the United States, Washington DC.

Fetkovich, M.J. 1980. Decline Curve Analysis Using Type Curves. *Journal of Petroleum Technology* **32** (6): 1065–1077. SPE-4629-PA.

Fetkovich, M.J., Bradley, M.D., Works, A.M., Thrasher, T.S. 1990. Depletion Performance of Layered Reservoirs Without Crossflow. *SPE Formation Evaluation* **5** (3): 310–318. SPE-18266-PA.

Fetkovich, M.J., Fetkovich, E.J., Fetkovich, M.D. 1996. Useful Concepts for Decline Curve Forecasting, Reserve Estimation, and Analysis. *SPE Reservoir Engineering* **11** (1): 13–22. SPE-28628-PA.

Fetkovich, M.J., Vienot, M.E., Bradley, M.D., Kiesow, U.G. 1987. Decline Curve Analysis Using Type Curves: Case Histories. *SPE Formation Evaluation* **2** (4): 637–656. SPE-13169-PA.

Fisher, M.K., Wright, C.A., Davidson, B.M., Steinsberger, N.P., Buckler, W.S., Goodwin, A., Fielder, E.O. 2005. Integrating Fracture-Mapping Technologies To Improve Stimulations in the Barnett Shale. *SPE Production & Operations* **20** (2): 85–93. SPE-77441-PA.

Fox, M.J., Chedburn, A.C.S., Stewart, G. 1988. Simple Characterization of Communication Between Reservoir Regions. Paper SPE 18360 presented at the European Petroleum Conference, London, United Kingdom, 16–19 October.

Fraim, M.L., Wattenbarger, R.A. 1987. Gas Reservoir Decline-Curve Analysis Using Type Curves With Real Gas Pseudopressure and Normalized Time. *SPE Formation Evaluation* **2** (4): 671–682. SPE-14238-PA.

Freeborn, R., Russell, B. 2012. How To Apply Stretched Exponential Equations to Reserve Evaluation. Paper SPE 162631 presented at the SPE Hydrocarbon Economics and Evaluation Symposium, Calgary, Alberta, Canada, 24–25 September.

Gao, C., Lee, W.J., Spivey, J.P., Semmelbeck, M.E. 1994. Modeling Multilayer Gas Reservoirs Including Sorption Effects. Paper SPE 29173 presented at the SPE Eastern Regional Meeting, Charleston, West Virginia, 8–10 November.

Gringarten, A.C., Ramey, H.J. 1973. The Use of Source and Green's Functions in Solving Unsteady-Flow Problems in Reservoirs. *Society of Petroleum Engineers Journal* **13** (5): 285–296. SPE-3818-PA.

Gringarten, A.C., Ramey, H.J. 1974. Unsteady-State Pressure Distributions Created by a Well With a Single Horizontal Fracture, Partial Penetration, or Restricted Entry. *Society of Petroleum Engineers Journal* **14** (4): 413–426. SPE-3819-PA.

Gringarten, A.C., Ramey, H.J., Raghavan, R. 1974. Unsteady-State Pressure Distributions Created by a Well With a Single Infinite-Conductivity Vertical Fracture. *Society of Petroleum Engineers Journal* **14** (4): 347–360. SPE-4051-PA.

Hamdi, H. 2012. Illumination of Channelised Fluvial Reservoirs Using Geological Well Testing and Seismic Modelling. PhD Thesis, Heriot-Watt University, Edinburgh.

Hassanzadeh, H., Pooladi-Darvish, M., Atabay, S. 2009. Shape factor in the drawdown solution for well testing of dual-porosity systems. *Advances in Water Resources* **32** (11): 1652–1663.

Hawkins, M.F. 1956. A Note on the Skin Effect. *Journal of Petroleum Technology* **8** (12): 65–66.

Hill, D.G., Nelson, C.R. 2000. Gas productive fractured shales: An overview and update. *Gas TIPS* **6** (2): 4–13.

Holditch, S.A. 2006. Tight Gas Sands. *Journal of Petroleum Technology* **58** (6): 86–93. SPE-103356-MS.

Hosseinpour-Zonoozi, N., Ilk, D., Blasingame, T.A. 2006. The Pressure Derivative Revisited--Improved Formulations and Applications. Paper SPE 103204 presented at the SPE Annual Technical Conference and Exhibition, San Antonio, Texas, USA, 24–27 September.

Ibrahim, M., Wattenbarger, R.A. 2006. Rate Dependence of Transient Linear Flow in Tight Gas Wells. *Journal of Canadian Petroleum Technology* **45** (10): 18–20. PETSOC-06-10-TN2.

Idorenyin, E., Okouma, V., Mattar, L. 2011. Analysis of Production Data Using the Beta-Derivative. Paper SPE 149361 presented at the Canadian Unconventional Resources Conference, Alberta, Canada, 15–17 November.

Ilk, D. 2010. Well performance analysis for low to ultra-low permeability reservoir systems. PhD Thesis, Texas A&M University, College Station, TX.

Ilk, D., Blasingame, T.A. 2013. Decline Curve Analysis for Unconventional Reservoir Systems-Variable Pressure Drop Case. Paper SPE 167253 presented at the SPE Unconventional Resources Conference–Canada, Calgary, Alberta, Canada, 5–7 November.

Ilk, D., Hosseinpour-Zonoozi, N., Amini, S., Blasingame, T.A. 2007. Application of the β-Integral Derivative Function to Production Analysis. Paper SPE 107967 presented at the Rocky Mountain Oil & Gas Technology Symposium, Denver, Colorado, USA, 16–18 April.

Ilk, D., Rushing, J.A., Perego, A.D., Blasingame, T.A. 2008. Exponential vs. Hyperbolic Decline in Tight Gas Sands–Understanding the Origin and Implications for Reserve Estimates Using Arps' Decline Curves. Paper SPE 116731 presented at the SPE Annual Technical Conference and Exhibition, Denver, Colorado, USA, 21–24 September.

Jenkins, C.D., Boyer, C.M. 2008. Coalbed- and Shale-Gas Reservoirs. *Journal of Petroleum Technology* **60** (2): 92–99. SPE-103514-MS.

Johnson, R.H., Bollens, A.L. 1927. The Loss Ratio Method of Extrapolating Oil Well Decline Curves. *Transactions of the AIME* **77** (1): 771–778.

Junkin, J.E., Sippel, M.A., Collins, R.E., Lord, M.E. 1992. Well Performance Evidence for Compartmented Geometry of Oil and Gas Reservoirs. Paper SPE 24356 presented

at the SPE Rocky Mountain Regional Meeting, Casper, Wyoming, USA, 18–21 May.

Kabir, C.S., Rasdi, F., Igboalisi, B. 2011. Analyzing Production Data From Tight Oil Wells. *Journal of Canadian Petroleum Technology* **50** (5): 48–58. SPE-137414-PA.

King, G.E. 2010. Thirty Years of Gas Shale Fracturing: What Have We Learned? Paper SPE 133456 presented at the SPE Annual Technical Conference and Exhibition, Florence, Italy, 19–22 September.

King, G.R., Ertekin, T., Schwerer, F.C. 1986. Numerical Simulation of the Transient Behavior of Coal-Seam Degasification Wells. *SPE Formation Evaluation* **1** (2): 165–183. SPE-12258-PA.

Kupchenko, C.L., Gault, B.W., Mattar, L. 2008. Tight Gas Production Performance Using Decline Curves. Paper SPE 114991 presented at the CIPC/SPE Gas Technology Symposium 2008 Joint Conference, Calgary, Alberta, Canada, 16–19 June.

Law, B.E. 2002. Basin-Centered Gas Systems. *AAPG Bulletin* **86** (11): 1891–1919.

Lee, W.J., Sidle, R. 2010. Gas-Reserves Estimation in Resource Plays. *SPE Economics & Management* **2** (2): 86–91. SPE-130102-PA.

Malavazos, M., McDonough, R.C.M. 1991. Pressure-Transient Response in Compartmentalised Gas Reservoirs: A South Australian Field Example. Paper SPE 23009 presented at the SPE Asia-Pacific Conference, Perth, Australia, 4–7 November.

Marhaendrajana, T., Blasingame, T.A. 2001. Decline Curve Analysis Using Type Curves - Evaluation of Well Performance Behavior in a Multiwell Reservoir System. Paper SPE 71517 presented at the SPE Annual Technical Conference and Exhibition, New Orleans, Louisiana, USA, 30 September–3 October.

Martin, S.O., Holditch, S.A., Ayers, W.B., McVay, D. 2010. PRISE Validates Resource Triangle Concept. *SPE Economics & Management* **2** (1): 51–60. SPE-117703-PA.

Martini, A.M., Walter, L.M., Budai, J.M., Ku, T.C.W., Kaiser, C.J., M.Schoell. 1998. Genetic and Temporal Relations between Formation Waters and Biogenic Methane—Upper Devonian Antrim Shale, Michigan basin. *Geochimica et Cosmochimica Acta* **62** (10): 1699–1720.

Massonnat, G.J., Norris, R.J., Chalmette, J-C. 1993. Well Test Interpretation in Geologically Complex Channelized Reservoirs. Paper 00026464 presented at the SPE Annual Technical Conference and Exhibition, Houston, Texas, 3-6 October 1993.

Masters, J.A. 1979. Deep Basin Gas Trap, Western Canada. *AAPG Bulletin* **63** (2): 152–181.

Mattar, L., McNeil, R. 1998. The "Flowing" Gas Material Balance. *Journal of Canadian Petroleum Technology* **37** (2). PETSOC-98-02-06.

Mattar, L., Moghadam, S. 2009. Modified Power Law Exponential Decline for Tight Gas. Paper PETSOC-2009-198 presented at the Canadian International Petroleum Conference, Calgary, Alberta, Canada, 16–18 June.

Maugeri, L. 2013. The Shale Oil Boom: A U.S. Phenomenon. Report No. 2013-05, Belfer Center for Science and International Affairs, Harvard Kennedy School (June).

Mayerhofer, M.J., Lolon, E., Warpinski, N.R., Cipolla, C.L., Walser, D.W., Rightmire, C.M. 2010. What Is Stimulated Reservoir Volume? *SPE Production & Operations* **25** (1): 89–98. SPE-119890-PA.

McNeil, R., Jeje, O., Renaud, A. 2009. Application of the Power Law Loss-Ratio Method of Decline Analysis. Paper PETSOC-2009-159 presented at the Canadian International Petroleum Conference, Calgary, Alberta, Canada, 16–18 June.

Medeiros, F., Ozkan, E., Kazemi, H. 2008. Productivity and Drainage Area of Fractured Horizontal Wells in Tight Gas Reservoirs. *SPE Reservoir Evaluation & Engineering* **11** (5): 902–911. SPE-108110-PA.

Meunier, D.F., Kabir, C.S., Wittmann, M.J. 1987. Gas Well Test Analysis: Use of Normalized Pseudovariables. *SPE Formation Evaluation* **2** (4): 629–636. SPE-13082-PA.

Mishra, S. 2012. A New Approach to Reserves Estimation in Shale Gas Reservoirs Using Multiple Decline Curve Analysis Models. Paper SPE 161092 presented at the SPE Eastern Regional Meeting, Lexington, Kentucky, USA, 3–5 October.

Moghadam, S., Jeje, O., Mattar, L. 2011. Advanced Gas Material Balance in Simplified Format. *Journal of Canadian Petroleum Technology* **50** (1): 90–98. SPE-139428-PA.

Moghadam, S., Mattar, L., Pooladi-Darvish, M. 2010. Dual Porosity Typecurves for Shale Gas Reservoirs. Paper SPE 137535 presented at the Canadian Unconventional Resources and International Petroleum Conference, Calgary, Alberta, Canada, 19–21 October.

Morrow, N.R., Buckley, J.S., Cather, M.E., Brower, K.R., Graham, M., Ma, S., Zhang, X. 1990. Rock Matrix and Fracture Analysis of Flow in Western Tight Gas Sands. Report No. DOE/MC/21179-2853, New Mexico Institute of Mining and Technology, Socorro, New Mexico.

Muskat, M. 1937. *The Flow of Homogeneous Fluids Through Porous Media*. New York, McGraw-Hill Book Co.

Nobakht, M., Clarkson, C.R. 2012a. A New Analytical Method for Analyzing Linear Flow in Tight/Shale Gas Reservoirs: Constant-Flowing-Pressure Boundary Condition. *SPE Reservoir Evaluation & Engineering* **15** (3): 370–384. SPE-143989-PA.

Nobakht, M., Clarkson, C.R. 2012b. A New Analytical Method for Analyzing Linear Flow in Tight/Shale Gas Reservoirs: Constant-Rate Boundary Condition. *SPE Reservoir Evaluation & Engineering* **15** (1): 51–59. SPE-143990-PA.

Nobakht, M., Mattar, L. 2012. Analyzing Production Data From Unconventional Gas Reservoirs With Linear Flow and Apparent Skin. *Journal of Canadian Petroleum Technology* **51** (1): 52–59. SPE-137454-PA.

Nobakht, M., Mattar, L., Moghadam, S., Anderson, D. 2012. Simplified Forecasting of Tight/Shale-Gas Production in Linear Flow. *Journal of Canadian Petroleum Technology* **51** (6): 476–486. SPE-133615-PA.

Okuszko, K.E., Gault, B.W., Mattar, L. 2008. Production Decline Performance of CBM Wells. *Journal of Canadian Petroleum Technology* **47** (7): 57–61. PETSOC-08-07-57.

Onur, M., Reynolds, A.C. 1988. A New Approach for Constructing Derivative Type Curves for Well Test Analysis. *SPE Formation Evaluation* **3** (1): 197-206. 00016473.

Onur, M., Yeh, N., Reynolds, A.C. 1989. New Applications of the Pressure Derivative in Well-Test Analysis. *SPE Formation Evaluation* **4** (3): 429-437. 00016810.

Palacio, J.C., Blasingame, T.A. 1993. Decline-Curve Analysis With Type Curves--Analysis of Gas Well Production Data. Paper SPE 25909 presented at the SPE Joint Rocky Mountain Regional and Low Permeability Reservoirs Symposium, Denver, Colorado, USA, 26–28.

Passey, Q.R., Creaney, S., Kulla, J.B., Moretti, F.J., Stroud, J.D. 1990. A Practical Model for Organic Richness from Porosity and Resistivity Logs. *AAPG Bulletin* **74** (12): 1777–1794.

Potter, P.E. 2003. Mudrocks. In *Encyclopedia of Sediments and Sedimentary Rocks*, ed. G.V. Middleton. Springer.

Pratikno, H., Rushing, J.A., Blasingame, T.A. 2003. Decline Curve Analysis Using Type Curves - Fractured Wells. Paper SPE 84287 presented at the SPE Annual Technical Conference and Exhibition, Denver, Colorado, USA, 5–8 October.

Pulle, C.V. 1982. A Hydrodynamic Analogy of Production Decline for Devonian Shale Wells. Paper SPE 10837 presented at the SPE/DOE Unconventional Gas Recovery Symposium, Pittsburgh, Pennsylvania, USA, 16–18 May.

Raghavan, R. 1993. *Well test analysis*, PTR Prentice Hall.

Rahman, N.M.A. 1998. Transient pressure analysis in compartmentalized reservoirs. PhD Thesis, University of Alberta, Edmonton, Alberta.

Ruppel, S.C., Loucks, R.G. 2008. Black Mudrocks: Lessons and Questions from the Mississippian Barnett Shale in the Southern Midcontinent. *The Sedimentary Record* **6** (2).

Sayarpour, M., Zuluaga, E., Kabir, C.S., Lake, L.W. 2009. The use of capacitance–resistance models for rapid estimation of waterflood performance and optimization. *Journal of Petroleum Science and Engineering* **69** (3–4): 227–238.

Schettler, P.D., Parmely, C.R. 1991. Contributions to Total Storage Capacity in Devonian Shales. Paper SPE 23422 presented at the SPE Eastern Regional Meeting, Lexington, Kentucky, USA, 22–25 October.

Schmoker, J.W. 2002. Resource-Assessment Perspectives for Unconventional Gas Systems. *AAPG Bulletin* **86** (11): 1993–1999.

Shahamat, M.S., Aguilera, R. 2010. A New Method for Production Decline Analysis of Tight Gas Formations. Paper SPE 138149 presented at the Canadian Unconventional Resources and International Petroleum Conference, Calgary, Alberta, Canada, 19–21 October.

Shahamat, M.S., Mattar, L., Aguilera, R. 2014. A Physics-Based Method for Production Data Analysis of Tight and Shale Petroleum Reservoirs Using Succession of Pseudo-Steady States. Paper SPE 167686 presented at the SPE/EAGE European Unconventional Resources Conference and Exhibition, Vienna, Austria, 25–27 February.

Shanley, K.W., Cluff, R.M., Robinson, J.W. 2004. Factors Controlling Prolific Gas Production from Low-Permeability Sandstone Reservoirs: Implications for

Resource Assessment, Prospect Development, and Risk Analysis. *AAPG Bulletin* **88** (8): 1083–1121.

Sondergeld, C.H., Newsham, K.E., Comisky, J.T., Rice, M.C., Rai, C.S. 2010. Petrophysical Considerations in Evaluating and Producing Shale Gas Resources. Paper SPE 131768 presented at the SPE Unconventional Gas Conference, Pittsburgh, Pennsylvania, USA, 23–25 February.

Spencer, C.W. 1989. Review of Characteristics of Low-Permeability Gas Reservoirs in Western United States. *AAPG Bulletin* **73** (5): 613–629.

Spencer, R.J., Pedersen, P.K., Clarkson, C.R., Aguilera, R. 2010a. SHALE GAS: Part 1 - Introduction. *Canadian Society of Petroleum Geologists* (8): 47–51.

Spencer, R.J., Pedersen, P.K., Clarkson, C.R., Aguilera, R. 2010b. SHALE GAS: Part 4 - Log Analysis and Shale Gas Petrophysics. *Canadian Society of Petroleum Geologists* (11): 27–31.

Spivey, J.P., Jr., J.H. Frantz, Williamson, J.R., Sawyer, W.K. 2001. Applications of the Transient Hyperbolic Exponent. Paper SPE 71038 presented at the SPE Rocky Mountain Petroleum Technology Conference, Keystone, Colorado, USA, 21–23 May.

Stalgorova, E., Mattar, L. 2012. Practical Analytical Model To Simulate Production of Horizontal Wells With Branch Fractures. Paper SPE 162515 presented at the SPE Canadian Unconventional Resources Conference, Calgary, Alberta, Canada, 30 October–1 November.

Stalgorova, E., Mattar, L. 2013. Analytical Model for Unconventional Multifractured Composite Systems. *SPE Reservoir Evaluation & Engineering* **16** (3): 246–256. SPE-162516-PA.

Stehfest, H. 1970. Numerical inversion of Laplace transforms. *Communications of the ACM* **13** (1): 47–49.

Stewart, G. 2011. *Well Test Design & Analysis*, PennWell.

Stewart, G., Whaballa, A.E. 1989. Pressure Behavior of Compartmentalized Reservoirs. Paper SPE 19779 presented at the SPE Annual Technical Conference and Exhibition, San Antonio, Texas, USA, 8–11 October.

Steyl, G., vanTonder, G.J. 2013. Hydrochemical and Hydrogeological Impact of Hydraulic Fracturing in the Karoo, South Africa. In *Effective and Sustainable Hydraulic Fracturing*, ed. A.P. Bunger, J. McLennan and R. Jeffrey.

Suabdi, I.N. 2001. Analysis of layered gas reservoir performance using a semi-analytical solution for rate and pressure behavior. PhD Thesis, Texas A&M University, College Station, TX.

Tabatabaie, S.H., Pooladi-Darvish, M., Mattar, L. 2013. Pseudotime Calculation in Low Permeability Gas Reservoirs. Paper SPE 167185 presented at the SPE Unconventional Resources Conference, Calgary, Alberta, Canada, 5–7 November.

Thompson, L.G., Manrique, J.L., Jelmert, T.A. 1991. Efficient Algorithms for Computing the Bounded Reservoir Horizontal Well Pressure Response. Paper SPE 21827 presented at the Low Permeability Reservoirs Symposium, Denver, Colorado, 15–17 April.

Tucker, M.E. 2001. *Sedimentary Petrology: An Introduction to the Origin of Sedimentary Rocks*, 3rd edition, Wiley-Blackwell.

Valko, P.P. 2009. Assigning Value to Stimulation in the Barnett Shale: A Simultaneous Analysis of 7000 Plus Production Histories and Well Completion Records. Paper SPE 119369 presented at the SPE Hydraulic Fracturing Technology Conference, The Woodlands, Texas, USA, 19–21 January.

Van Everdingen, A.F. 1953. The Skin Effect and Its Influence on the Productive Capacity of a Well. *Journal of Petroleum Technology* **5** (6): 171–176.

Van Everdingen, A.F., Hurst, W. 1949. The Application of the Laplace Transformation to Flow Problems in Reservoirs. *Journal of Petroleum Technology* **1** (12): 305–324.

Wahl, W.L., Mullins, L.D., Barham, R.H., Bartlett, W.R. 1962. Matching the Performance of Saudi Arabian Oil Fields With an Electrical Model. *Journal of Petroleum Technology* **14** (11): 1275–1282.

Wang, F.P., Reed, R.M. 2009. Pore Networks and Fluid Flow in Gas Shales. Paper SPE 124253 presented at the SPE Annual Technical Conference and Exhibition, New Orleans, Louisiana, USA, 4–7 October.

Warpinski, N.R., Mayerhofer, M.J., Vincent, M.C., Cipolla, C.L., Lolon, E.P. 2009. Stimulating Unconventional Reservoirs: Maximizing Network Growth While Optimizing Fracture Conductivity. *Journal of Canadian Petroleum Technology* **48** (10): 39–51. SPE-114173-PA.

Warren, J.E., Root, P.J. 1963. The Behavior of Naturally Fractured Reservoirs. *Society of Petroleum Engineers Journal* **3** (3): 245–255. SPE-426-PA.

Wattenbarger, R.A., El-Banbi, A.H., Villegas, M.E., Maggard, J.B. 1998. Production Analysis of Linear Flow Into Fractured Tight Gas Wells. Paper SPE 39931 presented at the SPE Rocky Mountain Regional/Low-Permeability Reservoirs Symposium, Denver, Colorado, USA, 5–8 April.

Weber, D., Edgar, T.F., Lake, L.W., Lasdon, L.S., Kawas, S., Sayarpour, M. 2009. Improvements in Capacitance-Resistive Modeling and Optimization of Large Scale Reservoirs. Paper SPE 121299 presented at the SPE Western Regional Meeting, San Jose, California, USA, 24–26 March.

Whittle, T.M., Gringarten, A.C. 2008. The Determination of Minimum Tested Volume From the Deconvolution of Well Test Pressure Transients. Paper SPE 116575 presented at the SPE Annual Technical Conference and Exhibition, Denver, Colorado, USA, 21–24 September.

Ye, P., Ayala, L.F. 2013. Straightline Analysis of Flow Rate vs. Cumulative-Production Data for the Explicit Determination of Gas Reserves. *Journal of Canadian Petroleum Technology* **52** (4): 296–305. SPE-165583-PA.

Yousef, A.A., Gentil, P.H., Jensen, J.L., Lake, L.W. 2006. A Capacitance Model To Infer Interwell Connectivity From Production- and Injection-Rate Fluctuations. *SPE Reservoir Evaluation & Engineering* **9** (6): 630–646. SPE-95322-PA.

Yu, S. 2013. Best Practice of Using Empirical Methods for Production Forecast and EUR Estimation in Tight/Shale Gas Reservoirs. Paper SPE 167118 presented at the SPE Unconventional Resources Conference, Canada, Calgary, Alberta, Canada, 5–7 November.

Yu, S., Lee, W.J., Miocevic, D.J., Li, D., Harris, S. 2013. Estimating Proved Reserves in Tight/Shale Wells Using the Modified SEPD Method. Paper SPE 166198 presented

at the SPE Annual Technical Conference and Exhibition, New Orleans, Louisiana, USA, 30 September–2 October.

Zaitlin, B.A., Moslow, T.F. 2006. A Review of Deep Basin Gas Reservoirs of the Western Canada Sedimentary Basin. *The Mountain Geologist* **43** (3): 257–262.

APPENDIX A: DERIVATION OF THE TRANSIENT SOLUTION FOR LINEAR FLOW

This Appendix explains derivation of the transient linear flow solutions with and without skin for both cases of constant rate and constant pressure production.

The governing partial differential equation for linear flow is according to Eq. A. 1:

$$\frac{\partial^2 p}{\partial y^2} = \frac{\phi \mu c}{\beta_2 k}\frac{\partial p}{\partial t} \qquad \text{Eq. A. 1}$$

Let's define the following dimensionless parameters for constant rate and constant pressure production scenarios:

Table A. 1: Dimensionless parameters defined for solving linear diffusivity equation.

Constant Rate	Constant p_{wf}
$y_D = \frac{y}{x_f}$	$y_D = \frac{y}{x_f}$
$t_D = t_{Dxf} = \frac{\eta t}{{x_f}^2}$	$t_D = t_{Dxf} = \frac{\eta t}{{x_f}^2}$
$p_D = \frac{2\pi kh}{\beta_1 q_{wb} B\mu}(p_i - p)$	$p_D = \frac{(p_i - p)}{(p_i - p_{wf})}$
$q_D = \frac{q(y,t)}{q}$	$q_D = \frac{\beta_1 qB\mu}{2\pi kh(p_i - p_{wf})}$

Where η is the hydraulic diffusivity and equal to $\eta = \frac{\beta_2 k}{\phi \mu c_t}$. Note that Darcy's Law gives:

$$q(y,t) = \frac{khx_f}{\beta_1 B\mu}\frac{\partial p}{\partial y} \qquad \text{Eq. A. 2}$$

In this equation $\beta_1 = 2\pi \times 141.2$. From dimensionless definitions for either of the production scenarios, the diffusivity equation to be solved will take on the following form:

$$\frac{\partial^2 p_D}{\partial {y_D}^2} = \frac{\partial p_D}{\partial t_D} \qquad \text{Eq. A. 3}$$

And Darcy's Law for both production scenarios will be of the following form:

$$q_D = -\frac{2}{\pi}\frac{\partial p_D}{\partial y_D} \qquad \text{Eq. A. 4}$$

Part I: Without Skin

When there is no skin, the IC and the BCs are defined as below:

Table A. 2: Initial and boundary conditions, transient linear flow without skin.

Constant Rate	Constant p_{wf}	Type
$p_D = 0$	$p_D = 0$	Initial Condition (IC), at $t_D = 0$
$\frac{\partial p_D}{\partial y_D} = -\frac{\pi}{2}$	$p_D = 1$	Inner Boundary Condition (IBC) , at $y_D = 0$
$p_D = 0$	$p_D = 0$	Outer Boundary Condition (OBC), at $y_D \to \infty$

The diffusivity equation with associated initial and boundary conditions are solved in Laplace space. As a result, first the diffusivity equation is written in Laplace domain:

$$\frac{d^2\overline{p_D}}{dy_D{}^2} - u\overline{p_D} = -IC = 0 \qquad \text{Eq. A. 5}$$

In addition to the diffusivity equation, the initial and boundary conditions have to be expressed in Laplace domain. Table A. 3 gives a summary of the conditions in Table A. 2:

Table A. 3: Initial and boundary conditions in Laplace domain, without skin.

Constant Rate	Constant p_{wf}	Type
$\overline{p_D} = 0$	$\overline{p_D} = 0$	Initial Condition (IC), at $t_D = 0$
$\frac{d\overline{p_D}}{dy_D} = -\frac{\pi}{2u}$	$\overline{p_D} = \frac{1}{u}$	Inner Boundary Condition (IBC) , at $y_D = 0$
$\overline{p_D} = 0$	$\overline{p_D} = 0$	Outer Boundary Condition (OBC), at $y_D \to \infty$

Characteristic equation of Eq. A. 5 has two real roots. As a result, its solution gets the following form:

$$\overline{p_D} = Ae^{y_D\sqrt{u}} + Be^{-y_D\sqrt{u}} \qquad \text{Eq. A. 6}$$

Satisfying the initial and boundary conditions of Table A. 3 in Eq. A. 6, the coefficients A and B for each of the production scenarios are obtained according to the following table:

Table A. 4: Constants obtained for the solutions in Laplace domain, without skin.

Constant	Constant Rate	Constant p_{wf}
A	0	0
B	$\frac{\pi}{2u\sqrt{u}}$	$\frac{1}{u}$

Therefore, the final complete solutions in Laplace domain and their real time inversions are given in the Table A. 5:

Table A. 5: Transient linear flow solutions without skin.

Solutions	Constant Rate	Constant p_{wf}
Laplace	$\overline{p_D} = \frac{\pi}{2u\sqrt{u}} e^{-y_D\sqrt{u}}$	$\overline{p_D} = \frac{1}{u} e^{-y_D\sqrt{u}}$
Real time	$p_D = \sqrt{\pi t_D} e^{-\frac{{y_D}^2}{4t_D}} - \frac{\pi}{2} y_D \operatorname{erfc}\left(\frac{y_D}{2\sqrt{t_D}}\right)$	$p_D = \operatorname{erfc}\left(\frac{y_D}{2\sqrt{t_D}}\right)$

Equations in the above table are new solutions obtained through this research. Substitution of $y_D = 0$ in Table A. 5 gives the dimensionless pressure at the wellbore ($p_{wD} = \sqrt{\pi t_D}$ for constant rate and $p_{wD} = 1$ for constant p_{wf} production). These equations are similar to the equations previously reported in the literature (Wattenbarger et al. 1998).

The equations in Table A. 5 are useful because they can be used to obtain the volumetric average pressure within the investigated region. In order to perform this task, the definition of distance of investigation (Eq. 3.1) is used. Fist the dimensionless average pressure is defined according to $(p_{avg})_D = \frac{2\pi kh(p_i - p_{avg})}{\alpha_1 qB\mu}$ for constant rate and $(p_{avg})_D = \frac{(p_i - p_{avg})}{(p_i - p_{wf})}$ for constant pressure production. The average pressure in these definitions are calculated volumetrically, i.e. $p_{avg} = \frac{\int_0^{y_{inv}} p dy}{\int_0^{y_{inv}} dy}$. Expressing all the pressure and distance terms in dimensionless form, calculating the integration and then simplifying the obtained equations yield the following results:

Table A. 6: Average pressure solutions in real time domain, transient without skin.

Production Type	Solution
Constant Rate	$\left(p_{avg}\right)_D = \frac{\pi}{2y_{invD}}\left\{t_D \operatorname{erf}\left(\frac{y_{invD}}{2\sqrt{t_D}}\right) + y_{Dinv}\sqrt{\frac{t_D}{\pi}}e^{-\frac{{y_{invD}}^2}{4t_D}} - \frac{{y_{invD}}^2}{2}\operatorname{erfc}\left(\frac{y_{invD}}{2\sqrt{t_D}}\right)\right\}$
Constant p_{wf}	$\left(p_{avg}\right)_D = \frac{1}{y_{invD}}\left\{y_{invD}\operatorname{erfc}\left(\frac{y_{invD}}{2\sqrt{t_D}}\right) - 2\sqrt{\frac{t_D}{\pi}}e^{-\frac{{y_{invD}}^2}{4t_D}} + 2\sqrt{\frac{t_D}{\pi}}\right\}$

Further simplification of these equations is obtained by substituting Eq. 3.1 in Table A. 6. Table A.7 shows the final results:

Table A. 7: Average pressure solutions in real time domain, transient without skin.

Production Type	Solution
Constant Rate	$\left(p_{avg}\right)_D = \left\{\frac{\sqrt{\pi}}{2}e^{-\frac{{\alpha_1}^2}{4}} + \frac{\pi\left(2+{\alpha_1}^2\right)}{4\alpha_1}\operatorname{erf}\left(\frac{\alpha_1}{2}\right) - \frac{\pi\alpha_1}{4}\right\}\sqrt{t_D} \cong 0.816\sqrt{t_D}$
Constant p_{wf}	$\left(p_{avg}\right)_D \cong 0.475$

Equations in Table A. 6 and Table A.7 are interesting results derived in this research. These equations indicate that the ratio of the dimensionless average pressure to the dimensionless wellbore pressure, i.e. $\frac{\left(p_{avg}\right)_D}{p_{wD}}$, is equal to 0.46 and 0.475, for constant rate and constant pressure production, respectively.

Part II: With Skin

In this section, diffusivity equation, dimensionless parameters and outer boundary conditions are the same as the previous section. The only difference is the inner boundary condition to account for skin (s):

$(\Delta p_D)_{skin} = \frac{\pi}{2} q_D(y_D = 0, t_D) \times s$ and $p_{wD} = p_D|_{y_D=0} + (\Delta p_D)_{skin}$

For constant rate production for example, we have:

$$p_{wD} = p_D|_{y_D=0} + \frac{\pi}{2} q_D(y_D = 0, t_D) \times s = p_D|_{y_D=0} + \frac{\pi}{2} s$$

For constant pressure also we have:

$$p_{wD} = p_D|_{y_D=0} + \frac{\pi}{2} q_D(y_D = 0, t_D) \times s \quad \Rightarrow \quad p_D|_{y_D=0} - \frac{\pi}{2} \frac{\partial p_D}{\partial y_D} \times s = 1$$

Therefore the IC and the BCs are defined as below:

Table A. 8: Initial and boundary conditions, transient linear flow with skin.

Constant Rate	Constant p_{wf}	Type
$p_D = 0$	$p_D = 0$	IC ($t_D = 0$)
$p_{wD} = p_D + s \,\&\, \frac{\partial p_D}{\partial y_D} = -\frac{\pi}{2}$	$p_D - s \frac{\partial p_D}{\partial y_D} = 1$	IBC ($y_D = 0$)
$p_D = 0$	$p_D = 0$	OBC ($y_D \to \infty$)

The IC and BCs in Table A. 8 should also be expressed in the Laplace domain:

Table A. 9: Initial and boundary conditions in Laplace domain, with skin.

Constant Rate	Constant p_{wf}	Type
$\overline{p_D} = 0$	$\overline{p_D} = 0$	IC ($t_D = 0$)
$\overline{p_{wD}} = \overline{p_D} + \frac{s}{u} \,\&\, \frac{d\overline{p_D}}{dy_D} = -\frac{\pi}{2u}$	$\overline{p_D} - s \frac{d\overline{p_D}}{dy_D} = \frac{1}{u}$	IBC ($y_D = 0$)
$\overline{p_D} = 0$	$\overline{p_D} = 0$	OBC ($y_D \to \infty$)

Using the above table with Eq. A. 6 gives the constants in the characteristic equation:

Table A. 10: Constants obtained for the solutions in Laplace domain, with skin.

	Constant Rate	Constant p_{wf}
A	0	0
B	$\frac{\pi}{2u\sqrt{u}}$	$\frac{1}{u(1+s\sqrt{u})}$

As a result of using these constants, the final solutions for pressure and rate profiles within the reservoir are obtained according to the following table:

Table A. 11: Transient linear flow solutions in Laplace domain, with skin.

Solutions	Constant Rate	Constant p_{wf}
Pressure profile	$\overline{p_D} = \frac{\pi}{2u\sqrt{u}} e^{-y_D\sqrt{u}}$ & $\overline{p_{wD}} = \overline{p_D} + \frac{s}{u}$	$\overline{p_D} = \frac{e^{-y_D\sqrt{u}}}{u(1+s\sqrt{u})}$
Rate profile	$\overline{q_D} = \frac{e^{-y_D\sqrt{u}}}{u}$	$\overline{q_D} = \frac{2}{\pi s}\frac{e^{-y_D\sqrt{u}}}{\sqrt{u}\left(\frac{1}{s}+\sqrt{u}\right)}$

Table A. 12 is used for inversion of Laplace space solutions in the above table back into the real time:

Table A. 12: Analytical inversion of Laplace functions into real time domain.

Function in Laplace domain	Inversion in real time domain
$F(u) = \frac{e^{-a\sqrt{u}}}{u}$	$f(t) = \text{erfc}\left(\frac{a}{2\sqrt{t}}\right)$
$F(u) = \frac{e^{-a\sqrt{u}}}{u^{\frac{3}{2}}}$	$f(t) = 2\sqrt{\frac{t}{\pi}} e^{\left(-\frac{a^2}{4t}\right)} - a \times \text{erfc}\left(\frac{a}{2\sqrt{t}}\right)$
$F(u) = \frac{e^{-a\sqrt{u}}}{\sqrt{u}(\sqrt{u}+b)}$	$f(t) = e^{b(bt+a)}\text{erfc}\left(b\sqrt{t} + \frac{a}{2\sqrt{t}}\right)$
$F(u) = \frac{ae^{-b\sqrt{u}}}{u(a+\sqrt{u})}$	$f(t) = -e^{a(b+at)}\text{erfc}\left(a\sqrt{t} + \frac{b}{2\sqrt{t}}\right) + \text{erfc}\left(\frac{b}{2\sqrt{t}}\right)$

Using this table, one gets the following rate and pressure profiles within the reservoir (in real time domain):

Table A. 13: Transient linear flow solutions in real time domain, with skin.

Solutions	Constant Rate	Constant p_{wf}
Pressure profile	$p_D = \sqrt{\pi t_D} e^{-\frac{{y_D}^2}{4t_D}} - \frac{\pi}{2} y_D \text{erfc}\left(\frac{y_D}{2\sqrt{t_D}}\right)$	$p_D = -e^{\frac{1}{s}\left(y_D+\frac{t_D}{s}\right)}\text{erfc}\left(\frac{\sqrt{t_D}}{s} + \frac{y_D}{2\sqrt{t_D}}\right) + \text{erfc}\left(\frac{y_D}{2\sqrt{t_D}}\right)$
Rate profile	$q_D = \text{erfc}\left(\frac{y_D}{2\sqrt{t_D}}\right)$	$q_D = \frac{2}{\pi s} e^{\frac{1}{s}\left(\frac{t_D}{s}+y_D\right)}\text{erfc}\left(\frac{\sqrt{t_D}}{s} + \frac{y_D}{2\sqrt{t_D}}\right)$

These new solutions are obtained as part of this research and give the pressure and rate profiles within a reservoir that has skin at the inner boundary. Substitution of $y_D = 0$ in Table A. 13 gives dimensionless pressure/rate at the wellbore:

Table A. 14: Transient linear flow solutions in real time domain, with skin.

Solutions	Constant Rate	Constant p_{wf}
Pressure profile	$p_{wD} = \sqrt{\pi t_D}+s$	$p_{wD} = -e^{\frac{1}{s}\left(\frac{t_D}{s}\right)}\text{erfc}\left(\frac{\sqrt{t_D}}{s}\right)$
Rate profile	$q_{wD} = 1$	$q_{wD} = \frac{2}{\pi s}e^{\frac{1}{s}\left(\frac{t_D}{s}\right)}\text{erfc}\left(\frac{\sqrt{t_D}}{s}\right)$

It is noted that the obtained equation for rate profile (q_{wD}) in constant wellbore pressure is similar to what Bello obtained in his thesis (Bello 2009). Similar to Part I, the real time pressure solutions in Table A. 13 were used to obtain the volumetric average reservoir pressure within the investigated region, using the definition of distance of investigation (Eq. 3.1). Table A. 15 shows the obtained results:

Table A. 15: Average pressure solutions in real time domain, transient with skin.

Production Type	Solution
Constant Rate	$\left(p_{avg}\right)_D = \frac{\pi}{2y_{invD}}\left\{t_D\text{erf}\left(\frac{y_{invD}}{2\sqrt{t_D}}\right) + y_{invD}\sqrt{\frac{t_D}{\pi}}e^{-\frac{{y_{invD}}^2}{4t_D}} - \frac{{y_{invD}}^2}{2}\text{erfc}\left(\frac{y_{invD}}{2\sqrt{t_D}}\right)\right\}$
Constant p_{wf}	$\left(p_{avg}\right)_D = \frac{1}{y_{invD}}\left\{s\left[1 + e^{\frac{1}{s}\left(y_{invD}+\frac{t_D}{s}\right)}\text{erf}\left(\frac{\sqrt{t_D}}{s} + \frac{y_{invD}}{2\sqrt{t_D}}\right) - e^{\frac{t_D}{s^2}}\left[e^{\frac{y_{invD}}{s}} + \text{erf}\left(\frac{\sqrt{t_D}}{s}\right) - 1\right]\right] + (y_{invD} - s)\text{erfc}\left(\frac{y_{invD}}{2\sqrt{t_D}}\right) + \frac{2\sqrt{t_D}}{\sqrt{\pi}}\left(1 - e^{-\frac{{y_{invD}}^2}{4t_D}}\right)\right\}$

The solutions in Table A. 15 are obtained as part of this research and calculate the average pressure within the reservoir with skin during transient linear flow.

The solution for the constant rate scenario is similar to the case where skin is zero (Table A. 6) therefore it can be simplified further. The constant pressure average pressure solution, though, is a complicated function of t_D, y_{Dinv} and skin, and substitution of the approximate equation for the distance of investigation cannot simplify the result any further.

APPENDIX B: DERIVATION OF THE COMPLETE SOLUTION FOR LINEAR FLOW

Part I: Without Skin

Here Eq. A. 1 is solved with initial and boundary conditions defined as below:

Table B. 1: Initial and boundary conditions, complete solution without skin.

Constant Rate	Constant p_{wf}	Type
$p_D = 0$	$p_D = 0$	Initial Condition (IC), at $t_D = 0$
$\frac{\partial p_D}{\partial y_D} = -\frac{\pi}{2}$	$p_D = 1$	Inner Boundary Condition (IBC) , at $y_D = 0$
$\frac{\partial p_D}{\partial y_D} = 0$	$\frac{\partial p_D}{\partial y_D} = 0$	Outer Boundary Condition (OBC), at $y_D = y_{eD}$

The diffusivity equation with associated initial and boundary conditions are solved in Laplace space. Writing the conditions of Table B. 1 in Laplace domain, one gets:

Table B. 2: Initial and boundary conditions in Laplace domain, complete solution without skin.

Constant Rate	Constant p_{wf}	Type
$\overline{p_D} = 0$	$\overline{p_D} = 0$	Initial Condition (IC), at $t_D = 0$
$\frac{d\overline{p_D}}{dy_D} = -\frac{\pi}{2u}$	$\overline{p_D} = \frac{1}{u}$	Inner Boundary Condition (IBC) , at $y_D = 0$
$\frac{d\overline{p_D}}{dy_D} = 0$	$\frac{d\overline{p_D}}{dy_D} = 0$	Outer Boundary Condition (OBC), at $y_D = y_{eD}$

The solution of the diffusivity equation gives:

$$\overline{p_D} = Ae^{y_D\sqrt{u}} + Be^{-y_D\sqrt{u}} \qquad \text{Eq. B. 1}$$

Satisfying the initial and boundary conditions of Table B. 2 in Eq. B. 1, the coefficients A and B for each of the production scenarios are obtained:

Table B. 3: Constants obtained for the solutions in Laplace domain, without skin.

	Constant Rate	Constant p_{wf}
A	$\frac{\pi}{2u\sqrt{u}\left(e^{2y_{eD}\sqrt{u}}-1\right)}$	$\frac{1}{u\left(1+e^{2y_{eD}\sqrt{u}}\right)}$
B	$\frac{\pi \times e^{2y_{De}\sqrt{u}}}{2u\sqrt{u}\left(e^{2y_{eD}\sqrt{u}}-1\right)}$	$\frac{e^{2y_{De}\sqrt{u}}}{u\left(1+e^{2y_{eD}\sqrt{u}}\right)}$

Using these constants and noting that $\overline{q_D} = -\frac{2}{\pi}\frac{\partial \overline{p_D}}{\partial y_D}$, the final complete solutions in Laplace domain (the pressure and rate profiles) are obtained according to the following table:

Table B. 4: Complete solutions in Laplace domain, without skin.

Solutions	Constant Rate	Constant p_{wf}
Pressure profile	$\overline{p_D} = \frac{\pi\left(e^{y_D\sqrt{u}} + e^{(2y_{eD}-y_D)\sqrt{u}}\right)}{2u\sqrt{u}\left(e^{2y_{eD}\sqrt{u}}-1\right)}$	$\overline{p_D} = \frac{\left(e^{y_D\sqrt{u}} + e^{(2y_{eD}-y_D)\sqrt{u}}\right)}{u\left(1+e^{2y_{eD}\sqrt{u}}\right)}$
Rate profile	$\overline{q_D} = \frac{\left(e^{y_D\sqrt{u}} - e^{(2y_{eD}-y_D)\sqrt{u}}\right)}{u\left(1-e^{2y_{eD}\sqrt{u}}\right)}$	$\overline{q_D} = \frac{2}{\pi}\frac{\left(e^{(2y_{eD}-y_D)\sqrt{u}} - e^{y_D\sqrt{u}}\right)}{\sqrt{u}\left(1+e^{2y_{eD}\sqrt{u}}\right)}$

Solutions in Table B. 4 cannot be inverted into real time domain analytically. In order to obtain the solutions in real time domain, another approach is taken to obtain series representation of the solutions expressed in real time domain.

For the case of constant rate, Ozisik has obtained solution for a situation analogous to ours here. Referring to his book, one gets:

$$p_D = \frac{\pi}{2}\left(\frac{t_D}{y_{eD}}\right) + \pi y_{eD}\sum_{n=1}^{\infty}\frac{\cos\left(n\pi\left(\frac{y_D}{y_{eD}}\right)\right)}{(n\pi)^2}\left\{1 - e^{-\left(\frac{n\pi}{y_{eD}}\right)^2 t_D}\right\} \qquad \text{Eq. B. 2}$$

For the constant pressure production, the separation of variables approach is used to find the solution in series. It is noted here that any PDE can be solved using the separation of variables if not only the PDE but also both the BCs are homogeneous. Homogeneity means that each term should have the dependent variable in it. Looking at the BCs for the constant pressure production, one can see that the IBC is not homogeneous. Therefore, the dependent dimensionless variables are changed and define in such a way that both the BCs are homogeneous and therefore solvable using the separation of variables.

The dimensionless pressure is defined as $\widehat{p_D} = \frac{(p-p_{wf})}{(p_i-p_{wf})}$. The initial and boundary conditions are therefore obtained according to the following table:

Table B. 5: Initial and boundary conditions for obtaining the constant pressure solution using the separation of variables.

Constant p_{wf}	Condition type
$\widehat{p_D} = 1$	IC, at $t_D = 0$
$\widehat{p_D} = 0$	IBC, at $y_D = 0$
$\frac{d\widehat{p_D}}{dy_D} = 0$	OBC, at $y_D = y_{eD}$

Using the separation of variables, first it is assumed that Eq. B.3 is the general solution of the partial differential equation given in Eq. A. 3:

$$\widehat{p_D} = F(y_D) \times G(t_D) \qquad \text{Eq. B. 3}$$

Substitution of this assumed solution into the diffusion equation results in two separate ordinary differential equations (ODEs) which are much easier to solve. The first ODE is $\frac{1}{G}\frac{d^2F}{dy_D{}^2} = -\chi^2$ whose general solution is according to $F(y_D) = C_1\sin(\chi y_D) + C_2\cos(\chi y_D)$. Using the entries in Table B. 5, IBC gives $C_2 = 0$ and OBC yields $\chi = \frac{(2n-1)\pi}{2y_{eD}}$. The second ODE is $\frac{1}{G}\frac{dG}{dt_D} = -\chi^2$ whose solution is according to $G(t_D) = C_3 e^{-\chi^2 t_D}$.

The general solution is a linear combination of the two ODEs: $\widehat{p_D} = \sum_{n=1}^{\infty}\left\{C_n\sin\left(\frac{(2n-1)\pi}{2y_{eD}}y_D\right)e^{-\left(\frac{(2n-1)\pi}{2y_{eD}}\right)^2 t_D}\right\}$, where $C_n = C_{1n}C_{3n}$. One can obtain a unique solution from the nonhomogeneous part of the problem (i.e. the initial condition (IC)). Upon substitution and using the orthogonality of sine function, one can simplify the solution to yield:

$$C_n = \frac{2}{y_{eD}} \int_0^{y_{eD}} \sin\left(\frac{(2n-1)\pi}{2y_{eD}} y_D\right) = \frac{4}{(2n-1)\pi} \quad \text{Eq. B. 4}$$

Therefore the final solution is according to Eq. B. 5:

$$\widehat{p_D} = \sum_{n=1}^{\infty} \left\{ \frac{4}{(2n-1)\pi} \sin\left(\frac{(2n-1)\pi}{2y_{eD}} y_D\right) e^{-\left(\frac{(2n-1)\pi}{2y_{eD}}\right)^2 t_D} \right\} \quad \text{Eq. B. 5}$$

It is noticed here that $p_D = 1 - \widehat{p_D}$.

Table B. 6 shows the final form of the solutions in real time domain. These solutions are equivalent to inversion of the equations in Table B. 4:

Table B. 6: Complete solutions (p_D) in real time domain, without skin.

Production Type	Solution
Constant Rate	$p_D = \frac{\pi}{2}\left(\frac{t_D}{y_{eD}}\right) + \pi y_{eD} \sum_{n=1}^{\infty} \left\{ \frac{cos\left(n\pi\left(\frac{y_D}{y_{eD}}\right)\right)}{(n\pi)^2} \left(1 - e^{-\left(\frac{n\pi}{y_{eD}}\right)^2 t_D}\right) \right\}$
Constant p_{wf}	$p_D = 1 - \sum_{n=1}^{\infty} \left\{ \frac{4}{(2n-1)\pi} sin\left(\frac{(2n-1)\pi}{2y_{eD}} y_D\right) e^{-\left(\frac{(2n-1)\pi}{2y_{eD}}\right)^2 t_D} \right\}$

Using Table B. 6, dimensionless average pressure is calculated according to Table B. 7:

Table B. 7: Complete solutions $(p_{avg})_D$ in real time domain, without skin.

Production Type	Solution
Constant Rate	$(p_{avg})_D = \frac{\pi}{2}\left(\frac{t_D}{y_{eD}}\right) + \pi \frac{{y_{eD}}^2}{y_{invD}} \sum_{n=1}^{\infty} \left\{ \frac{sin\left((n\pi)\frac{y_{invD}}{y_{eD}}\right)}{(n\pi)^3} \left(1 - e^{-\left(\frac{n\pi}{y_{invD}}\right)^2 t_D}\right) \right\}$
Constant p_{wf}	$(p_{avg})_D = 1 - 2\left(\frac{y_{eD}}{y_{invD}}\right) \sum_{n=1}^{\infty} \left\{ \left(\frac{2}{(2n-1)\pi}\right)^2 \left[1 - cos\left(\frac{(2n-1)\pi}{2y_{eD}} y_{invD}\right)\right] e^{-\left(\frac{(2n-1)\pi}{2y_{eD}}\right)^2 t_D} \right\}$

In addition, one can also obtain the dimensionless rate at different locations within the investigated region. Equivalent to real time inversions of solutions in Table B. 4, the rate profiles are obtained according to Table B. 8:

Table B. 8: Complete solutions (q_D) in real time domain, without skin.

Production Scenario	Solution
Constant Rate	$q_D = 2\sum_{n=1}^{\infty}\left\{\frac{sin\left(n\pi\left(\frac{y_D}{y_{eD}}\right)\right)}{n\pi}\left(1-e^{-\left(\frac{n\pi}{y_{eD}}\right)^2 t_D}\right)\right\}$
Constant p_{wf}	$q_D = \frac{4}{\pi y_{eD}}\sum_{n=1}^{\infty}\left\{cos\left(\frac{(2n-1)\pi}{2y_{eD}}y_D\right)e^{-\left(\frac{(2n-1)\pi}{2y_{eD}}\right)^2 t_D}\right\}$

Equations in Table B.6 through B.8 are obtained as part of the research done in this work. It is noted that substitution of $y_D = 0$ in Table B.6 and Table B.8 gives the solutions at the wellbore whose equations are similar to those obtained by Arevalo-Villagran (2001).

The equations obtained so far are still complex, as they involve addition of many terms for obtaining reasonable profiles. The integral method is then used to find the approximate pressure distributions during BDF. In the integral method, first it is assumed that the pressure distribution is a polynomial. For constant rate production a second degree polynomial is used, since the rate profile shows a linear behaviour at late times. For the case of constant rate production a third degree polynomial is used because the rate behaviour of this production scenario shows an almost quadratic profile.

Table B. 9: Approximate pressure distributions, during BDF without skin.

Production Scenario	Solution
Constant Rate	$p_D = a(t_D) + b(t_D)y_D + c(t_D){y_D}^2$
Constant p_{wf}	$p_D = a(t_D) + b(t_D)y_D + c(t_D){y_D}^2 + d(t_D){y_D}^3$

These equations can be used to obtain the rate profile within the reservoir by $q_D = -\frac{2}{\pi}\frac{\partial p_D}{\partial y_D}$.

Using the IC and BCs, the coefficients can be determined. Notice that for the case of constant pressure production one needs an additional boundary condition for determining all the coefficients of the assumed pressure profile:

Table B. 10: Linear flow initial and boundary conditions used in the integral method.

Constant Rate	Constant p_{wf}	Type
$p_D = 0$	$p_D = 0$	Initial Condition (IC), at $t_D = 0$
$\frac{\partial p_D}{\partial y_D} = -\frac{\pi}{2}$	$p_D = 1$	Inner Boundary Condition (IBC) , at $y_D = 0$
$\frac{\partial p_D}{\partial y_D} = 0$	$\frac{\partial p_D}{\partial y_D} = 0$	Outer Boundary Condition (OBC), at $y_D = y_{eD}$
	$\frac{\partial q_D}{\partial y_D} = 0$	Inner Boundary Condition (IBC), at $y_D = 0$

Using the inner and outer BCs one can get the following results:

Table B. 11: Obtained parameters based on boundary conditions used in the integral method.

Constant Rate	Constant p_{wf}	Type
$b(t_D) = -\frac{\pi}{2}$	$a(t_D) = 1$	Inner Boundary Condition (IBC) , at $y_D = 0$
$c(t_D) = \frac{\pi}{4y_{eD}}$	$d(t_D) = -\frac{b(t_D)}{3{y_{eD}}^2}$	Outer Boundary Condition (OBC), at $y_D = y_{eD}$
	$c(t_D) = 0$	Inner Boundary Condition (IBC), at $y_D = 0$

Table B. 11 shows that the obtained pressure profiles still contain one unknown parameter. Therefore, the obvious conditions below can be used to eliminate the unknowns left in the pressure profile equations:

a) For the constant rate production, $p_D = p_{wD}$ at $y_D = 0$, therefore $a(t_D) = p_{wD}$.

b) For the constant pressure production, $q_D = q_{wD}$ at $y_D = 0$, therefore $b(t_D) = -\frac{\pi}{2} q_{wD}$.

Substitution of these coefficients in the above pressure distribution equation gives:

Table B. 12: Approximate pressure distributions, during BDF without skin.

Production Scenario	Solution
Constant Rate	$p_D = p_{wD} - \frac{\pi}{2}\left(y_D - \frac{1}{2y_{eD}}{y_D}^2\right)$
Constant p_{wf}	$p_D = 1 - \frac{\pi}{2} q_{wD}\left(y_D - \frac{1}{3{y_{eD}}^2}{y_D}^3\right)$

Equations in table above are for the BDF period. During transient flow, one can use the same equations provided that y_{eD} is substitute by y_{invD}. The average pressure within the investigated region is obtained by volumetric averaging of the pressure profile equations ($(p_{avg})_D = \frac{\int_0^{y_{invD}} p_D dy_D}{y_{invD}}$). This yields:

Table B. 13: Approximate pressure distributions, during both transient and BDF without skin.

Solutions	Constant Rate	Constant p_{wf}
Dimensionless	$(p_{avg})_D = p_{wD} - \frac{\pi}{2}\left(\frac{1}{3}y_{invD}\right)$	$(p_{avg})_D = 1 - \frac{\pi}{2}q_{wD}\left(\frac{5}{12}y_{invD}\right)$
Dimensional	$p_{avg} = p_{wf} + \frac{\pi}{2}\frac{\alpha_1 q_{wb} B\mu}{2\pi kh}\left(\frac{1}{3}\frac{y_{inv}}{x_f}\right)$	$p_{avg} = p_{wf} + \frac{\pi}{2}\frac{\alpha_1 q_{wb} B\mu}{2\pi kh}\left(\frac{5}{12}\frac{y_{inv}}{x_f}\right)$

Equations in the above Table are new approximate solutions that are obtained using the integral method. As a result of using equations in Table above, productivity indices can be derived. The ratio of the productivity indices for the constant rate and constant pressure is calculated to be equal to $PI_{ratio} = \frac{J_{CR}}{J_{CP}} = 1.25$, which is comparable with $PI_{ratio} = \frac{12}{\pi^2} = 1.22$ obtained by Wattenbarger et al. (1998).

Because the pressure profiles in Table B. 13 are based on distance of investigation, one can impose a constraint that the pressure profiles are required to have a zero slope (and therefore no flow) at the farthest boundary. This means that the pressure at y_{inv} during transient flow is set equal to the initial pressure, i.e. $p_y = p_i \text{ at } y = y_{inv}$. In terms of dimensionless parameters, $p_D = 0 \text{ at } y_D = y_{Dinv}$. Using this condition and substitution of the appropriate transient flow equations ($p_{wD} = \sqrt{\pi t_D}$ for the constant terminal rate and $\frac{1}{q_{wD}} = \frac{\pi}{2}\sqrt{\pi t_D}$ for constant terminal pressure) lead to the Eq. B. 6 and Eq. B. 7 for the distance of investigation of constant rate and constant pressure production, respectively:

$$y_{invD} = \frac{4}{\sqrt{\pi}}\sqrt{t_D} \qquad \text{Eq. B. 6}$$

$$y_{invD} = \frac{3\sqrt{\pi}}{2}\sqrt{t_D} \qquad \text{Eq. B. 7}$$

These equations determine the distance of investigation as the distance at which the approximate pressure within the reservoir is equal to the initial pressure. The ratio of the distances of investigation for the cases of constant rate and constant pressure production is therefore equal to $\frac{y_{invD_{CP}}}{y_{invD_{CR}}} = \frac{3\pi}{8} = 1.18$, which is comparable with the value suggested by Wattenbarger which is about 1.414.

Finally one can determine the approximate distance at which the pressure is equal to the average pressure (within the investigated distance). Equating the right hand side of the equations for p_y (Table B. 12) and p_{avg} (Table B. 13) gives $y_{avg} = \left(1 - \sqrt{\frac{1}{3}}\right) y_{inv} \cong 0.4226 y_{inv}$ for constant rate and $\bar{y} \cong 0.4463 y_{inv}$ for constant pressure production. It is noted that substitution of y_{inv} by y_e gives the distance at which pressure equals average reservoir pressure during BDF. This is while in radial flow, the approximate location at which pressure equals average reservoir pressure is at $r_{avg} = r(p_{avg}) \cong 0.5493 r_e$ (Raghavan 1993).

APPENDIX C: DERIVATION OF THE DOUBLE TANK SOLUTION FOR CTR

As part of the work done in this research, this Appendix details derivation of the new CTR solutions for the double tank model.

Eq. 4.9 and Eq. 4.10, which are the result of simple combination of material balance and fluid-flow equations construct a coupled system of two ordinary differential equations for two unknown (p_{DM} and p_{DMs}) since knowledge of p_{DM} is required in order to find p_{DMs} and vice versa. Using the notation that $X_1 = p_{DM}$ and $X_2 = p_{DMs}$, one can solve this system using matrix algebra, where the system is written in the following manner:

$$X' = AX + g \qquad \text{Eq. C. 1}$$

In this equation, $X = \begin{bmatrix} X_1 \\ X_2 \end{bmatrix}$, $X' = \frac{dX}{dt_{DM}}$, A is the matrix of coefficients $A = \begin{bmatrix} -F_R & F_R \\ F_c F_R & -F_c F_R \end{bmatrix}$ and $g = \begin{bmatrix} 1 \\ 0 \end{bmatrix}$.

As evident, this is a linear nonhomogeneous system of differential equations. In order to solve the above system and find the general solutions, one need to obtain the homogeneous solution (i.e. solution to the homogeneous system of ODE). This can be achieved by first evaluating the eigenvalues of Eq. C. 1. The eigenvalues are obtained through finding the roots of the characteristic polynomial of the matrix of coefficients, i.e. $\det(A - \lambda I) = 0$. Since A in this case is a 2×2 matrix, then its characteristic polynomial is a second degree polynomial. Upon finding the roots, the following eigenvalues are obtained:

$$\begin{cases} \lambda_1 = 0 \\ \lambda_2 = -F_R(1 + F_c) \end{cases} \qquad \text{Eq. C. 2}$$

Then the eigenvectors $\vec{\alpha} = \begin{bmatrix} \alpha_1 \\ \alpha_2 \end{bmatrix}$ and $\vec{\beta} = \begin{bmatrix} \beta_1 \\ \beta_2 \end{bmatrix}$ corresponding to the first and second eigenvalues, respectively, should be obtained. Eq. C. 3 and Eq. C. 4 give the appropriate eigenvectors:

$$\vec{\alpha} = \begin{bmatrix} 1 \\ \frac{\lambda_1}{F_R} + 1 \end{bmatrix} \quad \text{Eq. C. 3}$$

$$\vec{\beta} = \begin{bmatrix} 1 \\ \frac{\lambda_2}{F_R} + 1 \end{bmatrix} \quad \text{Eq. C. 4}$$

After finding the eigenvectors, the homogeneous solution is obtained as below:

$$X_h(\mathrm{t_{DM}}) = \mathrm{C_1}\vec{\alpha}e^{\lambda_1 \mathrm{t_{DM}}} + \mathrm{C_2}\vec{\beta}e^{\lambda_2 \mathrm{t_{DM}}} \quad \text{Eq. C. 5}$$

Upon substitution and simplification, one can get:

$$X_h(\mathrm{t_{DM}}) = \mathrm{C_1}\begin{bmatrix} 1 \\ \frac{\lambda_1}{F_R} + 1 \end{bmatrix} e^{\lambda_1 \mathrm{t_{DM}}} + \mathrm{C_2}\begin{bmatrix} 1 \\ \frac{\lambda_2}{F_R} + 1 \end{bmatrix} e^{\lambda_2 \mathrm{t_{DM}}} \quad \text{Eq. C. 6}$$

After finding the homogeneous solution, the particular solution can be obtained using the method of variation of parameters. For this purpose, first the matrix M using coefficients of $\mathrm{C_1}$ and $\mathrm{C_2}$ of the homogeneous solution (Eq. C. 6) is constructed:

$$M = \begin{bmatrix} 1 & e^{\lambda_2 \mathrm{t_{DM}}} \\ 1 & \left(\frac{\lambda_2}{F_R} + 1\right) e^{\lambda_2 \mathrm{t_{DM}}} \end{bmatrix} \quad \text{Eq. C. 7}$$

Here, substitution of the first eigenvalue ($\lambda_1 = 0$) simplifies the resulting matrix. Then upon simplification of the inverse of M one yields:

$$M^{-1} = \frac{F_R}{\lambda_2}\begin{bmatrix} \left(\frac{\lambda_2}{F_R} + 1\right) & -1 \\ -e^{-\lambda_2 \mathrm{t_{DM}}} & e^{-\lambda_2 \mathrm{t_{DM}}} \end{bmatrix} \quad \text{Eq. C. 8}$$

The particular solution is then obtained by finding the below integration:

$$X_p(\mathrm{t_{DM}}) = M \int M^{-1} g d\mathrm{t_{DM}} \qquad \text{Eq. C. 9}$$

The resulting particular solution is then determined to be according to below equation:

$$X_p(\mathrm{t_{DM}}) = \begin{bmatrix} \left(\frac{\lambda_2+F_R}{\lambda_2}\right)\mathrm{t_{DM}} + \frac{F_R}{{\lambda_2}^2} \\ \left(\frac{\lambda_2+F_R}{\lambda_2}\right)\mathrm{t_{DM}} + \frac{F_R}{{\lambda_2}^2}\left(\frac{\lambda_2}{F_R}+1\right) \end{bmatrix} \qquad \text{Eq. C. 10}$$

After finding the particular solution, the general solution is determined by adding the homogeneous and particular solutions:

$$X_g(\mathrm{t_{DM}}) = \mathrm{C_1}\begin{bmatrix}1\\1\end{bmatrix} + \mathrm{C_2}\begin{bmatrix}1\\ \frac{\lambda_2}{F_R}+1\end{bmatrix} e^{\lambda_2 \mathrm{t_{DM}}} + \begin{bmatrix} \left(\frac{\lambda_2+F_R}{\lambda_2}\right)\mathrm{t_{DM}} + \frac{F_R}{{\lambda_2}^2} \\ \left(\frac{\lambda_2+F_R}{\lambda_2}\right)\mathrm{t_{DM}} + \frac{F_R}{{\lambda_2}^2}\left(\frac{\lambda_2}{F_R}+1\right) \end{bmatrix} \qquad \text{Eq. C. 11}$$

Using the initial conditions, the constants $\mathrm{C_1}$ and $\mathrm{C_2}$ can be determined. It is noted here that the obtained results are for the average pressure. Moreover, it is noted that for the case of production at a constant rate and after reaching the boundaries of the first tank, the wellbore pressure tracks the average pressure. As a result one can set the initial condition as the starting wellbore pressure during boundary dominated flow ($\mathrm{p_{DM,BDF}}$, as obtained by the conventional methods of pressure transient analysis). Therefore the initial conditions are:

$$X_g(\mathrm{t_{DM,BDF}}) = \begin{bmatrix}\mathrm{p_{DM,BDF}}\\ 0\end{bmatrix} \qquad \text{Eq. C. 12}$$

Substitution of these initial conditions and simplification of the results give the following equation for $\mathrm{C_1}$ and $\mathrm{C_2}$:

$$\mathrm{C_1} = \left(\frac{\lambda_2+F_R}{\lambda_2}\right)\left(\mathrm{p_{DM,BDF}} - \mathrm{t_{DM,BDF}}\right) \qquad \text{Eq. C. 13}$$

$$C_2 = \left(-\frac{F_R}{{\lambda_2}^2} - \frac{F_R}{\lambda_2} p_{DM,BDF}\right) e^{-\lambda_2 t_{DM,BDF}} \quad \text{Eq. C. 14}$$

Using these constants, the general solution $X_g(t_{DM})$ is therefore obtained. The first element of the matrix $X_g(t_{DM})$ is p_{DM} which upon simplification yields:

$$p_{DM} = p_{DM,BDF} + \left(1 + \frac{F_R}{\lambda_2}\right)(t_{DM} - t_{DM,BDF}) + \frac{F_R}{\lambda_2}\left(\frac{1}{\lambda_2} + p_{DM,BDF}\right)(1 - e^{\lambda_2(t_{DM} - t_{DM,BDF})}) \quad \text{Eq. C. 15}$$

And the first element of the matrix $X_g(t_{DM})$ is p_{DMs} which is according to Eq. C. 16:

$$p_{DMs} = \left(1 + \frac{F_R}{\lambda_2}\right)\left\{(t_{DM} - t_{DM,BDF}) + \left(\frac{1}{\lambda_2} + p_{DM,BDF}\right)\{1 - e^{\lambda_2(t_{DM} - t_{DM,BDF})}\}\right\} \quad \text{Eq. C. 16}$$

APPENDIX D: DERIVATION OF THE DOUBLE TANK SOLUTION FOR CTP

As part of the work done in this research, this Appendix details derivation of the new CTP solutions for the double tank model.

In this case, Eq. 4.14 and Eq. 4.15, construct a coupled system of two ordinary differential equations for two unknown (q_{DM} and q_{DMs}), since knowledge of q_{DM} is required in order to find q_{DMs} and vice versa. Using the notation that $X_1 = q_{DM}$ and $X_2 = q_{DMs}$, one can solve this system using matrix algebra, where the system is written in the following manner:

$$X' = AX \qquad \text{Eq. D. 1}$$

In this equation, $X = \begin{bmatrix} X_1 \\ X_2 \end{bmatrix}$, $X' = \frac{dX}{dt_{DM}}$ and A is the matrix of coefficients given by $A = \begin{bmatrix} -1 & 1 \\ F_R & -(F_R + F_c F_R) \end{bmatrix}$.

This is a linear homogeneous system of differential equations. In order to solve the above system and find the general solutions, one needs to obtain the homogeneous solution (i.e. solution to the homogeneous system of ODE). This can be achieved by first evaluating the eigenvalues of Eq. D. 1. The eigenvalues are obtained through finding the roots of the characteristic polynomial of the matrix of coefficients, i.e. $\det(A - \lambda I) = 0$. Since A in this case is a 2×2 matrix, its characteristic polynomial is of second degree, as below equation shows:

$$\lambda^2 + \big(1 + F_R(1 + F_c)\big)\lambda - F_R F_c = 0 \qquad \text{Eq. D. 2}$$

Depending on the discriminant for this equation, the solution can have real or imaginary roots. The discriminant for Eq. D. 2 is as below:

$$\Delta = \left(1 + F_R(1 + F_c)\right)^2 - 4F_R F_c \qquad \text{Eq. D. 3}$$

This equation can be manipulated to yield the following relation, which shows that the discriminant is positive and therefore Eq. D. 3 has two real roots:

$$\Delta = \left(1 - F_R(1 + F_c)\right)^2 + 4F_R \qquad \text{Eq. D. 4}$$

The roots are then obtained as below:

$$\lambda = \frac{-\left(1+F_R(1+F_c)\right) \pm \sqrt{\left(1-F_R(1+F_c)\right)^2 + 4F_R}}{2} \qquad \text{Eq. D. 5}$$

The convention adopted here is that λ_1 and λ_2 correspond to the positive (+) and negative (-) signs in Eq. D. 5, respectively.

Then one needs to find the eigenvectors $\vec{\alpha} = \begin{bmatrix}\alpha_1 \\ \alpha_2\end{bmatrix}$ and $\vec{\beta} = \begin{bmatrix}\beta_1 \\ \beta_2\end{bmatrix}$ corresponding to the first and second eigenvalues, respectively. These eigenvectors can be obtained according to the following equations:

$$\vec{\alpha} = \begin{bmatrix} 1 \\ 1 + \lambda_1 \end{bmatrix} \qquad \text{Eq. D. 6}$$

$$\vec{\beta} = \begin{bmatrix} 1 \\ \lambda_2 + 1 \end{bmatrix} \qquad \text{Eq. D. 7}$$

Similar the previous case and after finding the eigenvectors, the homogeneous solution is obtained using Eq. C. 5. Upon substitution and simplification, the homogeneous solution, which in this case is equal to the general solution gives:

$$X_g(t_{DM}) = X_h(t_{DM}) = C_1 \begin{bmatrix} 1 \\ \lambda_1 + 1 \end{bmatrix} e^{\lambda_1 t_{DM}} + C_2 \begin{bmatrix} 1 \\ \lambda_2 + 1 \end{bmatrix} e^{\lambda_2 t_{DM}} \qquad \text{Eq. D. 8}$$

The constants C_1 and C_2 can be found using the following initial conditions:

$$X_g(t_{DM,BDF}) = \begin{bmatrix} q_{DM,BDF} \\ 0 \end{bmatrix}$$ Eq. D. 9

Substitution of these initial conditions and simplification of the results give the following equation for C_1 and C_2:

$$C_1 = \left(\frac{\lambda_2+1}{\lambda_2-\lambda_1}\right) q_{DM,BDF} \times e^{-\lambda_1 t_{DM,BDF}}$$ Eq. D. 10

$$C_2 = -\left(\frac{\lambda_1+1}{\lambda_2-\lambda_1}\right) q_{DM,BDF} \times e^{-\lambda_2 t_{DM,BDF}}$$ Eq. D. 11

Therefore from the obtained general solution, the following equation for q_{DM} is resulted:

$$q_{DM} = q_{DM,BDF}\left\{\left(\frac{\lambda_2+1}{\lambda_2-\lambda_1}\right) \times e^{\lambda_1(t_{DM}-t_{DM,BDF})} - \left(\frac{\lambda_1+1}{\lambda_2-\lambda_1}\right) \times e^{\lambda_2(t_{DM}-t_{DM,BDF})}\right\}$$ Eq. D. 12

And for q_{DMs} one yields:

$$q_{DMs} = q_{DM,BDF}\left(\frac{(\lambda_1+1)(\lambda_2+1)}{(\lambda_2-\lambda_1)}\right)\left\{e^{\lambda_1(t_{DM}-t_{DM,BDF})} - e^{\lambda_2(t_{DM}-t_{DM,BDF})}\right\}$$ Eq. D. 13

APPENDIX E: ANALYSIS OF THE DOUBLE TANK MODEL BEHAVIOUR

As part of the work done in this research, this Appendix explains derivation of the new approximate equations for describing the double tank model behaviour.

Behaviour of a double compartment model is different from that of a single compartment and is a function of the contrasting properties of the two compartments. Using the simple concept of distance of investigation, one can determine the time where significant changes in its behaviour takes place. In order to simplify this task, the distance of investigation is written in terms of capacity and resistivity. Substituting Eq. 3.8 into Eq. 3.1, the following equation is obtained:

$$y_{inv} = \alpha_1 \sqrt{\frac{2}{\pi} \frac{t}{C^* \times R^*}} \qquad \text{Eq. E. 1}$$

Then the definition of t_{DM}, Eq. 4.6, and relation between $C^*\&R^*$ and C&R are used to write the dimensionless time used in the compartmentalized model:

$$t_{DM} = \frac{t}{(C^* y_{inv}) \times (R^* \alpha_2 \times y_{inv})} \qquad \text{Eq. E. 2}$$

Substituting y_{inv} from Eq. E. 1 into Eq. E. 2 gives the dimensionless time to reach BDF of the production tank:

$$t_{DM,BDF} = \frac{\pi}{2} \frac{1}{{\alpha_1}^2 \alpha_2} \qquad \text{Eq. E. 3}$$

As noticed, this time is a function of the constant α_1 which its value is different for CTR than CTP.

In order to approximate the time at which the total system BDF is evident, first the capacity and resistivity terms used in the distance of investigation equation (Eq. E. 1) are substituted

by those of the support tank. Using the definition of the dimensionless time (t_{DM}) and upon simplification, the following equation is obtained:

$$t_{DM,2} = \left(\frac{\pi}{2}\frac{1}{{\alpha_1}^2\alpha_2}\right)\frac{1}{F_c F_R} \qquad \text{Eq. E. 4}$$

Eq. E. 4 gives the time required to investigate the support tank capacity through a medium with support tank resistivity. Addition of $t_{DM,2}$ and $t_{DM,BDF}$ gives the time required to reach the total system BDF:

$$t_{DM} = t_{DM,BDF}\left(\frac{F_c F_R + 1}{F_c F_R}\right) \qquad \text{Eq. E. 5}$$

These calculations are for both cases of CTR and CTP. In order to obtain relevant relations for calculating the time where the support compartment becomes significant, each production scenario is analyzed separately.

(i) Constant terminal rate (CTR)

After investigating the production tank, depending on the characteristics of the support tank, sooner or later its behaviour becomes significant. When the support tank starts contribution, the production tank gets depleted, while being replenished by the transient flow of the support tank. The pressure difference between these two tanks can be obtained by subtracting Eq. 4.12 from Eq. 4.11 to get the following relation:

$$p_{DM} - p_{DMs} = p_{DM,BDF} - \left(\frac{1}{\lambda_2} + p_{DM,BDF}\right)\left(1 - e^{\lambda_2\left(t_{DM} - t_{DM,BDF}\right)}\right) \qquad \text{Eq. E. 6}$$

At late times, the exponential term becomes smaller and therefore eventually negligible. As a result, when the total system pseudo-steady state prevails (i.e. at late times), the two compartments are depleted at the same rate with a constant pressure difference between them, Eq. E.7:

$$p_{DM} - p_{DMs} = -\frac{1}{\lambda_2}$$ Eq. E. 7

In order to approximate the time at which the support tank starts sensible contribution to production, first the time for investigating the production tank with the resistance of support tank is obtained. This time can be simply obtained according to the following equation:

$$t_{DM,3} = \left(\frac{\pi}{2}\frac{1}{{\alpha_1}^2\alpha_2}\right)\frac{1}{F_R}$$ Eq. E. 8

The time where deviation from the single tank behaviour happens is determined by addition of $t_{DM,3}$ and $t_{DM,BDF}$ to yield Eq. E. 9:

$$t_{DM} = t_{DM,BDF}\left(\frac{F_R+1}{F_R}\right)$$ Eq. E. 9

(ii) Constant terminal pressure (CTP)

The time at which the support tank contribution becomes significant is determined by intersecting the second exponential decline (the first term in curled parenthesis in Eq. 4.16) with the traditional exponential decline (i.e. Eq. 4.27). Having done that, Eq. E. 10 is obtained:

$$q_{DM,BDF}\left(\frac{\lambda_2+1}{\lambda_2-\lambda_1}\right) \times e^{\lambda_1(t_{DM}-t_{DM,BDF})} = q_{DM,BDF} \times e^{-(t_{DM}-t_{DM,BDF})}$$ Eq. E. 10

Simplification of this equation gives Eq. E. 11 which is the time at which the support's contribution becomes sensible:

$$t_{DM} = t_{DM,BDF} + \left(\frac{1}{\lambda_1+1}\right) ln\left(\frac{\lambda_2-\lambda_1}{\lambda_2+1}\right)$$ Eq. E. 11

APPENDIX F: THE DEPLETION EQUATION FOR GAS

This Appendix demonstrates the gas material balance equation (p/Z vs. cumulative production) can be derived from the gas compressibility equation.

Depletion equation for a liquid is according to the compressibility equation. Its calculation is easy since the liquid compressibility can be assumed constant. For gas flow, however, the compressibility changes substantially with production and therefore depletion calculation according to simple liquid flow equations is not possible. In this section it is shown that the depletion for a gas reservoir can be calculated easily according to the familiar p/Z (material balance) equation. Let's start with the definition of the compressibility:

$$c_g = -\frac{1}{V}\frac{dV}{dp} \qquad \text{Eq. F. 1}$$

In the above equation, p means average pressure (p_{avg}). It is noted in Eq. F. 1 that V and dV are in ft^3. Replacing the former by GB_{gi} and the latter by $qB_g dt$ and then substituting them into the above compressibility equation gives:

$$c_g = -\frac{1}{GB_{gi}}\frac{qB_g dt}{dp} \qquad \text{Eq. F. 2}$$

From the definition of gas formation volume factor ($B_g = 0.0283\frac{ZT}{p}$) one can write following relation between B_g and B_{gi}:

$$\frac{B_g}{B_{gi}} = \frac{(Z/p)}{(Z/p)_i} \qquad \text{Eq. F. 3}$$

Its substitution in Eq. F. 2 gives:

$$c_g = -\frac{(Z/p)}{(Z/p)_i}\frac{1}{G}\frac{qdt}{dp} \qquad \text{Eq. F. 4}$$

There is an alternative definition for compressibility, based on formation volume factor, Eq. F. 5:

$$c_g = -\frac{1}{B_g}\frac{dB_g}{dp} \qquad \text{Eq. F. 5}$$

Upon substituting the equation for gas formation volume factor into Eq. F. 5 and performing the derivative with respect to pressure, Eq. F. 6 is obtained:

$$c_g = \frac{1}{p} - \frac{1}{Z}\frac{dZ}{dp} \qquad \text{Eq. F. 6}$$

Equating the right-hand sides of Eq. F. 4 and Eq. F. 6 and then rearranging the obtained equation yields:

$$\left(\frac{1}{Z} - \frac{p}{Z^2}\frac{dZ}{dp}\right) = -\left(\frac{p}{Z}\right)_i \frac{1}{G}\frac{qdt}{dp} \qquad \text{Eq. F. 7}$$

The left-hand side of this equation is equal to $\frac{d(p/Z)}{dp}$. Upon its substitution, one yields:

$$\frac{d(p/Z)}{dp} = -\left(\frac{p}{Z}\right)_i \frac{1}{G}\frac{qdt}{dp} \qquad \text{Eq. F. 8}$$

Multiplying through by dp, Eq. F. 9 is simply obtained:

$$d\left(\frac{p}{Z}\right) = -\left(\frac{p}{Z}\right)_i \frac{q_g dt}{G} \qquad \text{Eq. F. 9}$$

Integrating Eq. F. 9 over the entire production period gives:

$$\left(\frac{p}{Z}\right) = \left(\frac{p}{Z}\right)_i \left[1 - \frac{G_p}{G}\right] \qquad \text{Eq. F. 10}$$

As evident, Eq. F. 10 was resulted from the gas compressibility equation. This means that for flow of gases one can use the p/Z equation in place of the compressibility equation to calculate depletion. Using p/Z, therefore, one can account for the changes in gas compressibility with production.